

**Electron spectroscopy of ionic liquids:
experimental identification of atomic orbital contributions to valence electronic structure**

Richard M. Fogarty,¹ Robert G. Palgrave,² Richard A. Bourne,³ Karsten Handrup,⁴ Ignacio J. Villar-Garcia,⁵ David J. Payne,⁵ Patricia A. Hunt,¹ Kevin R. J. Lovelock.⁶

¹ Department of Chemistry, Imperial College London, UK

² Department of Chemistry, University College London, UK

³ Institute of Process Research and Development, Schools of Chemistry and Chemical and Process Engineering, University of Leeds, UK

⁴ MAX IV Laboratory, Lund University, Lund, Sweden

⁵ Department of Materials, Imperial College London, UK

⁶ Department of Chemistry, University of Reading, UK

Contact E-mail: k.r.j.lovelock@reading.ac.uk

1. Ionic Liquids Studied and Synthesis	S2-S5
2. Apparatus	S6
3. Synchrotron XPS. Sample charging	S7-S9
4. Data analysis. Peak fitting core level XP spectra	S10-S13
5. Data analysis. Charge referencing procedures	S14-S20
6. Data analysis. AO photoionisation cross-sections	S21-S23
7. Data analysis. Interpolation of electron spectra	S24-S25
8. Data analysis. Area normalisation	S26-S27
9. Data analysis. Obtaining individual cation and anion traces	S28-S29
10. Data analysis. Subtraction methods	S30-S31
11. Data analysis. Validating quantitative area normalisation and subtraction	S32
12. Data analysis. Obtaining $E_B(\text{ion HOFO})$ and $E_B(\text{ion onset})$	S33
13. Results. XPS: demonstrating purity	S34-S79
14. Results. Variable $h\nu$ valence XPS data	S80-S81
15. Results. Using NEXAFS spectroscopy to aid RAES	S82-S83
16. Results. RAES data: E_B heat maps	S84-S98
17. Results. RAES data: further descriptions	S99-S100
18. Results. RAES data: $[\text{NO}_3]^-$ comparison	S101
19. Results. Component identification: summary tables	S102
20. Results. Fingerprint method: area normalisation using valence levels	S103-S106
21. Results. Subtraction method: identifying cationic and anionic alkyl contributions	S107-S110
22. Results. Subtraction method: identifying cationic non-alkyl contributions	S111-S126
23. Results. Subtraction method: identifying anionic non-alkyl contributions	S127-S130
24. Results. Identification of MOs that were not the ion HOFO	S132
25. Results. $\Delta E_B(\text{valence level} - \text{valence level})$	S133
26. Results. $E_B(\text{ion HOFO})$ and $E_B(\text{ion onset})$	S134-S135
27. Results. HOMO identification	S136-S138
28. References	S139-S141

1. Ionic Liquids Studied and Synthesis

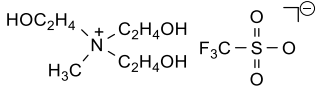
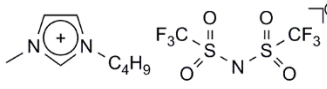
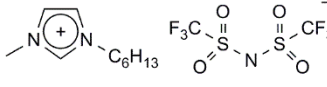
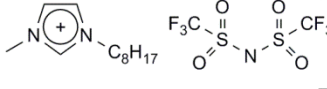
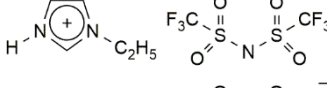
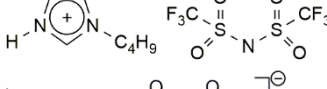
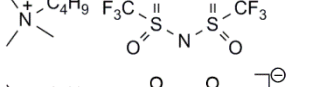
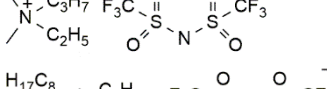
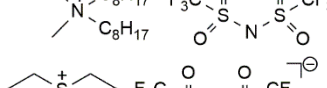
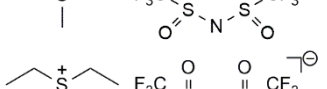
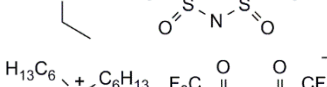
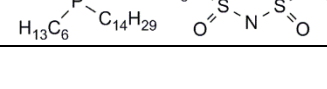
Select ionic liquids (ILs) were purchased from: Merck ($[\text{C}_6\text{C}_1\text{Im}][\text{B}(\text{CN})_4]$), Sigma–Aldrich ($[\text{C}_4\text{C}_1\text{Im}][\text{OcSO}_4]$, $[\text{C}_4\text{C}_1\text{Im}][\text{SCN}]$, $[\text{C}_4\text{C}_1\text{Im}][\text{N}(\text{CN})_2]$, $[\text{C}_8\text{C}_1\text{Im}][\text{TfO}]$, $[\text{N}_{4,1,1,1}][\text{NTf}_2]$, $[\text{N}_{3,2,1,1}][\text{NTf}_2]$, $[\text{N}_{8,8,8,1}][\text{NTf}_2]$, $[\text{P}_{6,6,6,14}][\text{NTf}_2]$, $[\text{P}_{6,6,6,14}]\text{Cl}$, $[\text{P}_{6,6,6,14}]\text{Br}$, $[\text{P}_{6,6,6,14}][\text{N}(\text{CN})_2]$, $[\text{S}_{2,2,2}][\text{NTf}_2]$) or Iolitec ($[\text{C}_2\text{C}_0\text{Im}][\text{NTf}_2]$, $[\text{C}_8\text{C}_1\text{Im}]\text{Br}$, $[\text{C}_6\text{C}_1\text{Im}]\text{I}$, $[\text{C}_8\text{C}_1\text{Im}][\text{BF}_4]$, $[\text{S}_{2,2,1}][\text{NTf}_2]$, $[\text{C}_8\text{C}_1\text{Im}][\text{SCN}]$, $[\text{C}_8\text{C}_1\text{Im}][\text{C}(\text{CN})_3]$ and $[\text{N}_{2,2,1,0}][\text{TfO}]$). Select ILs were prepared in our laboratories *via* established synthetic methods: $[\text{C}_8\text{C}_1\text{Im}][\text{HSO}_4]$,¹ $[\text{C}_4\text{C}_1\text{Im}][\text{HSO}_4]$,² $[\text{C}_4\text{C}_1\text{Im}][\text{MeSO}_4]$,² $[\text{P}_{6,6,6,14}][\text{NO}_3]$,³ $[\text{C}_4\text{C}_1\text{Im}][\text{NTf}_2]$,² $[\text{C}_6\text{C}_1\text{Im}][\text{NTf}_2]$,² $[\text{C}_8\text{C}_1\text{Im}][\text{NTf}_2]$,² $[\text{C}_4\text{C}_0\text{Im}][\text{NTf}_2]$,⁴ $[\text{C}_8\text{C}_1\text{Im}]\text{Cl}$,² $[\text{C}_4\text{C}_1\text{Im}][\text{TfO}]$,² $[\text{N}_{2\text{OH},2\text{OH},2\text{OH},1}][\text{TfO}]$,⁵ $[\text{C}_4\text{C}_1\text{Im}][\text{Me}_2\text{PO}_4]$,⁵ $[\text{C}_2\text{C}_1\text{Im}][\text{MeSO}_3]$,⁶ $[\text{C}_4\text{C}_0\text{Im}][\text{HSO}_4]$,⁷ or *via* a modified procedure ($[\text{N}_{4,1,1,0}][\text{HSO}_4]$ ⁸ and $[\text{N}_{8,1,1,0}][\text{HSO}_4]$). The purity of all IL samples synthesised in our laboratories was assessed using ¹H NMR and ¹³C NMR spectroscopy. Sample purity was also confirmed by XP survey spectra (ESI Section 13).

The seven ILs for which RAES experiments were carried out (Table S1) were chosen with N 1s RAES experiments in mind. Multiple $[\text{C}_n\text{C}_1\text{Im}]^+$ -based ILs were chosen as they are the most important cations for the IL community. A $[\text{C}_n\text{C}_1\text{Im}]^+$ cation was paired with an anion, Cl^- , that does not contain nitrogen to allow the RAE spectrum for the $[\text{C}_n\text{C}_1\text{Im}]^+$ cation to be recorded without any anionic nitrogen atom contributions. $[\text{C}_n\text{C}_1\text{Im}]^+$ cations were paired with anions that contain nitrogen ($[\text{C}(\text{CN})_3]^-$, $[\text{SCN}]^-$, $[\text{NTf}_2]^-$) so that both the anions and the cations could be studied using N 1s RAES (we knew in advance that the anionic N 1s XA contributions would come at energies different to those of the $[\text{C}_n\text{C}_1\text{Im}]^+$ cation contributions). The immense power of RAES to allow differentiation between different IL covalent bonding environments was particularly important for these three ILs. $[\text{P}_{6,6,6,14}][\text{NO}_3]$ was chosen to allow the N 1s RAE spectrum of the $[\text{NO}_3]^-$ anion to be recorded without any cationic nitrogen atom contributions. A similar rationale was used to choose the ammonium–based ILs; ILs were chosen that do not contain nitrogen atoms in the anion, so as to allow the RAE spectrum for the ammonium cations to be recorded. The 37 ILs for which lab-based XPS experiments were carried out (Table S1) were chosen with structural diversity in mind. 16 different cations and 16 different anions were studied using lab-based XPS experiments, giving a structurally very diverse data set. The seven ILs for which RAES experiments were carried out (Table S1) were also studied using lab-based XPS experiments, to give comparable data to the other 30 ILs studied using lab-based XPS experiments. For 34 of the 37 ILs studied here, at least one ion was studied using RAES experiments. The three ILs with no ion studied with RAES ($[\text{C}_2\text{C}_1\text{Im}][\text{MeSO}_3]$, $[\text{C}_6\text{C}_1\text{Im}]\text{I}$ and $[\text{C}_6\text{C}_1\text{Im}][\text{B}(\text{CN})_4]$) all have the $[\text{C}_n\text{C}_1\text{Im}]^+$ core, which has been studied with RAES. Therefore, the information and observations gained from the RAES experiments for seven ILs could be used to inform peak identification for the other 30 ILs. Five of the ILs in Table S1 were chosen because they have halide anions ($[\text{C}_8\text{C}_1\text{Im}]\text{Br}$, $[\text{C}_6\text{C}_1\text{Im}]\text{I}$, $[\text{P}_{6,6,6,14}]\text{Cl}$ and $[\text{P}_{6,6,6,14}]\text{Br}$), which makes them ideal candidates for using the fingerprint and subtraction methods to identify AO contributions to MOs. $[\text{C}_8\text{C}_1\text{Im}][\text{BF}_4]$ was chosen because it has been concluded in the literature (from a combination of experiments and calculations) that the HOMO for this IL was from the cation;⁹ hence, this IL is also an ideal candidate for using the fingerprint method to identify AO contributions to MOs.

Table S1. ILs investigated in this work.

IL no.	Abbreviation	Structure	Name	Variable $h\nu$ XPS	RAES	Lab-based XPS
1	[C ₈ C ₁ Im]Cl		1-octyl-3-methylimidazolium chloride	✓	✓	✓
2	[C ₈ C ₁ Im]Br		1-octyl-3-methylimidazolium bromide			✓
3	[C ₆ C ₁ Im]I		1-hexyl-3-methylimidazolium iodide			✓
4	[P _{6,6,6,14}]Cl		tetradecyl(trihexyl)phosphonium chloride			✓
5	[P _{6,6,6,14}]Br		tetradecyl(trihexyl)phosphonium bromide			✓
6	[C ₄ C ₁ Im][SCN]		1-butyl-3-methylimidazolium thiocyanate	✓	✓	✓
7	[C ₈ C ₁ Im][SCN]		1-octyl-3-methylimidazolium thiocyanate			✓
8	[C ₄ C ₁ Im][N(CN) ₂]		1-butyl-3-methylimidazolium dicyanamide			✓
9	[P _{6,6,6,14}][N(CN) ₂]		tetradecyl(trihexyl)phosphonium dicyanamide			✓
10	[C ₈ C ₁ Im][C(CN) ₃]		1-octyl-3-methylimidazolium tricyanomethanide		✓	✓
11	[C ₆ C ₁ Im][B(CN) ₄]		1-hexyl-3-methylimidazolium tetracyanoborate			✓
12	[C ₈ C ₁ Im][BF ₄]		1-octyl-3-methylimidazolium tetrafluoroborate			✓
13	[P _{6,6,6,14}][NO ₃]		tetradecyl(trihexyl)phosphonium nitrate	✓	✓	✓

14	[C ₄ C ₁ Im][HSO ₄]		1-butyl-3-methylimidazolium hydrogensulfate				✓
15	[C ₈ C ₁ Im][HSO ₄]		1-octyl-3-methylimidazolium hydrogensulfate				✓
16	[C ₄ C ₀ Im][HSO ₄]		1-butyl-imidazolium hydrogensulfate				✓
17	[N _{4,1,1,0}][HSO ₄]		butyl(dimethyl)ammonium hydrogensulfate	✓	✓		✓
18	[N _{8,1,1,0}][HSO ₄]		octyl(dimethyl)ammonium hydrogensulfate				✓
19	[C ₄ C ₁ Im][MeSO ₄]		1-butyl-3-methylimidazolium methylsulfate				✓
20	[C ₄ C ₁ Im][OcSO ₄]		1-butyl-3-methylimidazolium octylsulfate				✓
21	[C ₂ C ₁ Im][MeSO ₃]		1-ethyl-3-methylimidazolium methanesulfonate				✓
22	[C ₄ C ₁ Im][Me ₂ PO ₄]		1-butyl-3-methylimidazolium dimethylphosphate				✓
23	[C ₄ C ₁ Im][TfO]		1-butyl-3-methylimidazolium trifluoromethylsulfonate				✓
24	[C ₈ C ₁ Im][TfO]		1-octyl-3-methylimidazolium trifluoromethylsulfonate				✓
25	[N _{2,2,1,0}][TfO]		diethyl(methyl)ammonium trifluoromethylsulfonate	✓	✓		✓

26	[N _{2OH,2OH,2OH,1}][TfO]		triethanol(methyl)ammonium triflate				✓
27	[C ₄ C ₁ Im][NTf ₂]		1-butyl-3-methylimidazolium bis[(trifluoromethane)sulfonyl]imide				✓
28	[C ₆ C ₁ Im][NTf ₂]		1-hexyl-3-methylimidazolium bis[(trifluoromethane)sulfonyl]imide				✓
29	[C ₈ C ₁ Im][NTf ₂]		1-octyl-3-methylimidazolium bis[(trifluoromethane)sulfonyl]imide	✓	✓		✓
30	[C ₂ C ₀ Im][NTf ₂]		1-ethyl-imidazolium bis[(trifluoromethane)sulfonyl]imide				✓
31	[C ₄ C ₀ Im][NTf ₂]		1-butyl-imidazolium bis[(trifluoromethane)sulfonyl]imide				✓
32	[N _{4,1,1,1}][NTf ₂]		butyl(trimethyl)ammonium bis[(trifluoromethane)sulfonyl]imide				✓
33	[N _{3,2,1,1}][NTf ₂]		propyl(ethyl)(dimethyl)ammonium bis[(trifluoromethane)sulfonyl]imide				✓
34	[N _{8,8,8,1}][NTf ₂]		trioctyl(methyl)ammonium bis[(trifluoromethane)sulfonyl]imide				✓
35	[S _{2,2,1}][NTf ₂]		diethyl(methyl)sulfonium bis[(trifluoromethane)sulfonyl]imide				✓
36	[S _{2,2,2}][NTf ₂]		triethylsulfonium bis[(trifluoromethane)sulfonyl]imide				✓
37	[P _{6,6,6,14}][NTf ₂]		hexadecyl(trihexyl)phosphonium bis[(trifluoromethane)sulfonyl]imide				✓

2. Apparatus

Laboratory-based XPS was carried out using two Thermo K-alpha spectrometers utilising Al K α radiation ($h\nu = 1486.6$ eV) and a quartz crystal monochromator set in a 250 mm Rowland circle. The X-ray spot was focussed at the sample to a size of 400 μm . The base pressure was 10^{-9} mbar, and the analyser was a double focusing 180° hemisphere with mean radius 125 mm which was run in constant analyser energy mode. The pass energy was set to 200 eV for the survey scan, 20 eV for core level spectra and 50 eV for valence XP spectra. The detector was a 128 channel position sensitive detector. The energy scale of the instrument was regularly calibrated using a three point (Cu, Ag, Au) scale. A drop of IL was placed directly onto a stainless steel plate. This was placed in a loadlock and the pressure reduced to 10^{-7} mbar by pumping down overnight. After attaining the required pressure, the IL was transferred to the analysis chamber. Etching was carried out using a 500 eV Ar $^+$ ion gun. Charge compensation was achieved using a dual beam flood gun which applies both electrons and low energy Ar $^+$ ions to the sample.

Valence XP spectra with $h\nu \neq 1486.6$ eV and all RAES data were collected on beamline I311 at the MAX-II storage ring (Lund, Sweden). A drop of IL was deposited onto a molybdenum sample plate. The sample was placed in a load lock and pumped down slowly to 10^{-6} mbar before being transferred to an analysis chamber (10^{-9} mbar). Etching was carried out with a 500 eV Ar $^+$ ion gun. The detector was a Scienta SES200 hemispherical electron analyser. The pass energy was set to 100 eV for the survey spectrum and to 20 eV for the high resolution valence XP spectra.

For both instruments used here, the source-detector angle was 54.7°, *i.e.* the magic angle. At this angle, the anisotropy parameter is zero.^{10, 11} Therefore, the asymmetry parameter component was not considered when analysing the variable $h\nu$ XPS results.

Etching using an Ar $^+$ ion gun was necessary to remove small amounts of surface contaminants, *e.g.* silicon and oxygen contamination from grease from synthesis of the ionic liquids. It has been concluded previously using XPS and low energy ion scattering (LEIS) that ionic liquid sample surfaces were not left permanently damaged in the region studied after bombardment with Ar $^+$ ions (~ 1 keV).^{2, 12, 13} Sample charging has been noted to be a problem for XPS analysis;¹⁴ therefore, charge compensation was used to attempt to remove any problems with sample charging.

3. Data analysis. Synchrotron XPS: sample charging

For two of the ILs studied at the synchrotron, $[\text{C}_8\text{C}_1\text{Im}]\text{Cl}$ and $[\text{N}_{4,1,1,0}][\text{HSO}_4]$, sample charging was observed over time under X-ray irradiation during XPS experiments (ESI Figure S1 and ESI Figure S2 respectively). Previously, IL charging under X-ray irradiation during XPS experiments has only been reported for solid ILs that were cooled from room temperature.^{15, 16} This is the first time that the flux from electrons leaving the sample after photoemission was greater than the charge compensation mechanism provided by the IL. These two ILs have relatively large viscosity; for the lower viscosity ILs studied at the synchrotron, *e.g.* $[\text{C}_8\text{C}_1\text{Im}][\text{NTf}_2]$, no sample charging over time was observed. Therefore, we expect that for the more viscous ILs, ionic transport to compensate for the electrons leaving was insufficient to overcome the sample charging. To overcome this problem, the sample was moved during synchrotron experiments. Whilst this procedure overcame the problem of sample charging, it introduced a further problem for $[\text{C}_8\text{C}_1\text{Im}]\text{Cl}$; differences in the sample thickness led to a small number of data points giving less signal than expected (however, this issue did not cause a significant problem for data analysis).

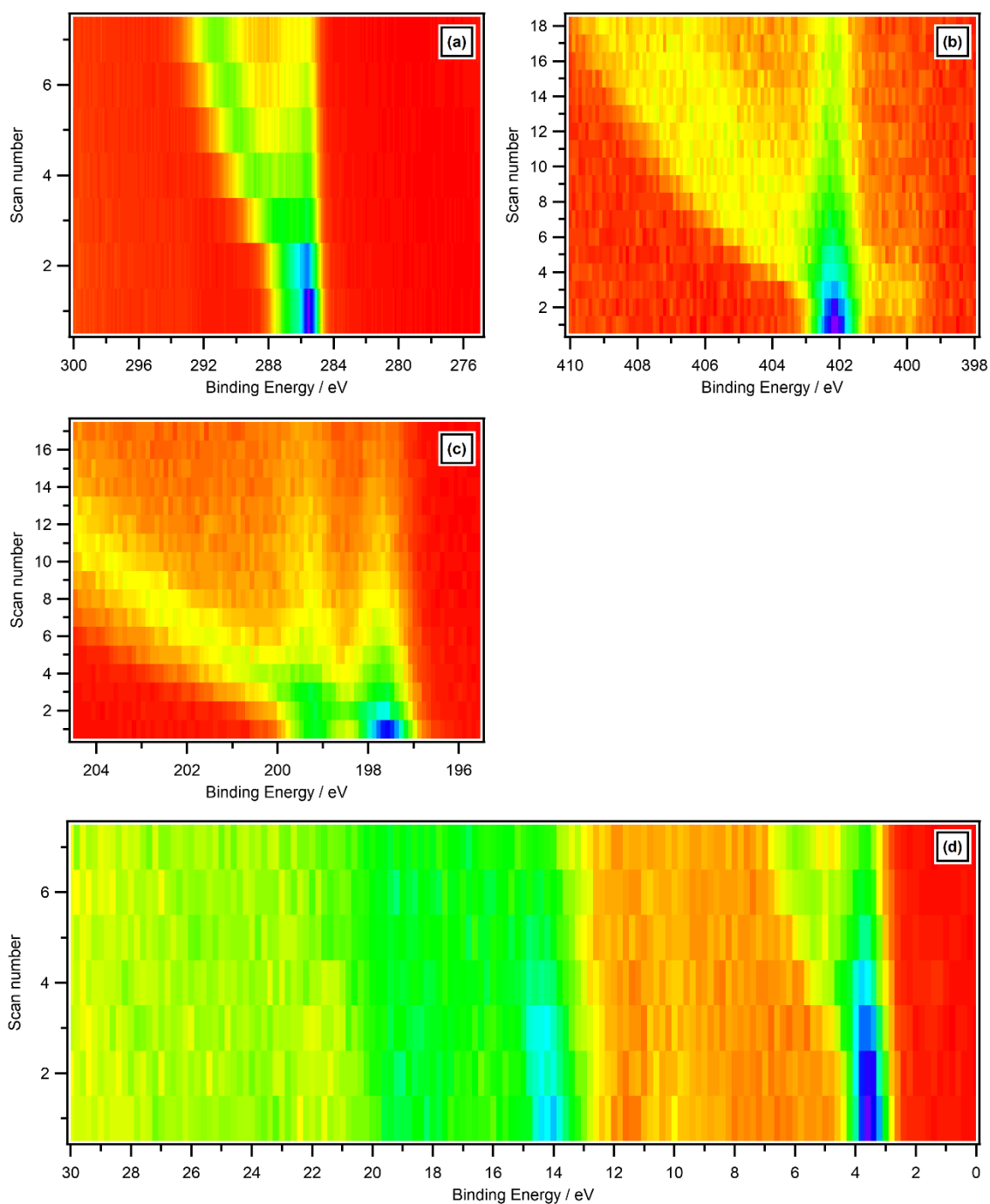


Figure S1. XP spectra for $[\text{C}_8\text{C}_1\text{Im}]\text{Cl}$ over time with a stationary sample recorded on synchrotron-based XPS at $h\nu = 850$ eV: (a) C 1s, (b) N 1s, (c) Cl 2p, (d) valence. No charge referencing was applied to these spectra. These XP spectra were recorded one after the other; hence, different numbers of XP spectra were recorded for each region. Red corresponds to low intensity, blue corresponds to high intensity.

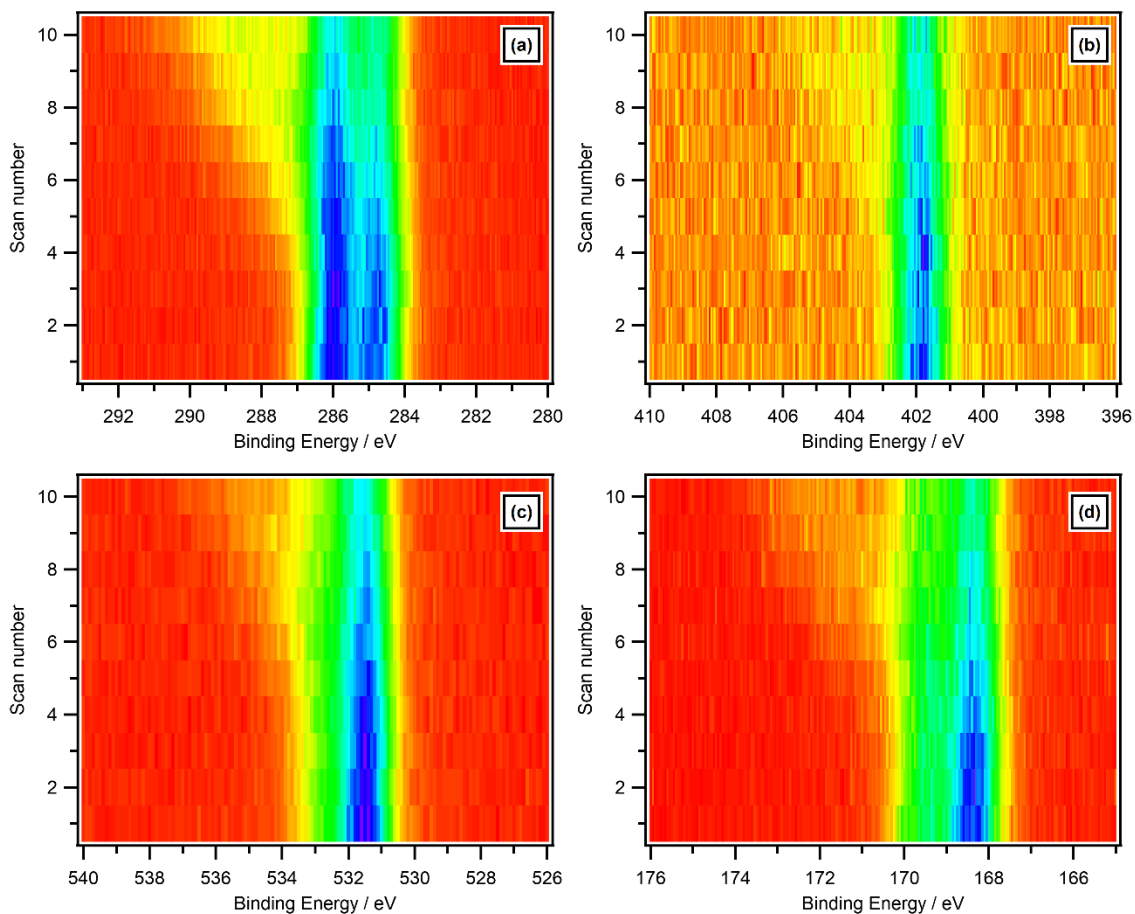


Figure S2. XP spectra for $[N_{4,1,1,0}][HSO_4]$ over time with a stationary sample recorded on synchrotron-based XPS at $h\nu = 850$ eV: (a) C 1s, (b) N 1s, (c) O 1s, (d) S 2p. No charge referencing was applied to these spectra. Red corresponds to low intensity, blue corresponds to high intensity.

4. Data analysis. Peak fitting core level XP spectra

All core-level XP spectra were fitted using CASAXPS™ software. Spectra were fitted with a GL30 lineshape (70% Gaussian, 30% Lorentzian) and a Shirley background. How the core level XP spectra were fitted is given in Table S2.

Fitting C 1s XP Spectra: $[C_nC_1Im][A]$ ILs with no anionic contributions in the C 1s region $284 \text{ eV} < E_B < 289 \text{ eV}$

For all 23 $[C_nC_1Im][A]$ ILs studied here using XPS, two clear peaks and a shoulder at larger E_B were observed at $284 \text{ eV} < E_B < 289 \text{ eV}$. Therefore, three components were used to fit the C 1s XP spectra for $[C_nC_1Im][A]$ at $284 \text{ eV} < E_B < 289 \text{ eV}$. For each IL, once it was established that no carbon contamination was present (by checking the measured and nominal IL compositions match, ESI Table S7), area constraints were used to fit the C 1s XP spectra.

For the 14 $[C_nC_1Im][A]$ ILs studied here for which there were no anionic contributions in the C 1s region $284 \text{ eV} < E_B < 289 \text{ eV}$, the component areas were constrained to $1:4:(n-1)$ for $C^2:C_{\text{hetero}}:C_{\text{alkyl}}$, reflecting the stoichiometry of the $[C_nC_1Im]^+$ cations. This fitting procedure is different to most of the literature for ILs, where either two components (non-monochromated X-ray source) or four components (monochromated X-ray source) have been used to fit the C 1s region $284 \text{ eV} < E_B < 289 \text{ eV}$.¹³ We conclude that as two peaks and a shoulder were readily observed, ideally three components should be used to fit the C 1s region $284 \text{ eV} < E_B < 289 \text{ eV}$, as long as peaks with physically-realistic full width half maxima (*e.g.* $0.8 \text{ eV} < \text{FWHM} < 1.4 \text{ eV}$ for C 1s peaks) are produced. Three components have also been used by the group of Newburg and co-workers to fit the C 1s region for $[C_2C_1Im][\text{NTf}_2]$.^{17, 18}

Fitting C 1s XP Spectra: $[C_nC_1Im][A]$ ILs with anionic contributions in the C 1s region $284 \text{ eV} < E_B < 289 \text{ eV}$

For the five $[C_nC_1Im][A]$ ILs that contain cyano carbon atoms it can be concluded, using C 1s area subtraction,¹⁹ that these cyano carbon atoms should be fitted as C_{hetero} atoms. For $[C_4C_1Im][\text{MeSO}_4]$ and $[C_4C_1Im][\text{OcSO}_4]$ it can be concluded, using C 1s area subtraction,¹⁹ that the C-O carbon atom should be fitted as a C_{hetero} atom, and the C-C carbon atoms should be fitted as C_{alkyl} atoms. For $[C_2C_1Im][\text{MeSO}_3]$ it can be concluded, using C 1s area subtraction,¹⁹ that the C-S carbon atom should be fitted as a C_{alkyl} atom. For $[C_4C_1Im][\text{Me}_2\text{PO}_4]$ it can be concluded, using C 1s area subtraction,¹⁹ that the C-O carbon atoms should be fitted as C_{hetero} atoms. Therefore, the peak area constraints given in Table S2 were used to fit the C 1s region at $284 \text{ eV} < E_B < 289 \text{ eV}$ for these ILs.

Fitting C 1s XP Spectra: $[P_{6,6,6,14}][A]$ ILs

For the three $[P_{6,6,6,14}][A]$ ILs studied here for which there were no anionic contributions in the C 1s region $284 \text{ eV} < E_B < 289 \text{ eV}$, a large peak with a small shoulder at larger E_B (*i.e.* a very large but slightly asymmetric peak) was observed. The component areas were constrained to 4:28 for $C_{\text{hetero}}:C_{\text{alkyl}}$, reflecting the stoichiometry of the $[P_{6,6,6,14}]^+$ cations; four carbon atoms directly bonded to P, and then 28 carbon atoms bonded only to other carbons (and hydrogen). This fitting procedure is the same as the literature for ILs.^{20, 21} Using just this area constraint, a FWHM of 2.44 eV was obtained for the C_{hetero} 1s peak for $[P_{6,6,6,14}]\text{Cl}$. Therefore, to obtain a satisfactory fit the constraint $\text{FWHM}(C_{\text{hetero}}) = \text{FWHM}(C_{\text{alkyl}})$ was also used. $[P_{6,6,6,14}][\text{N}(\text{CN})_2]$ there was an anionic contribution in the C 1s region $284 \text{ eV} < E_B < 289 \text{ eV}$. A visual inspection clearly showed a third peak due to $[\text{N}(\text{CN})_2]^-$ carbon atoms. Therefore, the component areas were constrained to 2:4:28 for $C_{\text{cyano}}:C_{\text{hetero}}:C_{\text{alkyl}}$. As for the three other $[P_{6,6,6,14}][A]$ ILs studied here, a satisfactory fit was obtained by constraining the FWHM; therefore, $\text{FWHM}(C_{\text{cyano}}) = \text{FWHM}(C_{\text{hetero}}) = \text{FWHM}(C_{\text{alkyl}})$ was used.

Fitting C 1s XP Spectra: [ammonium][A] ILs

For the seven ammonium-based ILs studied here using XPS ($[N_{4,1,1,0}][HSO_4]$, $[N_{8,1,1,0}][HSO_4]$, $[N_{2,2,1,0}][TfO]$, $[N_{2OH,2OH,2OH,1}][TfO]$, $[N_{4,1,1,1}][NTf_2]$, $[N_{3,2,1,1}][NTf_2]$ and $[N_{8,8,8,1}][NTf_2]$) the C 1s region showed two peaks in the C 1s region $284 \text{ eV} < E_B < 289 \text{ eV}$. For tetraalkylammonium-based ILs, the C 1s region has been fitted with three components in the literature.^{20, 22, 23} These components represent the carbon atoms directly bonded to the nitrogen atom (labelled C_{hetero}), the carbon atoms next along the alkyl chain (labelled C_{inter}) and then the alkyl carbon atoms further away from the nitrogen atom (labelled C_{alkyl}).²² The three component model for ammonium ILs was developed for ILs that contain three C_{inter} atoms. $[N_{4,1,1,0}][HSO_4]$, $[N_{8,1,1,0}][HSO_4]$, $[N_{2,2,1,0}][TfO]$ and $[N_{3,2,1,1}][NTf_2]$ contain only one C_{inter} atom. Only two components were used here to fit the C 1s region for these four ILs (with constraints used for the component area ratios, see Table S2), due to the inherent unreliability of fitting a component due to a single carbon atom that has more intense components at both larger and smaller E_B . $[N_{3,2,1,1}][NTf_2]$ contains two C_{inter} atoms and one C_{alkyl} atom. When three components were fitted for the C 1s region $284 \text{ eV} < E_B < 289 \text{ eV}$ and the FWHM constrained to be equal for all three components, the fit was essentially identical to that produced when using two components. Therefore, for $[N_{3,2,1,1}][NTf_2]$ only two components were used to fit the C 1s region $284 \text{ eV} < E_B < 289 \text{ eV}$. $[N_{8,8,8,1}][NTf_2]$ contains three C_{inter} atoms and 18 C_{alkyl} atoms. The fit using three components was superior in terms of FWHM than the fit using two components (the FWHM for the C_{alkyl} peak was significantly larger for the two component fit than the three component fit). Therefore, for $[N_{8,8,8,1}][NTf_2]$ three components were used to fit the C 1s region $284 \text{ eV} < E_B < 289 \text{ eV}$. The $E_B(C_{alkyl} \text{ 1s})$ component was shifted by 0.07 eV going from the two component to the three component fitting model. $[N_{2OH,2OH,2OH,1}][TfO]$ gave a single, relatively Gaussian-shaped peak in the C 1s region $284 \text{ eV} < E_B < 289 \text{ eV}$. Therefore, for $[N_{2OH,2OH,2OH,1}][TfO]$ only one component was used to fit the C 1s region $284 \text{ eV} < E_B < 289 \text{ eV}$. $[N_{2OH,2OH,2OH,1}][TfO]$ was the only IL studied in this article for which no C 1s fitting constraints were used. Anion peaks were used for charge referencing six of the seven ammonium-based ILs studied here $[N_{4,1,1,0}][HSO_4]$, $[N_{8,1,1,0}][HSO_4]$, $[N_{2,2,1,0}][TfO]$, $[N_{2OH,2OH,2OH,1}][TfO]$, $[N_{4,1,1,1}][NTf_2]$ and $[N_{3,2,1,1}][NTf_2]$ (Table S3), meaning that the C 1s region fitting procedure will not have an impact upon the E_B of the valence XP spectra used for further analysis in this article.

Fitting C 1s XP Spectra: $[S_{2,2,n}][A]$ ILs

As far as we are aware, the only XP spectrum for C 1s for a sulfonium IL published was for a cyclic sulfonium; a single peak was used in the C 1s region $284 \text{ eV} < E_B < 289 \text{ eV}$, which probably worked because there were two electronic environments, both of which had four carbon atoms, giving a roughly Gaussian-shaped single peak.²⁴ For $[S_{2,2,2}][NTf_2]$, a roughly Gaussian-shaped single peak was observed in the C 1s region $284 \text{ eV} < E_B < 289 \text{ eV}$; a relatively large FWHM, 1.64 eV, was observed if a single peak was used, and the fit did not visually match the spectrum well. Therefore, two peaks were used, with an area constraint 3:3 for $C_{hetero}:C_{alkyl}$. For $[S_{2,2,1}][NTf_2]$, in the C 1s region $284 \text{ eV} < E_B < 289 \text{ eV}$ a peak was observed in the C_{hetero} 1s region, with a shoulder in the C_{alkyl} 1s region at lower E_B . Therefore, two peaks were used, with an area constraint 3:2 for $C_{hetero}:C_{alkyl}$.

Fitting core level XP spectra: spin-orbit coupling

Most other regions were easy to fit for this selection of ILs as each region had only one clear peak; therefore, each region can be fitted with one component with no constraints used (e.g. F 1s for [cation][NTf₂]). For four elements, spin-orbit coupling occurred that required fitting constraints to be used: Cl 2p (for [cation]Cl), S 2p (for $[C_nC_1Im][SCN]$, [cation][HSO₄], $[C_4C_1Im][MeSO_4]$, $[C_4C_1Im][OcSO_4]$, $[C_2C_1Im][MeSO_3]$, [cation][TfO], [cation][NTf₂]), P 2p (for $[P_{6,6,6,14}][A]$) and Br 3d (for [cation]Br). Peak ratios were constrained at 1:2 for $2p_{1/2}:2p_{3/2}$ and at 2:3 for $3d_{3/2}:3d_{5/2}$; no FWHM constraints or peak separation constraints were used.

Fitting core level XP spectra: O 1s

For [cation][HSO₄], [C₄C₁Im][MeSO₄] and [C₄C₁Im][OCSO₄] the O 1s region contained a large peak with a clearly visible shoulder at larger E_B. This region was fitted with two components with an area ratio fixed at 1:3 for O_{anion} (bridging) 1s and O_{anion} (terminal) 1s. This constraint is consistent with that used for ILs containing sulfate anions.²⁵ [N₂O_{H,2}O_{H,2}O_{H,1}][TfO] contains three oxygen atoms in the cation and three oxygen atoms in the anion. For [N₂O_{H,2}O_{H,2}O_{H,1}][TfO] the O 1s region contained a broad, relatively Gaussian-shaped peak with a FWHM of 1.69 eV; this FWHM was judged as too large for one electronic environment (by comparison, for [C₈C₁Im][TfO] gave a FWHM of 1.19 eV for the [TfO]⁻ O 1s peak). Therefore, for [N₂O_{H,2}O_{H,2}O_{H,1}][TfO] the O 1s region was fitted with two peaks, with an area ratio fixed at 1:1 for O_{anion} 1s and O_{cation} 1s.

Component labelling

For the seven ILs for which RAES was used, individual spectral features (peaks) in valence XP spectra are labelled with a component number. Selection of these components was based upon RAES and variable *hν* XPS results; no fitting procedure for the valence XP spectra was used as a standard procedure (peak fitting of component 1 to obtain E_B was carried out only when component 1 gave easily fitted peaks, *e.g.* for [C_nC₁Im][SCN] and [C₈C₁Im]Cl). Component labelling for [C₈C₁Im]Cl is relatively tricky, given that peaks are not clearly distinguishable from 4.5 eV < E_B < 10 eV. Therefore, for [C₈C₁Im]Cl components were chosen based upon the components chosen for [C₄C₁Im][SCN] and also the RAES results given in Section 3.2.

Table S2. Fitting constraints used for core level X-ray photoelectron spectroscopy (XPS) for each ionic liquid

IL no.	IL	Core level	Fitting constraints used
1	[C ₈ C ₁ Im]Cl	C 1s Cl 2p	1:4:7 for C ² :C _{hetero} :C _{alkyl} 1:2 for 2p _{1/2} :2p _{3/2}
2	[C ₈ C ₁ Im]Br	C 1s Br 3d	1:4:7 for C ² :C _{hetero} :C _{alkyl} 2:3 for 3d _{3/2} :3d _{5/2}
3	[C ₆ C ₁ Im]I	Valence C 1s	1:2 for 5p _{1/2} :5p _{3/2} 1:4:5 for C ² :C _{hetero} :C _{alkyl}
4	[P _{6,6,6,14}]Cl	C 1s Cl 2p P 2p	4:28 for C _{hetero} :C _{alkyl} FWHM(C _{hetero}) = FWHM(C _{alkyl}) 1:2 for 2p _{1/2} :2p _{3/2} 1:2 for 2p _{1/2} :2p _{3/2}
5	[P _{6,6,6,14}]Br	C 1s P 2p Br 3d	4:28 for C _{hetero} :C _{alkyl} FWHM(C _{hetero}) = FWHM(C _{alkyl}) 1:2 for 2p _{1/2} :2p _{3/2} 2:3 for 3d _{3/2} :3d _{5/2}
6	[C ₄ C ₁ Im][SCN]	N 1s C 1s S 2p	Shake-up peak (anionic) included 1:5:3 for C ² :C _{hetero} :C _{alkyl} 1:2 for 2p _{1/2} :2p _{3/2}
7	[C ₈ C ₁ Im][SCN]	N 1s C 1s S 2p	Shake-up peak (anionic) included 1:5:7 for C ² :C _{hetero} :C _{alkyl} 1:2 for 2p _{1/2} :2p _{3/2}
8	[C ₄ C ₁ Im][N(CN) ₂]	C 1s	1:6:3 for C ² :C _{hetero} :C _{alkyl} FWHM(C ²) = FWHM(C _{hetero})
9	[P _{6,6,6,14}][N(CN) ₂]	C 1s P 2p	2:4:28 for C _{cyano} :C _{hetero} :C _{alkyl} FWHM(C _{cyano}) = FWHM(C _{hetero}) = FWHM(C _{alkyl}) 1:2 for 2p _{1/2} :2p _{3/2}
10	[C ₈ C ₁ Im][C(CN) ₃]	N 1s C 1s C 1s	Shake-up peak (anionic) included 1:8:7 for C ² :C _{hetero} :C _{alkyl} 1:8:5 for C ² :C _{hetero} :C _{alkyl}
11	[C ₆ C ₁ Im][B(CN) ₄]	C 1s	1:8:5 for C ² :C _{hetero} :C _{alkyl}
12	[C ₈ C ₁ Im][BF ₄]	C 1s	1:4:7 for C ² :C _{hetero} :C _{alkyl}
13	[P _{6,6,6,14}][NO ₃]	C 1s P 2p	4:28 for C _{hetero} :C _{alkyl} FWHM(C _{hetero}) = FWHM(C _{alkyl}) 1:2 for 2p _{1/2} :2p _{3/2}
14	[C ₄ C ₁ Im][HSO ₄]	C 1s S 2p	1:4:3 for C ² :C _{hetero} :C _{alkyl} 1:2 for 2p _{1/2} :2p _{3/2}

15	[C ₈ C ₁ Im][HSO ₄]	C 1s S 2p	1:4:7 for C ² :C _{hetero} :C _{alkyl} 1:2 for 2p _{1/2} :2p _{3/2}
16	[C ₄ C ₀ Im][HSO ₄]	C 1s S 2p	1:3:3 for C ² :C _{hetero} :C _{alkyl} 1:2 for 2p _{1/2} :2p _{3/2}
17	[N _{4,1,1,0}][HSO ₄]	C 1s S 2p	3:3 for C _{hetero} :C _{alkyl} 1:2 for 2p _{1/2} :2p _{3/2}
18	[N _{8,1,1,0}][HSO ₄]	C 1s S 2p	3:7 for C _{hetero} :C _{alkyl} 1:2 for 2p _{1/2} :2p _{3/2}
19	[C ₄ C ₁ Im][MeSO ₄]	C 1s S 2p	1:5:3 for C ² :C _{hetero} :C _{alkyl} 1:2 for 2p _{1/2} :2p _{3/2}
20	[C ₄ C ₁ Im][OcSO ₄]	C 1s S 2p	1:5:10 for C ² :C _{hetero} :C _{alkyl} 1:2 for 2p _{1/2} :2p _{3/2}
21	[C ₂ C ₁ Im][MeSO ₃]	C 1s S 2p	1:4:2 for C ² :C _{hetero} :C _{alkyl} 1:2 for 2p _{1/2} :2p _{3/2}
22	[C ₄ C ₁ Im][Me ₂ PO ₄]	C 1s P 2p	1:6:3 for C ² :C _{hetero} :C _{alkyl} 1:2 for 2p _{1/2} :2p _{3/2}
23	[C ₄ C ₁ Im][TfO]	C 1s S 2p	1:4:3 for C ² :C _{hetero} :C _{alkyl} 1:2 for 2p _{1/2} :2p _{3/2}
24	[C ₈ C ₁ Im][TfO]	C 1s S 2p	1:4:7 for C ² :C _{hetero} :C _{alkyl} 1:2 for 2p _{1/2} :2p _{3/2}
25	[N _{2,2,1,0}][TfO]	C 1s S 2p	3:2 for C _{hetero} :C _{alkyl} 1:2 for 2p _{1/2} :2p _{3/2}
26	[N _{2OH,2OH,2OH,1}][TfO]	O 1s S 2p	1:1 for O _{anion} :O _{cation} 1:2 for 2p _{1/2} :2p _{3/2}
27	[C ₄ C ₁ Im][NTf ₂]	C 1s S 2p	1:4:3 for C ² :C _{hetero} :C _{alkyl} 1:2 for 2p _{1/2} :2p _{3/2}
28	[C ₆ C ₁ Im][NTf ₂]	C 1s S 2p	1:4:5 for C ² :C _{hetero} :C _{alkyl} 1:2 for 2p _{1/2} :2p _{3/2}
29	[C ₈ C ₁ Im][NTf ₂]	C 1s S 2p	1:4:7 for C ² :C _{hetero} :C _{alkyl} 1:2 for 2p _{1/2} :2p _{3/2}
30	[C ₂ C ₀ Im][NTf ₂]	C 1s S 2p	1:3:1 for C ² :C _{hetero} :C _{alkyl} 1:2 for 2p _{1/2} :2p _{3/2}
31	[C ₄ C ₀ Im][NTf ₂]	C 1s S 2p	1:3:3 for C ² :C _{hetero} :C _{alkyl} 1:2 for 2p _{1/2} :2p _{3/2}
32	[N _{4,1,1,1}][NTf ₂]	C 1s S 2p	4:3 for C _{hetero} :C _{alkyl} 1:2 for 2p _{1/2} :2p _{3/2}
33	[N _{3,2,1,1}][NTf ₂]	C 1s S 2p	4:3 for C _{hetero} :C _{alkyl} 1:2 for 2p _{1/2} :2p _{3/2}
34	[N _{8,8,8,1}][NTf ₂]	C 1s S 2p	4:3:18 for C _{hetero} :C _{inter} :C _{alkyl} 1:2 for 2p _{1/2} :2p _{3/2}
35	[S _{2,2,1}][NTf ₂]	C 1s S 2p	3:2 for C _{hetero} :C _{alkyl} 1:2 for 2p _{1/2} :2p _{3/2}
36	[S _{2,2,2}][NTf ₂]	C 1s S 2p	3:3 for C _{hetero} :C _{alkyl} 1:2 for 2p _{1/2} :2p _{3/2}
37	[P _{6,6,6,14}][NTf ₂]	C 1s S 2p P 2p	4:28 for C _{hetero} :C _{alkyl} FWHM(C _{hetero}) = FWHM(C _{alkyl}) 1:2 for 2p _{1/2} :2p _{3/2} 1:2 for 2p _{1/2} :2p _{3/2}

5. Data analysis. Charge referencing procedures

In the literature, all experimental E_B (*i.e.* XP spectra) for ILs have effectively been charge referenced to a Fermi level, E_F .^{9, 26-34} In this paper, both lab- and synchrotron-based XP and RAE spectra were charge referenced to E_F using the peaks and E_B values given in Table S3. The rationalisations for these choices are explained in reference¹⁹. For charge referencing, $E_B(\text{C}_{\text{alkyl}} 1s)$ was used where we were confident that the alkyl carbons were not affected by the R group they were covalently bonded to in the IL.

The E_B values that the valence XP spectra were shifted for the charge referencing procedure are given in Table S3. The values were in the range $-0.57 \text{ eV} < E_B < 0.22 \text{ eV}$.

Table S3. Experimental X-ray photoelectron spectroscopy (XPS) details on the charge correction applied for each ionic liquid

IL no.	IL	Core orbital used for charge referencing	E_B for core orbital used for charge referencing / eV	Rationale for choosing core orbital used for charge referencing	E_B value shifted for valence XP spectrum / eV
1	[C ₈ C ₁ Im]Cl	C _{alkyl} 1s	285.0	Long alkyl chain	-0.57
2	[C ₈ C ₁ Im]Br	C _{alkyl} 1s	285.0	Long alkyl chain	-0.31
3	[C ₆ C ₁ Im]I	N _{cation} 1s	401.9	N _{cation} 1s for [C ₈ C ₁ Im] ¹⁴	0.05
4	[P _{6,6,6,14}]Cl	C _{alkyl} 1s	285.0	Long alkyl chain	-0.19
5	[P _{6,6,6,14}]Br	C _{alkyl} 1s	285.0	Long alkyl chain	-0.42
6	[C ₄ C ₁ Im][SCN]	N _{cation} 1s	401.9	N _{cation} 1s for [C ₈ C ₁ Im][SCN]	0.10
7	[C ₈ C ₁ Im][SCN]	C _{alkyl} 1s	285.0	Long alkyl chain	-0.13
8	[C ₄ C ₁ Im][N(CN) ₂]	N _{cation} 1s	402.0	N _{cation} 1s for [C ₈ C ₁ Im][N(CN) ₂] ¹⁴	0.04
9	[P _{6,6,6,14}][N(CN) ₂]	C _{alkyl} 1s	285.0	Long alkyl chain	0.22
10	[C ₈ C ₁ Im][C(CN) ₃]	C _{alkyl} 1s	285.0	Long alkyl chain	0.01
11	[C ₆ C ₁ Im][B(CN) ₄]	C _{alkyl} 1s	285.0	Long alkyl chain	-0.24
12	[C ₈ C ₁ Im][BF ₄]	C _{alkyl} 1s	285.0	Long alkyl chain	-0.10
13	[P _{6,6,6,14}][NO ₃]	C _{alkyl} 1s	285.0	Long alkyl chain	-0.10
14	[C ₄ C ₁ Im][HSO ₄]	N _{cation} 1s	401.8	N _{cation} 1s for [C ₈ C ₁ Im][HSO ₄]	-0.38
15	[C ₈ C ₁ Im][HSO ₄]	C _{alkyl} 1s	285.0	Long alkyl chain	-0.39
16	[C ₄ C ₀ Im][HSO ₄]	C _{alkyl} 1s	285.0	C _{alkyl} 1s for [C ₄ C ₁ Im][HSO ₄]	-0.21
17	[N _{4,1,1,0}][HSO ₄]	S _{anion} 2p _{3/2}	168.7	S _{anion} 2p _{3/2} for [N _{8,1,1,0}][HSO ₄]	-0.28
18	[N _{8,1,1,0}][HSO ₄]	C _{alkyl} 1s	285.0	Long alkyl chain	0.11
19	[C ₄ C ₁ Im][MeSO ₄]	N _{cation} 1s	401.7	N _{cation} 1s for [C ₄ C ₁ Im][OCSO ₄]	-0.26
20	[C ₄ C ₁ Im][OCSO ₄]	C _{alkyl} 1s	285.0	Long alkyl chain	0.02
21	[C ₂ C ₁ Im][MeSO ₃]	N _{cation} 1s	401.9	Average N _{cation} 1s for [C ₈ C ₁ Im][A] ¹⁹	0.12
22	[C ₄ C ₁ Im][Me ₂ PO ₄]	N _{cation} 1s	401.9	Average N _{cation} 1s for [C ₈ C ₁ Im][A] ¹⁹	-0.17
23	[C ₄ C ₁ Im][TfO]	N _{cation} 1s	402.0	N _{cation} 1s for [C ₈ C ₁ Im][TfO]	-0.83
24	[C ₈ C ₁ Im][TfO]	C _{alkyl} 1s	285.0	Long alkyl chain	-0.46
25	[N _{2,2,1,0}][TfO]	F _{anion} 1s	688.4	F _{anion} 1s for [C ₈ C ₁ Im][TfO]	-0.49
26	[N _{2OH,2OH,2OH,1}][TfO]	F _{anion} 1s	688.4	F _{anion} 1s for [C ₈ C ₁ Im][TfO]	-0.44
27	[C ₄ C ₁ Im][NTf ₂]	N _{cation} 1s	402.1	N _{cation} 1s for [C ₈ C ₁ Im][NTf ₂]	0.04
28	[C ₆ C ₁ Im][NTf ₂]	N _{cation} 1s	402.1	N _{cation} 1s for [C ₈ C ₁ Im][NTf ₂]	0.04
29	[C ₈ C ₁ Im][NTf ₂]	C _{alkyl} 1s	285.0	Long alkyl chain	-0.03
30	[C ₂ C ₀ Im][NTf ₂]	F _{anion} 1s	688.8	F _{anion} 1s for [N _{8,8,8,1}][NTf ₂]	-0.01
31	[C ₄ C ₀ Im][NTf ₂]	F _{anion} 1s	688.8	F _{anion} 1s for [N _{8,8,8,1}][NTf ₂]	0.07
32	[N _{4,1,1,1}][NTf ₂]	F _{anion} 1s	688.8	F _{anion} 1s for [N _{8,8,8,1}][NTf ₂]	-0.30
33	[N _{3,2,1,1}][NTf ₂]	F _{anion} 1s	688.8	F _{anion} 1s for [N _{8,8,8,1}][NTf ₂]	-0.07
34	[N _{8,8,8,1}][NTf ₂]	C _{alkyl} 1s	285.0	Long alkyl chain	0.03
35	[S _{2,2,1}][NTf ₂]	F _{anion} 1s	688.8	F _{anion} 1s for [N _{8,8,8,1}][NTf ₂]	-0.36
36	[S _{2,2,2}][NTf ₂]	F _{anion} 1s	688.8	F _{anion} 1s for [N _{8,8,8,1}][NTf ₂]	-0.10
37	[P _{6,6,6,14}][NTf ₂]	C _{alkyl} 1s	285.0	Long alkyl chain	0.01

For four of the ILs studied here ([C₈C₁Im][BF₄], [N_{8,1,1,0}][HSO₄], [N_{8,8,8,1}][NTf₂] and [P_{6,6,6,14}][NTf₂]) an interpolation method, which has proven to be effective for charge referencing XP spectra for ILs,¹⁹ was used to charge reference the data recorded at $h\nu = 1486.6 \text{ eV}$. For the other 33 ILs studied here using XPS recorded at $h\nu = 1486.6 \text{ eV}$, a single E_B value was used for charge referencing.

As explained in reference ¹⁹, charge referencing for ILs with protic cations is not yet fully understood. Therefore, we have less confidence for the charge referencing procedure for $[N_{4,1,1,0}][HSO_4]$ in particular.

For the ILs studied here using RAES and variable $h\nu$ XPS, the electron spectra were charge referenced by shifting the electron spectra to visually match the valence XP spectrum recorded on the lab XPS apparatus (which has already been charge referenced). This data is shown in ESI Figure S3 to ESI Figure S9, and is summarised in Table S4.

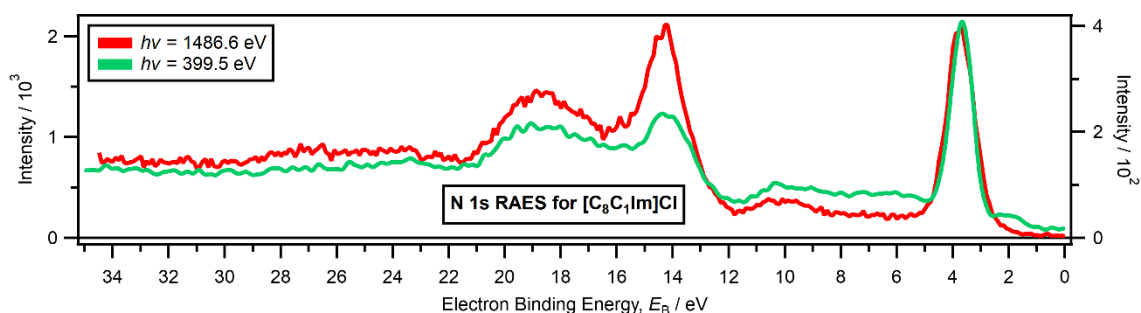


Figure S3. XP spectra for $[C_8C_1Im]Cl$ recorded on laboratory-based XPS recorded at $h\nu = 1486.6$ eV (charge referenced using data in Table S3) and synchrotron-based XPS (charge referenced by visually matching to the laboratory-based XP spectrum, summarised in Table S4) recorded at $h\nu = 399.5$ eV, used for charge referencing N 1s RAES data.

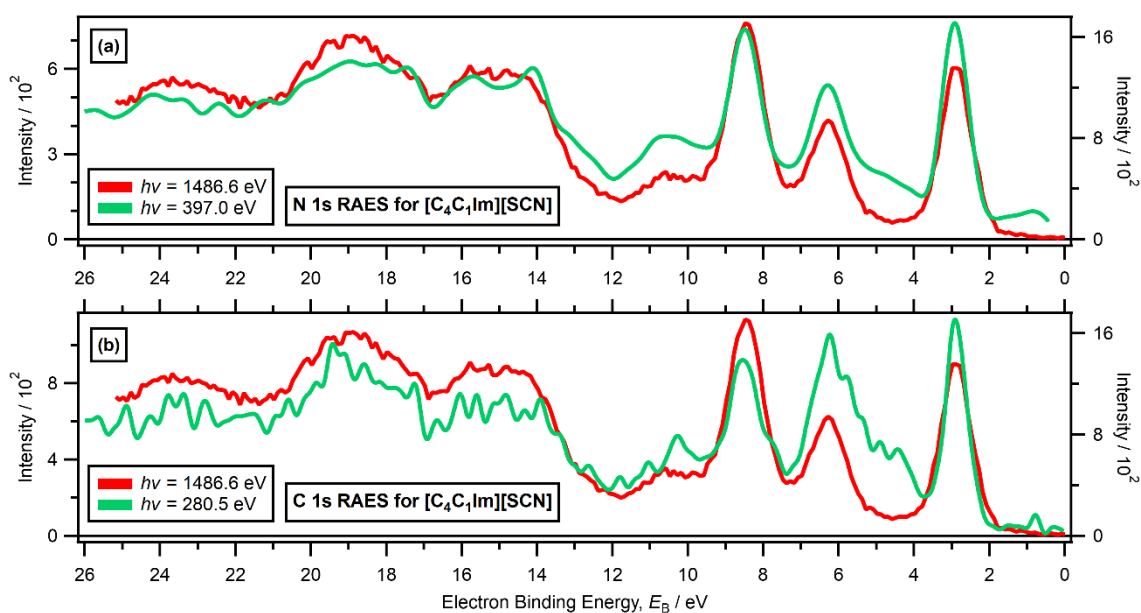


Figure S4. XP spectra for $[C_4C_1Im][SCN]$ recorded on laboratory-based XPS recorded at $h\nu = 1486.6$ eV (charge referenced using data in Table S3) and synchrotron-based XPS (charge referenced by visually matching to the laboratory-based XP spectrum, summarised in Table S4) recorded at: (a) $h\nu = 397.0$ eV, used for charge referencing N 1s RAES data, (b) $h\nu = 280.5$ eV, used for charge referencing C 1s RAES data.

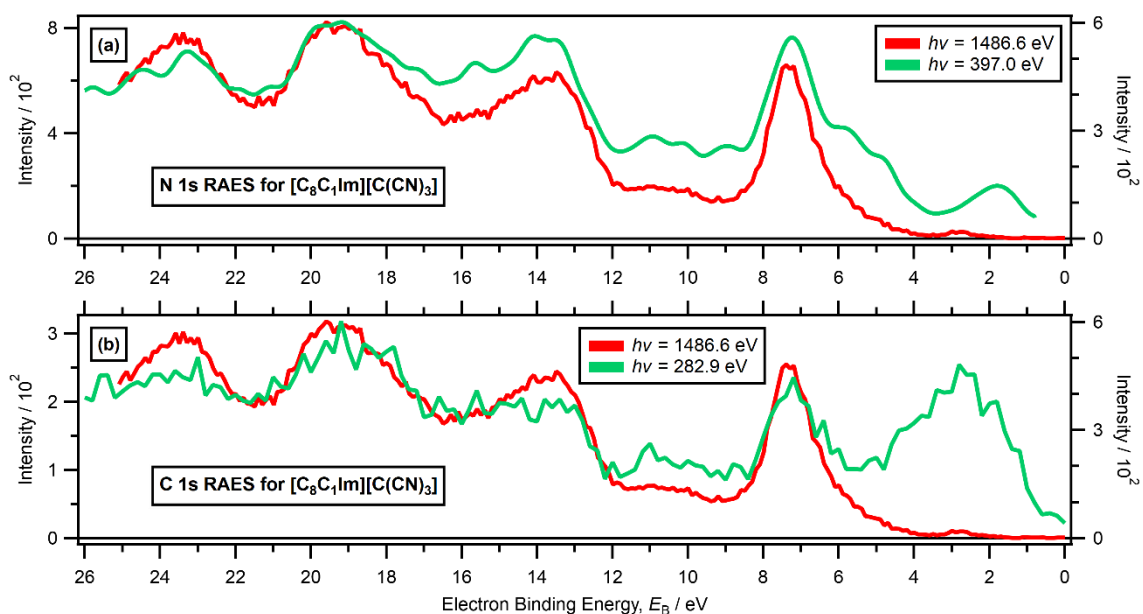


Figure S5. XP spectra for $[\text{C}_8\text{C}_1\text{Im}][\text{C}(\text{CN})_3]$ recorded on laboratory-based XPS recorded at $h\nu = 1486.6$ eV (charge referenced using data in Table S3) and synchrotron-based XPS (charge referenced by visually matching to the laboratory-based XP spectrum, summarised in Table S4) recorded at: (a) $h\nu = 397.0$ eV, used for charge referencing N 1s RAES data, (b) $h\nu = 282.9$ eV, used for charge referencing C 1s RAES data.

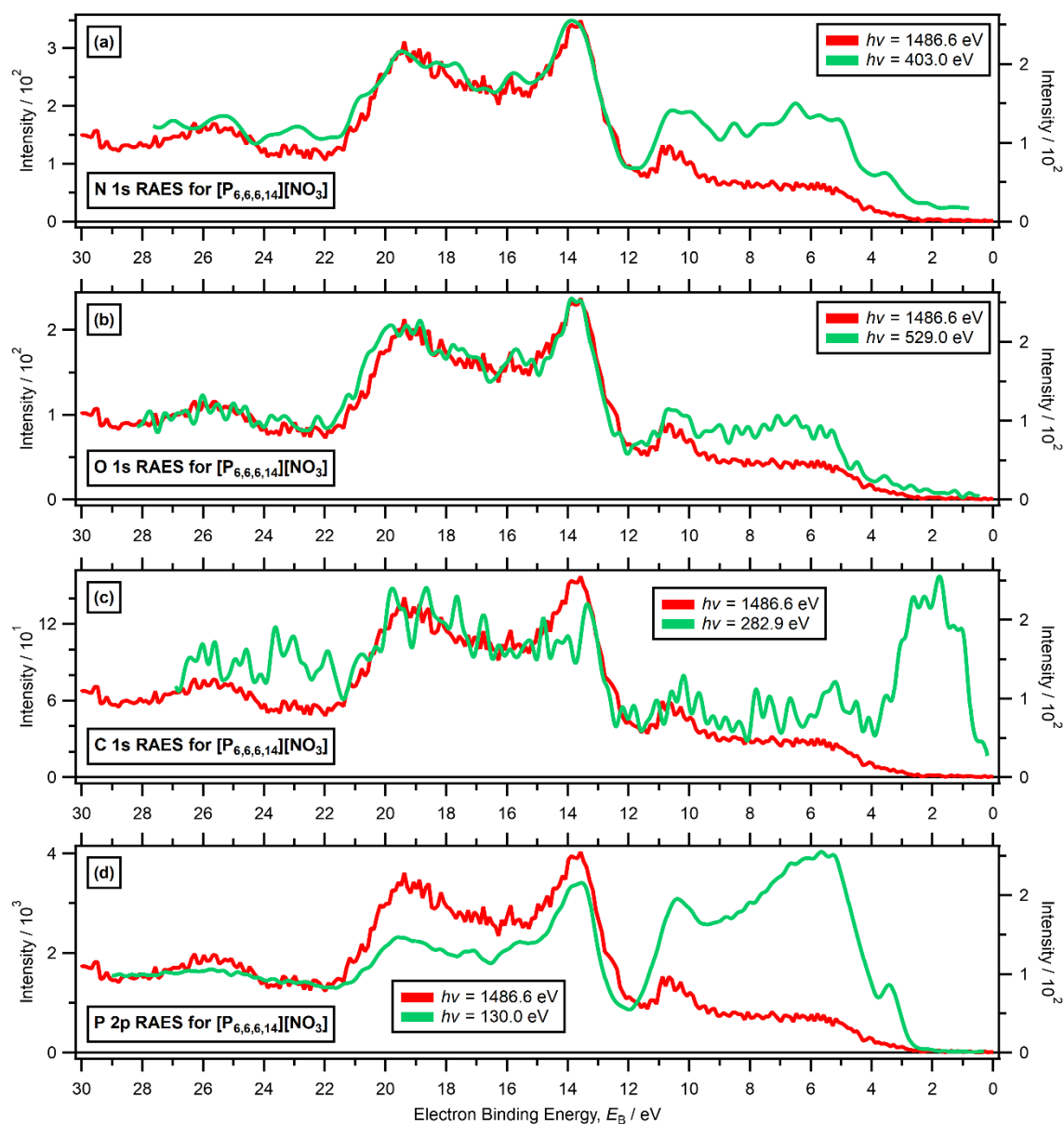


Figure S6. XP spectra for $[P_{6,6,6,14}][NO_3]$ recorded on laboratory-based XPS recorded at $h\nu = 1486.6$ eV (charge referenced using data in Table S3) and synchrotron-based XPS (charge referenced by visually matching to the laboratory-based XP spectrum, summarised in Table S4) recorded at: (a) $h\nu = 403.0$ eV, used for charge referencing N 1s RAES data, (b) $h\nu = 529.0$ eV, used for charge referencing O 1s RAES data, (c) $h\nu = 282.9$ eV, used for charge referencing C 1s RAES data, (d) $h\nu = 130.0$ eV, used for charge referencing P 2p RAES data.

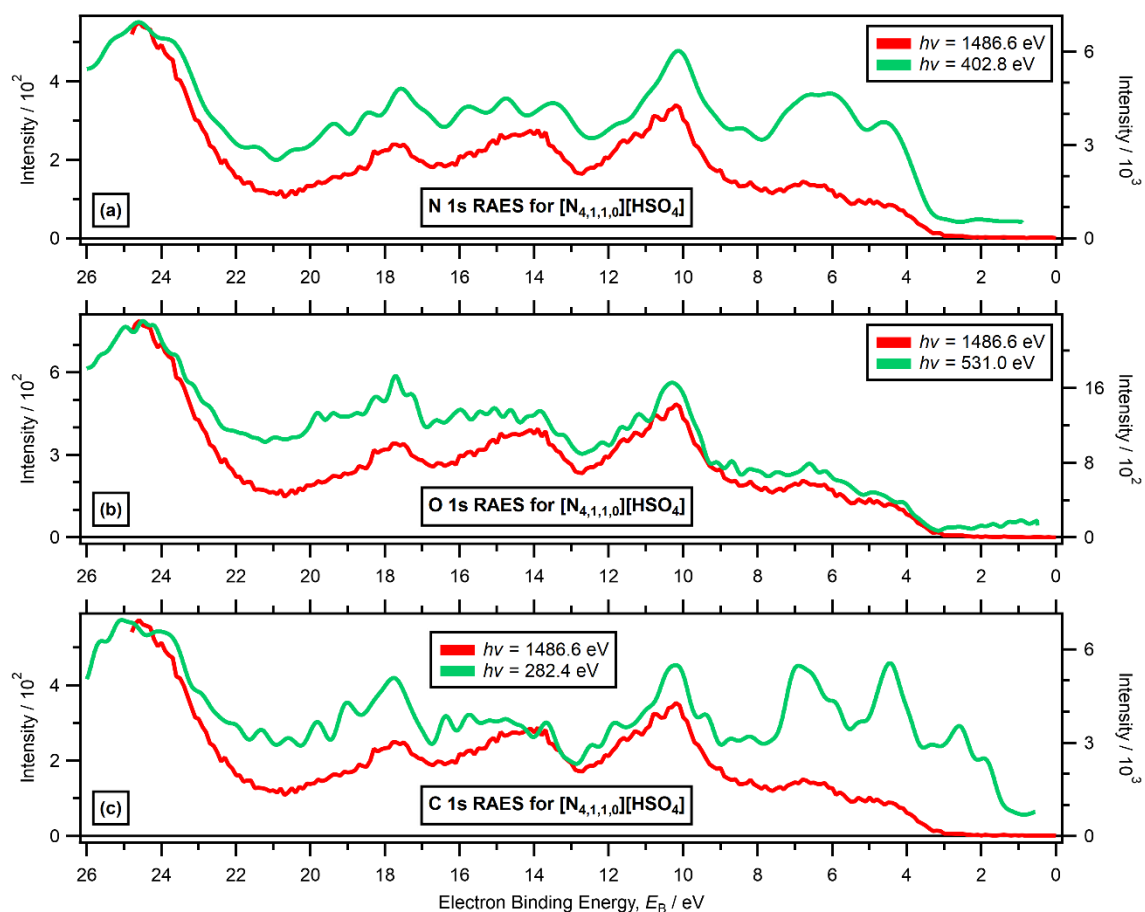


Figure S7. XP spectra for $[N_{4,1,1,0}][HSO_4]$ recorded on laboratory-based XPS recorded at $h\nu = 1486.6$ eV (charge referenced using data in Table S3) and synchrotron-based XPS (charge referenced by visually matching to the laboratory-based XP spectrum, summarised in Table S4) recorded at: (a) $h\nu = 402.8$ eV, used for charge referencing N 1s RAES data, (b) $h\nu = 531.0$ eV, used for charge referencing O 1s RAES data, (c) $h\nu = 282.4$ eV, used for charge referencing C 1s RAES data.

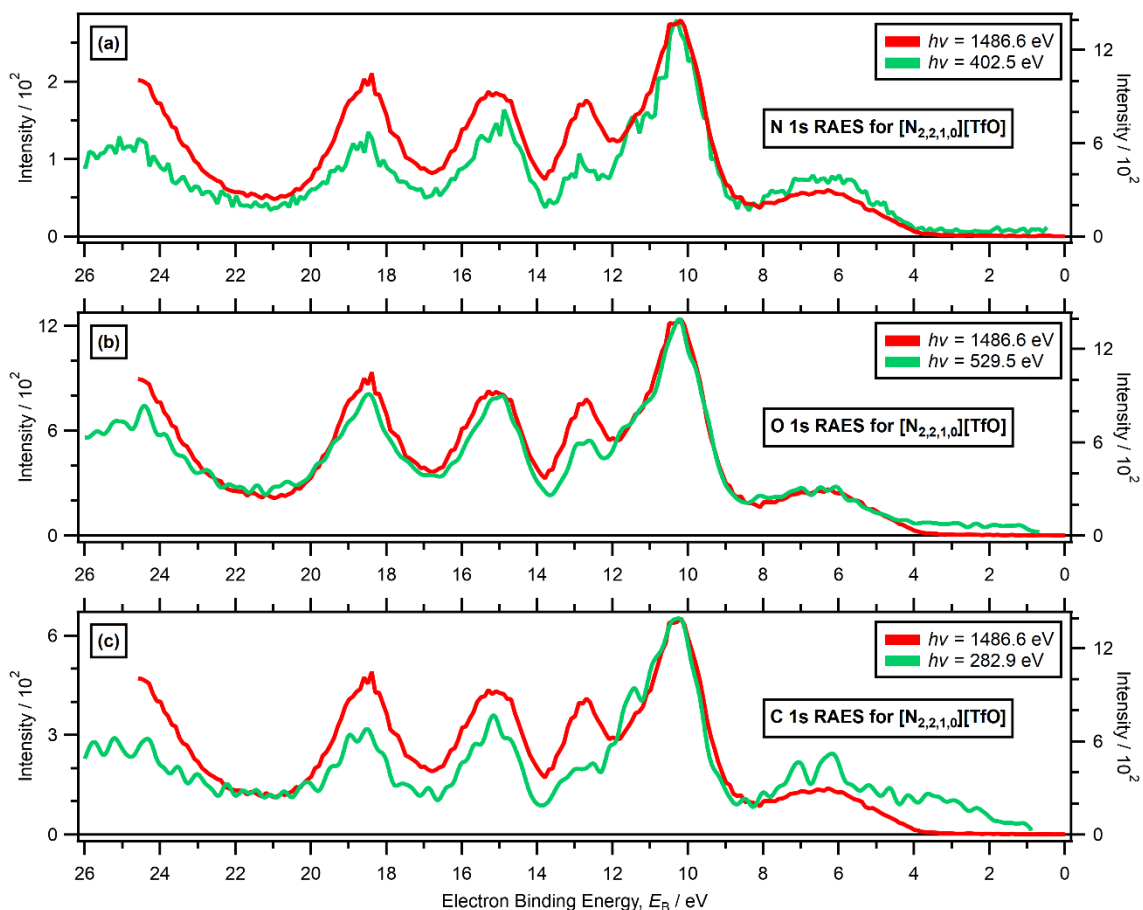


Figure S8. XP spectra for $[N_{2,2,1,0}][TfO]$ recorded on laboratory-based XPS recorded at $h\nu = 1486.6$ eV (charge referenced using data in Table S3) and synchrotron-based XPS (charge referenced by visually matching to the laboratory-based XP spectrum, summarised in Table S4) recorded at: (a) $h\nu = 402.5$ eV, used for charge referencing N 1s RAES data, (b) $h\nu = 529.5$ eV, used for charge referencing O 1s RAES data, (c) $h\nu = 282.9$ eV, used for charge referencing C 1s RAES data.

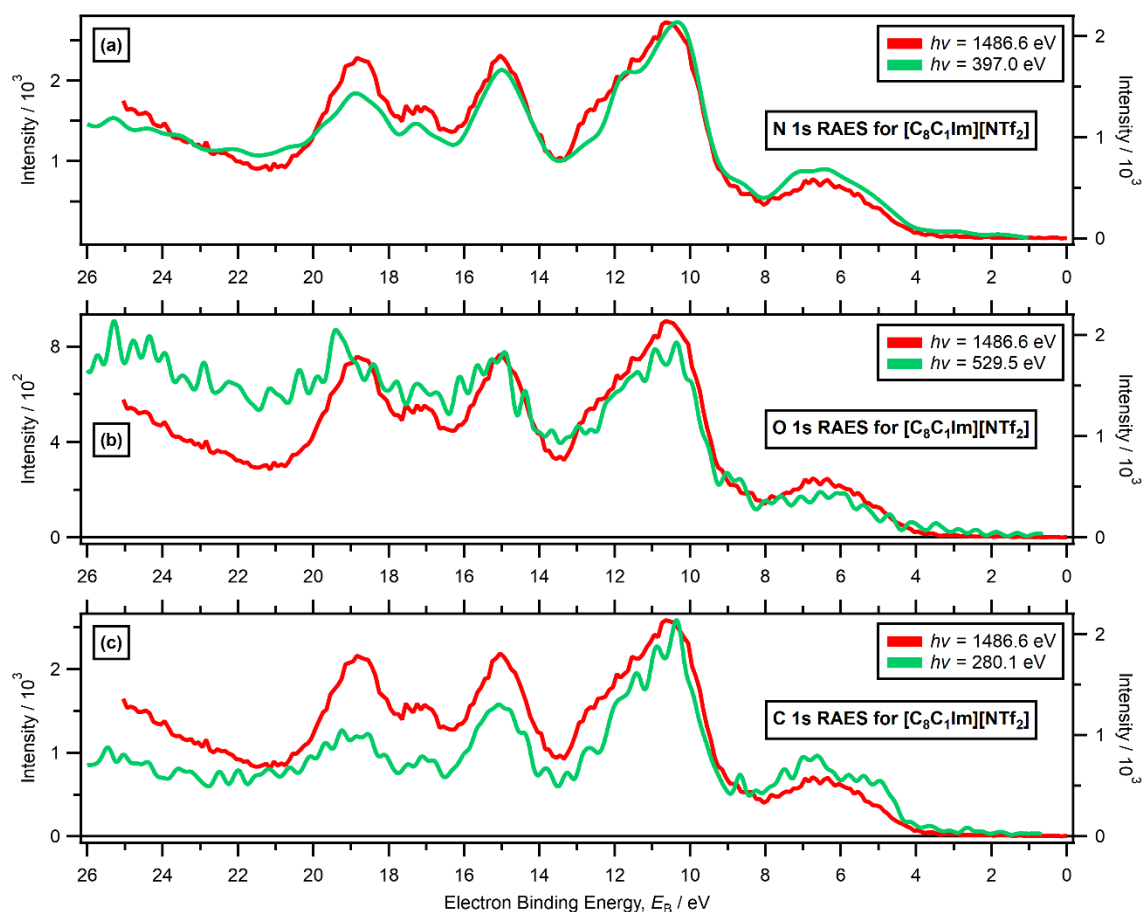


Figure S9. XP spectra for $[\text{C}_8\text{C}_1\text{Im}][\text{NTf}_2]$ recorded on laboratory-based XPS recorded at $h\nu = 1486.6$ eV (charge referenced as explained above) and synchrotron-based XPS (charge referenced by visually matching to the laboratory-based XP spectrum, summarised in Table S4) recorded at: (a) $h\nu = 397.0$ eV, used for charge referencing N 1s RAES data, (b) $h\nu = 529.5$ eV, used for charge referencing O 1s RAES data, (c) $h\nu = 280.1$ eV, used for charge referencing C 1s RAES data.

Table S4. Experimental resonant Auger electron spectroscopy (RAES) details on the charge correction applied for each ionic liquid

IL no.	IL	Element and orbital for RAES	E_B value shifted for RAE spectrum / eV
1	$[\text{C}_8\text{C}_1\text{Im}]\text{Cl}$	N 1s	-0.50
6	$[\text{C}_4\text{C}_1\text{Im}][\text{SCN}]$	N 1s	0.25
6	$[\text{C}_4\text{C}_1\text{Im}][\text{SCN}]$	C 1s	-0.13
10	$[\text{C}_8\text{C}_1\text{Im}][\text{C}(\text{CN})_3]$	N 1s	0.40
10	$[\text{C}_8\text{C}_1\text{Im}][\text{C}(\text{CN})_3]$	C 1s	0.00
13	$[\text{P}_{6,6,6,14}][\text{NO}_3]$	N 1s	0.50
13	$[\text{P}_{6,6,6,14}][\text{NO}_3]$	O 1s	0.28
13	$[\text{P}_{6,6,6,14}][\text{NO}_3]$	C 1s	0.00
13	$[\text{P}_{6,6,6,14}][\text{NO}_3]$	P 2p	0.11
17	$[\text{N}_{4,1,1,0}][\text{HSO}_4]$	N 1s	0.50
17	$[\text{N}_{4,1,1,0}][\text{HSO}_4]$	O 1s	0.30
17	$[\text{N}_{4,1,1,0}][\text{HSO}_4]$	C 1s	0.26
25	$[\text{N}_{2,2,1,0}][\text{TfO}]$	N 1s	0.48
25	$[\text{N}_{2,2,1,0}][\text{TfO}]$	O 1s	0.50
25	$[\text{N}_{2,2,1,0}][\text{TfO}]$	C 1s	0.70
29	$[\text{C}_8\text{C}_1\text{Im}][\text{NTf}_2]$	N 1s	0.83
29	$[\text{C}_8\text{C}_1\text{Im}][\text{NTf}_2]$	O 1s	0.47
29	$[\text{C}_8\text{C}_1\text{Im}][\text{NTf}_2]$	C 1s	0.46

Calibration of the energy scale for the NEXAFS spectra

An extensive explanation of the energy scale calibration for the NEXAFS data is given in reference ¹.

6. Data analysis. AO photoionisation cross-sections

It is difficult to obtain direct experimental evidence on the make-up of the valence MOs using a single $h\nu$ source. If the source $h\nu$ are sufficiently different, the MO photoionisation cross-sections will change relative to each other.³⁵ Relative peak intensities change with varying source $h\nu$ due to changes in MO photoionisation cross-sections. The Gelius approximation states that an MO photoionisation cross-section is a linear summation of the photoionisation cross-sections of the atomic orbitals (AOs) of which the MO is composed.^{36, 37} If a relative peak intensity decreases with decreasing $h\nu$ then the MOs which give rise to that peak must be composed of AOs with relative photoionisation cross-sections which also decrease with decreasing $h\nu$.

For the 37 ILs studied here, almost all (and all in the case of $[\text{C}_4\text{C}_1\text{Im}][\text{N}(\text{CN})_2]$, $[\text{C}_8\text{C}_1\text{Im}][\text{C}(\text{CN})_3]$, $[\text{C}_6\text{C}_1\text{Im}][\text{B}(\text{CN})_4]$ and $[\text{C}_8\text{C}_1\text{Im}][\text{BF}_4]$) of the atoms were from 2nd row elements (B, C, N, O, F). There were a small number atoms from 3rd row elements, *e.g.* P, S, Cl; in addition, Br and I were studied too.

Most XPS experiments were carried out at $h\nu = 1486.6$ eV. However, variable $h\nu$ XPS experiments also involved XPS experiments at $129 \text{ eV} < h\nu < 200 \text{ eV}$. Therefore, for comparisons of photoionisation cross-sections with respect to $h\nu$, the lower $h\nu$ value used was $h\nu = 165.0$ eV, approximately the average lower $h\nu$ value used (Table S5).

For the valence 2p AOs for the atoms from 2nd row elements, there are not significant variations in $h\nu$ dependence in the photoionisation cross-sections from *e.g.* $h\nu = 1486.6$ eV to $h\nu = 165.0$ eV.³⁸ However, for the atoms from 2nd row elements there are significant variations in $h\nu$ dependence in the photoionisation cross-sections from *e.g.* $h\nu = 1486.6$ eV to $h\nu = 165.0$ eV for the valence 2p AOs versus the valence 2s AOs.³⁸ Furthermore, for the valence 2p AOs for the atoms from 2nd row elements versus the valence 3p AOs for the atoms from 3rd row elements, there are large variations in $h\nu$ dependence in the photoionisation cross-sections from *e.g.* $h\nu = 1486.6$ eV to $h\nu = 165.0$ eV.³⁸

The ratio of AO photoionisation cross-section between Cl 3p and both N 2p and C 2p increases with decreasing $h\nu$ (the cross-sections ratio Cl 3p:N 2p:C 2p is 1.00:0.05:0.01 at $h\nu = 1486.6$ eV compared to 1.00:0.33:0.10 at $h\nu = 165.0$ eV).³⁸

The ratio of AO photoionisation cross-section between Cl 3p and Cl 3s decreases with decreasing $h\nu$ (the cross-sections ratio Cl 3p:Cl 3s is 1.00:1.33 at $h\nu = 1486.6$ eV compared to 1.00:0.36 at $h\nu = 165.0$ eV).³⁸ Therefore, components with significant contribution from N 2p and C 2p AOs will increase in area as $h\nu$ decreases, relative to components with significant contribution from Cl 3p AOs.

The ratio of AO photoionisation cross-section between S 3p and both N 2p and C 2p decreases with decreasing $h\nu$ (the cross-sections ratio S 3p:N 2p:C 2p is 1.00:0.09:0.02 at $h\nu = 1486.6$ eV compared to 1.00:0.52:0.15 at $h\nu = 165.0$ eV).³⁸ Components with significant contribution from S 3p AOs will decrease in area as $h\nu$ decreases, relative to components with no significant contribution from S 3p AOs.

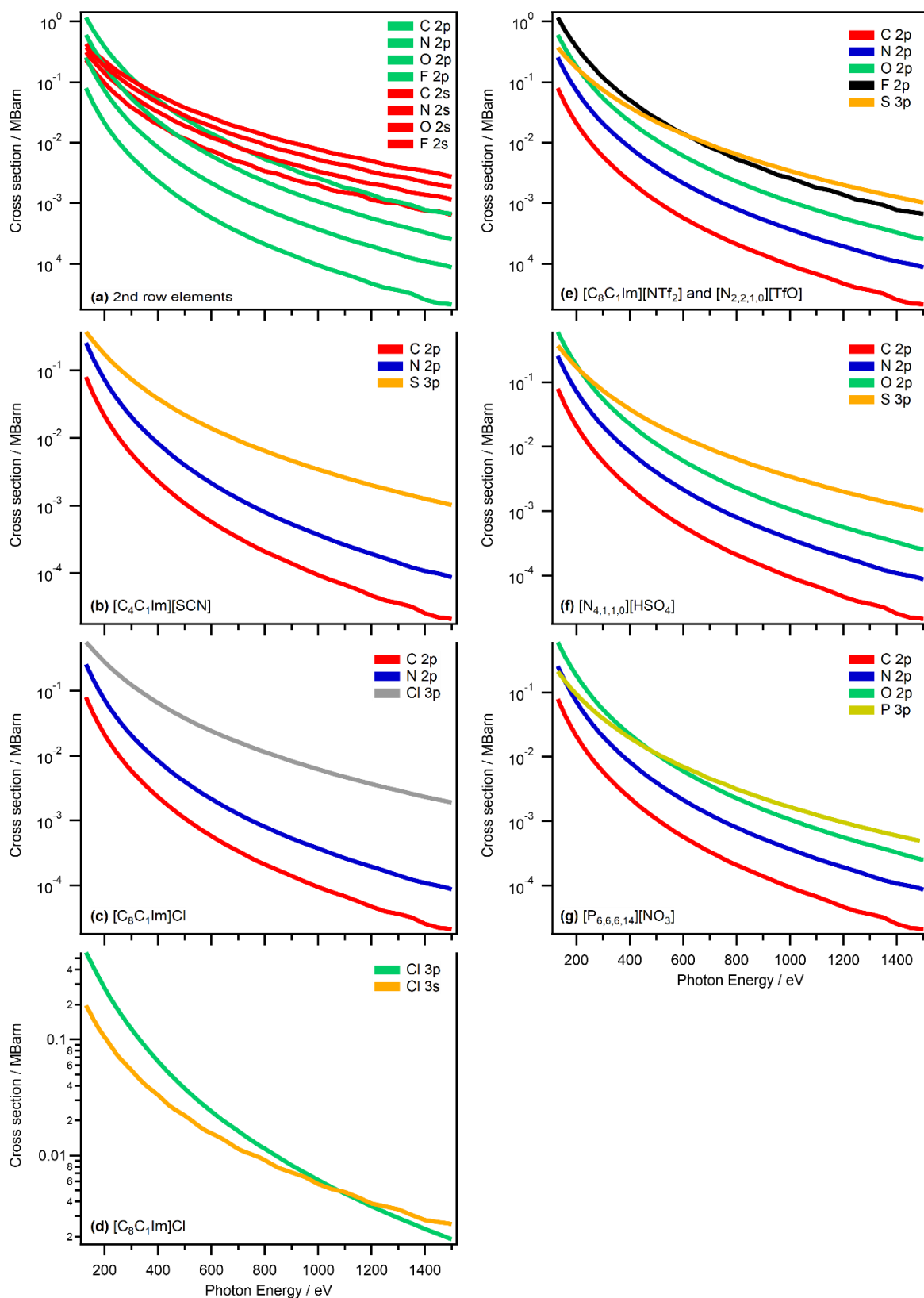


Figure S10. Calculated photoionisation cross-sections for $130 \text{ eV} < h\nu < 1500 \text{ eV}$, taken from reference ³⁸ (a) Key period 2 element AOs. (b) Valence p AOs for $[\text{C}_4\text{C}_1\text{Im}][\text{SCN}]$. (c) Valence p AOs for $[\text{C}_8\text{C}_1\text{Im}]\text{Cl}$. (d) Valence Cl AOs for $[\text{C}_8\text{C}_1\text{Im}]\text{Cl}$. (e) Valence p AOs for $[\text{C}_8\text{C}_1\text{Im}][\text{NTf}_2]$ and $[\text{N}_{2,2,1,0}][\text{TfO}]$. (f) Valence p AOs for $[\text{N}_{4,1,1,0}][\text{HSO}_4]$. (g) Valence p AOs for $[\text{P}_{6,6,6,14}][\text{NO}_3]$.

Table S5. Calculated photoionisation cross-sections at high $h\nu$ ($h\nu = 1486.6$ eV) and low $h\nu$ ($h\nu = 165.0$ eV), taken from reference ³⁸

Elements	Orbital	Photoionisation cross-section at $h\nu = 1486.6$ eV (high $h\nu$) / 10^{-6}	Photoionisation cross-section at $h\nu = 165.0$ eV (low $h\nu$) / 10^{-6}	Orbital	Photoionisation cross-section at $h\nu = 1486.6$ eV (high $h\nu$) / 10^{-6}	Photoionisation cross-section at $h\nu = 165.0$ eV (low $h\nu$) / 10^{-6}
B	2s	281	85460	2p	3	6411
C	2s	665	143100	2p	21	38310
N	2s	1192	204200	2p	91	128700
O	2s	1902	259200	2p	260	317300
F	2s	2846	301300	2p	682	633700
P	3s	1471	94080	3p	500	137300
S	3s	1935	118600	3p	1053	247700
Cl	3s	2598	139500	3p	1952	391000
Br	4s	2559	87980	4p	4503	130900
I	5s	1977	66200	5p	3812	83570

7. Data analysis. Interpolation of electron spectra

Interpolation of the x axes of traces was used for both IL valence XP spectra and RAES data.

7.1. Why interpolation was needed

Interpolation of IL valence XP spectra was needed to allow both quantitative area normalisation to be achieved and individual ion traces (both cation and anion traces) to be obtained. Each of the IL valence XP spectra were charge referenced, as explained in ESI Section 5. The E_B values used for charge referencing are given in ESI Table S3; all values used were to two decimal places. The data all have step sizes of 0.1 eV (*i.e.* to one decimal place). Once the charge referencing shifts of two decimal places were applied, the x axis values for each IL valence XP spectra no longer matched (which is needed for both area normalisation and obtaining individual ion traces). Therefore, to make each x axis match, we interpolated our data with a very low level of smoothing, giving us x axes to two decimal places.

Interpolation was needed to generate our RAES data heat maps. The RAES data was recorded in constant kinetic energy mode. The step sizes for kinetic energy and $h\nu$ did not match. Therefore, to plot our RAES data in constant binding energy mode, we interpolated our data.

7.2. Explaining the interpolation method

To make each x axis have the same number of data points, we interpolated our data with a very low level of smoothing, giving us x axes to two decimal places. We then chopped the data so all x axes had the same number of data points. The interpolation did not affect the quality or validity of the data, as demonstrated in ESI Figure S11a. In this article, subtraction has been carried out such that the subtracted trace usually has more positive peaks than negative peaks, for ease of interpretation.

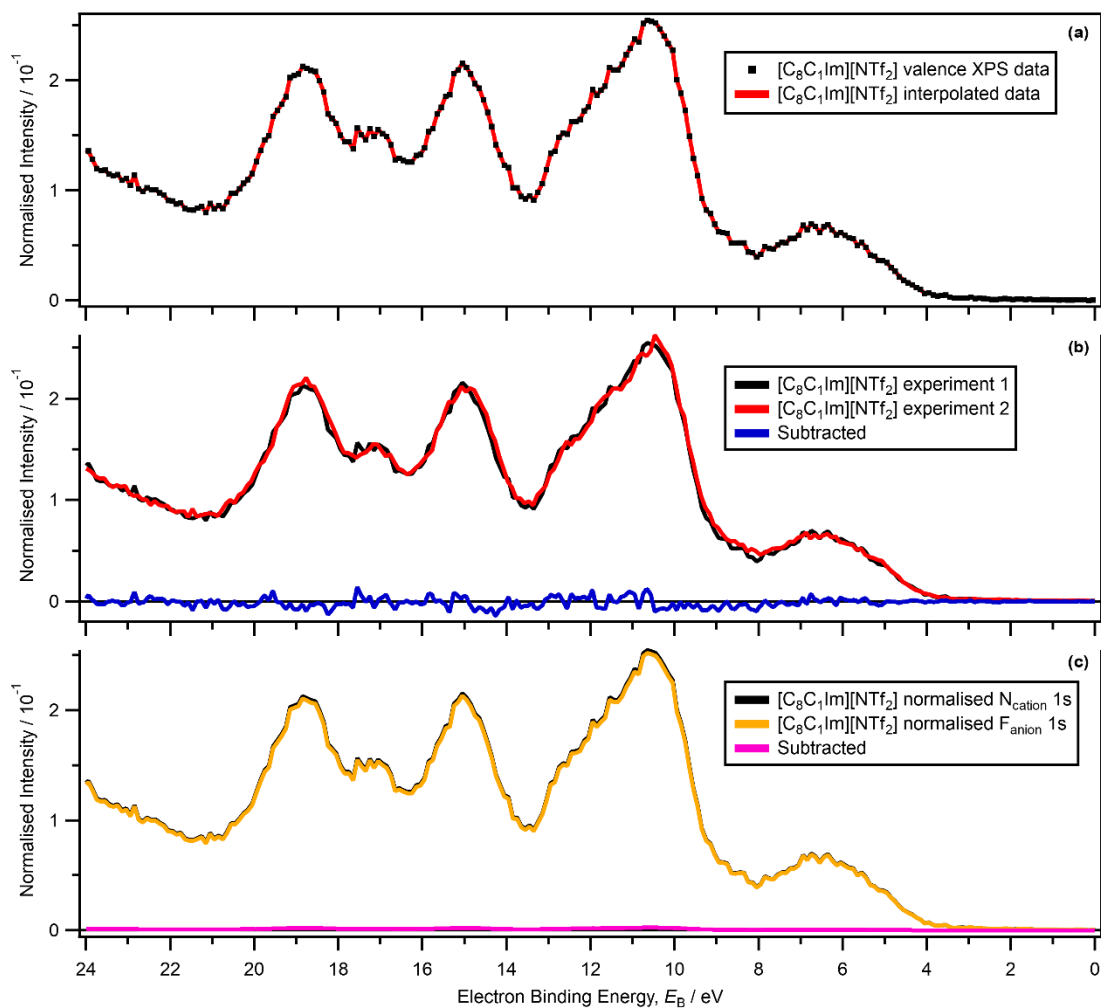


Figure S11. (a) Area normalised valence XP spectra for $[\text{C}_8\text{C}_1\text{Im}][\text{NTf}_2]$ recorded at $h\nu = 1486.6$ eV, and interpolated data. (b) Area normalised valence XP spectra for $[\text{C}_8\text{C}_1\text{Im}][\text{NTf}_2]$ recorded at $h\nu = 1486.6$ eV on two different days (18 months apart), and the subtracted trace ($[\text{C}_8\text{C}_1\text{Im}][\text{NTf}_2]$ minus $[\text{C}_8\text{C}_1\text{Im}][\text{NTf}_2]$). The areas were normalised to the area of the $\text{N}_{\text{cation}} 1\text{s}$ region. (c) Area normalised valence XP spectra for $[\text{C}_8\text{C}_1\text{Im}][\text{NTf}_2]$ recorded at $h\nu = 1486.6$ eV. The areas were normalised to the areas of the: (i) $\text{N}_{\text{cation}} 1\text{s}$ peak and (ii) $\text{F}_{\text{anion}} 1\text{s}$ peak, and then subtracted. The data plotted in black on each of (a), (b) and (c) have had the same area normalisation performed.

8. Data analysis. Area normalisation

8.1. Qualitative area normalisation

Qualitative area normalisation, achieved by using the judgement of the user to make peak areas/intensities match, was used to aid visual interpretation of XP spectra and RAES traces in Section 3.3.

8.2. Quantitative area normalisation

If data is sufficiently high quality, a significantly better, quantitative method can be used: area normalisation using core level peak areas. For high quality XP spectra of high purity ILs, the experimental stoichiometry matches the nominal stoichiometry. Therefore, the relative number of atoms of each element (and potentially, the number of atoms in different electronic environments for each element) in the sample is known. This information can be used for quantitative area normalisation.

Quantitative area normalisation to aid visual interpretation of core level XP spectra has been successfully used for a range of ILs, with the focus on identifying the different C 1s electronic environments for ILs with common structural features, *e.g.* to compare the C 1s XP spectra for $[\text{C}_7\text{C}_1\text{Im}][\text{TfO}]$.^{22, 39} However, such a visual fingerprint method, let alone the subtraction method, has not been demonstrated for identification of valence MOs for ILs to date, most likely due to the relatively complex valence XP spectra of ILs and the relatively small number of ILs studied using valence XPS. Recently, area normalised core level XP spectra have been subtracted to give difference traces, *e.g.* to identify E_b for the cyano carbon atom contribution to the C 1s region for $[\text{B}(\text{CN})_4]^-$.¹⁹

The simplest way to area normalise XP spectra for ILs quantitatively is to use a peak common to both ILs, *i.e.* all XP spectra for two ILs are divided by the peak area for the peak common to both ILs. For example, for subtraction of $[\text{C}_8\text{C}_1\text{Im}][\text{HSO}_4]$ minus $[\text{C}_4\text{C}_1\text{Im}][\text{HSO}_4]$ the peak areas of $\text{N}_{\text{cation}} 1s$ could be used; alternatively, $\text{S}_{\text{anion}} 2p$ or $\text{O}_{\text{anion}} 1s$ peak areas could be used. The C 1s area was never used for area normalisation, as we deemed that this region was the most likely to contain any small amount of contamination. In addition, peaks that showed relatively large shake-up peaks (*e.g.* $\text{N}_{\text{anion}}(\text{cyano}) 1s$) were also not used. Area normalisation can also be achieved using different elements, which is slightly more complex than area normalisation using a common element. For example, for $[\text{C}_8\text{C}_1\text{Im}]\text{Cl}$ and $[\text{P}_{6,6,6,14}]\text{Br}$ the peaks areas for *e.g.* $\text{N}_{\text{cation}} 1s$ for $[\text{C}_8\text{C}_1\text{Im}]\text{Cl}$ and $\text{P}_{\text{cation}} 2p$ for $[\text{P}_{6,6,6,14}]\text{Br}$ can be used. To obtain the correct area normalisation, both the number of atoms of each element and the core level photoionisation cross-sections need to be accounted for. This area normalisation was used at all times in this article. The element and orbital used for area normalisation, as well as the number of atoms of each of these elements and the core level relative sensitivity factors (RSFs), are listed in ESI Table S6.

Table S6. Peak used for area normalisation for each ionic liquid

IL no.	IL	Element used for area normalisation	Orbital used for area normalisation	Peak identity	No. of atoms	RSF ^a
1	[C ₈ C ₁ Im]Cl	N	1s	cation	2	0.350
3	[C ₆ C ₁ Im]I	N	1s	cation	2	0.350
4	[P _{6,6,6,14}]Cl	P	2p _{3/2}	cation	1	0.200
5	[P _{6,6,6,14}]Br	P	2p _{3/2}	cation	1	0.200
6	[C ₄ C ₁ Im][SCN]	N	1s	cation	2	0.350
8	[C ₄ C ₁ Im][N(CN) ₂]	N	1s	cation	2	0.350
9	[P _{6,6,6,14}][N(CN) ₂]	P	2p _{3/2}	cation	1	0.200
10	[C ₈ C ₁ Im][C(CN) ₃]	N	1s	cation	2	0.350
11	[C ₆ C ₁ Im][B(CN) ₄]	N	1s	cation	2	0.350
12	[C ₈ C ₁ Im][BF ₄]	N	1s	cation	2	0.350
13	[P _{6,6,6,14}][NO ₃]	P	2p _{3/2}	cation	1	0.200
14	[C ₄ C ₁ Im][HSO ₄]	N	1s	cation	2	0.350
15	[C ₈ C ₁ Im][HSO ₄]	N	1s	cation	2	0.350
16	[C ₄ C ₀ Im][HSO ₄]	N	1s	cation	2	0.350
17	[N _{4,1,1,0}][HSO ₄]	N	1s	cation	1	0.350
18	[N _{8,1,1,0}][HSO ₄]	N	1s	cation	1	0.350
19	[C ₄ C ₁ Im][MeSO ₄]	N	1s	cation	2	0.350
20	[C ₄ C ₁ Im][OCSO ₄]	N	1s	cation	2	0.350
21	[C ₂ C ₁ Im][MeSO ₃]	N	1s	cation	2	0.350
22	[C ₄ C ₁ Im][Me ₂ PO ₄]	N	1s	cation	2	0.350
24	[C ₈ C ₁ Im][TfO]	N	1s	cation	2	0.350
25	[N _{2,2,1,0}][TfO]	N	1s	cation	1	0.350
26	[N _{2OH,2OH,2OH,1}][TfO]	N	1s	cation	1	0.350
29	[C ₈ C ₁ Im][NTf ₂]	N	1s	cation	2	0.350
30	[C ₂ C ₀ Im][NTf ₂]	N	1s	cation	2	0.350
31	[C ₄ C ₀ Im][NTf ₂]	N	1s	cation	2	0.350
32	[N _{4,1,1,1}][NTf ₂]	N	1s	cation	1	0.350
33	[N _{3,2,1,1}][NTf ₂]	N	1s	cation	1	0.350
34	[N _{8,8,8,1}][NTf ₂]	N	1s	cation	1	0.350
35	[S _{2,2,1}][NTf ₂]	S	2p _{3/2}	cation	1	0.267
36	[S _{2,2,2}][NTf ₂]	S	2p _{3/2}	cation	1	0.267
37	[P _{6,6,6,14}][NTf ₂]	P	2p _{3/2}	cation	1	0.200

^a RSF = relative sensitivity factors, taken from reference ⁴⁰

9. Data analysis. Obtaining individual cation and anion traces

By splicing together sections of the area normalised valence XP spectra for $[\text{C}_8\text{C}_1\text{Im}][\text{BF}_4]$ ($0 \text{ eV} < E_B < 5.95 \text{ eV}$) and $[\text{C}_8\text{C}_1\text{Im}]\text{Cl}$ ($5.96 \text{ eV} < E_B < 11.5 \text{ eV}$) (ESI Figure S12a and ESI Figure S12b) an area normalised trace for $[\text{C}_8\text{C}_1\text{Im}]^+$ was obtained for the region at $0 \text{ eV} < E_B < 11.5 \text{ eV}$ at $h\nu = 1486.6 \text{ eV}$ (Figure 9 and ESI Figure S12c). Given the relatively small contribution from alkyl carbon-based C 2p AOs to the region at $0 \text{ eV} < E_B < 11.5 \text{ eV}$, this $[\text{C}_8\text{C}_1\text{Im}]^+$ trace can be used as the $[\text{C}_n\text{C}_1\text{Im}]^+$ trace (where $n = 2, 4, 6$) at $h\nu = 1486.6 \text{ eV}$.

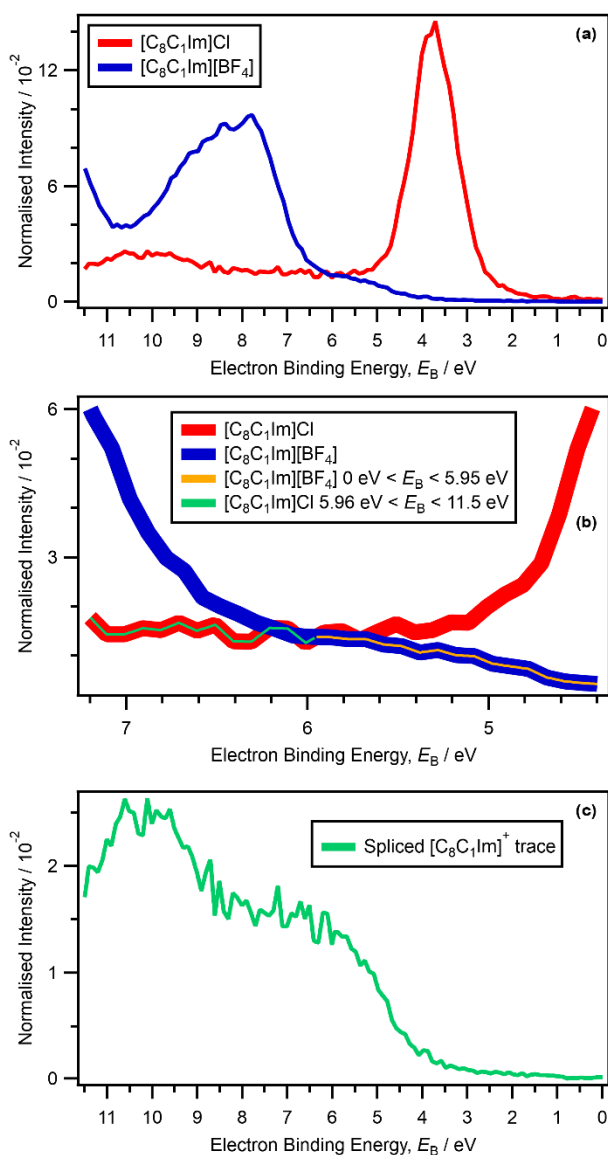


Figure S12. (a) Area normalised valence XP spectra recorded at $h\nu = 1486.6 \text{ eV}$ for $[\text{C}_8\text{C}_1\text{Im}][\text{BF}_4]$ and $[\text{C}_8\text{C}_1\text{Im}]\text{Cl}$, plotted in the region $0 \text{ eV} < E_B < 11.5 \text{ eV}$. (b) The same traces as in graph (a), plotted in the region $4.4 \text{ eV} < E_B < 7.2 \text{ eV}$. Interpolated data for $[\text{C}_8\text{C}_1\text{Im}][\text{BF}_4]$ plotted over the region $0 \text{ eV} < E_B < 5.95 \text{ eV}$ and for $[\text{C}_8\text{C}_1\text{Im}]\text{Cl}$ plotted over the region $5.96 \text{ eV} < E_B < 11.5 \text{ eV}$ (*i.e.* using the traces used to plot graph (b)). (c) Spliced $[\text{C}_8\text{C}_1\text{Im}]^+$ trace; the data was produced using interpolated data for $[\text{C}_8\text{C}_1\text{Im}][\text{BF}_4]$ over the region $0 \text{ eV} < E_B < 5.95 \text{ eV}$ and for $[\text{C}_8\text{C}_1\text{Im}]\text{Cl}$ over the region $5.96 \text{ eV} < E_B < 11.5 \text{ eV}$ (*i.e.* using the traces used to plot graph (b)). The areas were normalised using procedures outlined in ESI Section 8.2. The spliced $[\text{C}_8\text{C}_1\text{Im}]^+$ trace was obtained using procedures outlined in ESI Section 9. All electron spectra were charge referenced using procedures outlined in ESI Section 5.

The $[\text{C}_n\text{C}_1\text{Im}]^+$ trace was subtracted from all $[\text{C}_n\text{C}_1\text{Im}][\text{A}]$ ILs for which area normalised valence XP spectra were obtained, giving the anion $[\text{A}]^-$ trace at $h\nu = 1486.6 \text{ eV}$ for 14 different anions. The 14 anions for which anion traces were obtained are: Cl^- , I^- , $[\text{SCN}]^-$, $[\text{N}(\text{CN})_2]^-$, $[\text{C}(\text{CN})_3]^-$, $[\text{B}(\text{CN})_4]^-$, $[\text{BF}_4]^-$, $[\text{HSO}_4]^-$, $[\text{MeSO}_4]^-$, $[\text{OCsO}_4]^-$, $[\text{MeSO}_3]^-$, $[\text{Me}_2\text{PO}_4]^-$, $[\text{TfO}]^-$, $[\text{NTf}_2]^-$. These anion traces were subtracted

from [cation][A] IL area normalised valence XP spectra, where the [cation]⁺ was not [C_nC₁Im]⁺, to give cation traces at $h\nu = 1486.6$ eV for nine cations. The nine cations for which cations traces were obtained (in addition to that for [C₈C₁Im]⁺) are: [N_{3,2,1,1}]⁺, [N_{4,1,1,1}]⁺, [S_{2,2,1}]⁺, [S_{2,2,2}]⁺, [N_{8,8,8,1}]⁺, [N_{2OH,2OH,2OH,1}]⁺, [N_{2,2,1,0}]⁺, [N_{4,1,1,0}]⁺ and [N_{8,1,1,0}]⁺.

10. Data analysis. Subtraction methods

For the subtraction method, both area normalisation and charge referencing must be used. The subtraction method allows comparison of both peak areas and peak E_B . This subtraction method has the potential to be far more quantitative than the fingerprint method.

10.1. Explaining area subtraction for valence level XP spectra

Area normalisation is not reported for $[C_8C_1Im]Br$, $[C_8C_1Im][SCN]$, $[C_4C_1Im][TfO]$, $[C_4C_1Im][NTf_2]$ and $[C_6C_1Im][NTf_2]$. For $[C_8C_1Im]Br$, $[C_8C_1Im][SCN]$ and $[C_4C_1Im][TfO]$ the XP spectra were recorded on the Imperial XPS apparatus, not the UCL XPS apparatus. The area normalised valence XP spectra for these three ILs were found to not match the area normalised valence XP spectra for comparable ILs (the differences were very large). Despite being recorded on the same XPS apparatus, clearly some settings were different, leading to valence XP spectra that could not be compared using area normalisation. For $[C_4C_1Im][NTf_2]$ and $[C_6C_1Im][NTf_2]$ the XP spectra were recorded on the UCL XPS apparatus. However, the area normalised valence XP spectra for these two ILs were found to not match the area normalised valence XP spectra for comparable ILs. It is unclear why this was the case, as area normalisation of valence XP spectra was successful for 32 other ILs recorded on the UCL XPS apparatus. For these five ILs, area normalisation using the intensity of valence peaks was reported, to determine whether the shape of the valence XP spectra were comparable to other ILs (for $[C_8C_1Im][SCN]$, $[C_4C_1Im][TfO]$, $[C_4C_1Im][NTf_2]$ and $[C_6C_1Im][NTf_2]$) and to identify anion contributions (for $[C_8C_1Im]Br$). This approach has been used by Krischok and co-workers to identify alkyl contributions for $[C_nC_1Im][NTf_2]$ (where $n = 2$ and 8).³⁰

10.2. How to decide whether a valence level XP spectrum subtraction peak can be used for MO identification

We have used a number of guidelines to decide whether a peak/feature in a subtraction trace can be used for MO identification.

(1) Compare to other subtracted traces

The subtracted trace for $[C_8C_1Im][NTf_2]$ minus $[C_8C_1Im][NTf_2]$ (recorded on two different days 18 months apart on the same UCL XPS apparatus) provides an excellent guide to the level of noise expected when no peaks were present in the subtracted trace. Therefore, any feature in the subtracted trace of interest that was significantly more intense than this guide trace could potentially be used for MO identification.

(2) Charge referencing challenges

As explained in detail in reference ¹⁹, for $[cation][A]$ ILs (where the cations were different and the anion was the same) $E_B(\text{anion valence})$ did not always match. For example, for $[P_{6,6,6,14}]Cl$ and $[C_8C_1Im]Cl$ charge referenced using $E_B(C_{alkyl} 1s)$, the Cl 3p peaks were different by 0.5 eV.¹⁹ In such cases, the subtraction method can potentially give confusing results, as the subtracted trace can give both positive and negative peaks for what is essentially the same anion peak. Therefore, care must be taken; one possible solution is to charge reference using an anion peak. As explained in reference ¹⁹, charge referencing for ILs with protic cations is not yet fully understood. These differences make analysis of subtraction traces challenging for ILs with protic cations; any differences from the zero line should be treated with caution when making MO identifications.

(3) High intensity peak minus high intensity peak giving a low intensity subtracted peak

As a guide, ideally one would want the peak in the subtracted trace and the peak in the area normalised XP spectrum used to subtract to be of similar intensity. For example, for $[S_{2,2,2}][NTf_2]$ minus

[N_{3,2,1,1}][NTf₂] the feature at $E_B \sim 6$ eV in the subtracted trace was approximately the same intensity as the peak at $E_B \sim 6$ eV in the area normalised XP spectrum for [N_{3,2,1,1}][NTf₂] (Figure 11a); MO identifications can be made with confidence for the peak in the subtracted trace. For certain ILs, two large peaks in the area normalised valence XP spectra subtracted to give a relatively low intensity peak in the subtracted trace; the intensity of the peak in the subtracted trace was significantly smaller than peaks in both of the area normalised valence XP spectra. For example, for [P_{6,6,6,14}][NTf₂] minus [N_{8,8,8,1}][NTf₂] the peak at $E_B \sim 10$ eV in the subtracted trace was much lower intensity than the peak at $E_B \sim 10$ eV in the area normalised XP spectrum for [N_{8,8,8,1}][NTf₂] (ESI Figure S94). In such cases, any differences from the zero line should be treated with caution when making MO identifications.

(4) Large differences in AO photoionisation cross-sections

Ideally, the two ILs used for subtraction, one of the ILs will have a key atom which has one (or more) AO which has a significantly larger photoionisation cross-section than the other contributing AOs. In such a scenario, any significant deviation from the zero line for the subtracted trace can be attributed to the AO with the larger photoionisation cross-section, allowing MO identification.

10.3. Obtaining subtracted resonant Auger electron spectra traces

The electron spectra recorded at resonant $h\nu$, *e.g.* at $h\nu = 401.8$ eV for N_{cation} for [C_nC₁Im][A], had contributions from both RAE processes and non-resonant valence level XP processes. To obtain subtracted resonant Auger electron spectra traces, it is necessary to subtract the contribution from non-resonant valence level XP processes. For some of the RAES data here, this subtraction was achieved by subtracting using non-resonant valence level XP spectra from just below the resonant $h\nu$, *e.g.* at $h\nu = 397.0$ eV for [C₄C₁Im][SCN]. However, for certain RAES data (N 1s RAES for [C₈C₁Im][C(CN)₃]), subtraction using non-resonant valence level XP spectra from just below the resonant $h\nu$ did not work well due to the relatively low quality, caused by a number of different issues, *e.g.* peaks from 2nd order light. For these ILs, subtraction using non-resonant valence level XP spectra from just above the resonant $h\nu$, *e.g.* at $h\nu = 404.0$ eV for [C₈C₁Im][C(CN)₃]. At such $h\nu$ values, features due to Auger processes were not observed at $0 \text{ eV} < E_B < 12 \text{ eV}$ (at $E_B > 12 \text{ eV}$ features due to Auger processes were observed, so this subtraction method should not be used if data at $E_B > 12 \text{ eV}$ is of interest). At such $h\nu$ values, problems due to peaks from 2nd order light were also removed, as these features appear at negative E_B at such $h\nu$. The reliability of this method is demonstrated by subtracted O_{anion} resonant Auger electron spectra for [P_{6,6,6,14}][NO₃] (ESI Figure S13), where the subtracted traces were essentially identical whether the subtraction was performed using data below or above the edge.

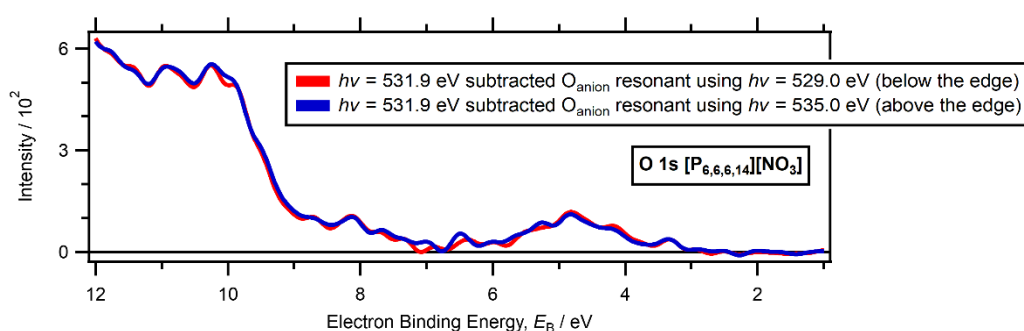


Figure S13. Subtracted O_{anion} resonant Auger electron spectra ($h\nu = 531.9$ eV) for [P_{6,6,6,14}][NO₃]; subtraction was carried out using two different non-resonant $h\nu$ ($h\nu = 529.0$ eV and $h\nu = 535.0$ eV).

11. Data analysis. Validating quantitative area normalisation and subtraction

As both quantitative area normalisation and the subtraction method have not been demonstrated previously for analysing valence XP spectra for ILs, we will demonstrate their validity here.

Area normalised valence XP spectra for $[\text{C}_8\text{C}_1\text{Im}][\text{NTf}_2]$ recorded at $h\nu = 1486.6$ eV on two different days (18 months apart) on the same UCL XPS apparatus, and the subtracted trace for this ($[\text{C}_8\text{C}_1\text{Im}][\text{NTf}_2]$ minus $[\text{C}_8\text{C}_1\text{Im}][\text{NTf}_2]$) are given in Figure S3b. The areas were normalised to the area of the $\text{N}_{\text{cation}} 1\text{s}$ peak. This peak was chosen as no complex fitting model was required to obtain this peak area; in addition, many ILs contain a $[\text{C}_n\text{C}_1\text{Im}]^+$ cation, allowing comparisons to be made relatively straightforwardly for a wide range of ILs. Clearly, the visual match of the two area normalised XP spectra was outstanding, demonstrating the validity of using quantitative area normalisation for analysing valence XP spectra for ILs.

To demonstrate the validity of our subtraction method, for $[\text{C}_8\text{C}_1\text{Im}][\text{NTf}_2]$ the valence XP spectrum was area normalised using both the area of the $\text{N}_{\text{cation}} 1\text{s}$ peak and the area of the $\text{F}_{\text{anion}} 1\text{s}$ peak (ESI Figure S11c). There are two N_{cation} atoms for every six F_{anion} atoms, and the photoionisation cross-sections (*i.e.* the relative sensitivity factors, taken from reference ⁴⁰) for N 1s and F 1s are 0.350 and 1.000 respectively. The visual match of the two area normalised XP spectra is excellent, and subtraction trace shows just noise with no discernible peaks, demonstrating the validity of the subtraction method for analysing valence XP spectra for ILs.

12. Data analysis. Obtaining $E_B(\text{ion HOFO})$ and $E_B(\text{ion onset})$

12.1. Obtaining $E_B(\text{ion HOFO})$

Our $E_B(\text{ion HOFO})$ values reported here are designed to capture the peak E_B of the lowest E_B anionic and cation contributions. Therefore, the ideal XP spectrum for obtaining $E_B(\text{ion HOFO})$ is one that gives a readily fitted peak for the lowest E_B (anionic or cation) contribution, *e.g.* determining $E_B(\text{anion HOFO})$ for $[\text{C}_7\text{C}_1\text{Im}][\text{SCN}]$. However, for determining many $E_B(\text{ion HOFO})$ values, no readily fitted peak occurred. Therefore, a combination of different data sources was used to estimate a peak E_B ; thus, $E_B(\text{ion HOFO})$ was obtained, *e.g.* $E_B(\text{anion HOFO})$ for $[\text{N}_{4,1,1,0}][\text{HSO}_4]$ was determined using a combination of variable $h\nu$ XPS and RAES data. This process of estimating a peak E_B can be challenging for XP spectra that gave a broad feature for the lowest E_B contribution; such features could be potentially be fitted with more than one peak. For such situations, the error given with the value was larger reflecting the greater challenge obtaining $E_B(\text{ion HOFO})$ values for such features.

A general observation is that the lowest E_B anionic feature in XP spectra was far more likely to be a sharp peak than the lowest E_B cationic feature in XP spectra. For example, for $[\text{C}_4\text{C}_1\text{Im}][\text{SCN}]$ and $[\text{C}_8\text{C}_1\text{Im}]\text{Cl}$ the lowest E_B anionic feature in XP spectra gave a single, relatively intense near-Gaussian shaped peak, whereas the lowest E_B cationic feature in XP spectra for both ILs was a relatively broad feature. This finding was likely the result of a combination of two factors: (i) for anions such as $[\text{SCN}]^-$ and Cl^- it is expected that multiple MOs of very similar E_B contribute to the lowest E_B anionic feature, giving rise to a relatively intense peak, (ii) the anions are in general structurally simpler than cations with fewer different atoms potentially contributing to the MOs, meaning that cations have a number of MOs at relatively similar E_B values.

12.2. Obtaining $E_B(\text{ion onset})$

$E_B(\text{ion onset})$ values represent the experimental HOMO energy. $E_B(\text{ion onset})$ was determined by fitting a linear curve to the lowest E_B component (*i.e.* component 1) in a valence XP spectrum. The x-intercept of this curve is equal to $E_B(\text{ion onset})$. The fitting E_B range was chosen by the user to give a good visual fit to the XP spectrum. In Figure S5 two example fits are presented; a good E_B range and a poor E_B range. All reported $E_B(\text{ion onset})$ values were determined from charge-referenced lab-based valence XP spectra.

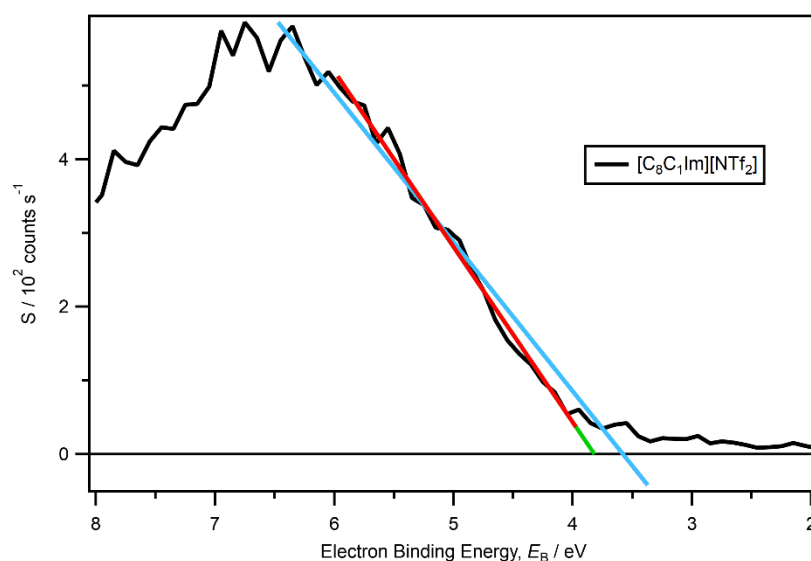


Figure S14. Valence XP spectrum for $[\text{C}_8\text{C}_1\text{Im}][\text{NTf}_2]$ recorded at $h\nu = 1486.6$ eV. The red trace (fitting range $4.0 \text{ eV} < E_B < 6.0 \text{ eV}$) is judged as a good fit; the green trace is the extrapolation to the x-intercept. The light blue trace (fitting range $3.4 \text{ eV} < E_B < 6.5 \text{ eV}$) is judged as a poor fit; the E_B chosen was too large. $E_B(\text{ion onset})$ is the x-intercept.

13. Results. XPS: demonstrating purity

Survey and core level XP spectra showed the expected peaks for both lab and synchrotron experiments, as shown by the XP spectra given in ESI Figure S15 to ESI Figure S51 (lab data) and ESI Figure S52 to ESI Figure S58 (synchrotron data).

Lab experiments

For the lab-based XP spectra for all 37 ILs studied in the lab (ESI Table S1), excellent matches were observed between the experimental and nominal stoichiometries (ESI Table S7). For $[P_{6,6,6,14}][NTf_2]$ a very small O 1s contamination peak was observed. Therefore, it can be concluded that for 36 of the 37 ILs studied on the lab source no impurities were observed after Ar^+ ion sputtering (ESI Table S7). A very small peak due to radiation damage was observed in the N 1s XP spectrum for $[C_8C_1Im]Br$ (ESI Figure S16c). The impurity/damage were observed in such small quantities that we expect them to have no impact on the valence XP spectra recorded for these two ILs.

Synchrotron experiments

A very small O 1s peak due to an impurity was observed in the synchrotron-based survey XP spectrum for $[C_8C_1Im][C(CN)_3]$ (ESI Figure S54a). Therefore, for six of the seven ILs studied at the synchrotron no impurities were observed after Ar^+ ion sputtering. A very small peak due to radiation damage was observed in the N 1s XP spectrum for $[C_8C_1Im]Cl$ (ESI Figure S53b). For $[C_8C_1Im][NTf_2]$, after ~12 hours under X-ray irradiation at the same sample spot, a small amount of impurity was observed in the N 1s NEXAFS spectrum (ESI Figure S61b); this has been detailed in a previous publication¹. These impurity/damage were not expected to have significant impact on the RAE spectra and valence XP spectra recorded for these three ILs.

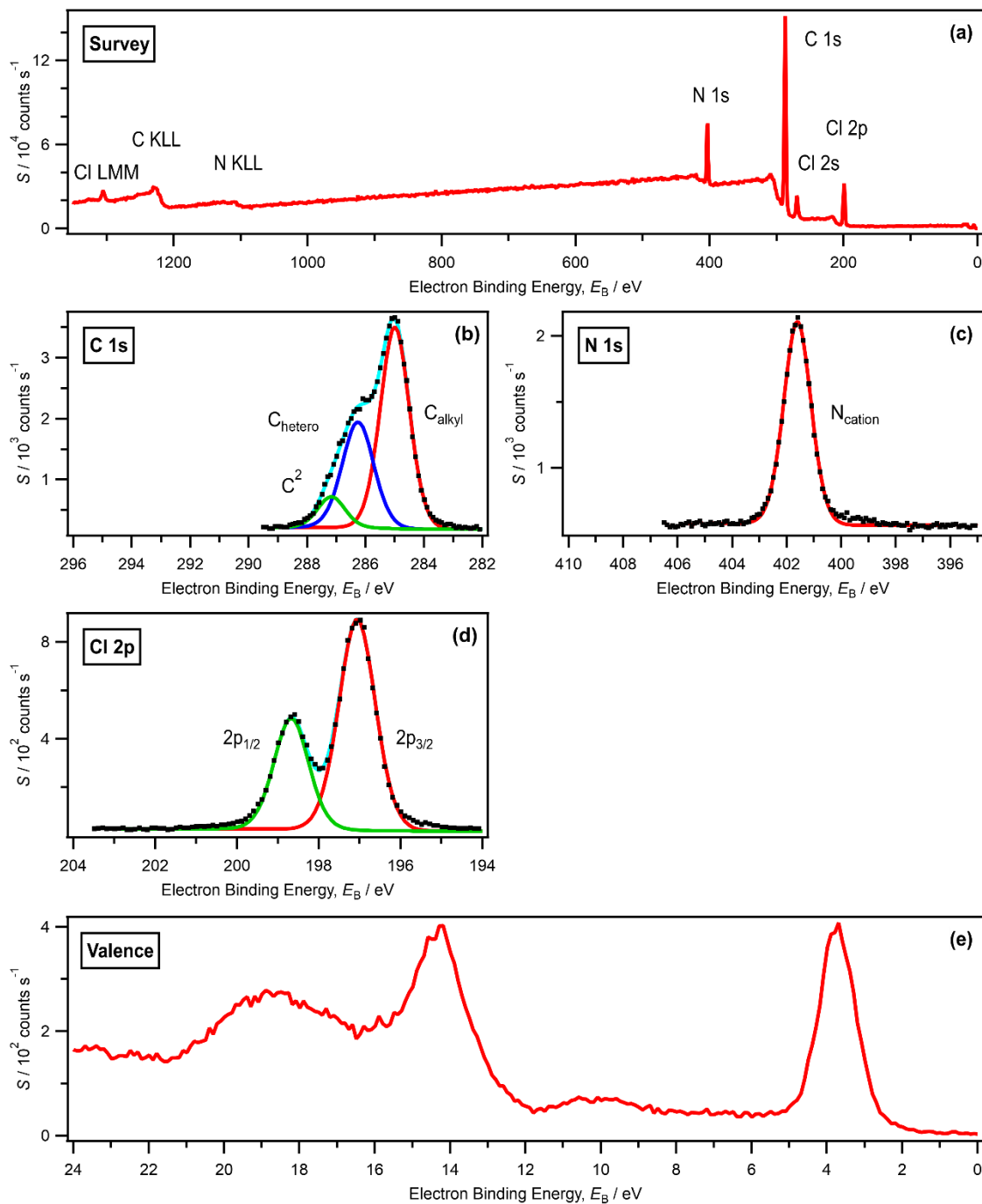


Figure S15. (a) Survey, (b-d) core (with fits) and (e) valence XP spectra for $[C_8C_1Im]Cl$ recorded on laboratory-based XPS apparatus at $h\nu = 1486.6$ eV. All electron spectra were charge referenced using procedures outlined in ESI Section 5.

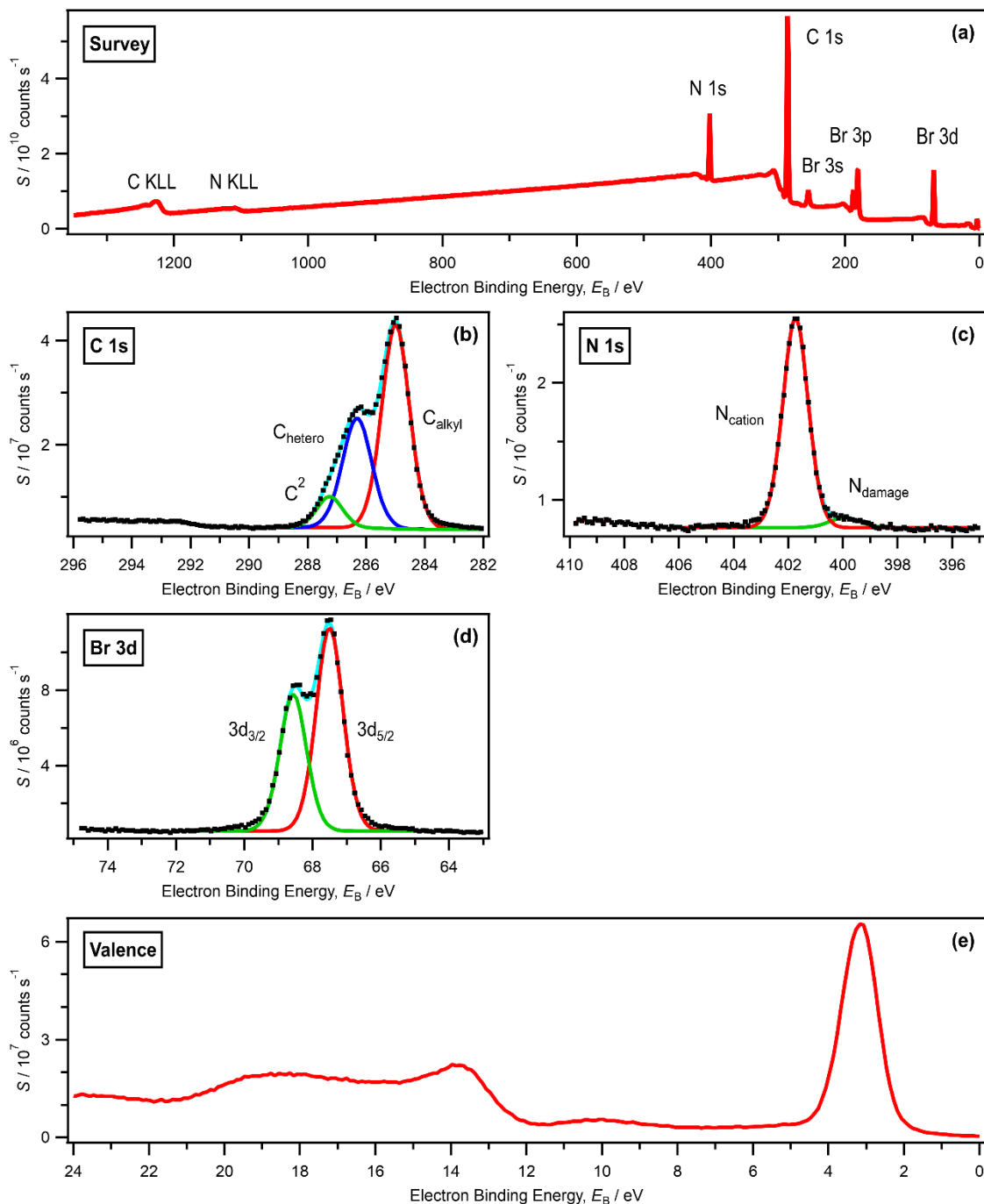


Figure S16. (a) Survey, (b-d) core (with fits) and (e) valence XP spectra for $[C_8C_1Im]Br$ recorded on laboratory-based XPS apparatus at $h\nu = 1486.6$ eV. All electron spectra were charge referenced using procedures outlined in ESI Section 5. The N 1s spectrum showed a very small amount of damage, which has been observed previously for imidazolium-based ILs.⁴⁰

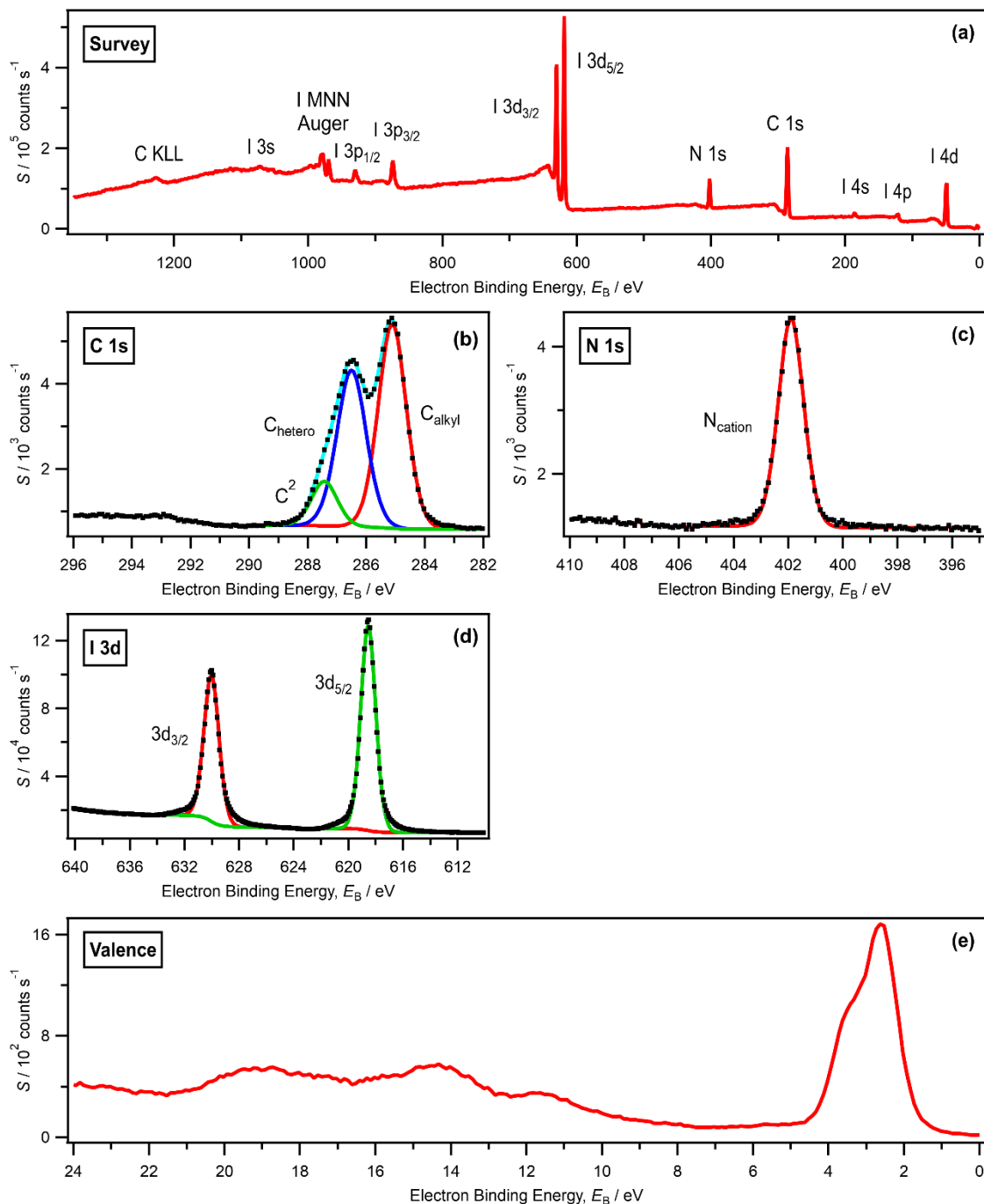


Figure S17. (a) Survey, (b-d) core (with fits) and (e) valence XP spectra for $[C_6C_3Im]I$ recorded on laboratory-based XPS apparatus at $h\nu = 1486.6$ eV. All electron spectra were charge referenced using procedures outlined in ESI Section 5.

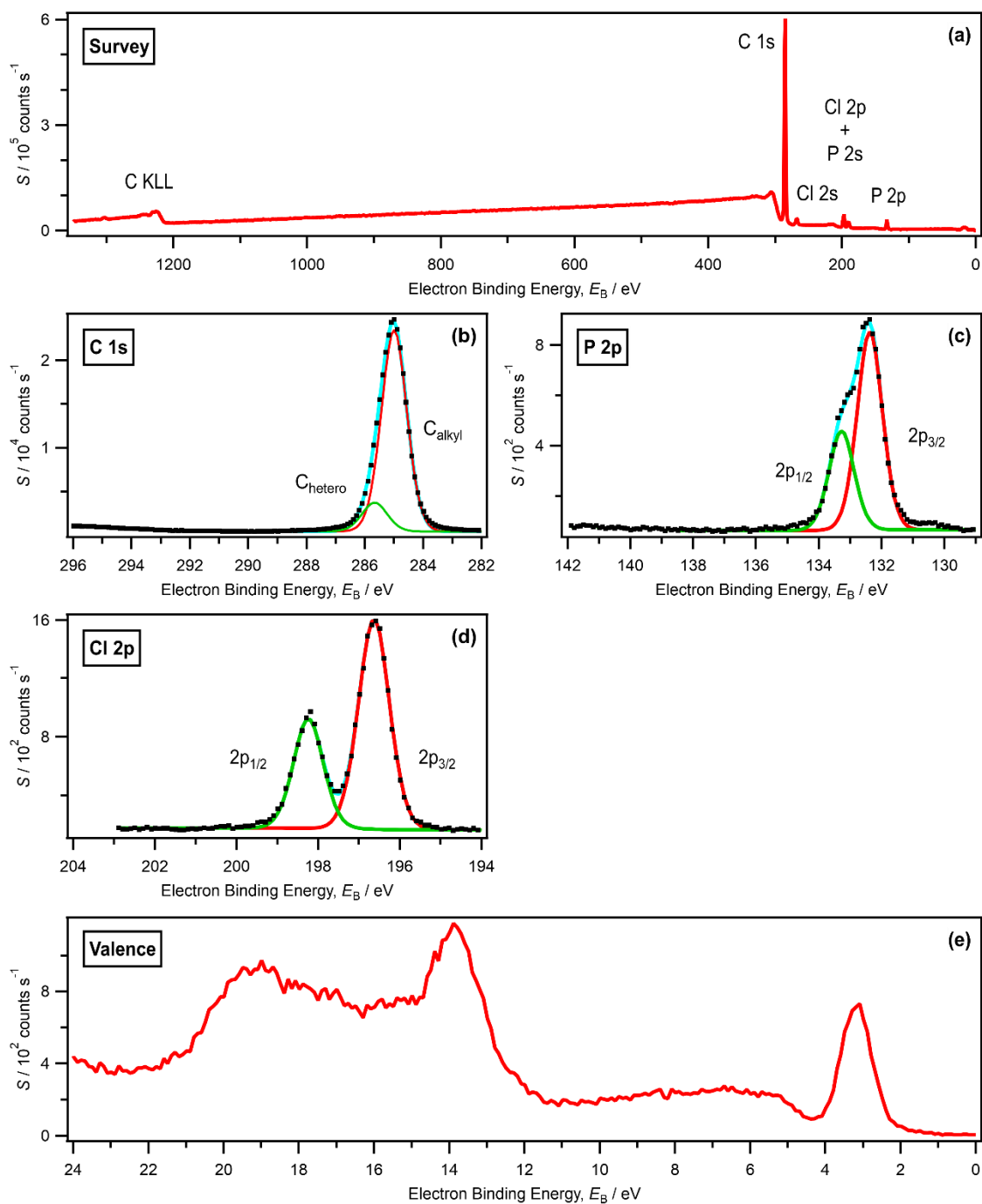


Figure S18. (a) Survey, (b-d) core (with fits) and (e) valence XP spectra for $[P_{6,6,6,14}]Cl$ recorded on laboratory-based XPS apparatus at $h\nu = 1486.6$ eV. All electron spectra were charge referenced using procedures outlined in ESI Section 5.

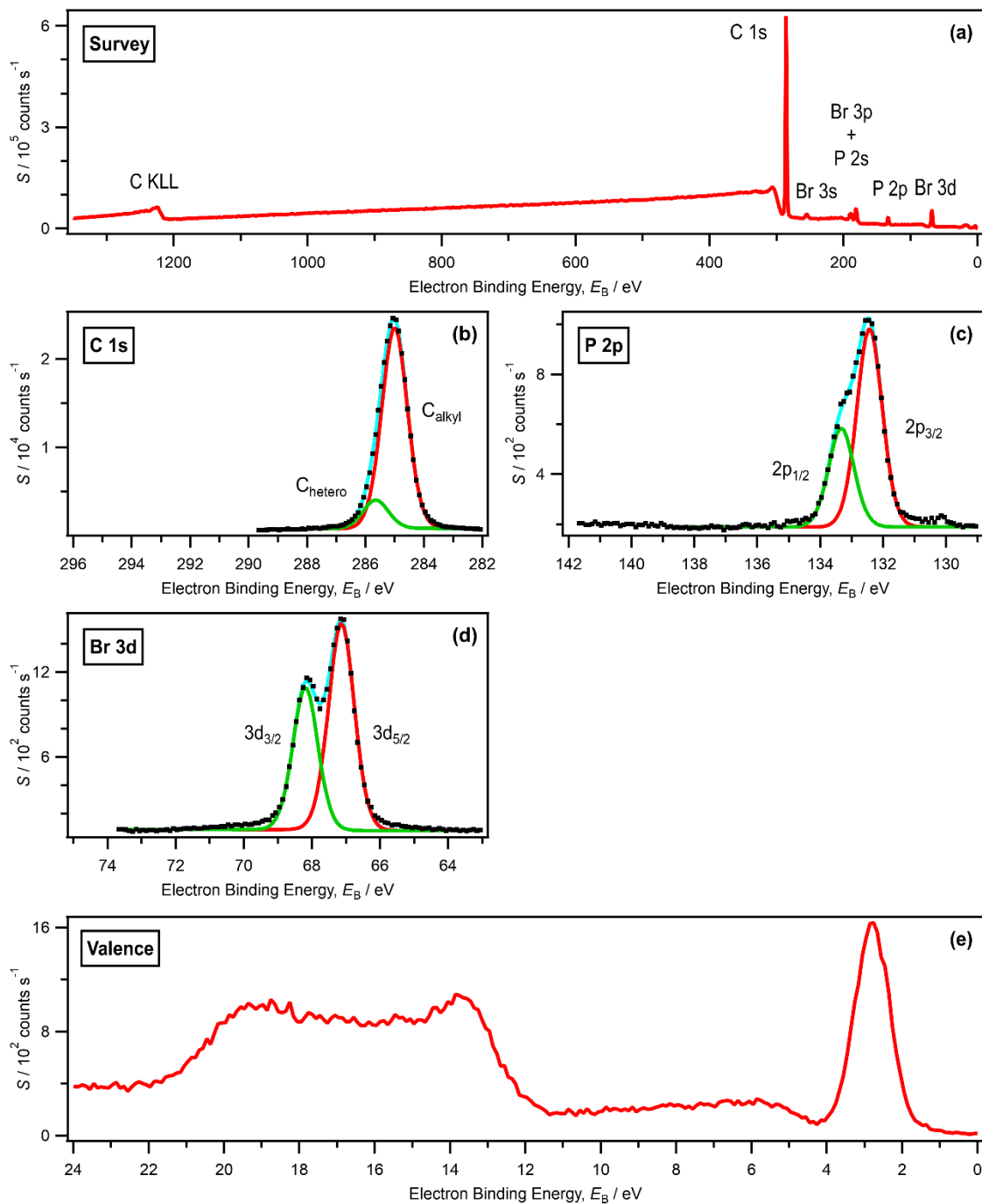


Figure S19. (a) Survey, (b-d) core (with fits) and (e) valence XP spectra for $[P_{6,6,6,14}]Br$ recorded on laboratory-based XPS apparatus at $h\nu = 1486.6$ eV. All electron spectra were charge referenced using procedures outlined in ESI Section 5.

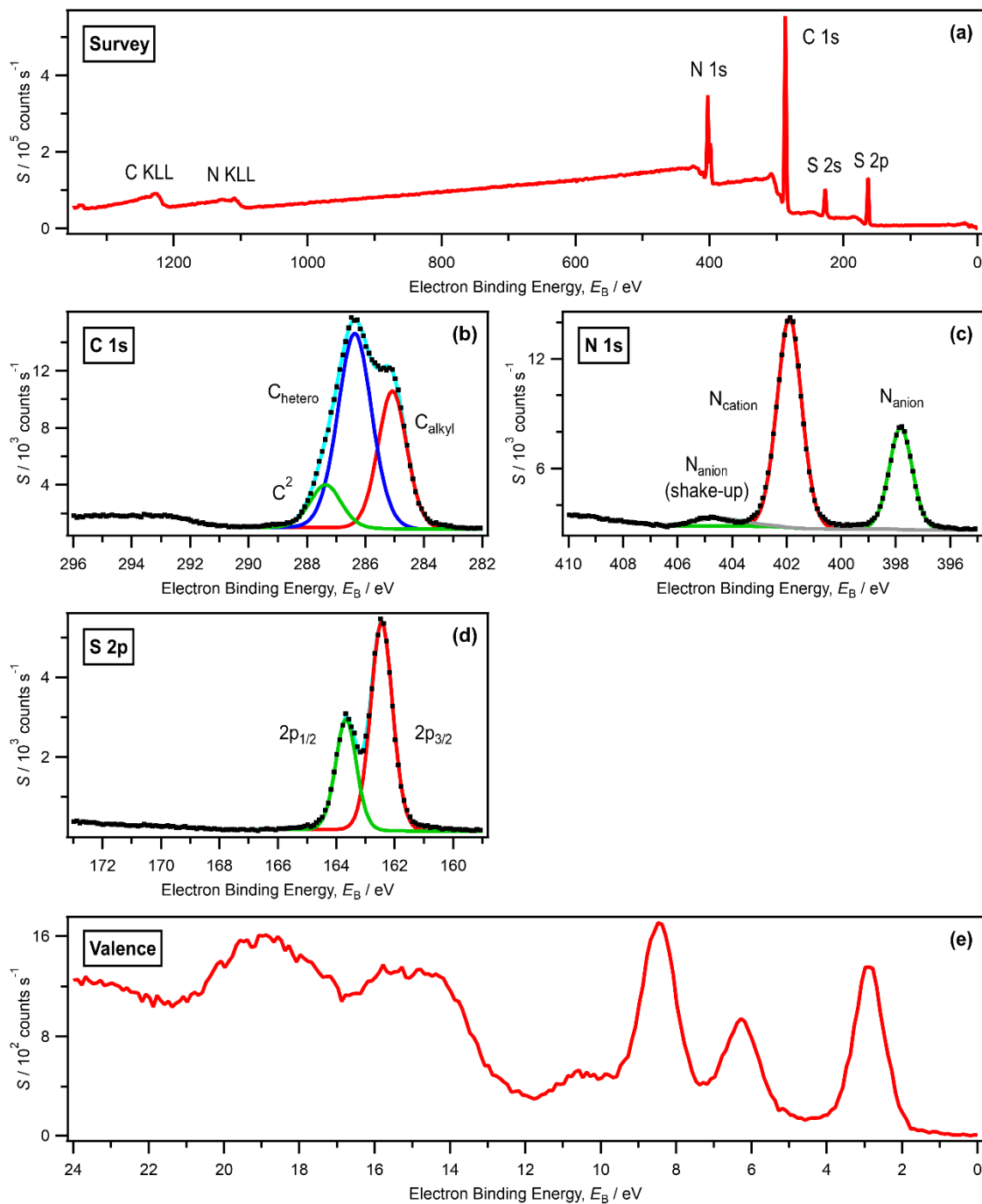


Figure S20. (a) Survey, (b-d) core (with fits) and (e) valence XP spectra for $[C_4C_1Im][SCN]$ recorded on laboratory-based XPS apparatus at $h\nu = 1486.6$ eV. All electron spectra were charge referenced using procedures outlined in ESI Section 5.

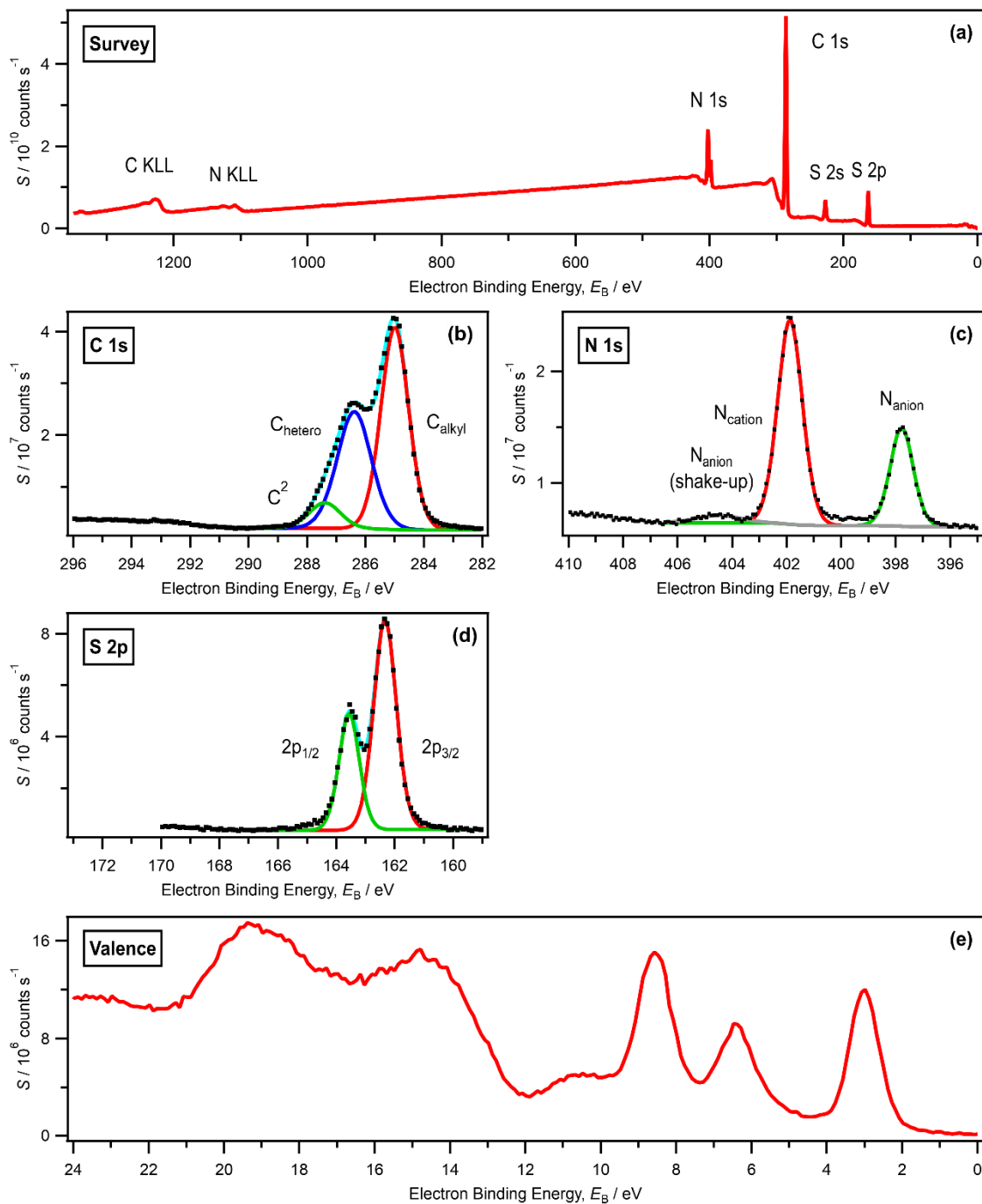


Figure S21. (a) Survey, (b-d) core (with fits) and (e) valence XP spectra for $[C_8C_1Im][SCN]$ recorded on laboratory-based XPS apparatus at $h\nu = 1486.6$ eV. All electron spectra were charge referenced using procedures outlined in ESI Section 5.

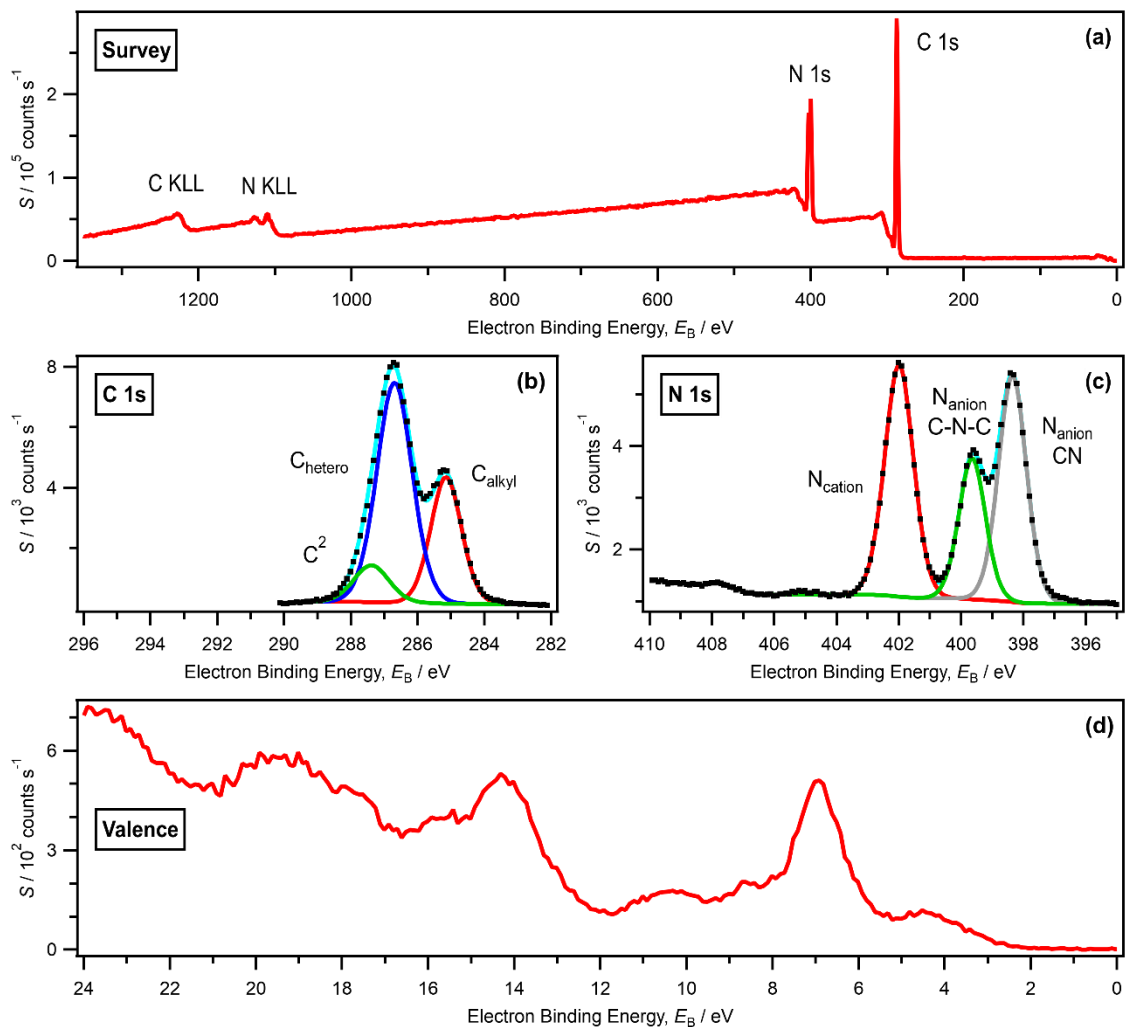


Figure S22. (a) Survey, (b and c) core (with fits) and (d) valence XPS spectra for $[C_4C_1Im][N(CN)_2]$ recorded on laboratory-based XPS apparatus at $h\nu = 1486.6 \text{ eV}$. All electron spectra were charge referenced using procedures outlined in ESI Section 5.

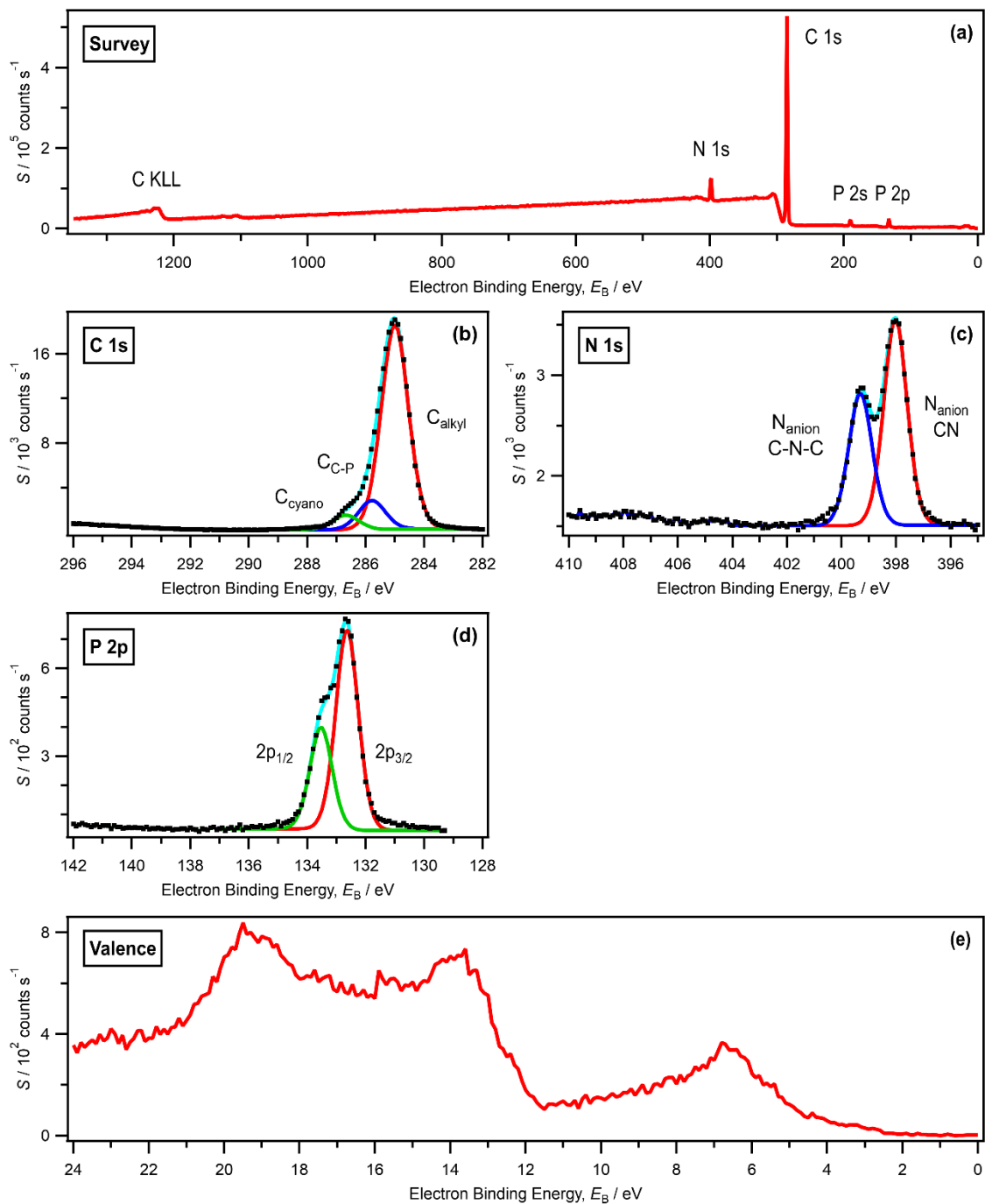


Figure S23. (a) Survey, (b-d) core (with fits) and (e) valence XP spectra for $[P_{6,6,6,14}][N(CN)_2]$ recorded on laboratory-based XPS apparatus at $h\nu = 1486.6$ eV. All electron spectra were charge referenced using procedures outlined in ESI Section 5.

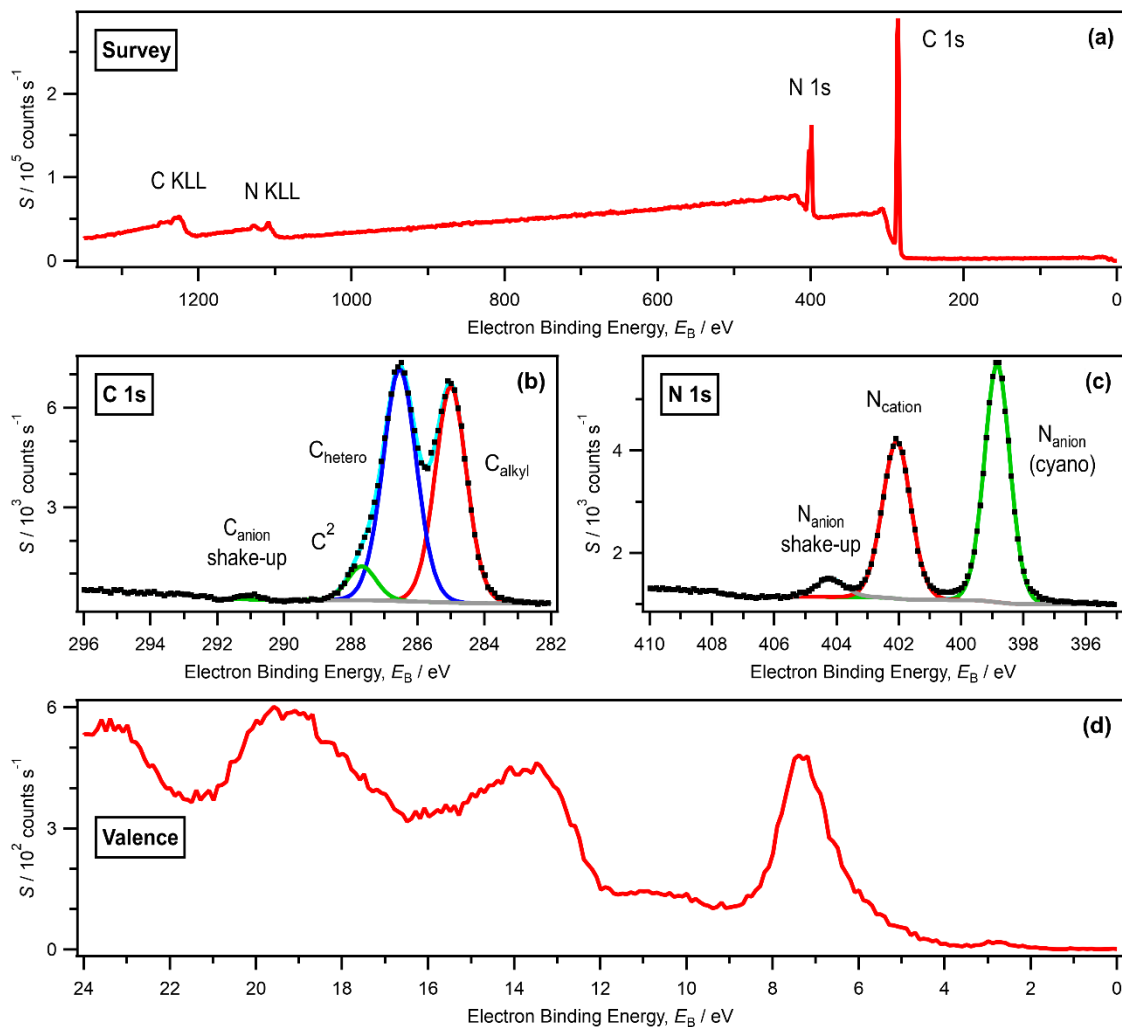


Figure S24. (a) Survey, (b and c) core (with fits) and (d) valence XP spectra for $[C_8C_1Im][C(CN)_3]$ recorded on laboratory-based XPS apparatus at $h\nu = 1486.6 \text{ eV}$. All electron spectra were charge referenced using procedures outlined in ESI Section 5.

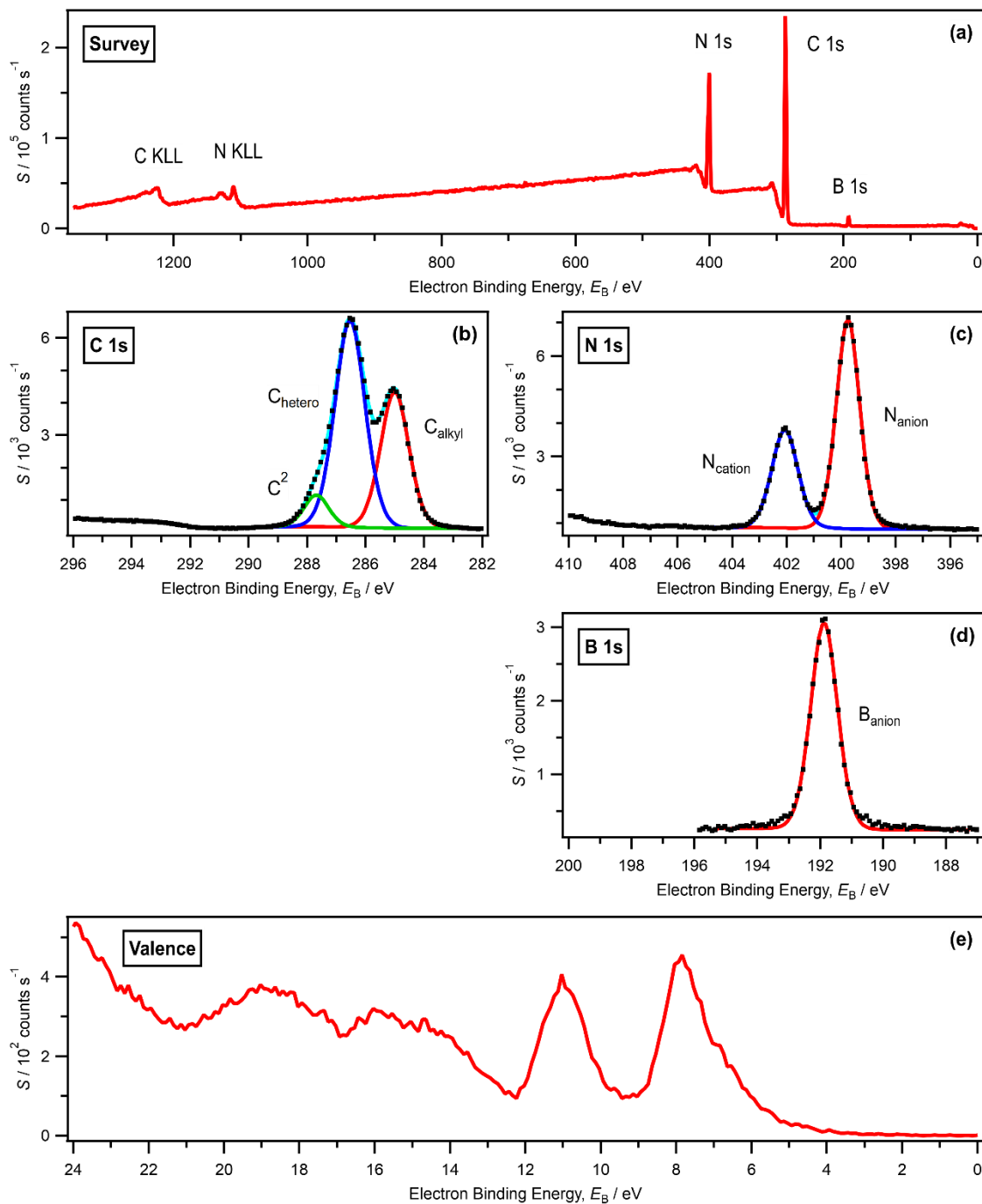


Figure S25. (a) Survey, (b-d) core (with fits) and (e) valence XPS spectra for $[\text{C}_6\text{C}_1\text{Im}][\text{B}(\text{CN})_4]$ recorded on laboratory-based XPS apparatus at $h\nu = 1486.6 \text{ eV}$. All electron spectra were charge referenced using procedures outlined in ESI Section 5.

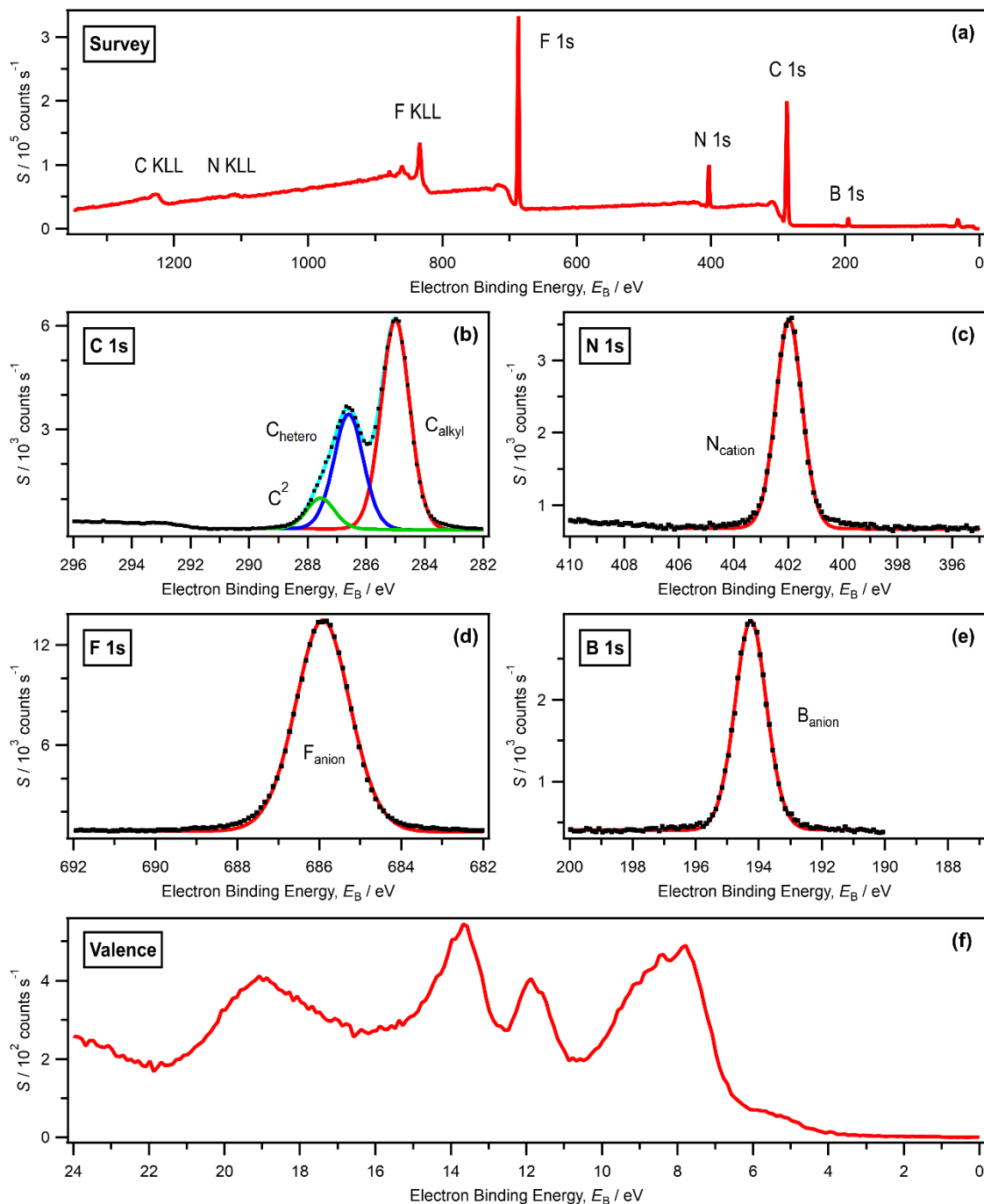


Figure S26. (a) Survey, (b-e) core (with fits) and (f) valence XP spectra for $[\text{C}_8\text{C}_1\text{Im}][\text{BF}_4]$ recorded on laboratory-based XPS apparatus at $h\nu = 1486.6 \text{ eV}$. All electron spectra were charge referenced using procedures outlined in ESI Section 5.

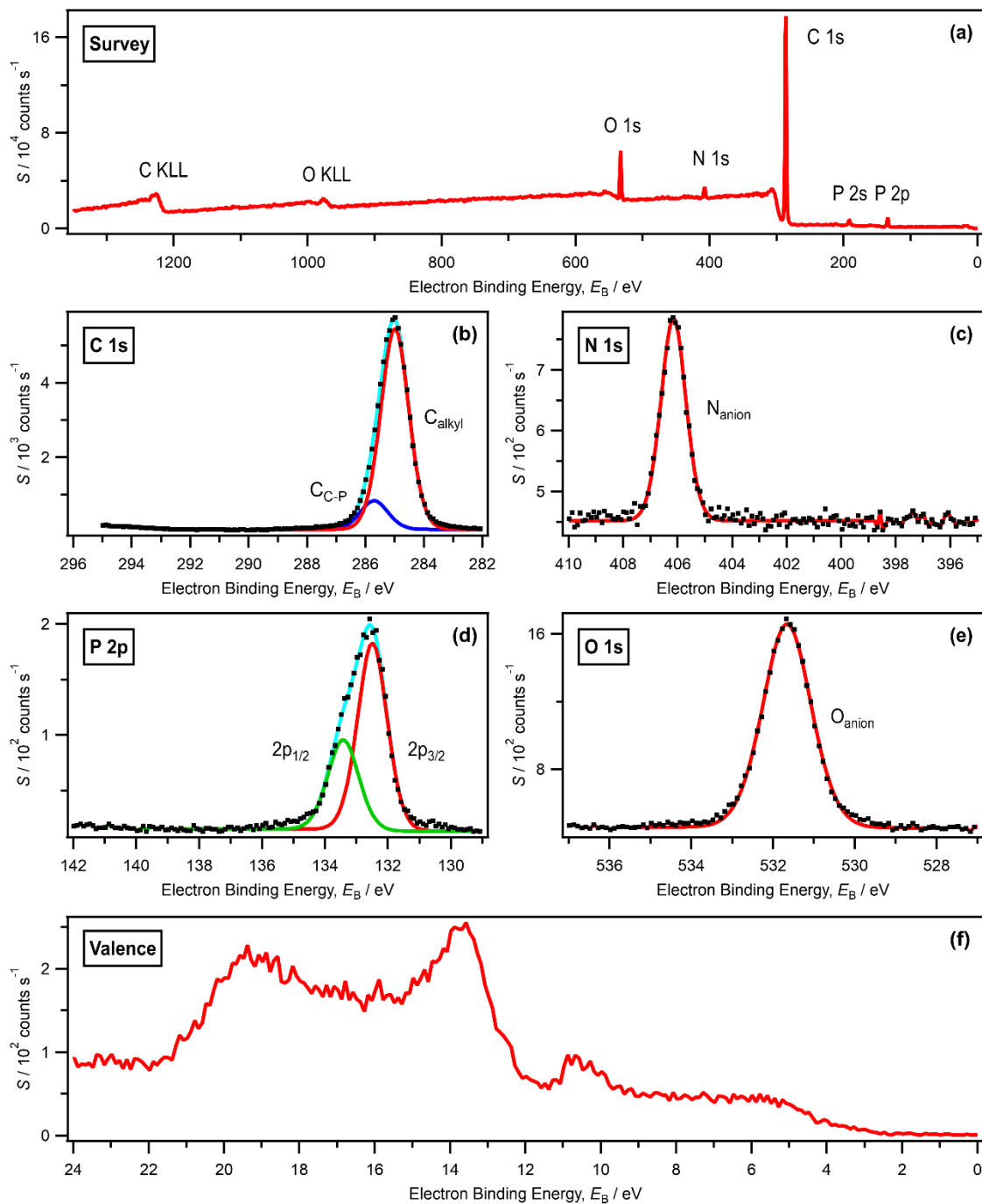


Figure S27. (a) Survey, (b-e) core (with fits) and (f) valence XP spectra for $[P_{6,6,6,14}][NO_3]$ recorded on laboratory-based XPS apparatus at $h\nu = 1486.6$ eV. All electron spectra were charge referenced using procedures outlined in ESI Section 5.

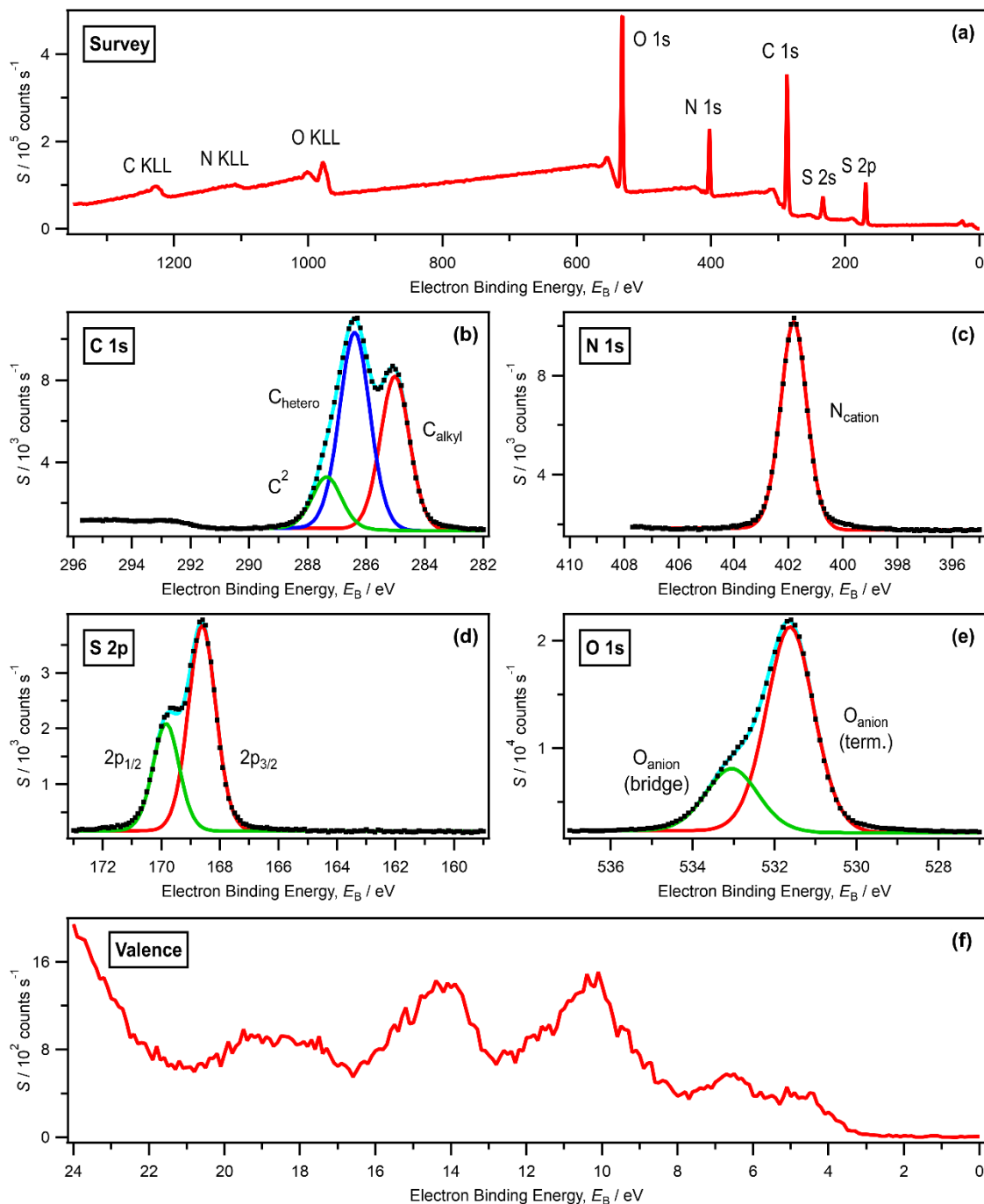


Figure S28. (a) Survey, (b-e) core (with fits) and (f) valence XP spectra for $[C_4C_1Im][HSO_4]$ recorded on laboratory-based XPS apparatus at $h\nu = 1486.6$ eV. All electron spectra were charge referenced using procedures outlined in ESI Section 5.

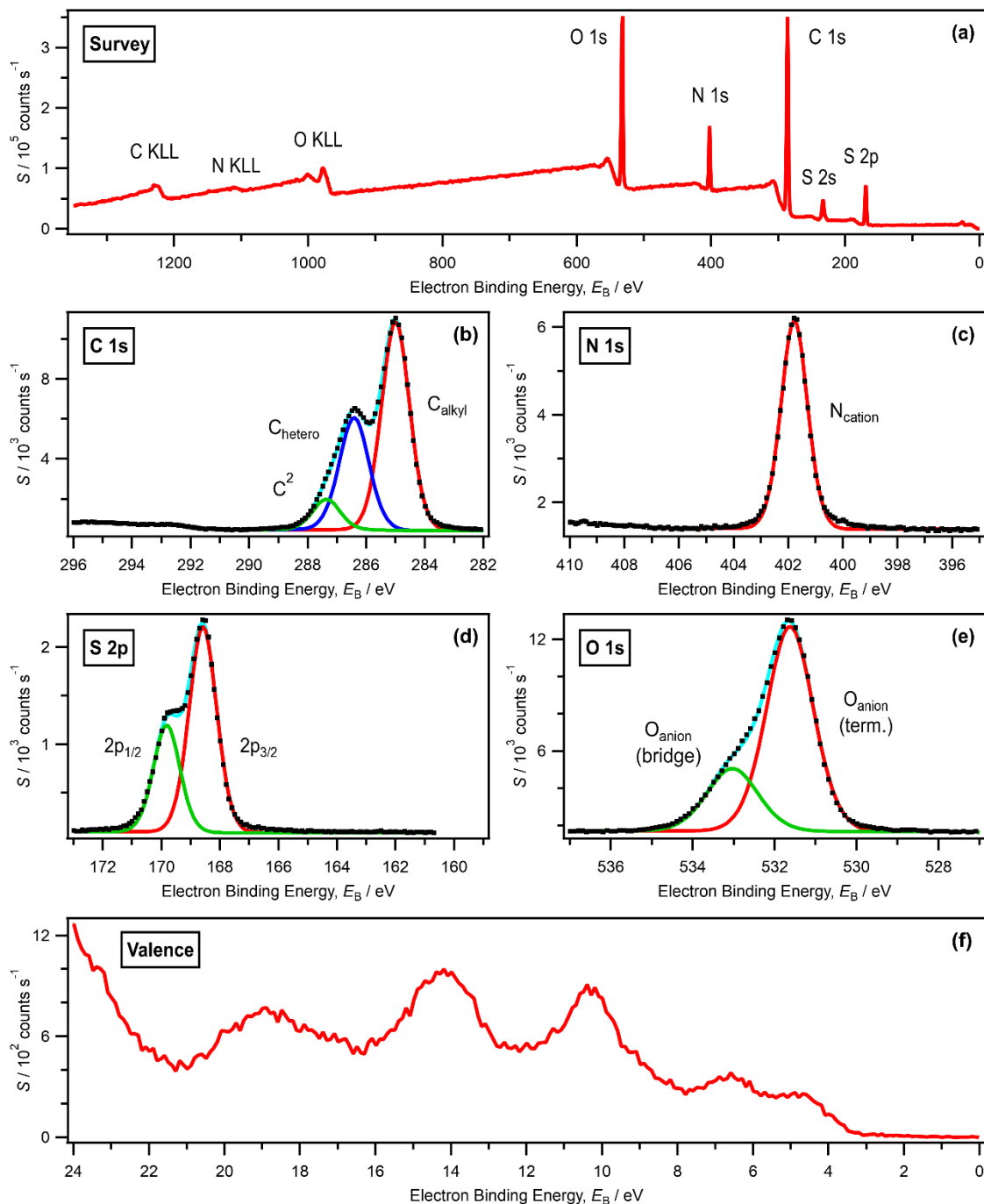


Figure S29. (a) Survey, (b-e) core (with fits) and (f) valence XP spectra for $[C_8C_1Im][HSO_4]$ recorded on laboratory-based XPS apparatus at $h\nu = 1486.6 \text{ eV}$. All electron spectra were charge referenced using procedures outlined in ESI Section 5.

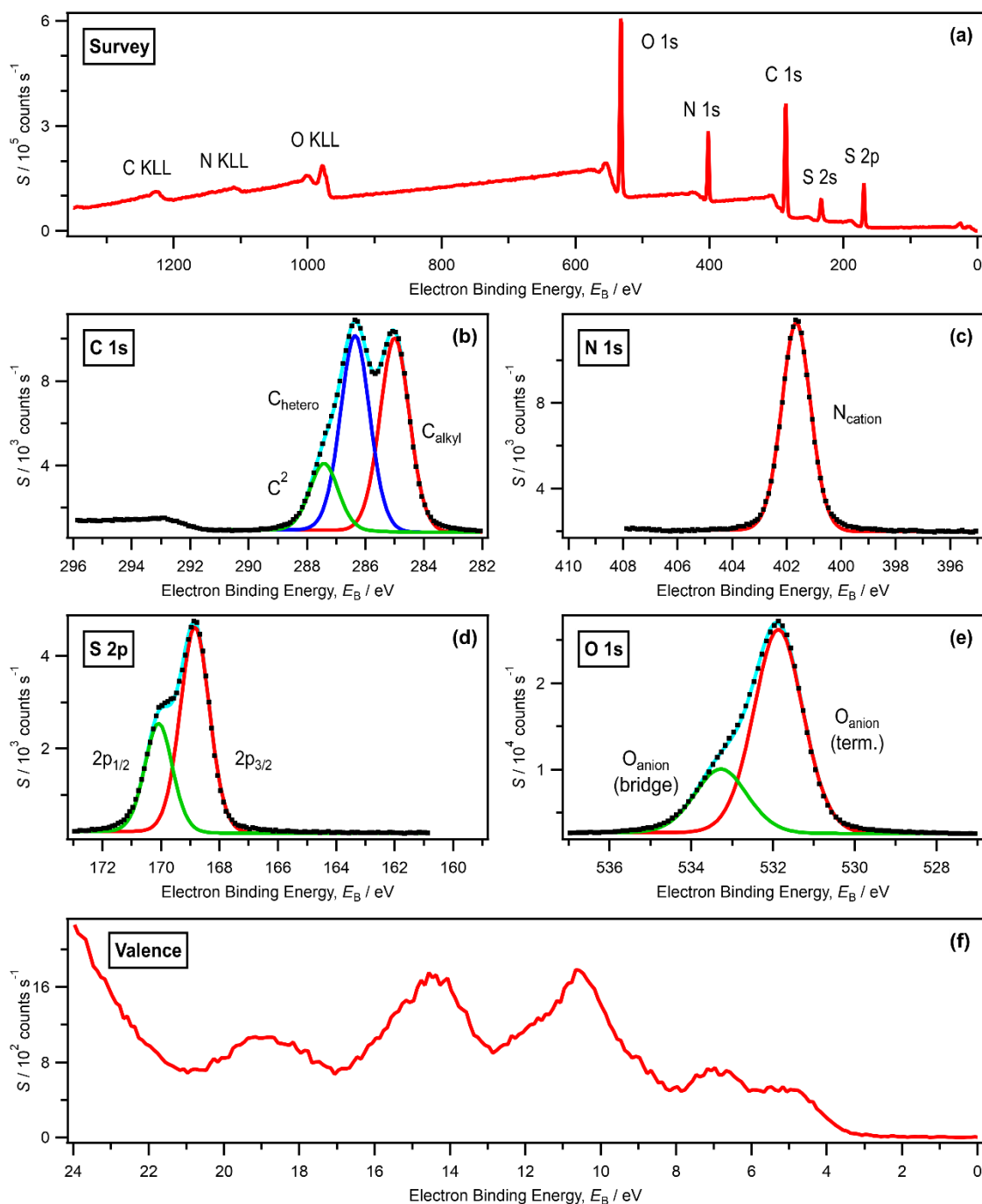


Figure S30. (a) Survey, (b-e) core (with fits) and (f) valence XP spectra for $[C_4C_0Im][HSO_4]$ recorded on laboratory-based XPS apparatus at $h\nu = 1486.6 \text{ eV}$. All electron spectra were charge referenced using procedures outlined in ESI Section 5.

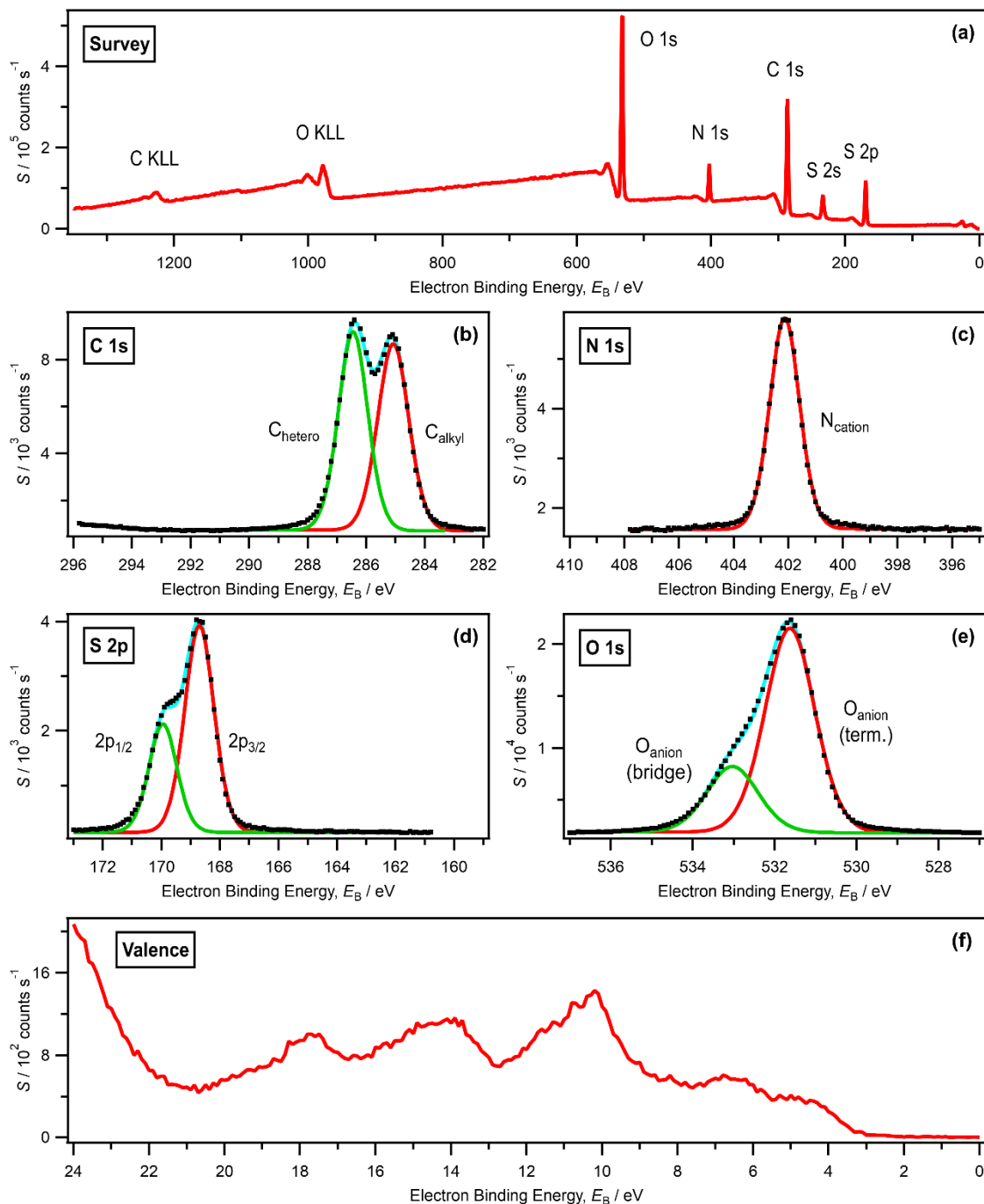


Figure S31. (a) Survey, (b-e) core (with fits) and (f) valence XP spectra for $[N_{4,1,1,0}][HSO_4]$ recorded on laboratory-based XPS apparatus at $h\nu = 1486.6 \text{ eV}$. All electron spectra were charge referenced using procedures outlined in ESI Section 5.

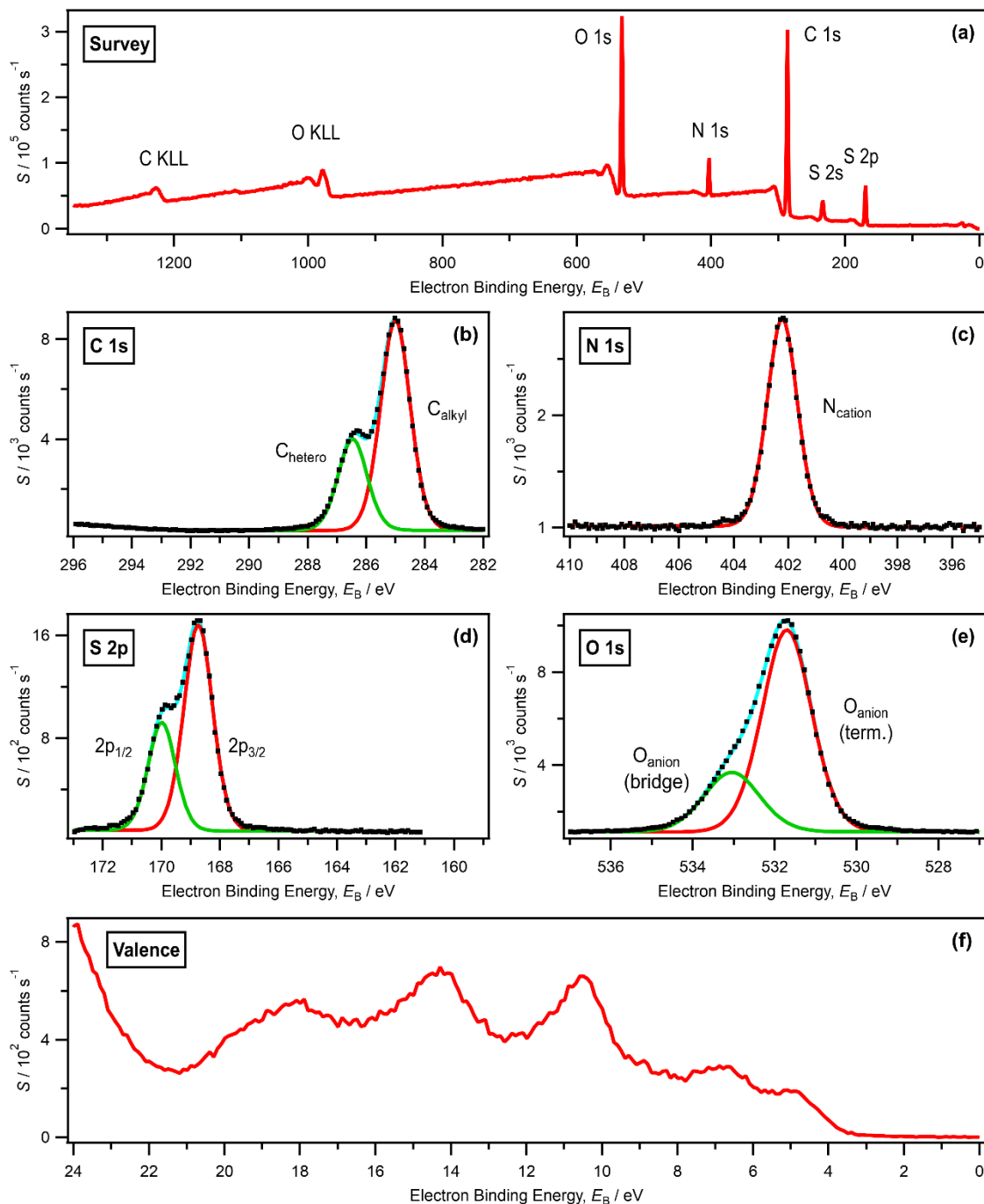


Figure S32. (a) Survey, (b-e) core (with fits) and (f) valence XP spectra for $[N_{8,1,1,0}][HSO_4]$ recorded on laboratory-based XPS apparatus at $h\nu = 1486.6$ eV. All electron spectra were charge referenced using procedures outlined in ESI Section 5.

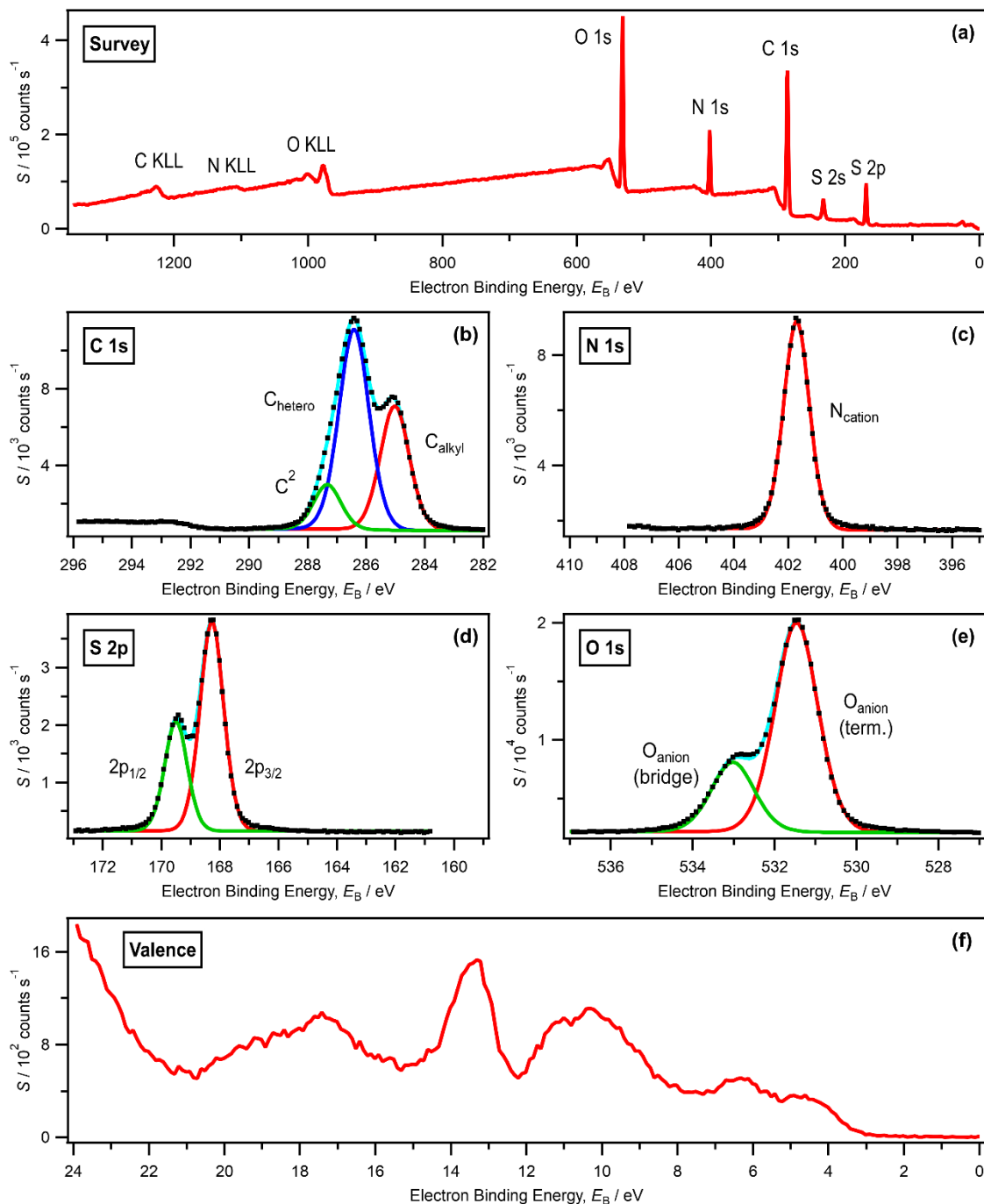


Figure S33. (a) Survey, (b-e) core (with fits) and (f) valence XPS spectra for $[C_4C_1Im][MeSO_4]$ recorded on laboratory-based XPS apparatus at $h\nu = 1486.6$ eV. All electron spectra were charge referenced using procedures outlined in ESI Section 5.

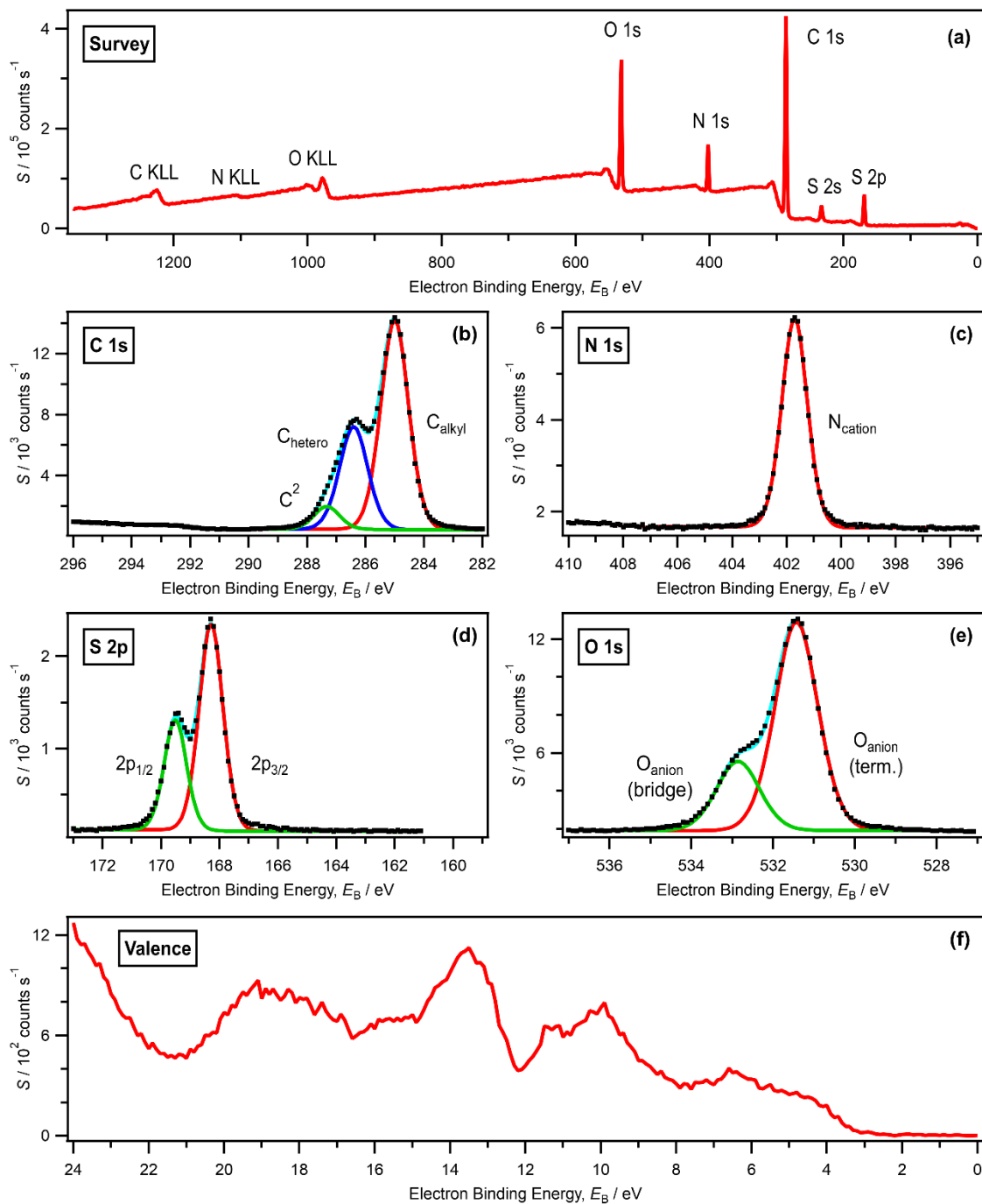


Figure S34. (a) Survey, (b-e) core (with fits) and (f) valence XP spectra for $[C_4C_1Im][OcSO_4]$ recorded on laboratory-based XPS apparatus at $h\nu = 1486.6$ eV. All electron spectra were charge referenced using procedures outlined in ESI Section 5.

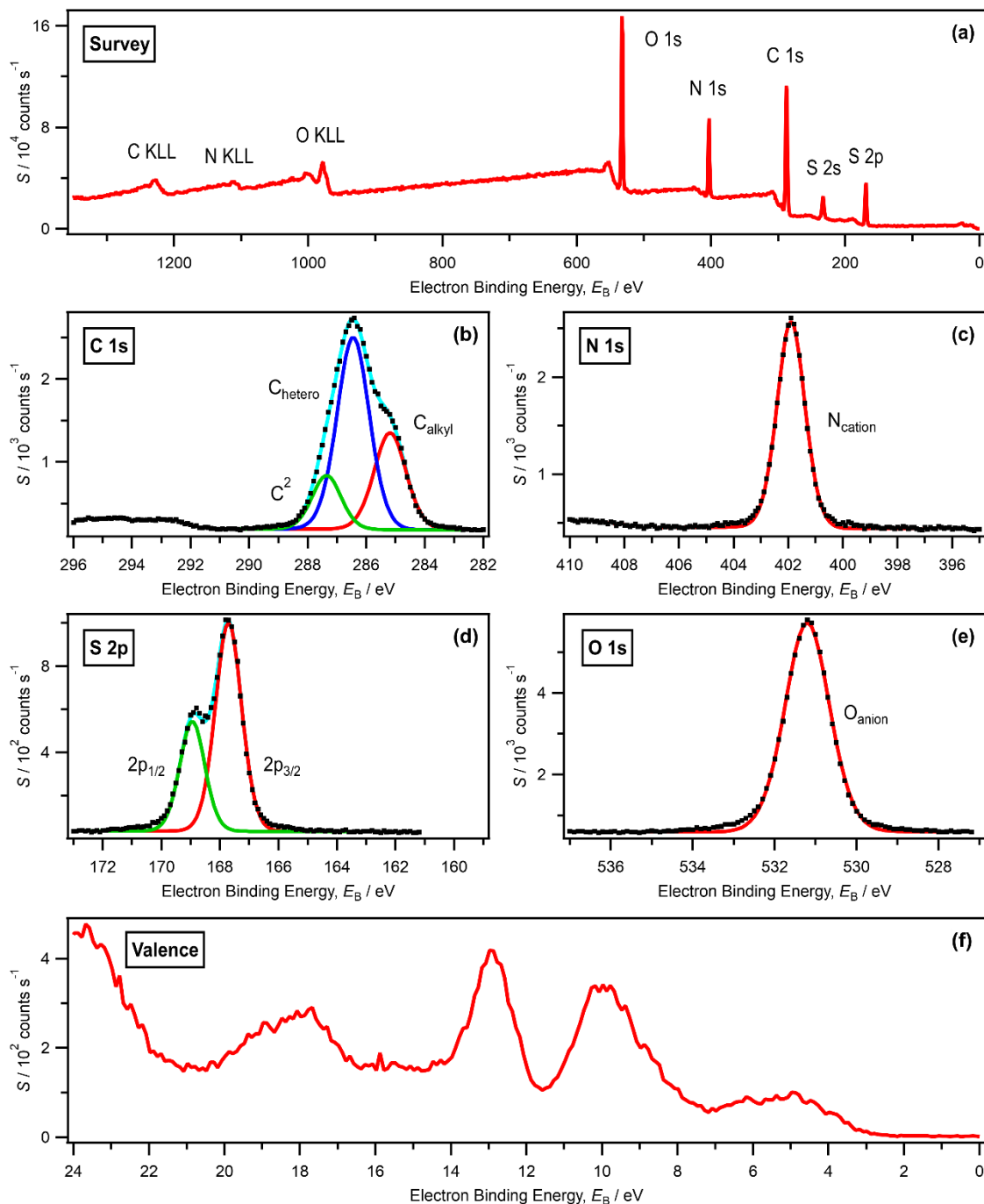


Figure S35. (a) Survey, (b-e) core (with fits) and (f) valence XPS spectra for $[C_2C_1Im][MeSO_3]$ recorded on laboratory-based XPS apparatus at $h\nu = 1486.6$ eV. All electron spectra were charge referenced using procedures outlined in ESI Section 5.

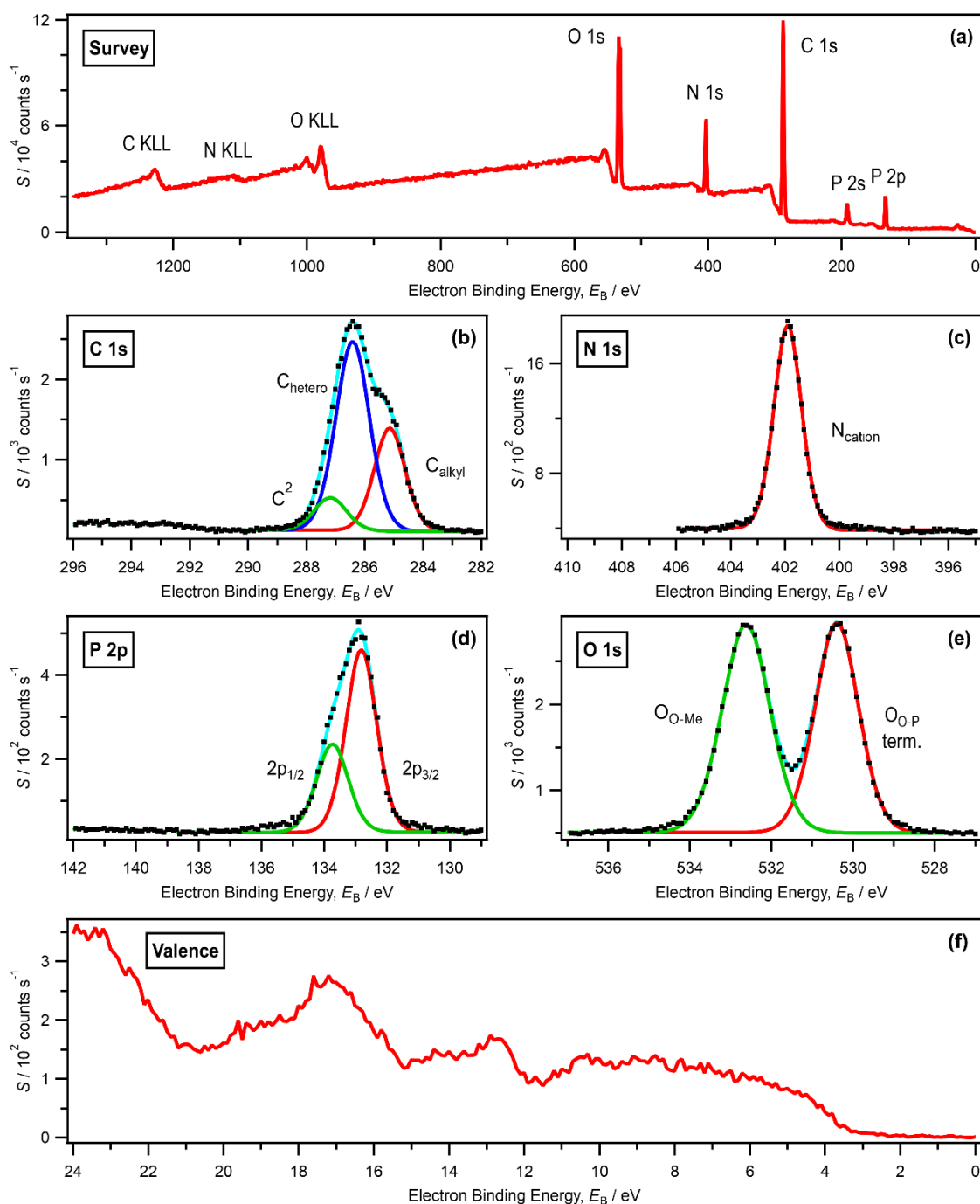


Figure S36. (a) Survey, (b-e) core (with fits) and (f) valence XP spectra for $[\text{C}_4\text{C}_1\text{Im}][\text{Me}_2\text{PO}_4]$ recorded on laboratory-based XPS apparatus at $h\nu = 1486.6 \text{ eV}$. All electron spectra were charge referenced using procedures outlined in ESI Section 5.

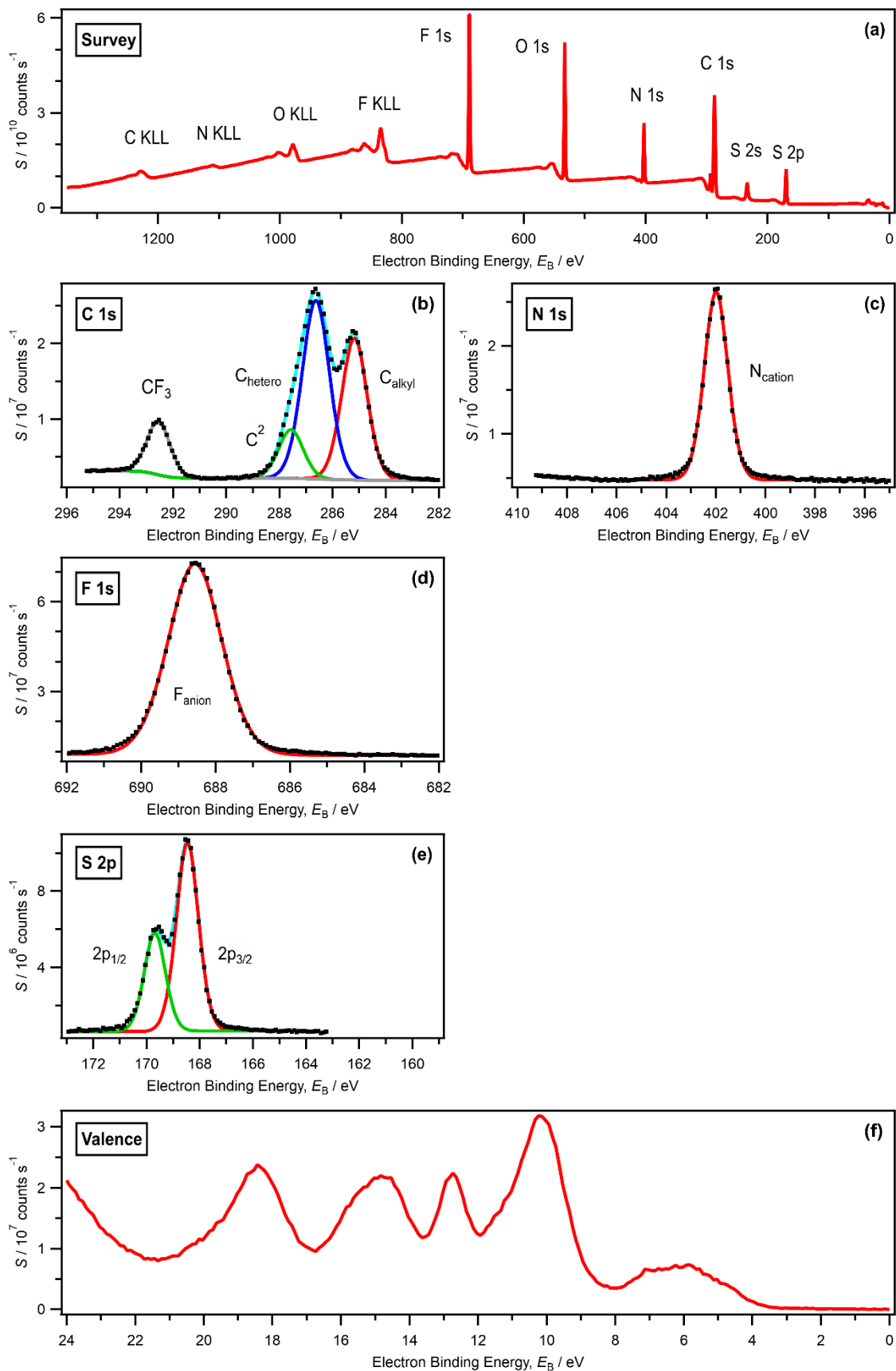


Figure S37. (a) Survey, (b-e) core (with fits) and (f) valence XP spectra for $[C_4C_1Im][TfO]$ recorded on laboratory-based XPS apparatus at $h\nu = 1486.6$ eV. All electron spectra were charge referenced using procedures outlined in ESI Section 5. No O 1s XP spectrum was recorded for this IL.

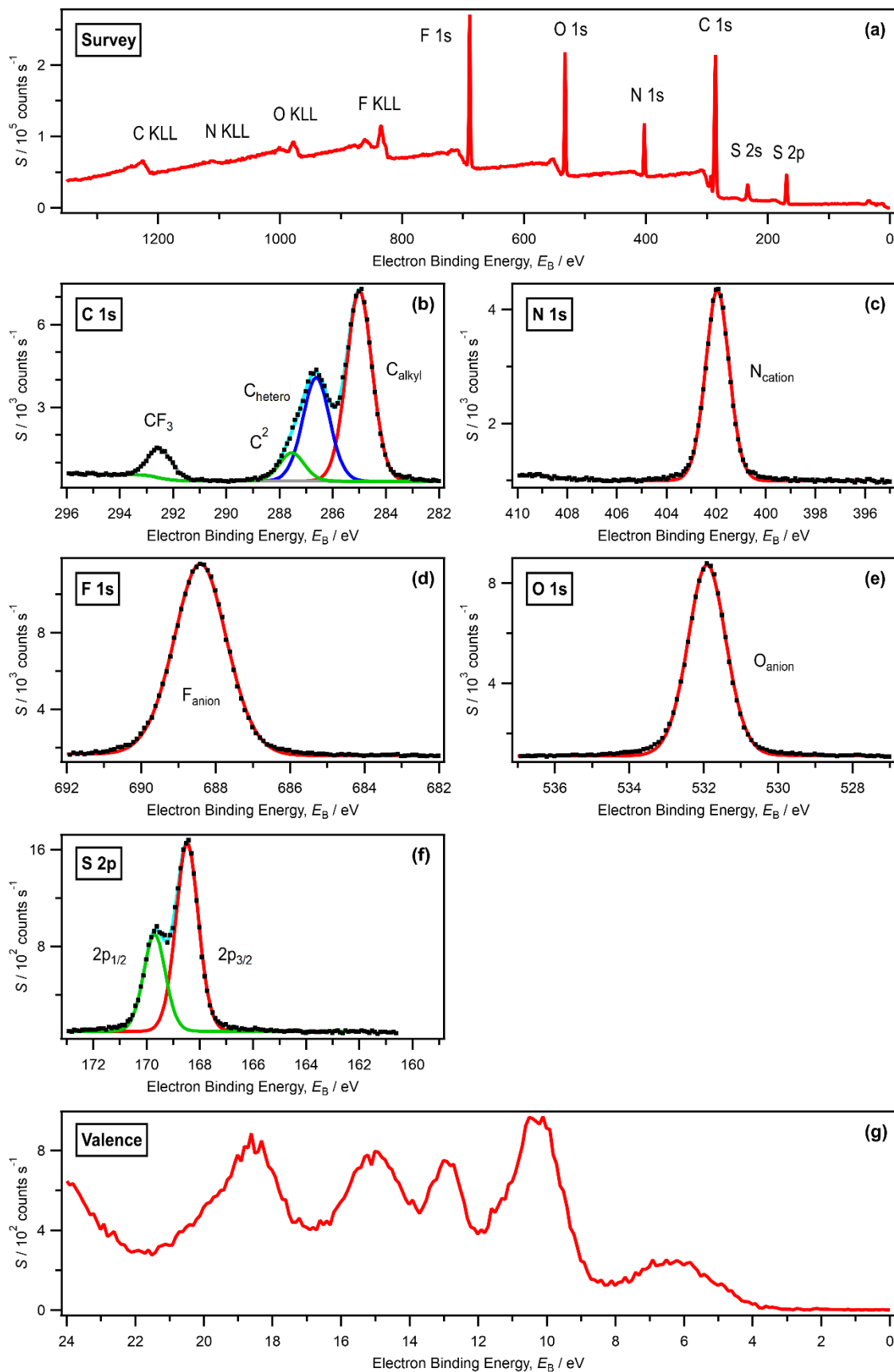


Figure S38. (a) Survey, (b-f) core (with fits) and (g) valence XP spectra for $[\text{C}_8\text{C}_1\text{Im}][\text{TfO}]$ recorded on laboratory-based XPS apparatus at $h\nu = 1486.6$ eV. All electron spectra were charge referenced using procedures outlined in ESI Section 5.

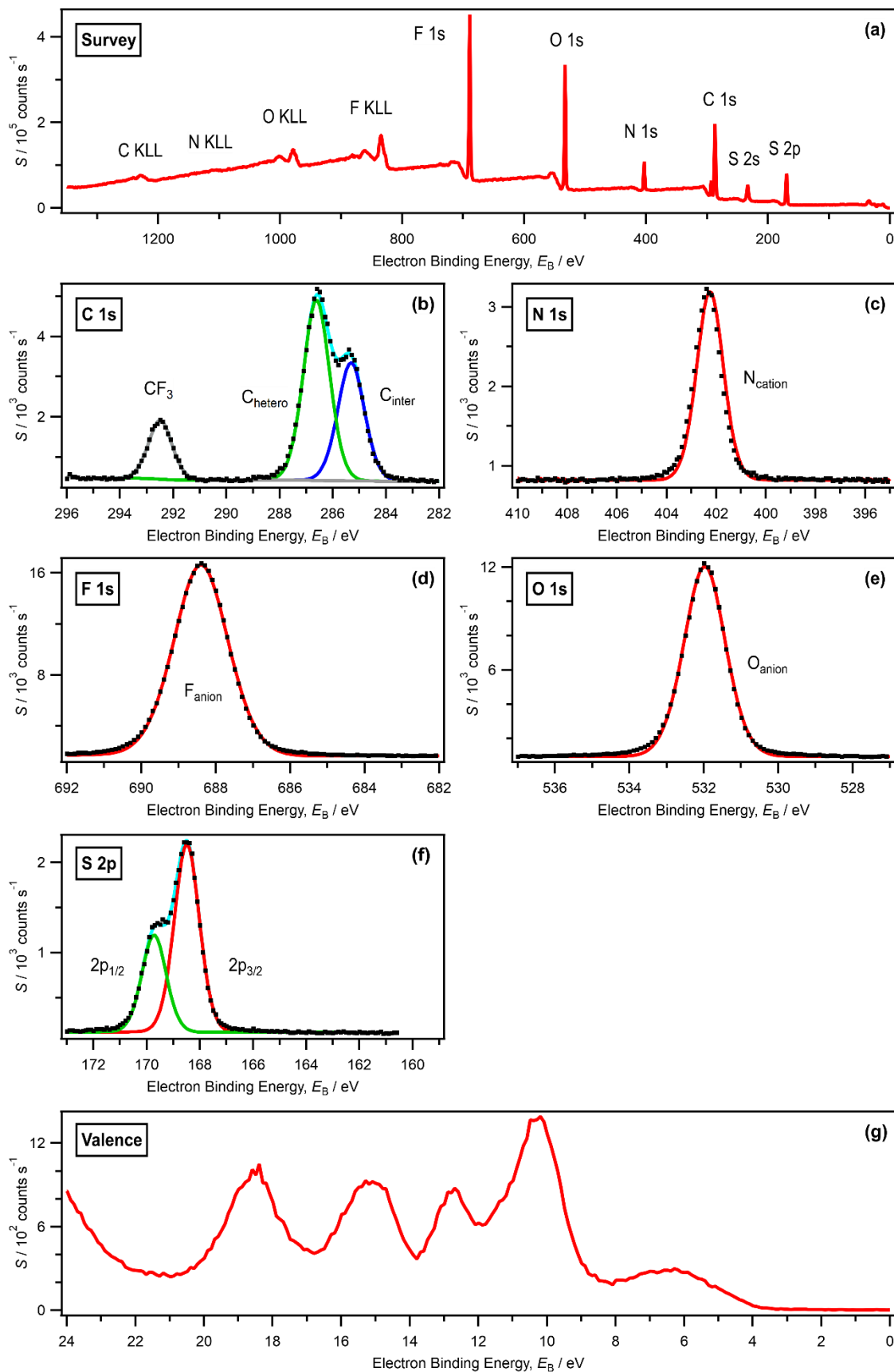


Figure S39. (a) Survey, (b-f) core (with fits) and (g) valence XP spectra for $[N_{2,2,1,0}][TfO]$ recorded on laboratory-based XPS apparatus at $h\nu = 1486.6$ eV. All electron spectra were charge referenced using procedures outlined in ESI Section 5.

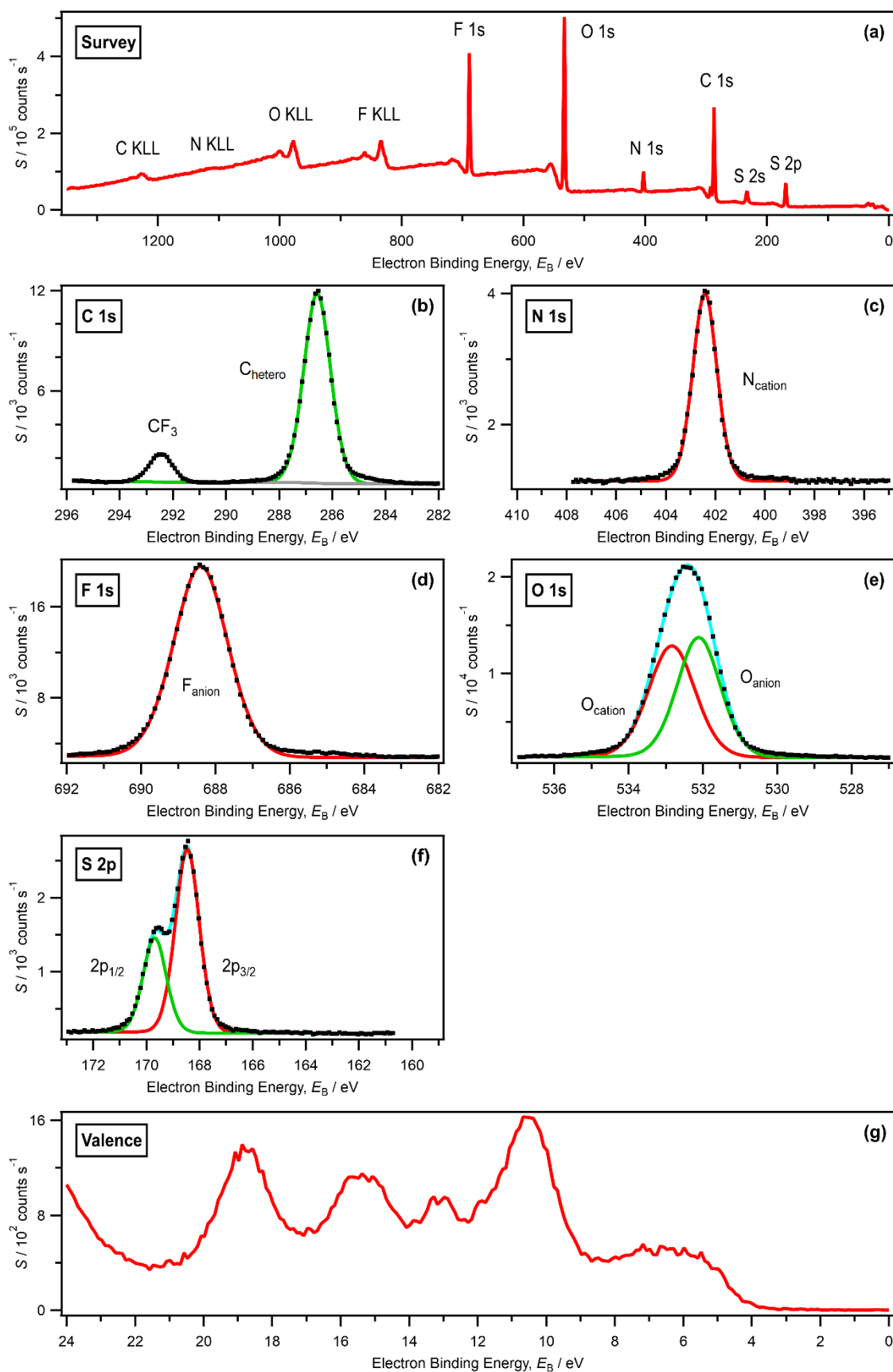


Figure S40. (a) Survey, (b-f) core (with fits) and (g) valence XPS spectra for $[N_{2OH,2OH,2OH,1}][TfO]$ recorded on laboratory-based XPS apparatus at $h\nu = 1486.6$ eV. All electron spectra were charge referenced using procedures outlined in ESI Section 5.

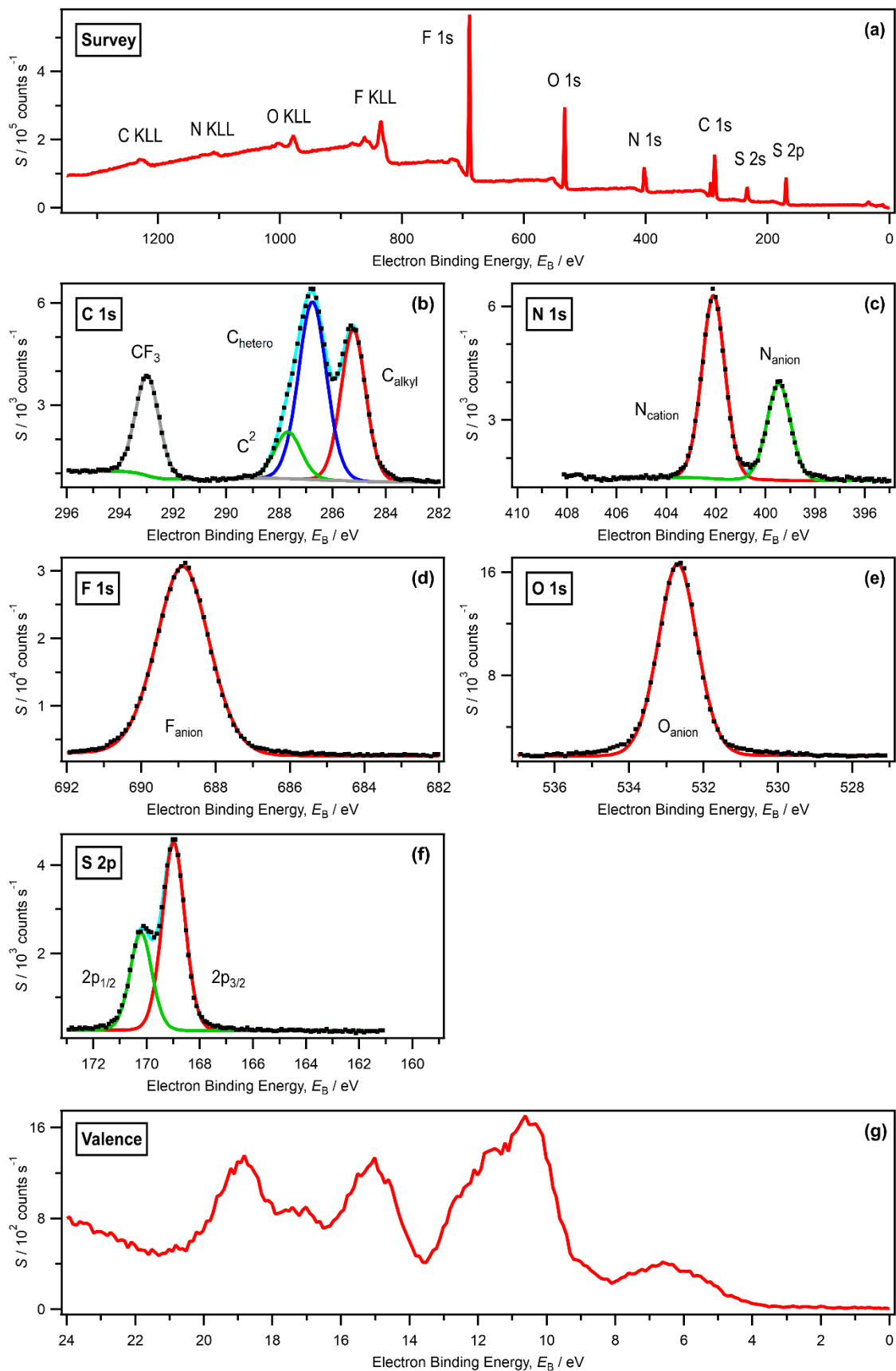


Figure S41. (a) Survey, (b–f) core (with fits) and (g) valence XP spectra for $[\text{C}_4\text{C}_1\text{Im}][\text{NTf}_2]$ recorded on laboratory-based XPS apparatus at $h\nu = 1486.6$ eV. All electron spectra were charge referenced using procedures outlined in ESI Section 5.

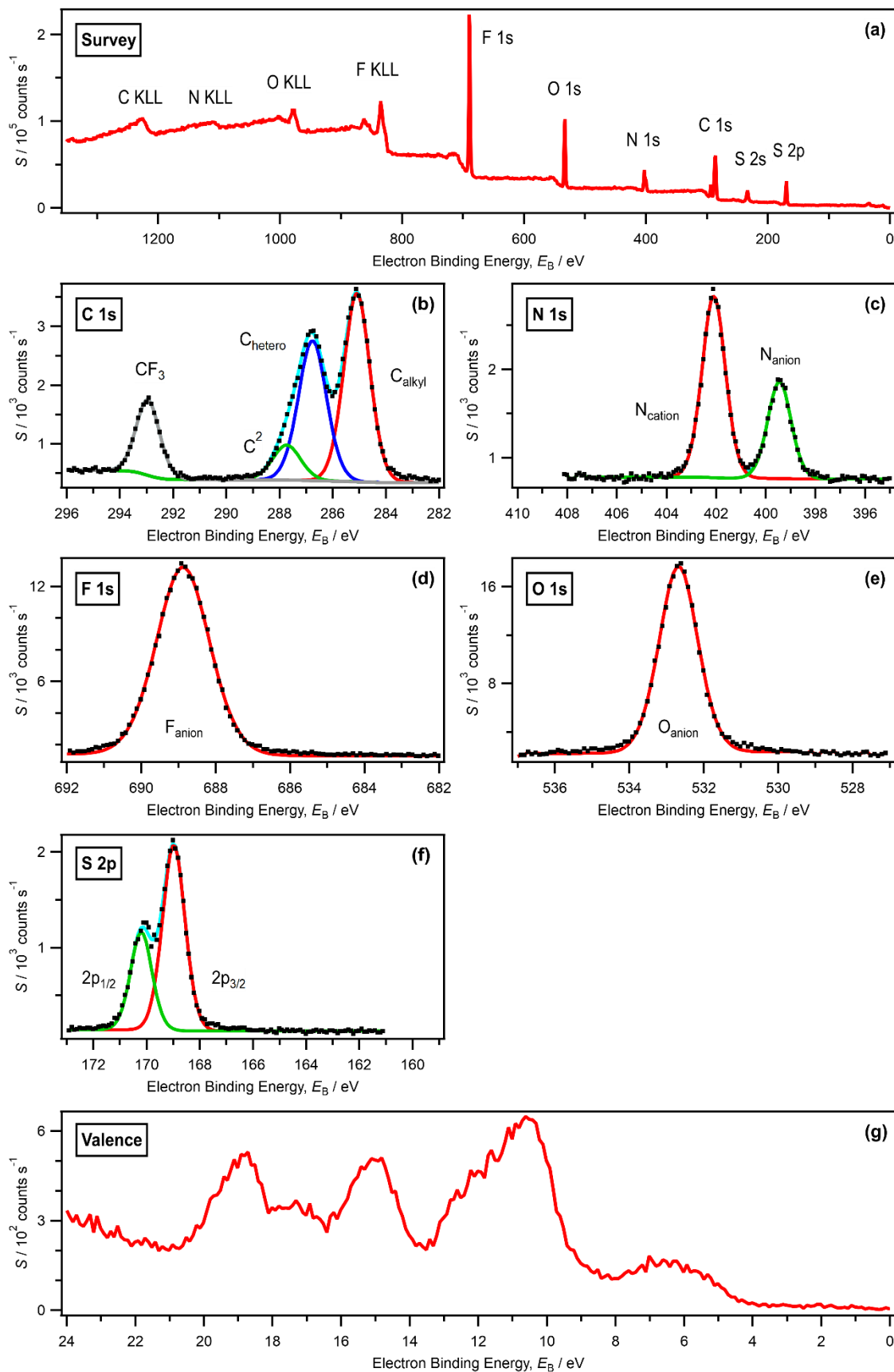


Figure S42. (a) Survey, (b-f) core (with fits) and (g) valence XP spectra for $[\text{C}_6\text{C}_1\text{Im}][\text{NTf}_2]$ recorded on laboratory-based XPS apparatus at $h\nu = 1486.6$ eV. All electron spectra were charge referenced using procedures outlined in ESI Section 5.

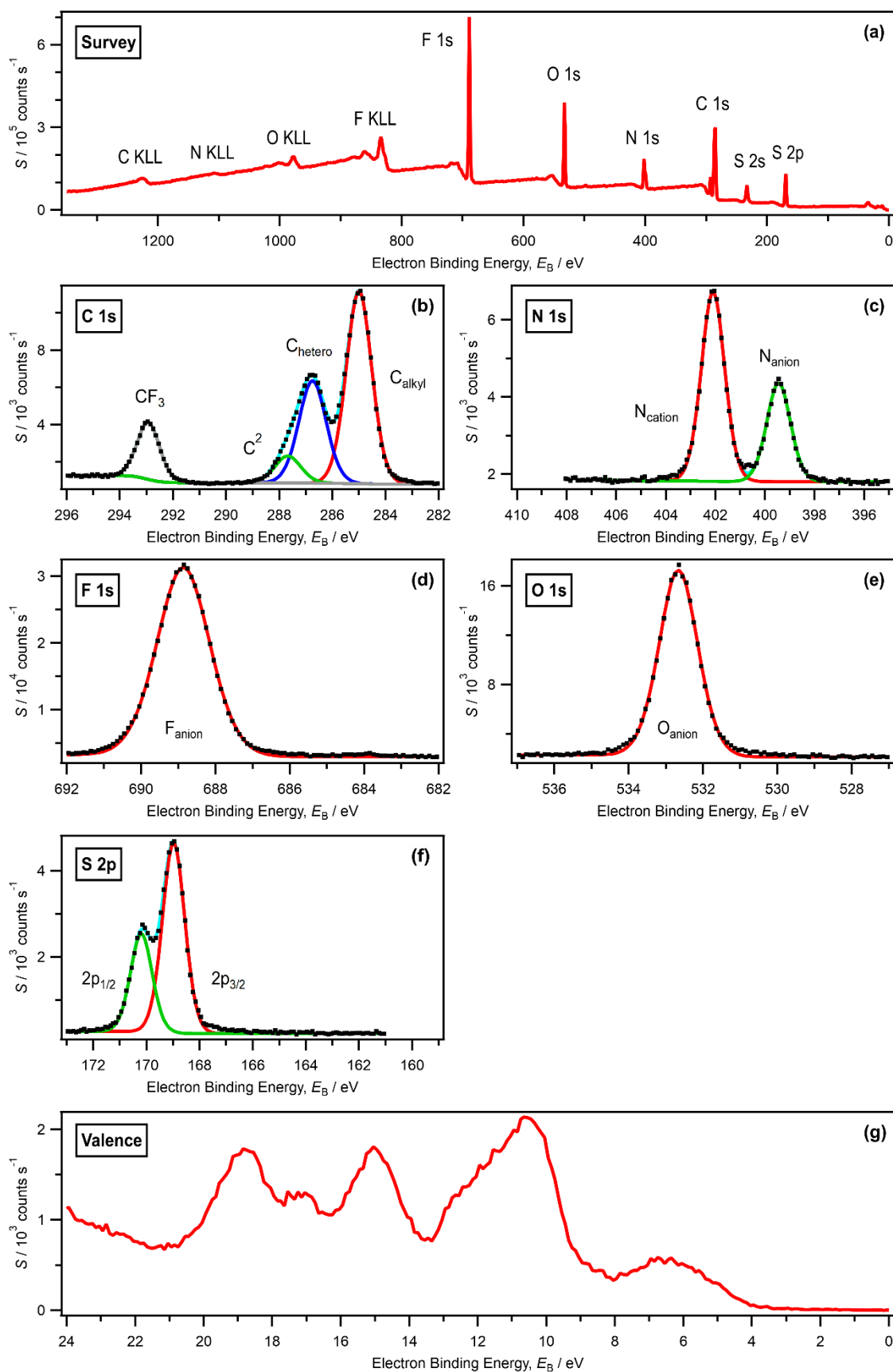


Figure S43. (a) Survey, (b-f) core (with fits) and (g) valence XP spectra for $[\text{C}_8\text{C}_1\text{Im}][\text{NTf}_2]$ recorded on laboratory-based XPS apparatus at $h\nu = 1486.6$ eV. All electron spectra were charge referenced using procedures outlined in ESI Section 5.

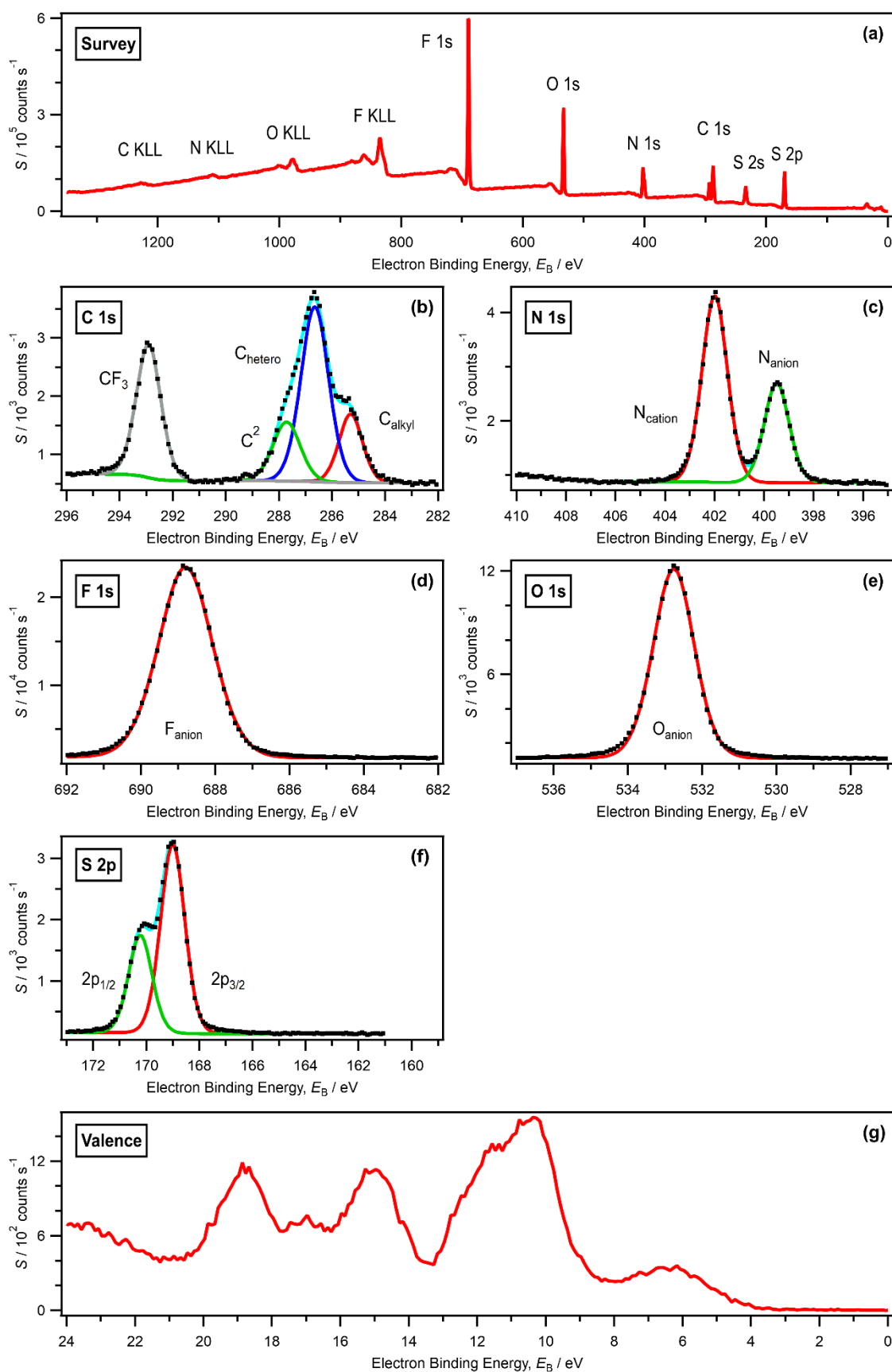


Figure S44. (a) Survey, (b-f) core (with fits) and (g) valence XP spectra for $[\text{C}_2\text{C}_0\text{Im}][\text{NTf}_2]$ recorded on laboratory-based XPS apparatus at $h\nu = 1486.6$ eV. All electron spectra were charge referenced using procedures outlined in ESI Section 5.

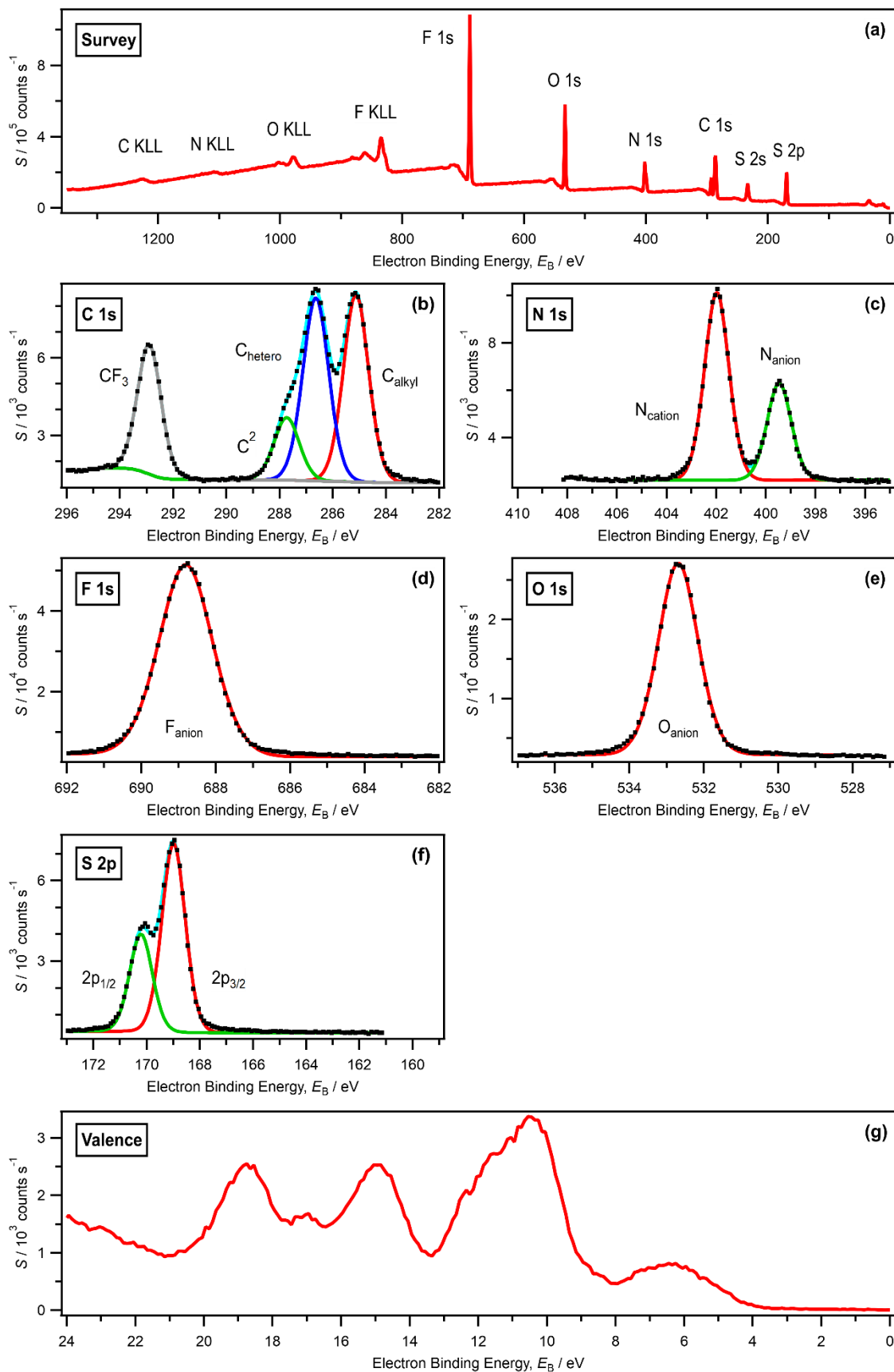


Figure S45. (a) Survey, (b-f) core (with fits) and (g) valence XP spectra for $[C_4C_0Im][NTf_2]$ recorded on laboratory-based XPS apparatus at $h\nu = 1486.6 \text{ eV}$. All electron spectra were charge referenced using procedures outlined in ESI Section 5.

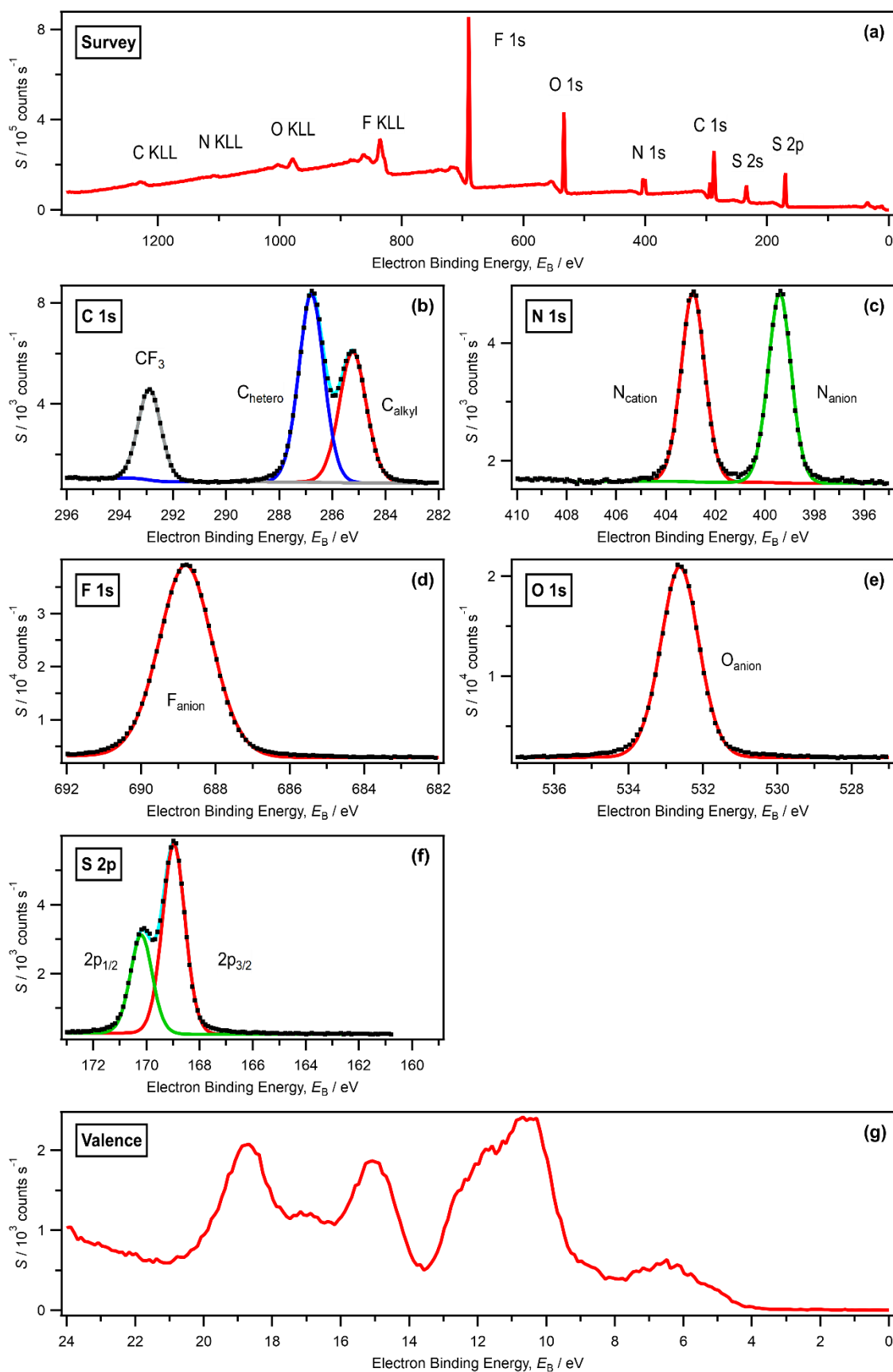


Figure S46. (a) Survey, (b-f) core (with fits) and (g) valence XP spectra for $[N_{4,1,1,1}][NTf_2]$ recorded on laboratory-based XPS apparatus at $h\nu = 1486.6 \text{ eV}$. All electron spectra were charge referenced using procedures outlined in ESI Section 5.

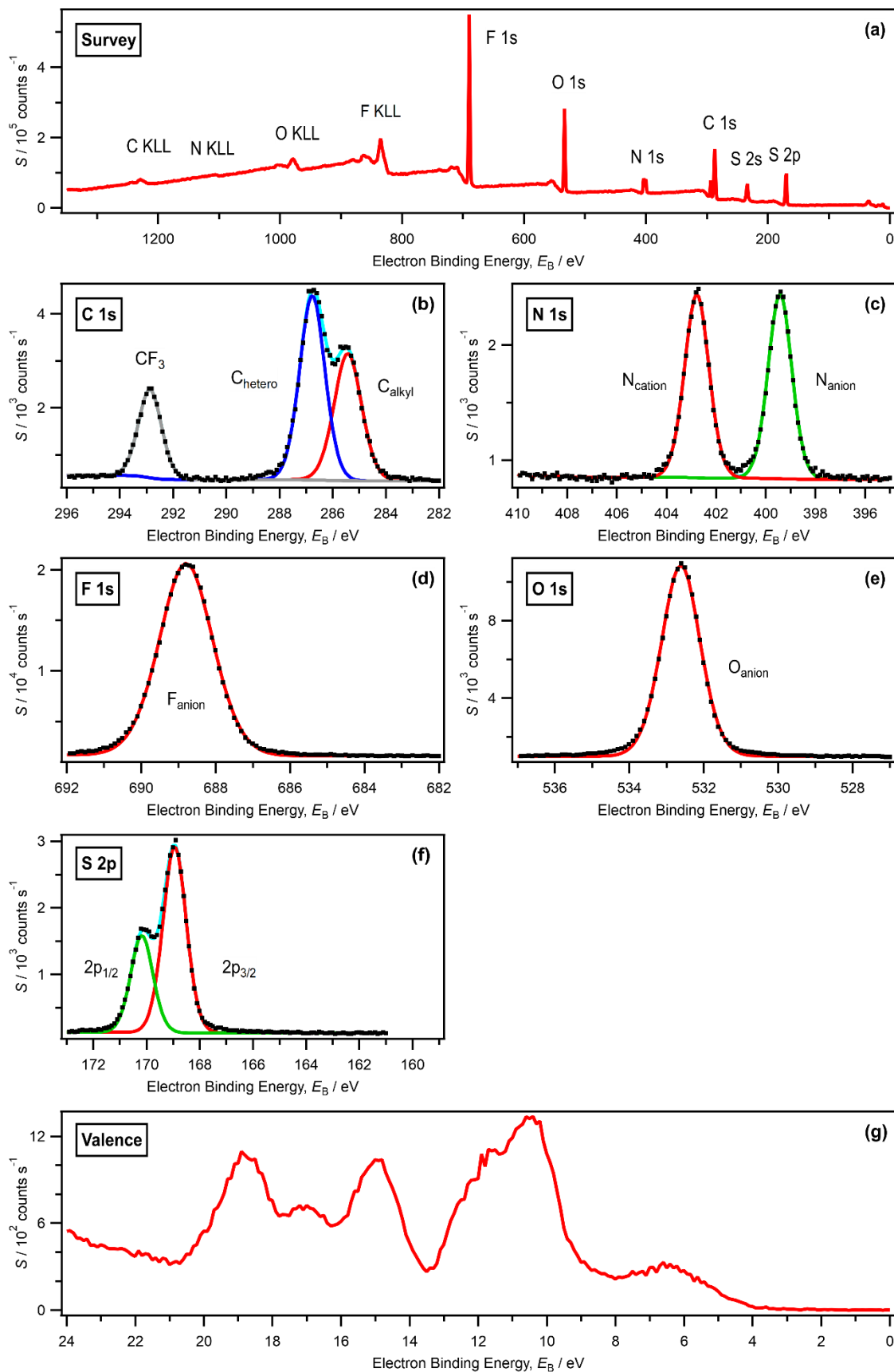


Figure S47. (a) Survey, (b-f) core (with fits) and (g) valence XP spectra for $[N_{3,2,1,1}][NTf_2]$ recorded on laboratory-based XPS apparatus at $h\nu = 1486.6$ eV. All electron spectra were charge referenced using procedures outlined in ESI Section 5.

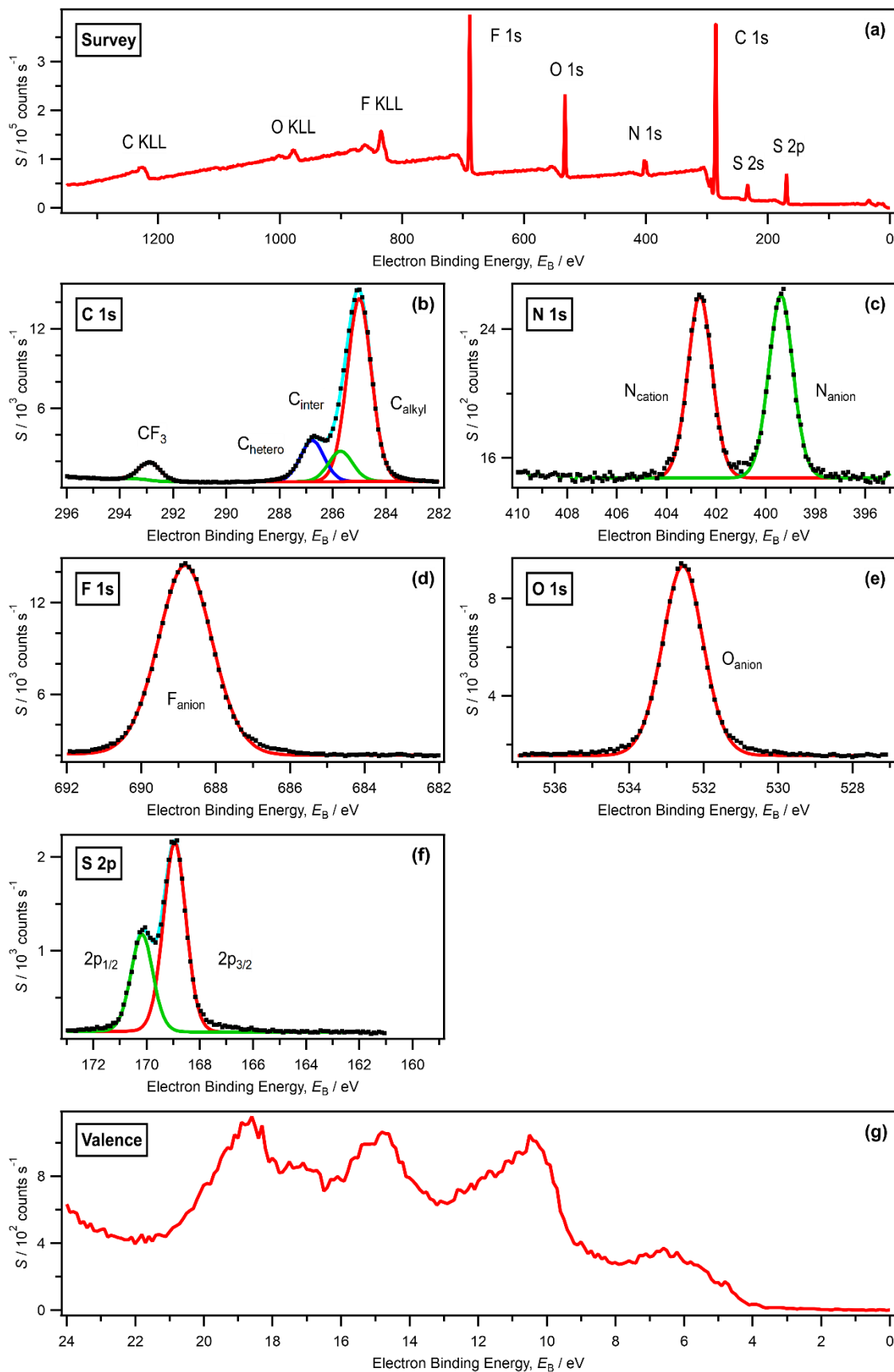


Figure S48. (a) Survey, (b-f) core (with fits) and (g) valence XP spectra for $[N_{8,8,8,1}][NTf_2]$ recorded on laboratory-based XPS apparatus at $h\nu = 1486.6$ eV. All electron spectra were charge referenced using procedures outlined in ESI Section 5.

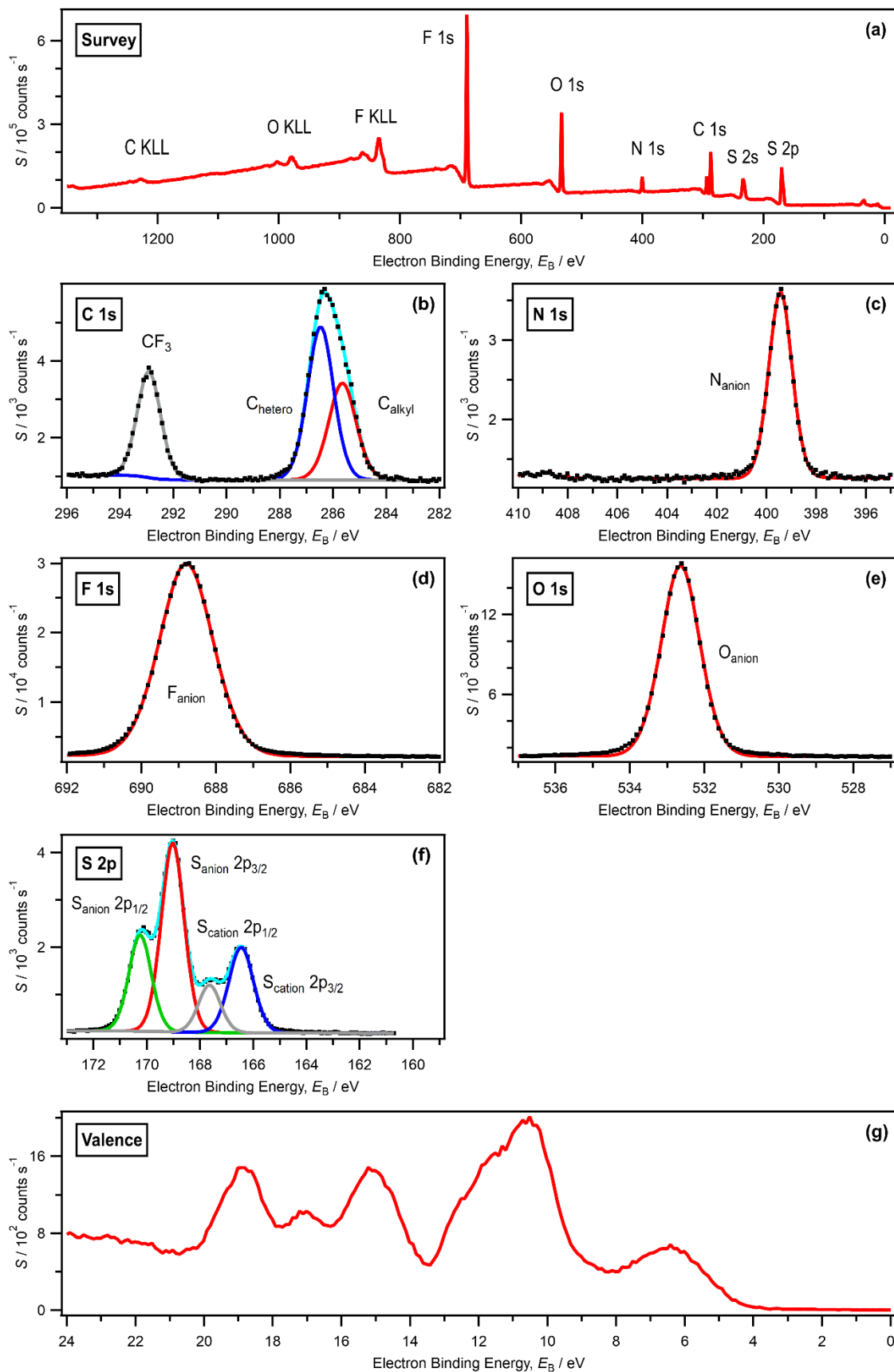


Figure S49. (a) Survey, (b-f) core (with fits) and (g) valence XP spectra for $[S_{2,2,1}][NTf_2]$ recorded on laboratory-based XPS apparatus at $h\nu = 1486.6$ eV. All electron spectra were charge referenced using procedures outlined in ESI Section 5.

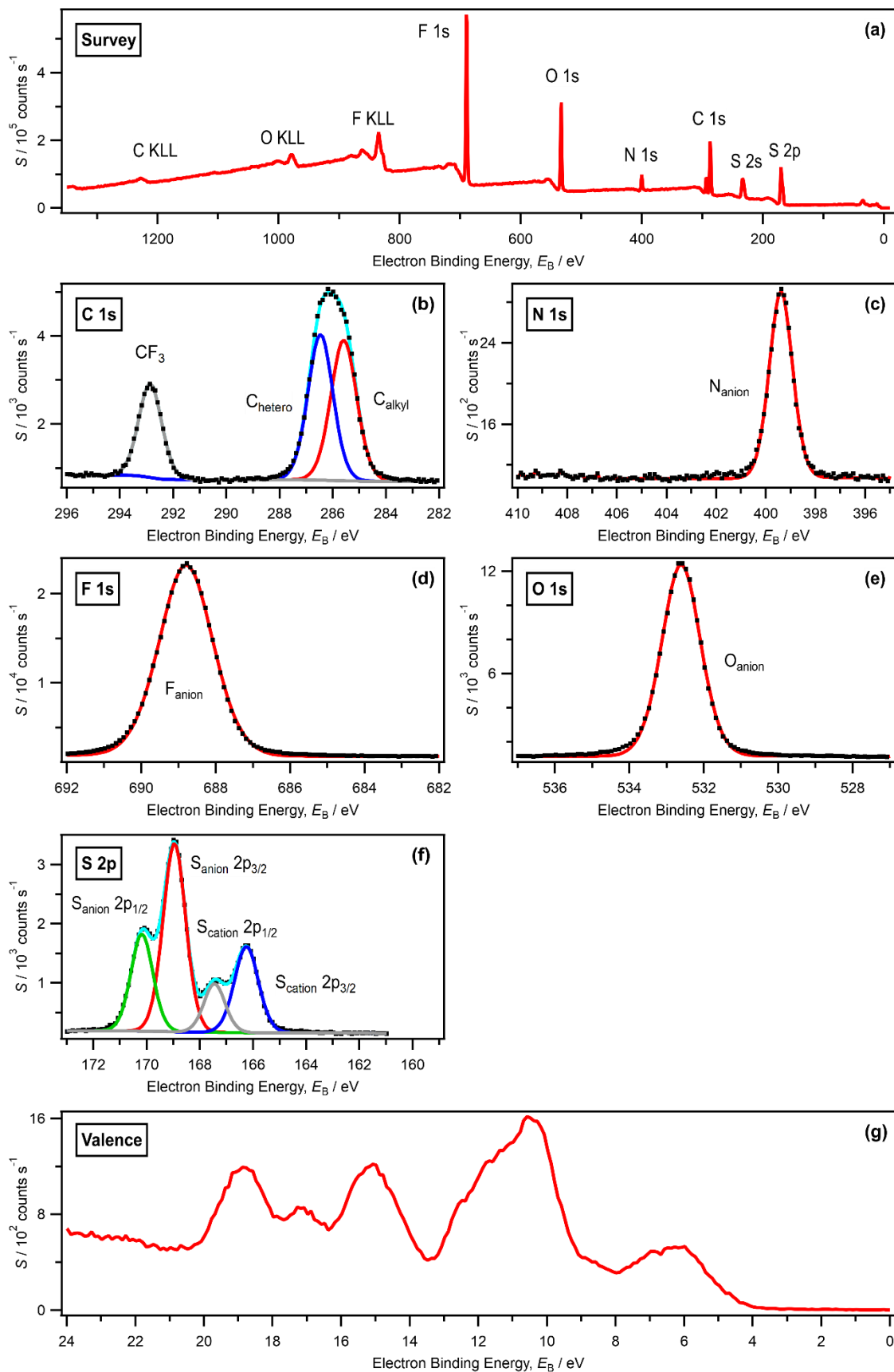


Figure S50. (a) Survey, (b-f) core (with fits) and (g) valence XP spectra for $[S_{2,2,2}][NTf_2]$ recorded on laboratory-based XPS apparatus at $h\nu = 1486.6$ eV. All electron spectra were charge referenced using procedures outlined in ESI Section 5.

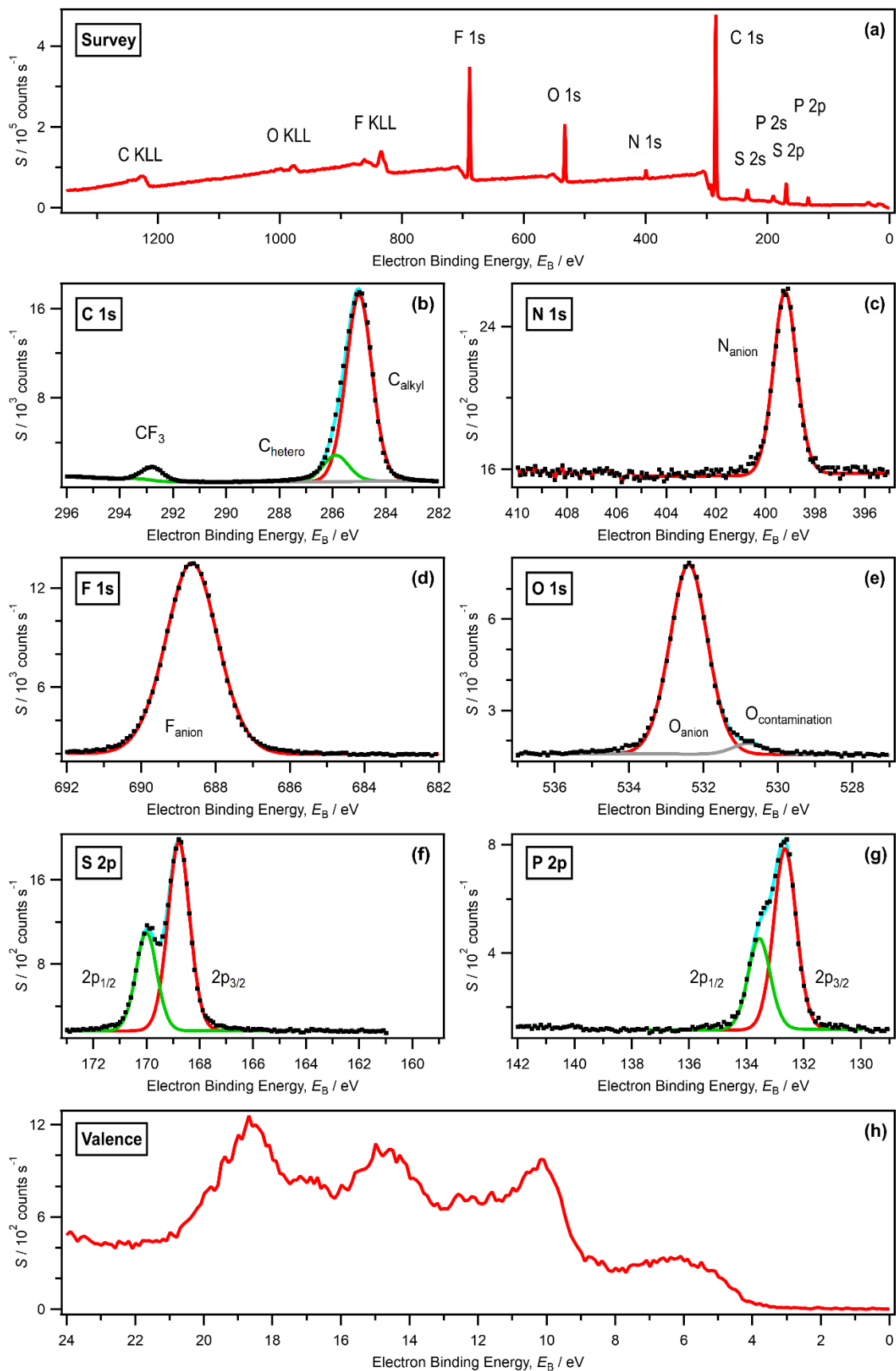


Figure S51. (a) Survey, (b-g) core (with fits) and (h) valence XP spectra for $[P_{6,6,6,14}][NTf_2]$ recorded on laboratory-based XPS apparatus at $h\nu = 1486.6$ eV. All electron spectra were charge referenced using procedures outlined in ESI Section 5.

Table S7. Measured experimental and nominal (in brackets) stoichiometries for the ionic liquids studied in this work, recorded on laboratory-based XPS at $h\nu = 1486.6$ eV.

IL no.	Cation	Anion	RSF ^a	B 1s	C 1s	N 1s	O 1s	F 1s	P 2p	S 2p	Cl 2p	Br 3d	I 4d
				0.115	0.205	0.350	0.580	1.000	0.200 ^b	0.267 ^b	0.367 ^b	0.330 ^c	5.610 ^d
1	[C ₈ C ₁ Im] ⁺	Cl ⁻	Measured (nominal)		12.1 (12)	1.9 (2)					0.9 (1)		
2	[C ₈ C ₁ Im] ⁺	Br ⁻	Measured (nominal)		12.1 (12)	1.9 (2)						1.0 (1)	
3	[C ₆ C ₁ Im] ⁺	I ⁻	Measured (nominal)		10.1 (10)	1.9 (2)							^e (1)
4	[P _{6,6,6,14}] ⁺	Cl ⁻	Measured (nominal)		32.2 (32)				0.9 (1)		0.9 (1)		
5	[P _{6,6,6,14}] ⁺	Br ⁻	Measured (nominal)		32.1 (32)				0.9 (1)			1.0 (1)	
6	[C ₄ C ₁ Im] ⁺	[SCN] ⁻	Measured (nominal)		9.2 (9)	2.8 (3)				1.0 (1)			
7	[C ₈ C ₁ Im] ⁺	[SCN] ⁻	Measured (nominal)		13.3 (13)	2.7 (3)				0.9 (1)			
8	[C ₄ C ₁ Im] ⁺	[N(CN) ₂] ⁻	Measured (nominal)		10.2 (10)	4.8 (5)							
9	[P _{6,6,6,14}] ⁺	[N(CN) ₂] ⁻	Measured (nominal)		34.3 (34)	2.8 (3)			0.9 (1)				
10	[C ₈ C ₁ Im] ⁺	[C(CN) ₃] ⁻	Measured (nominal)		16.4 (16)	4.6 (5)							
11	[C ₆ C ₁ Im] ⁺	[B(CN) ₄] ⁻	Measured (nominal)	0.9 (1)	14.3 (14)	5.9 (6)							
12	[C ₈ C ₁ Im] ⁺	[BF ₄] ⁻	Measured (nominal)	^e (1)	12.0 (12)	1.9 (2)		4.1 (4)					
13	[P _{6,6,6,14}] ⁺	[NO ₃] ⁻	Measured (nominal)		32.3 (32)	1.0 (1)	2.8 (3)		0.9 (1)				
14	[C ₄ C ₁ Im] ⁺	[HSO ₄] ⁻	Measured (nominal)		7.9 (8)	1.9 (2)	4.1 (4)			1.1 (1)			
15	[C ₈ C ₁ Im] ⁺	[HSO ₄] ⁻	Measured (nominal)		11.9 (12)	1.9 (2)	4.1 (4)			1.1 (1)			
16	[C ₄ C ₀ Im] ⁺	[HSO ₄] ⁻	Measured (nominal)		6.8 (7)	1.9 (2)	4.2 (4)			1.1 (1)			
17	[N _{4,1,1,0}] ⁺	[HSO ₄] ⁻	Measured (nominal)		6.1 (6)	0.9 (1)	3.9 (4)			1.0 (1)			
18	[N _{8,1,1,0}] ⁺	[HSO ₄] ⁻	Measured (nominal)		9.9 (10)	1.0 (1)	4.1 (4)			1.0 (1)			
19	[C ₄ C ₁ Im] ⁺	[MeSO ₄] ⁻	Measured (nominal)		8.9 (9)	1.9 (2)	4.1 (4)			1.0 (1)			
20	[C ₄ C ₁ Im] ⁺	[OcSO ₄] ⁻	Measured (nominal)		15.8 (16)	1.9 (2)	4.2 (4)			1.1 (1)			
21	[C ₂ C ₁ Im] ⁺	[MeSO ₃] ⁻	Measured (nominal)		6.9 (7)	2.0 (2)	3.1 (3)			1.0 (1)			
22	[C ₄ C ₁ Im] ⁺	[Me ₂ PO ₄] ⁻	Measured (nominal)		9.9 (10)	1.9 (2)	4.2 (4)		1.0 (1)				
23	[C ₄ C ₁ Im] ⁺	[TfO] ⁻	Measured (nominal)		8.9 (9)	1.9 (2)	^f (3)	3.1 (3)		1.0 (1)			
24	[C ₈ C ₁ Im] ⁺	[TfO] ⁻	Measured (nominal)		13.0 (13)	2.0 (2)	2.9 (3)	3.1 (3)		1.1 (1)			
25	[N _{2,2,1,0}] ⁺	[TfO] ⁻	Measured (nominal)		5.9 (6)	1.0 (1)	3.0 (3)	3.1 (3)		1.0 (1)			
26	[N _{2OH,2OH,2OH,1}] ⁺	[TfO] ⁻	Measured (nominal)		7.8 (8)	1.0 (1)	6.2 (6)	3.0 (3)		1.0 (1)			
27	[C ₄ C ₁ Im] ⁺	[NTf ₂] ⁻	Measured (nominal)		10.0 (10)	3.0 (3)	4.0 (4)	6.1 (6)		2.1 (2)			
28	[C ₆ C ₁ Im] ⁺	[NTf ₂] ⁻	Measured (nominal)		12.3 (12)	2.9 (3)	3.9 (4)	5.8 (6)		2.1 (2)			
29	[C ₈ C ₁ Im] ⁺	[NTf ₂] ⁻	Measured (nominal)		14.0 (14)	3.0 (3)	4.0 (4)	6.0 (6)		2.0 (2)			
30	[C ₂ C ₀ Im] ⁺	[NTf ₂] ⁻	Measured (nominal)		6.9 (7)	3.0 (3)	4.0 (4)	6.1 (6)		2.0 (2)			
31	[C ₄ C ₀ Im] ⁺	[NTf ₂] ⁻	Measured (nominal)		8.9 (9)	3.0 (3)	4.0 (4)	6.1 (6)		2.1 (2)			
32	[N _{4,1,1,1}] ⁺	[NTf ₂] ⁻	Measured (nominal)		8.8 (9)	2.0 (2)	4.0 (4)	6.1 (6)		2.1 (2)			
33	[N _{3,2,1,1}] ⁺	[NTf ₂] ⁻	Measured (nominal)		8.9 (9)	2.0 (2)	3.9 (4)	6.1 (6)		2.1 (2)			
34	[N _{8,8,8,1}] ⁺	[NTf ₂] ⁻	Measured (nominal)		27.2 (27)	1.9 (2)	4.4 (4)	5.5 (6)		1.9 (2)			
35	[S _{2,2,1}] ⁺	[NTf ₂] ⁻	Measured (nominal)		6.8 (7)	1.0 (1)	4.0 (4)	6.2 (6)		2.0 (2)			
36	[S _{2,2,2}] ⁺	[NTf ₂] ⁻	Measured (nominal)		7.9 (8)	1.0 (1)	4.0 (4)	6.1 (6)		2.0 (2)			
37	[P _{6,6,6,14}] ⁺	[NTf ₂] ⁻	Measured (nominal)		34.3 (34)	1.0 (1)	3.9 (4)	5.8 (6)	0.9 (1)	2.0 (2)			

^a RSF = relative sensitivity factors, taken from reference ⁴⁰

^b The RSFs for Cl 2p, S 2p and P 2p refer to the 2p_{3/2} orbital only.

^c The RSF for Br 3d refers to the 3d_{5/2} orbital only.

^d The RSF for I 4d refers to the 4d_{5/2} orbital only.

^e For [C₈C₁Im][BF₄] and [C₆C₁Im]I the B 1s and I 3d regions were recorded with pass energy = 50 eV, respectively; hence, no experimental stoichiometries are given for these regions.

^f For [C₄C₁Im][TfO] no O 1s region was recorded; hence, no experimental stoichiometry is given for this region.

The measured experimental and nominal stoichiometries (ESI Table S7) match very well for all 37 ILs investigated here. This match, along with the high quality XP spectra given in ESI Figure S15 to ESI Figure S51, demonstrates the high purity of the IL samples presented here; [C₈C₁Im]Br showed a small amount of impurity in the N 1s XP spectrum caused by damage to the sample by X-ray irradiation (ESI Figure S16c).

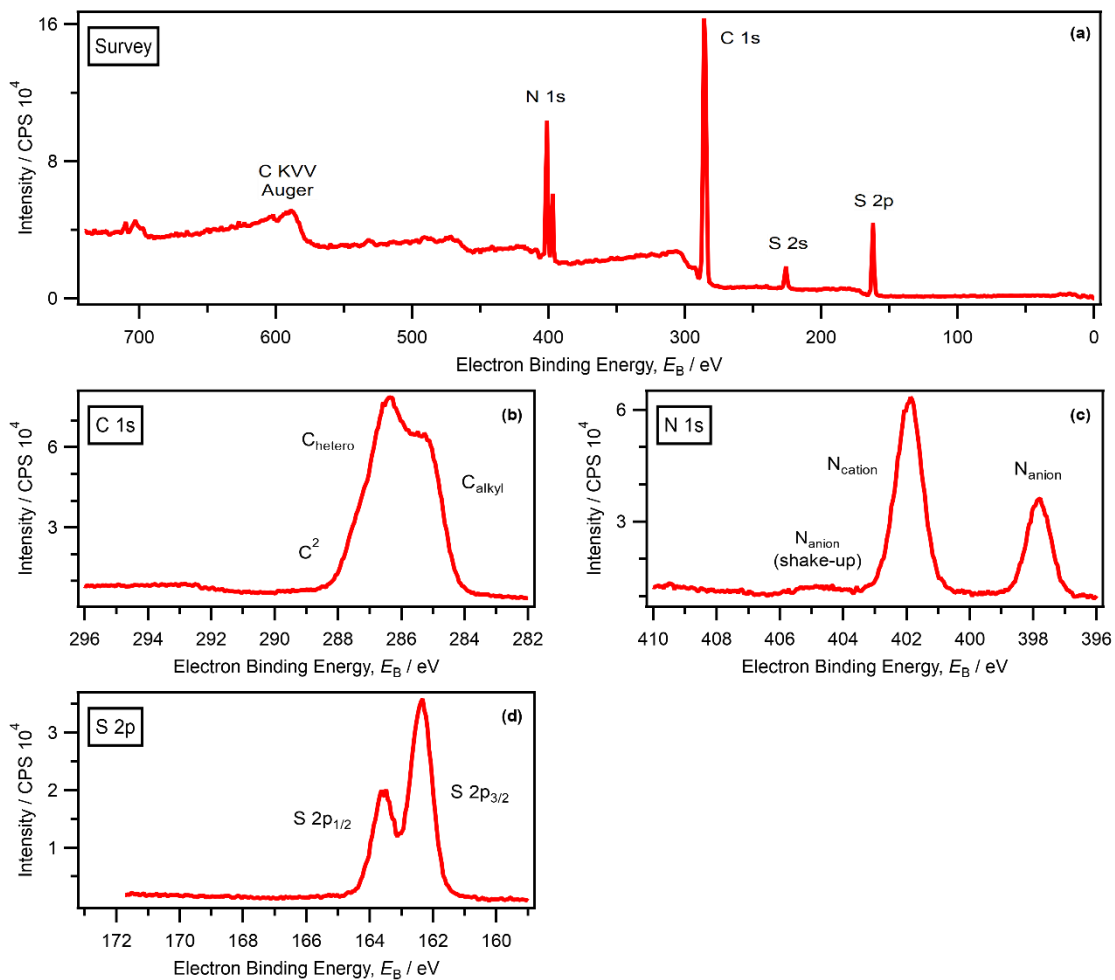


Figure S52. a) Survey and b-d) core level XP spectra for $[C_4C_1Im][SCN]$ recorded on synchrotron-based XPS at $h\nu = 850$ eV. All electron spectra were charge referenced using procedures outlined in ESI Section 5.

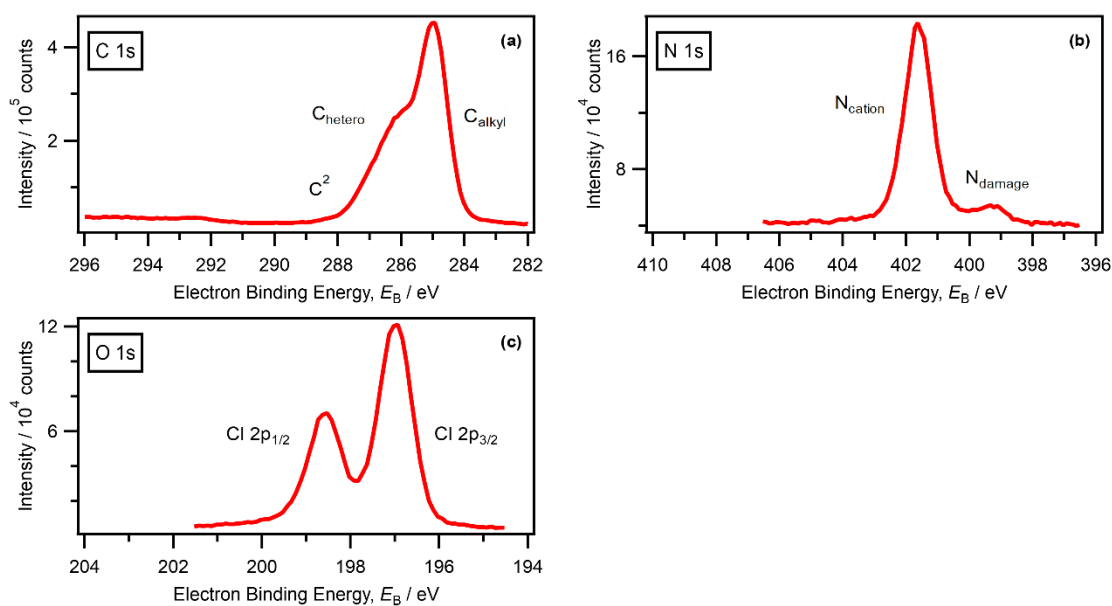


Figure S53. a-c) core level XP spectra for $[C_8C_1Im]Cl$ recorded on synchrotron-based XPS at $h\nu = 850$ eV. No survey scan was recorded. The N 1s spectrum showed a very small amount of damage, which has been observed previously for imidazolium-based ILs.^{32, 40} All electron spectra were charge referenced using procedures outlined in ESI Section 5.

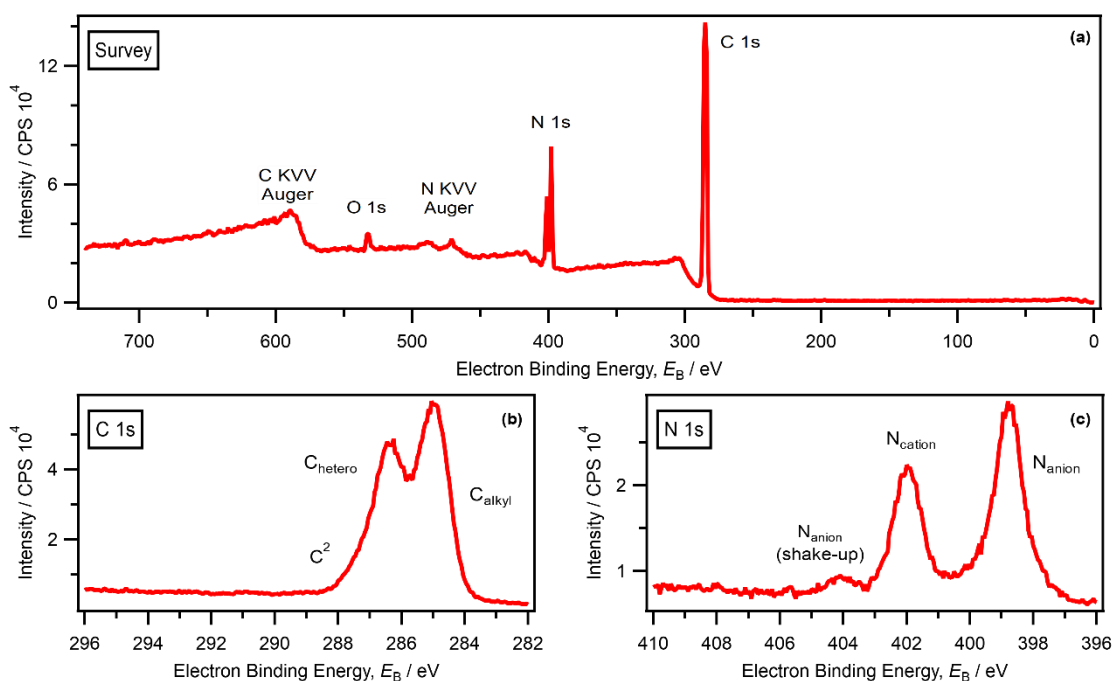


Figure S54. a) Survey and b-c) core level XP spectra for $[C_8C_1Im][C(CN)_3]$ recorded on synchrotron-based XPS at $h\nu = 850$ eV. There was a very small O 1s peak at ~ 530 eV, showing that there was a very small amount of O 1s contamination present. All electron spectra were charge referenced using procedures outlined in ESI Section 5.

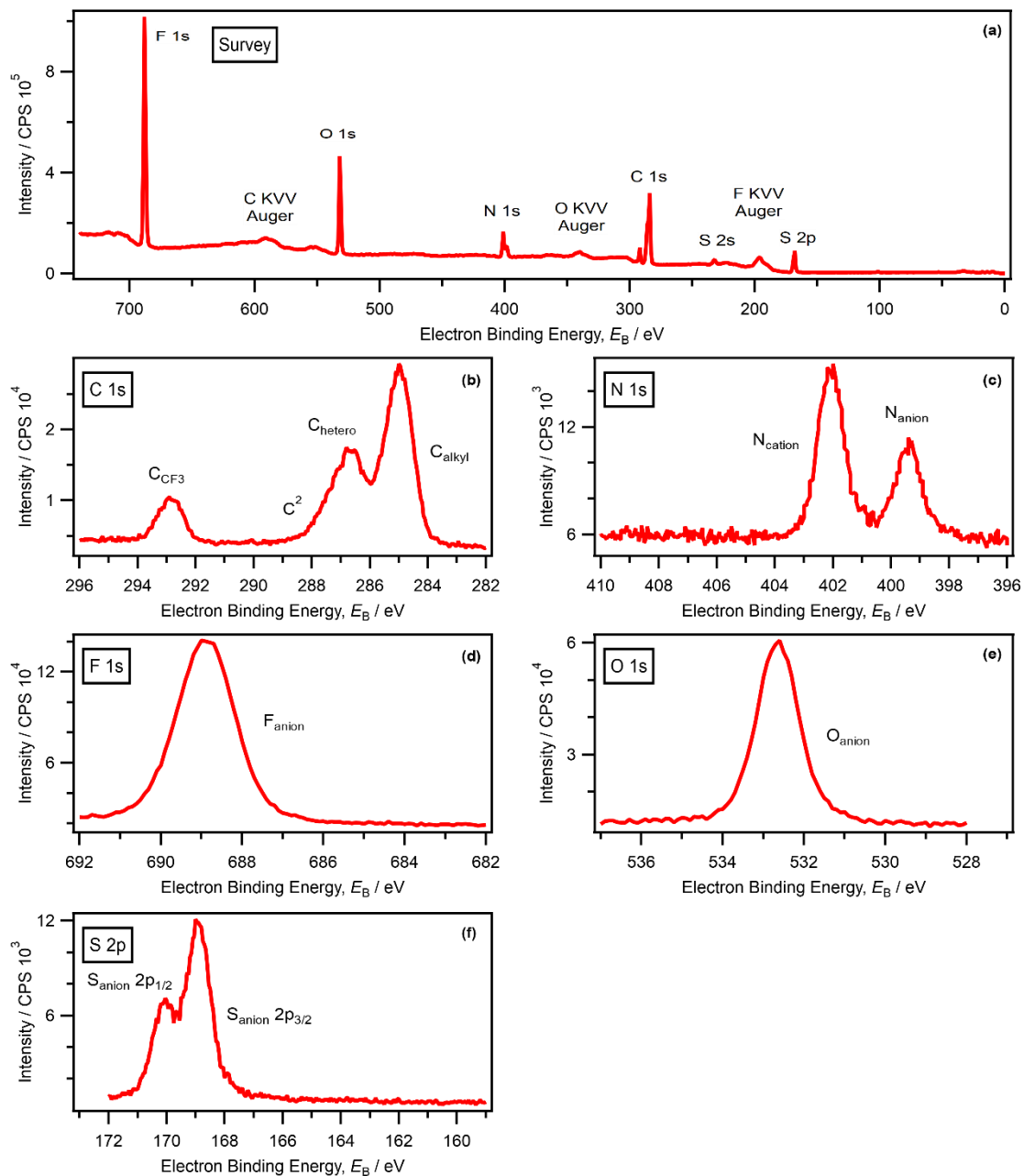


Figure S55. a) Survey and b-f) core level XP spectra for $[C_8C_1Im][NTf_2]$ recorded on synchrotron-based XPS at $h\nu = 850$ eV. All electron spectra were charge referenced using procedures outlined in ESI Section 5.

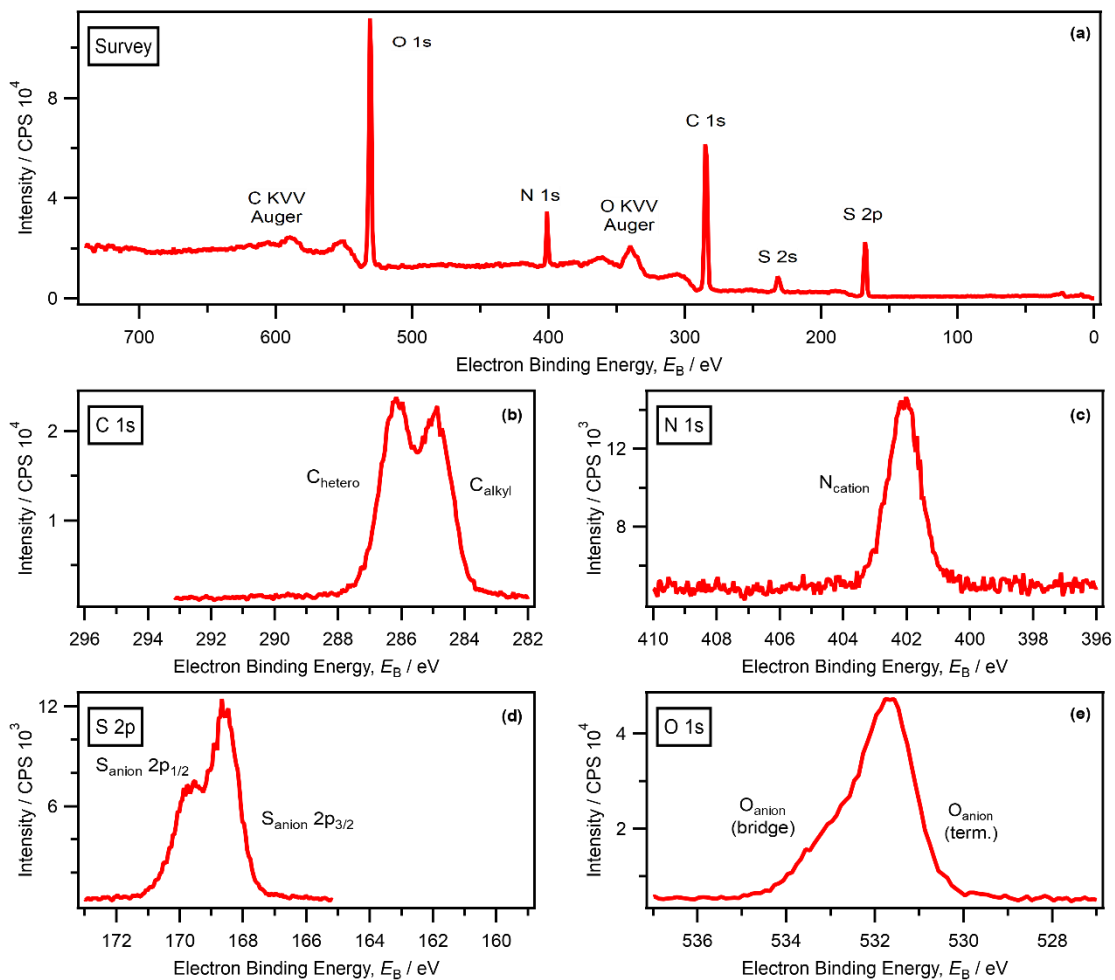


Figure S56. a) Survey and b-e) core level XP spectra for $[N_{4,1,1,0}][HSO_4]$ recorded on synchrotron-based XPS at $h\nu = 850$ eV. All electron spectra were charge referenced using procedures outlined in ESI Section 5.

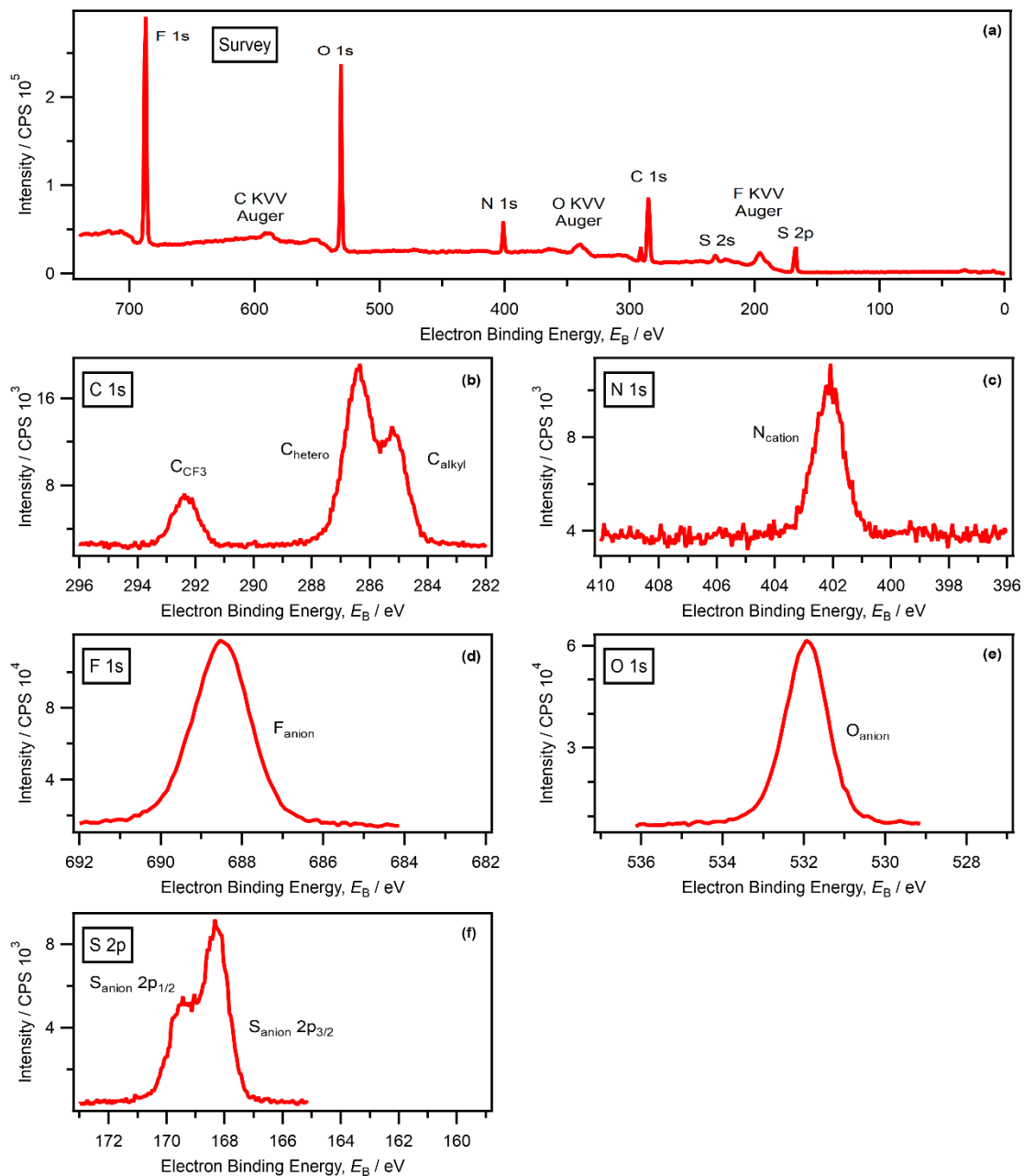


Figure S57. a) Survey and b-f) core level XP spectra for $[N_{2,2,1,0}][TfO]$ recorded on synchrotron-based XPS at $h\nu = 850$ eV. All electron spectra were charge referenced using procedures outlined in ESI Section 5.

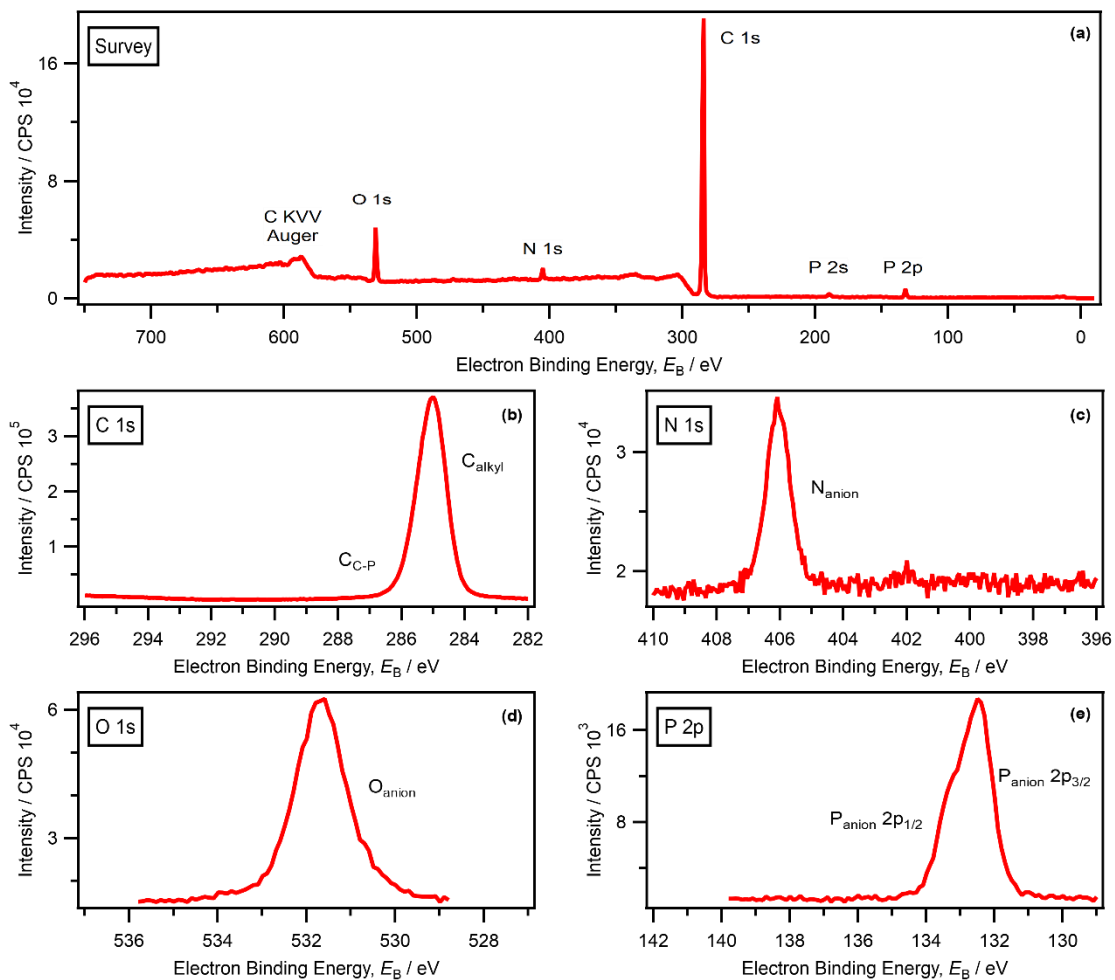


Figure S58. a) Survey and b-e) core level XP spectra for $[P_{6,6,6,14}][NO_3]$ recorded on synchrotron-based XPS at $h\nu = 850$ eV. All electron spectra were charge referenced using procedures outlined in ESI Section 5.

14. Results. Variable $h\nu$ valence XPS data

At $h\nu = 1486.6$ eV, the photoionisation cross-section for S 3p is ~ 50 times greater than that for C 2p and ~ 12 times greater than that for N 2p (ESI Section 6).³⁸ At $h\nu = 1486.6$ eV, the photoionisation cross-section for S 3p is four times greater than that for O 2p and only two times greater than that for F 2p (ESI Section 6).³⁸ Given the relatively large amount of both O and F atoms in $[\text{HSO}_4]^-$, $[\text{TfO}]^-$ and $[\text{NTf}_2]^-$, these photoionisation cross-sections explain why clear features due to S atoms were not observed from our variable $h\nu$ XP valence XP spectra.

For four of the ILs studied here ($[\text{P}_{6,6,6,14}][\text{NO}_3]$, $[\text{N}_{4,1,1,0}][\text{HSO}_4]$, $[\text{C}_8\text{C}_1\text{Im}][\text{NTf}_2]$ and $[\text{N}_{2,2,1,0}][\text{TfO}]$) no area variations were observed with respect to $h\nu$ that could be used to identify atomic contributions to MOs (ESI Figure S59). Therefore, no further AO contributions to MOs were identified from this experimental data. However, variable $h\nu$ valence XP spectra for all six of these ILs will be very valuable when attempting to validate MO calculations.

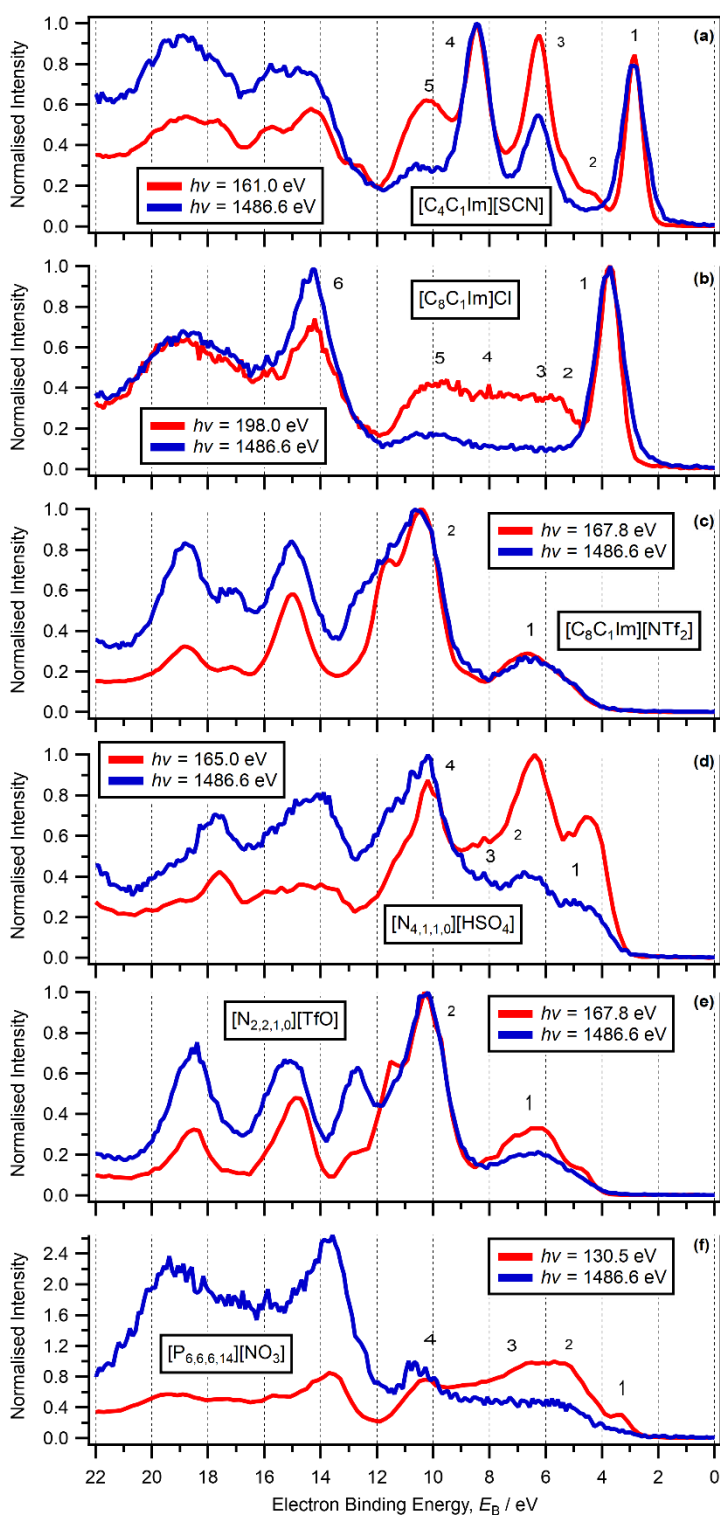


Figure S59. Variable $h\nu$ valence XP spectra for: (a) $[\text{C}_4\text{C}_1\text{Im}][\text{SCN}]$ at $h\nu = 1486.6$ eV and $h\nu = 161.0$ eV, (b) $[\text{C}_8\text{C}_1\text{Im}]\text{Cl}$ at $h\nu = 1486.6$ eV and $h\nu = 198.0$ eV, (c) $[\text{C}_8\text{C}_1\text{Im}][\text{NTf}_2]$ at $h\nu = 1486.6$ eV and $h\nu = 167.8$ eV, (d) $[\text{N}_{4,1,1,0}][\text{HSO}_4]$ at $h\nu = 1486.6$ eV and $h\nu = 165.0$ eV. (e) $[\text{N}_{2,2,1,0}][\text{TfO}]$ at $h\nu = 1486.6$ eV and $h\nu = 167.8$ eV, and (f) $[\text{P}_{6,6,6,14}][\text{NO}_3]$ at $h\nu = 1486.6$ eV and $h\nu = 130.5$ eV. The numbers on each graph represent component labels. The areas of all valence XP spectra in all graphs are normalised to the area of the most intense component in the region $0 \text{ eV} < E_B < 12 \text{ eV}$. All electron spectra were charge referenced using procedures outlined in ESI Section 5.

15. Results. Using NEXAFS spectroscopy to aid RAES

NEXAFS spectroscopy: the number of electronic environments

For many of the edges studied here, there was only one electronic environment present in the IL (as judged using core level XPS), which makes identification of NEXAFS spectra straightforward. For example, $[\text{N}_{2,2,1,0}][\text{TfO}]$ contains three oxygen atoms which were electronically indistinguishable by core level XPS (ESI Figure S39e, ESI Figure S57e and reference ⁴¹); the O 1s NEXAFS spectrum for $[\text{N}_{2,2,1,0}][\text{TfO}]$ gave just one intense resonant peak due to absorption (Figure 6b). The exceptions are the O 1s NEXAFS spectrum for $[\text{N}_{4,1,1,0}][\text{HSO}_4]$ and the C 1s NEXAFS spectra for all ILs studied here. For $[\text{N}_{4,1,1,0}][\text{HSO}_4]$, the O 1s XP spectrum showed two peaks (ESI Figure S31e, ESI Figure S56e and reference ⁴¹); as these peaks are at relatively similar XPS E_B , we could not distinguish their contributions to the O 1s NEXAFS spectrum (which contains only a broad feature).

NEXAFS spectroscopy: N 1s edge

All peaks in the N 1s NEXAFS spectra for these ILs have been identified previously, using a combination of core level XPS, NEXAFS spectroscopy and time-dependent density functional theory (TDDFT) calculations.¹ For example, for $[\text{C}_4\text{C}_1\text{Im}][\text{SCN}]$ the peak at $h\nu = 401.8$ eV was assigned to the two (indistinguishable by NEXAFS spectroscopy) cationic nitrogen atoms from $[\text{C}_4\text{C}_1\text{Im}]^+$, where there was promotion of a N 1s core level electron to a π^* conduction MO;^{28, 42, 43} the peak at $h\nu = 399.5$ eV is assigned to absorption by anionic $[\text{SCN}]^-$ nitrogen atoms (Figure 4b).⁴⁴ Contributions from cationic and anionic nitrogen can be distinguished using RAES for $[\text{C}_8\text{C}_1\text{Im}][\text{C}(\text{CN})_3]$ (Figure 5). For $[\text{C}_7\text{C}_1\text{Im}][\text{NTf}_2]$, calculations suggest that the lowest energy peak due to the $[\text{NTf}_2]^-$ anion in the N 1s NEXAFS spectrum would appear at a similar energy to the lowest energy peak for the imidazolium ring.^{1, 43, 45, 46} Therefore, distinguishing between cationic and anionic N 1s absorption is challenging for $[\text{C}_7\text{C}_1\text{Im}][\text{NTf}_2]$.

NEXAFS spectroscopy: C 1s edge

There was a significant carbon dip (a decrease in intensity due to absorption of X-rays by carbon-based material on the beamline apparatus) for the C 1s NEXAFS spectra for all ILs studied here (Figure 7 and Figures S58 to S62). This dip makes analysing the C 1s NEXAFS spectra more challenging. For RAES data taken at a particular $h\nu$, the carbon dip does not impact on the comparisons made between the peak areas of two different peaks due to participator Auger transitions; therefore, conclusions can readily be drawn from the C 1s RAE spectra. Analysis of C 1s RAE spectra is easier for ILs that showed strong absorption at the C 1s edge. The carbon dip showed the most dramatic effect on the C 1s RAES data for $[\text{N}_{2,2,1,0}][\text{TfO}]$ compared to the other ILs studied here (Figure 7 and ESI Figure S68 to ESI Figure S72); this is because the $[\text{N}_{2,2,1,0}]^+$ cation contains no π^* MOs and relatively few alkyl carbon atoms, meaning that absorption at the C 1s edge for this IL is relatively weak.

For $[\text{C}_8\text{C}_1\text{Im}][\text{NTf}_2]$ the peaks in the C 1s NEXAFS spectrum (Figure 7b) were identified using NEXAFS spectra and calculations from an article on $[\text{C}_4\text{C}_1\text{Im}][\text{I}]$ and $[\text{C}_4\text{C}_1\text{Im}][\text{NTf}_2]$.⁴⁵ Peaks at $h\nu \sim 287$ eV correspond to absorption by the imidazolium ring carbon atoms, peaks at $h\nu \sim 289.5$ eV correspond to absorption by the cation alkyl carbon atoms and peaks at $h\nu \sim 294.5$ eV correspond to absorption by the CF_3 carbon atoms.

For $[\text{C}_4\text{C}_1\text{Im}][\text{SCN}]$ the C 1s NEXAFS spectrum showed two distinct peaks (ESI Figure S68) at $h\nu \sim 286.6$ eV and ~ 287.2 eV; similar peaks were observed for $[\text{C}_8\text{C}_1\text{Im}][\text{C}(\text{CN})_3]$ (ESI Figure S69). For the core level C 1s XP spectra of $[\text{C}_4\text{C}_1\text{Im}][\text{SCN}]$ and $[\text{C}_8\text{C}_1\text{Im}][\text{C}(\text{CN})_3]$, the cationic and anionic contributions could not be distinguished (ESI Figure S20b, ESI Figure S24b and reference ¹⁹). Therefore, we cannot differentiate between the contributions of anionic carbon and cationic carbon to a valence component.

For three ILs [N_{4,1,1,0}][HSO₄], [N_{2,2,1,0}][TfO] and [P_{6,6,6,14}][NO₃] no peaks were observed in the region $h\nu \sim 287$ eV; peaks due to C 1s absorption were observed at $h\nu \sim 288.5$ eV for all three ILs (ESI Figure S70b, ESI Figure S71b and ESI Figure S72b). The absorption energies for the C 1s edge for these three ILs were larger than for the [C_nC₁Im][A] ILs. In addition, the cationic C 1s absorption features for these ILs were relatively low intensity and broad. These observations are as expected, based on the lack of aromaticity in the cations for these three ILs. For three ILs [N_{2,2,1,0}][TfO], [N_{4,1,1,0}][HSO₄] and [P_{6,6,6,14}][NO₃], unlike for the [C_nC₁Im][A] ILs studied here, there was no significant π^* system on the cation (or the anion).

16. Results. RAES data: E_B heat maps

RAES: alternative names

Resonant Auger electron spectroscopy (RAES) is sometimes known as de-excitation electron spectroscopy.⁴⁷ Participator Auger emission is also known as direct recombination⁴⁸ or resonant photoemission⁴⁹.

RAES: simple one-electron picture

Observations from reference⁵⁰ indicate that the participator Auger spectrum can be well described by a simple one-electron picture.⁵⁰ Small exceptions have been noted, where the peak due to a participator Auger transition does not increase linearly in E_K with a concomitant increase in photon energy (unlike for peaks due to direct photoemission), called anti-Raman behaviour. Peaks due to direct photoemission remain at constant E_B as the $h\nu$ is changed, whereas peaks due to a participator Auger transition vary E_B slightly as the photon energy is increased. The excess energy in the system may go into occupation of different vibrational sub-levels.⁵¹⁻⁵⁴

RAES: E_B at which peaks due to participator Auger and spectator Auger transitions occur

The E_B at which peaks due to participator Auger and spectator Auger transitions occur is system dependent.^{55, 56} As a guide, peaks due to participator Auger transitions occur from E_F to $E_B \sim 16$ eV, and peaks due to spectator Auger transitions occur from $E_B \sim 20$ eV upwards. Using this guide, for $16 \text{ eV} < E_B < 20 \text{ eV}$ identification of peaks as originating from participator Auger or spectator Auger is hard to achieve.⁵⁵ However, we have been relatively conservative in our identification of a peak as originating from participator Auger transitions. We have not used any peaks at $E_B > 12$ eV to identify AO contributions to MOs (*i.e.* we have not identified any peaks at $E_B > 12$ eV as originating from participator Auger transitions). In addition, we have mainly focused on identification of peaks/components near in E_B to the HOMO.

Subtracted resonant Auger electron spectra traces can be obtained using non-resonant XP spectra from above or below the edge for subtraction (when focusing only on the participator region at $0 \text{ eV} < E_B < 12 \text{ eV}$, ESI Section 10.3). For $[\text{C}_8\text{C}_{11}\text{Im}]\text{Cl}$, the N 1s RAES data was subtracted to produce a subtracted resonant Auger electron spectrum trace. However, due to problems caused by sample charging (ESI Section 3) the subtraction process was not perfect. Therefore, subtraction was carried out using non-resonant XP spectra recorded at four different $h\nu$ (ESI Figure S60). The four traces matched very well at $E_B > 4$ eV, but differences were observed at $3 \text{ eV} < E_B < 4 \text{ eV}$ (ESI Figure 60c), caused by subtraction of the relatively intense non-resonant Cl 3p valence XPS contribution.

16.1. N 1s

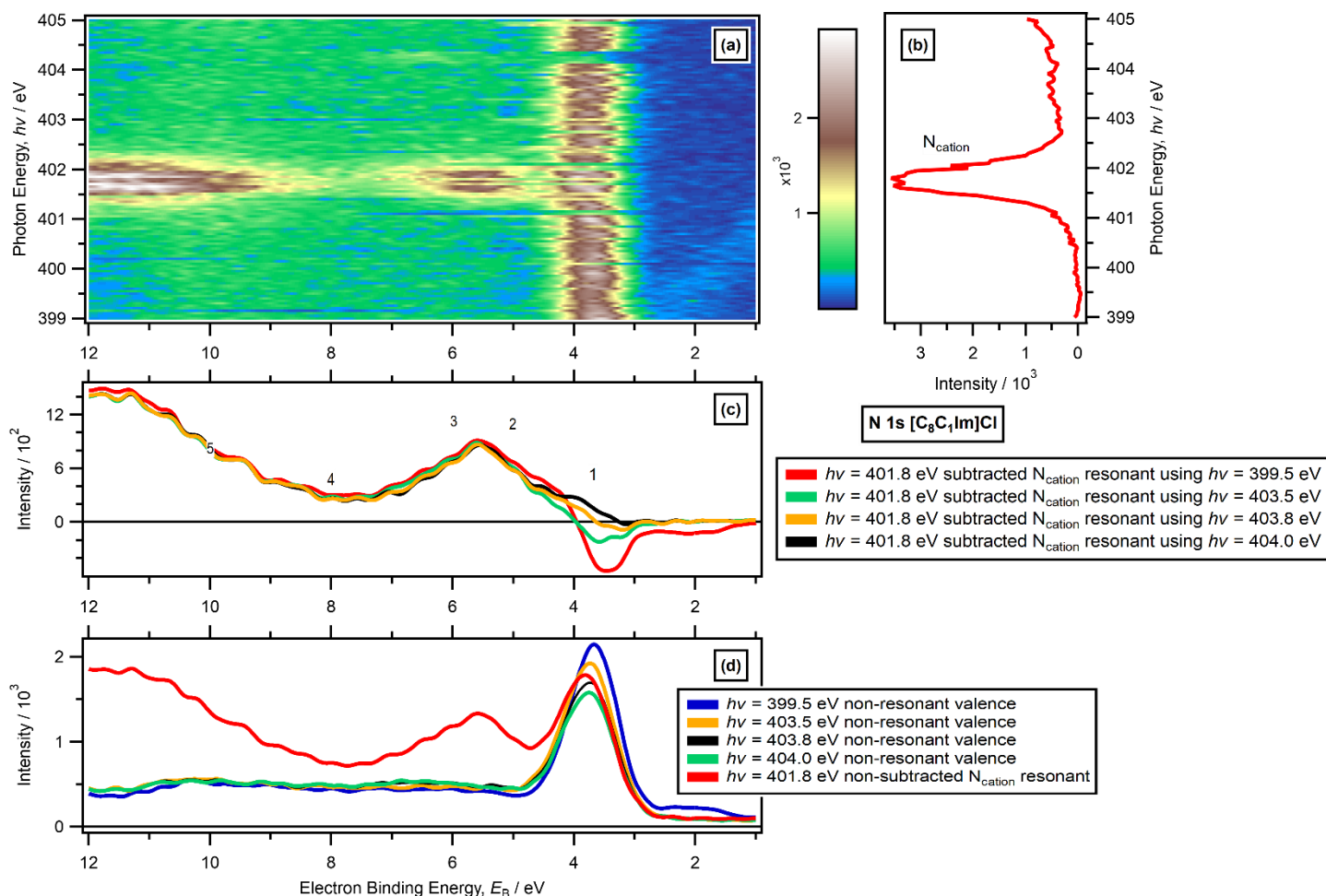


Figure S60. RAES N 1s edge data for [C₈C₁Im]Cl. (a) Heat map of $h\nu$ against E_B for the N 1s edge (produced by combining individual electron spectra taken at varying $h\nu$). (b) Partial electron yield NEXAFS spectrum for the N 1s edge. (c) Subtracted N_{cation} resonant Auger electron spectra ($h\nu = 401.8$ eV); subtraction was carried out using four different non-resonant $h\nu$ ($h\nu = 399.5$ eV, $h\nu = 403.5$ eV, $h\nu = 403.8$ eV and $h\nu = 404.0$ eV). (d) Non-resonant valence XP spectrum below the N 1s absorption edge ($h\nu = 399.5$ eV), and non-resonant valence XP spectra above the N 1s absorption edge ($h\nu = 403.5$ eV, $h\nu = 403.8$ eV and $h\nu = 404.0$ eV) and subtracted N_{cation} resonant Auger electron spectrum ($h\nu = 401.8$ eV). The RAES traces were produced by subtraction of non-resonant XP contributions using the procedure outlined in ESI Section 10.3. Component labels 1 to 4 are given in (c). All electron spectra were charge referenced using procedures outlined in ESI Section 5.

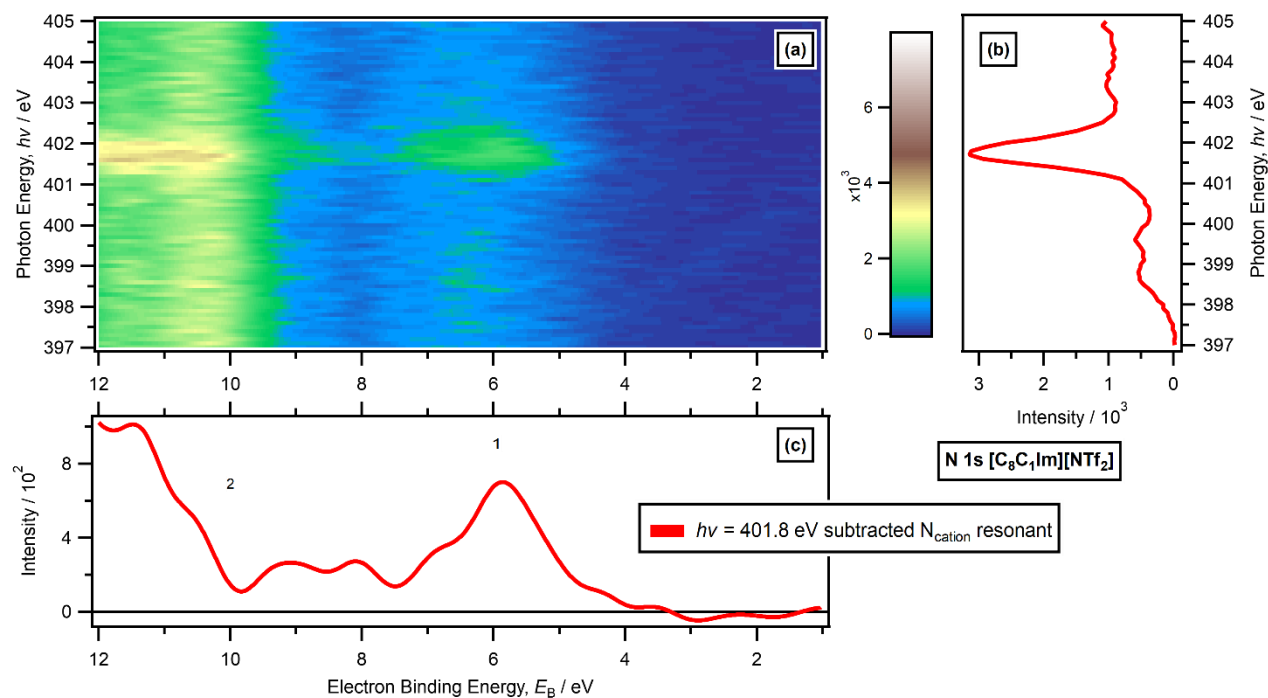


Figure S61. RAES N 1s edge data for $[\text{C}_8\text{C}_1\text{Im}][\text{NTf}_2]$. (a) Heat map of $h\nu$ against E_B for the N 1s edge (produced by combining individual electron spectra taken at varying $h\nu$). (b) Partial electron yield NEXAFS spectrum for the N 1s edge. (c) Subtracted N_{cation} resonant Auger electron spectrum ($h\nu = 401.8$ eV). The RAES trace was produced by subtraction of non-resonant XP contributions using the procedure outlined in ESI Section 10.3. Component labels 1 and 2 are given in (c). All electron spectra were charge referenced using procedures outlined in ESI Section 5.

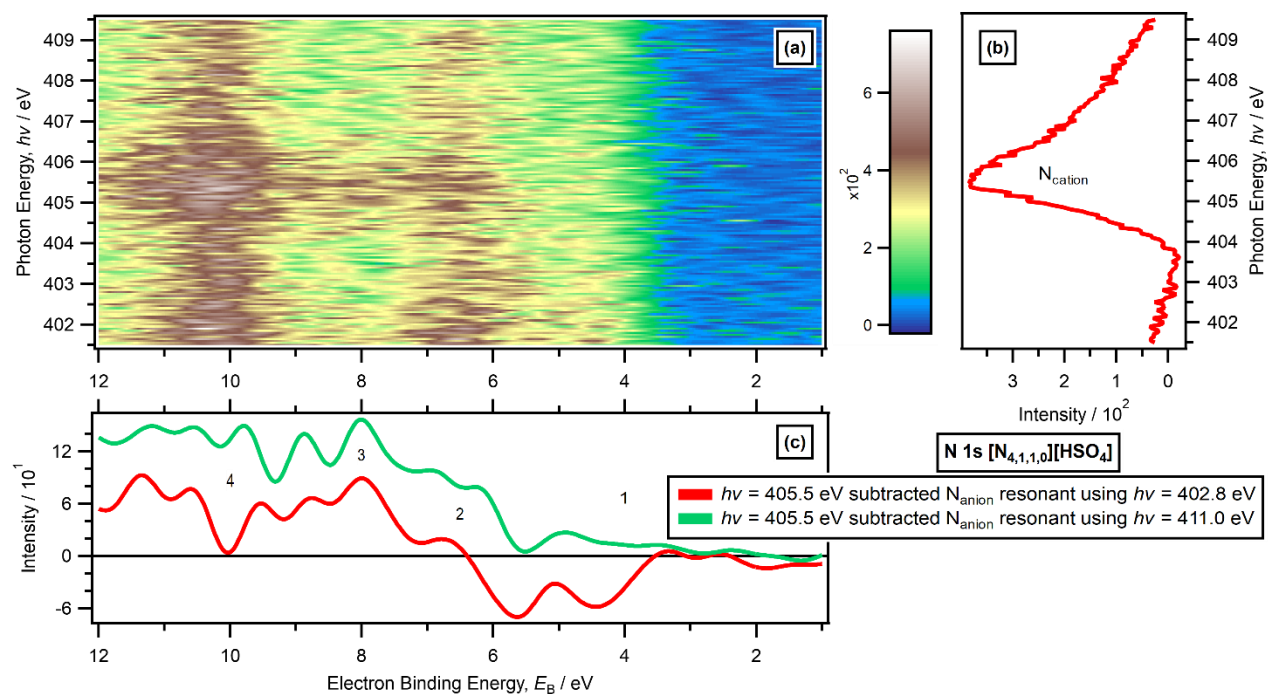


Figure S62. RAES N 1s edge data for $[N_{4,1,1,0}][HSO_4]$. (a) Heat map of $h\nu$ against E_B for the N 1s edge (produced by combining individual electron spectra taken at varying $h\nu$). (b) Partial electron yield NEXAFS spectrum for the N 1s edge. (c) Subtracted N_{cation} resonant Auger electron spectra ($h\nu = 405.5$ eV); subtraction was carried out using two different non-resonant $h\nu$ ($h\nu = 402.8$ eV and $h\nu = 411.0$ eV). The RAES traces were produced by subtraction of non-resonant XP contributions using the procedure outlined in ESI Section 10.3. Component labels 1 to 4 are given in (c). All electron spectra were charge referenced using procedures outlined in ESI Section 5.

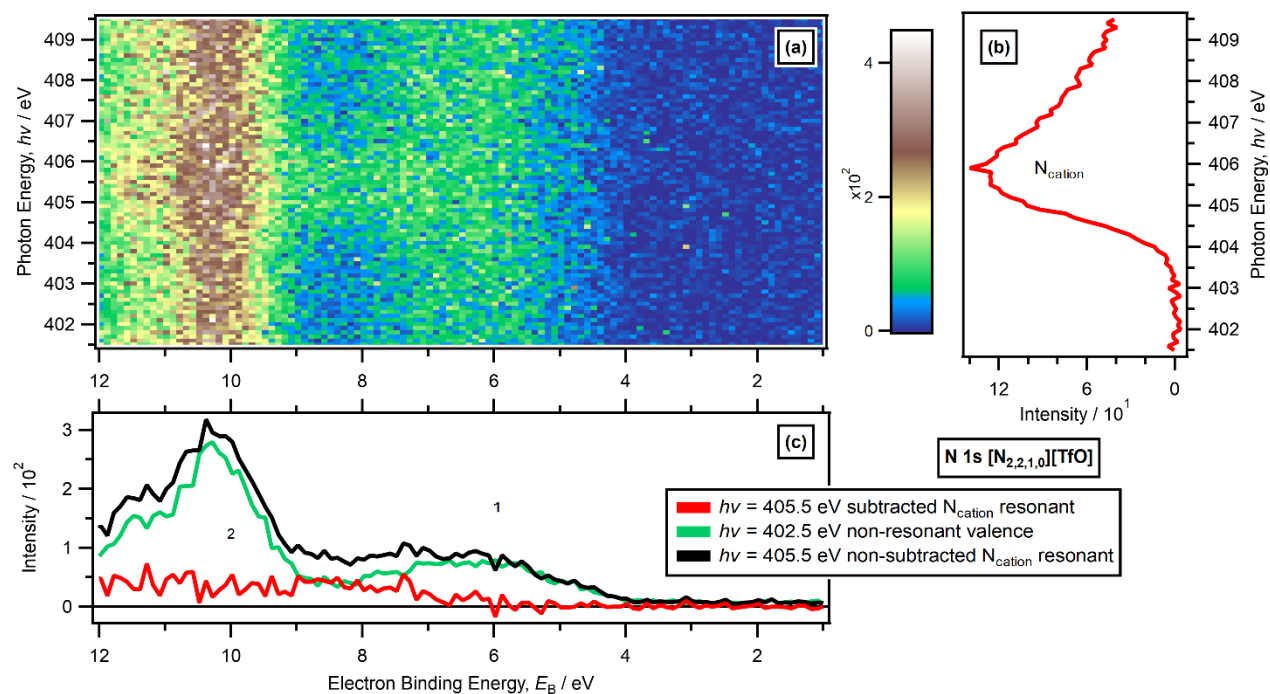


Figure S63. RAES N 1s edge data for $[N_{2,2,1,0}][TfO]$. (a) Heat map of $h\nu$ against E_B for the N 1s edge (produced by combining individual electron spectra taken at varying $h\nu$). (b) Partial electron yield NEXAFS spectrum for the N 1s edge. (c) Non-resonant valence XP spectrum below the edge ($h\nu = 402.5$ eV), electron spectrum at the resonant edge energy ($h\nu = 405.5$ eV) and subtracted N_{cation} resonant Auger electron spectrum ($h\nu = 405.5$ eV). The RAES trace was produced by subtraction of non-resonant XP contributions using the procedure outlined in ESI Section 10.3. Component labels 1 and 2 are given in (c). All electron spectra were charge referenced using procedures outlined in ESI Section 5.

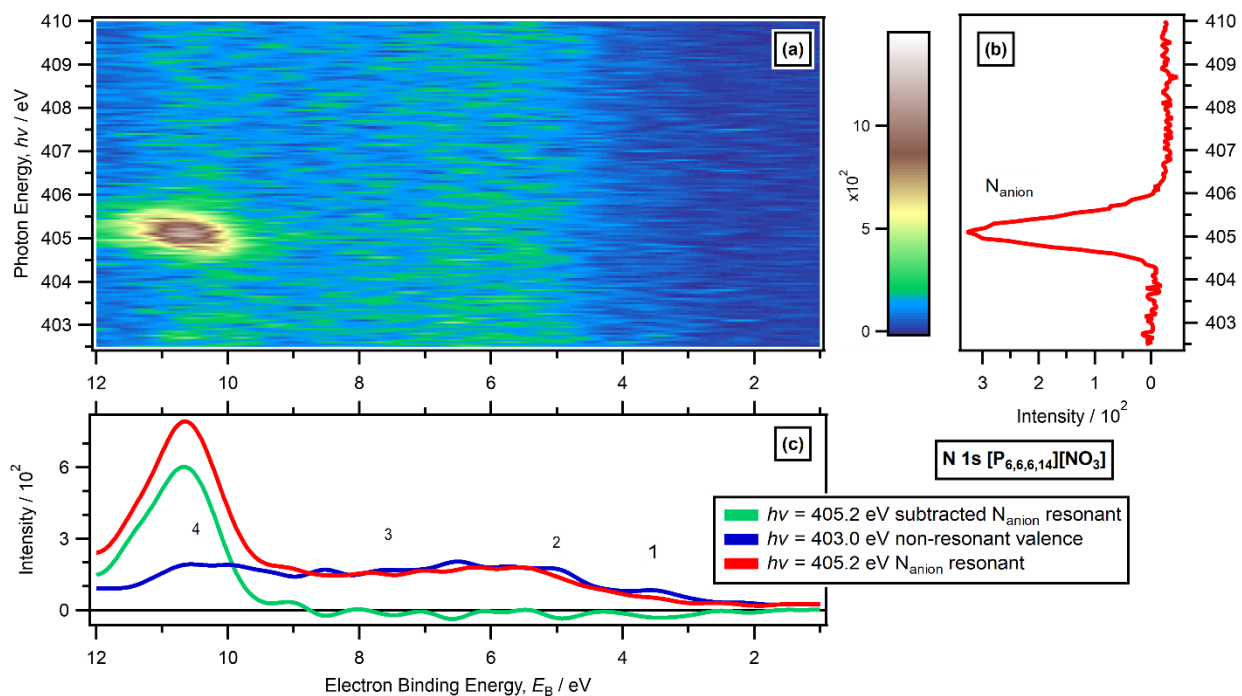


Figure S64. RAES N 1s edge data for $[P_{6,6,6,14}][NO_3]$. (a) Heat map of $h\nu$ against E_B for the N 1s edge (produced by combining individual electron spectra taken at varying $h\nu$). (b) Partial electron yield NEXAFS spectrum for the N 1s edge. (c) Non-resonant valence XP spectrum below the edge ($h\nu = 403.0$ eV), electron spectrum at the resonant edge energy ($h\nu = 405.2$ eV) and subtracted N_{cation} resonant Auger electron spectrum ($h\nu = 405.2$ eV). The RAES trace was produced by subtraction of non-resonant XP contributions using the procedure outlined in ESI Section 10.3. Component labels 1 to 4 are given in (c). All electron spectra were charge referenced using procedures outlined in ESI Section 5.

16.2. O 1s

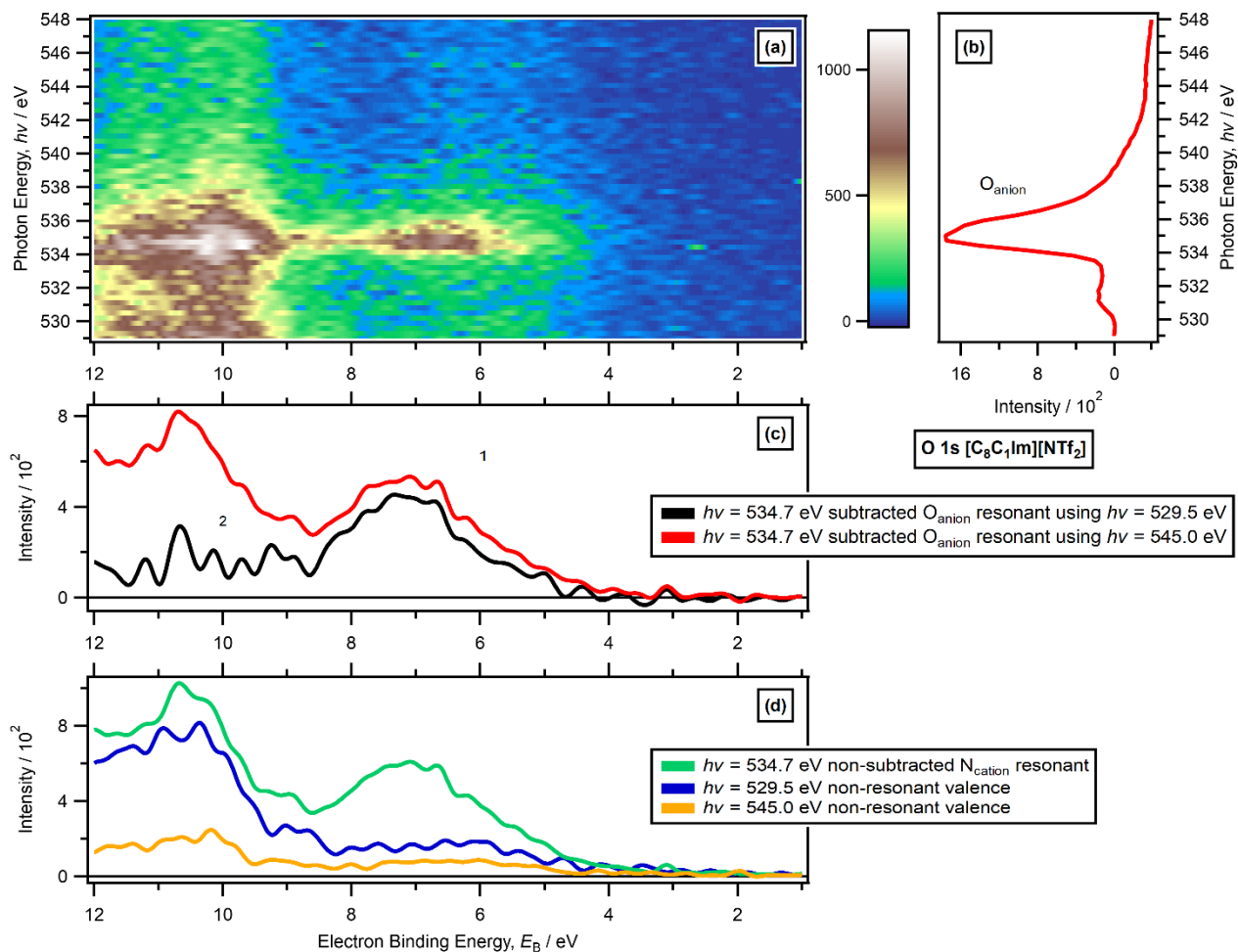


Figure S65. RAES O 1s edge data for $[C_8C_1Im][NTf_2]$. (a) Heat map of $h\nu$ against E_B for the O 1s edge (produced by combining individual electron spectra taken at varying $h\nu$). (b) Partial electron yield NEXAFS spectrum for the O 1s edge. (c) Subtracted O_{anion} resonant Auger electron spectra ($h\nu = 534.7$ eV); subtraction was carried out using two different non-resonant $h\nu$ ($h\nu = 529.5$ eV and $h\nu = 545.0$ eV). (d) Non-resonant valence XP spectrum below the edge (529.5 eV), non-subtracted electron spectrum at the resonant edge energy ($h\nu = 534.7$ eV) and non-resonant valence XP spectrum above the edge ($h\nu = 545.0$ eV). The RAES traces were produced by subtraction of non-resonant XP contributions using the procedure outlined in ESI Section 10.3. Component labels 1 and 2 are given in (c). All electron spectra were charge referenced using procedures outlined in ESI Section 5.

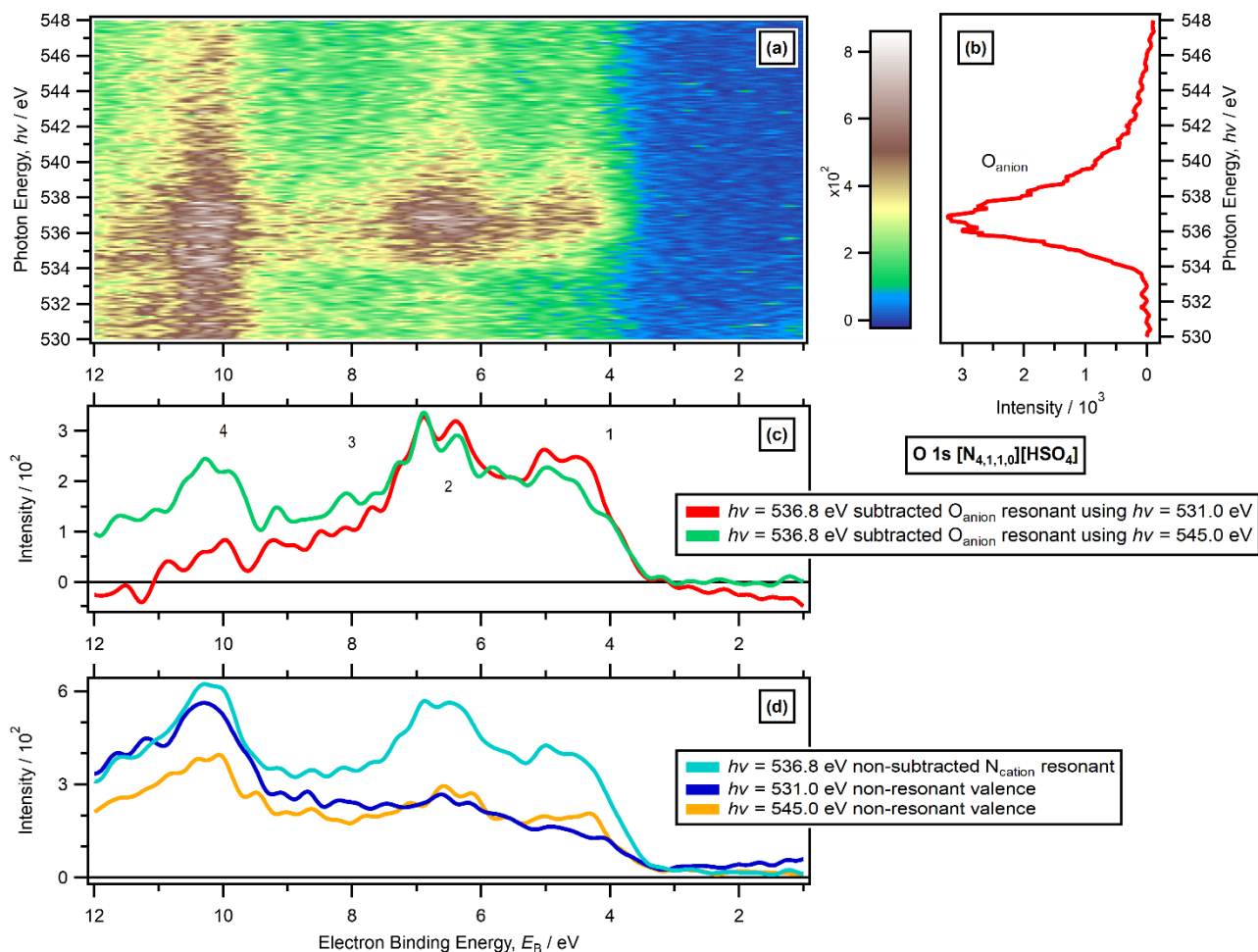


Figure S66. RAES O 1s edge data for $[N_{4,1,1,0}][HSO_4]$. (a) Heat map of $h\nu$ against E_B for the O 1s edge (produced by combining individual electron spectra taken at varying $h\nu$). (b) Partial electron yield NEXAFS spectrum for the O 1s edge. (c) Subtracted O_{anion} resonant Auger electron spectra ($h\nu = 536.8$ eV); subtraction was carried out using two different non-resonant $h\nu$ ($h\nu = 531.0$ eV and $h\nu = 545.0$ eV). (d) Non-resonant valence XP spectrum below the edge (531.0 eV), non-subtracted electron spectrum at the resonant edge energy ($h\nu = 536.8$ eV) and non-resonant valence XP spectrum above the edge ($h\nu = 545.0$ eV). The RAES traces were produced by subtraction of non-resonant XP contributions using the procedure outlined in ESI Section 10.3. Component labels 1 to 4 are given in (c). All electron spectra were charge referenced using procedures outlined in ESI Section 5.

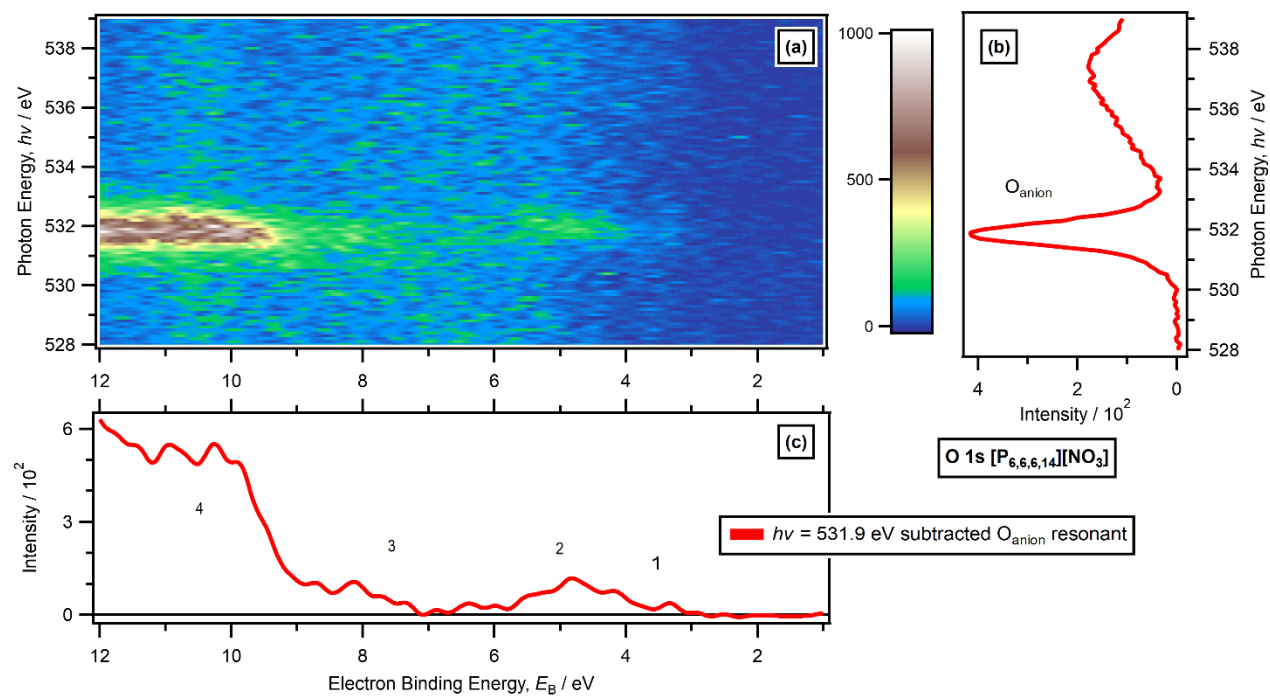


Figure S67. RAES O 1s edge data for $[P_{6,6,6,14}][NO_3]$. (a) Heat map of $h\nu$ against E_B for the O 1s edge (produced by combining individual electron spectra taken at varying $h\nu$). (b) Partial electron yield NEXAFS spectrum for the O 1s edge. (c) Subtracted O_{anion} resonant Auger electron spectra ($h\nu = 531.9$ eV). The RAES trace was produced by subtraction of non-resonant XP contributions using the procedure outlined in ESI Section 10.3. Component labels 1 to 4 are given in (c). All electron spectra were charge referenced using procedures outlined in ESI Section 5.

16.3. C 1s

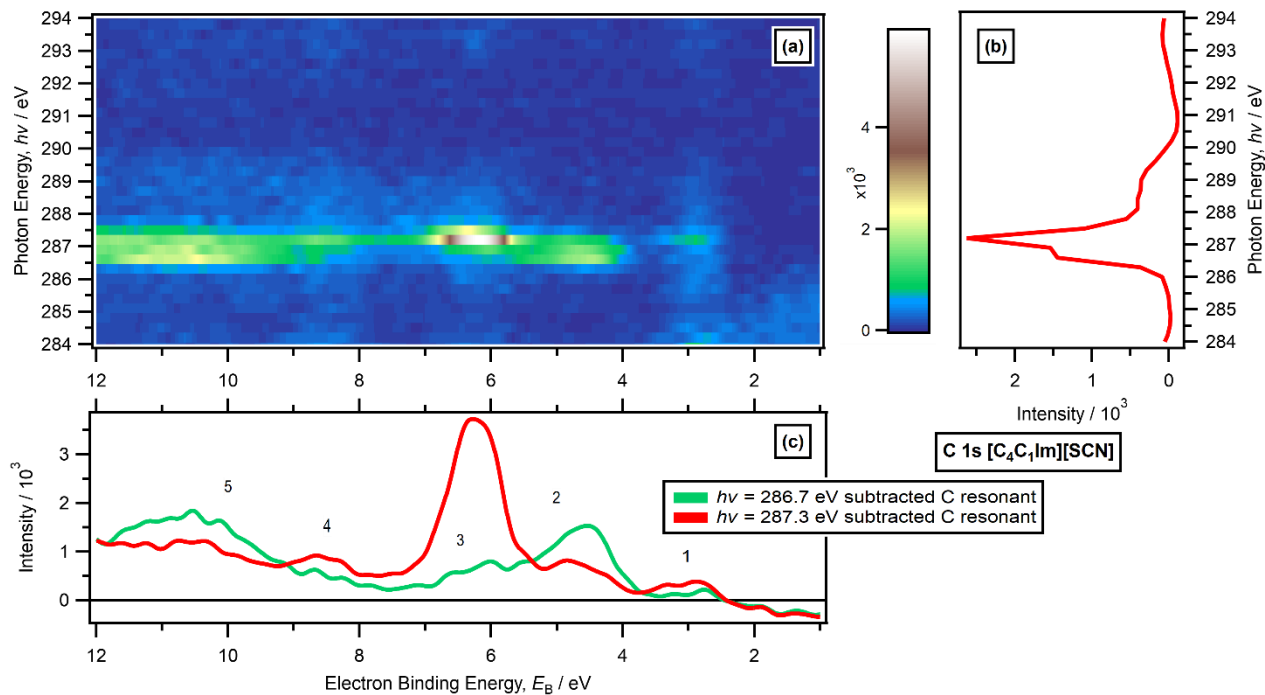


Figure S68. RAES C 1s edge data for [C₄C₁Im][SCN]. (a) Heat map of $h\nu$ against E_B for the C 1s edge (produced by combining individual electron spectra taken at varying $h\nu$). (b) Partial electron yield NEXAFS spectrum for the C 1s edge. (c) Subtracted C resonant Auger electron spectra ($h\nu = 286.7$ eV and $h\nu = 287.3$ eV). The RAES traces were produced by subtraction of non-resonant XP contributions using the procedure outlined in ESI Section 10.3. Component labels 1 to 5 are given in (c). All electron spectra were charge referenced using procedures outlined in ESI Section 5.

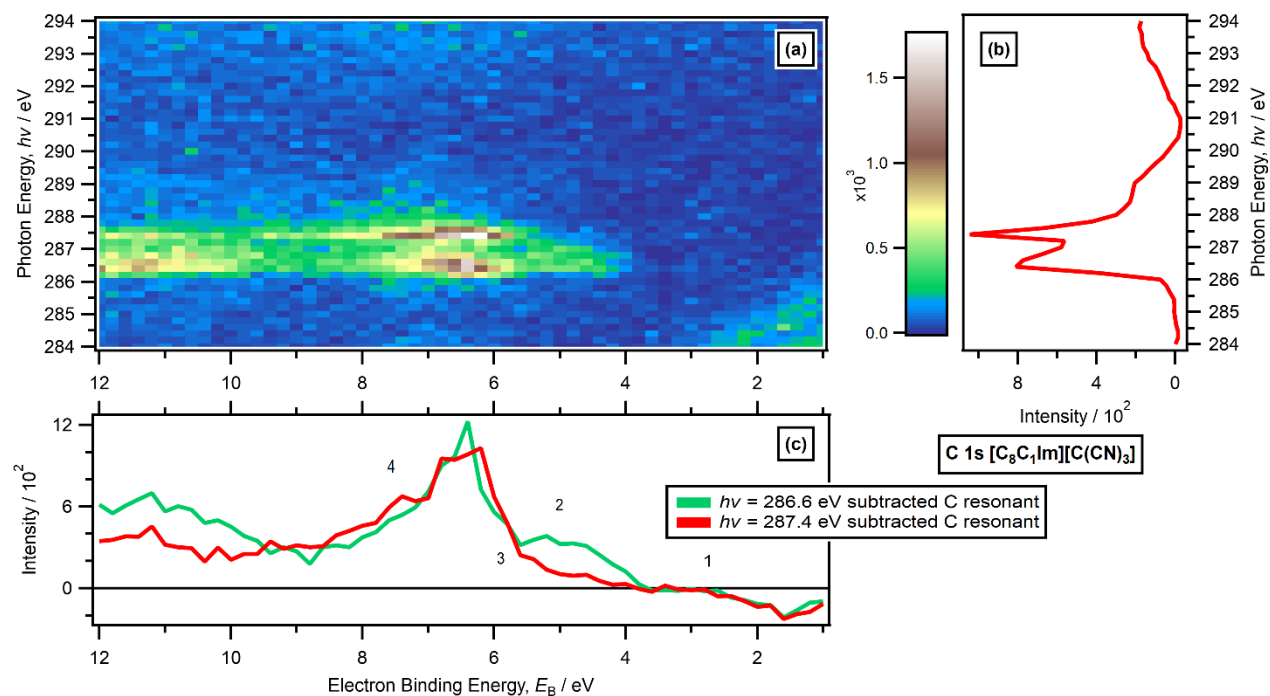


Figure S69. RAES C 1s edge data for $[C_8C_1Im][C(CN)_3]$. (a) Heat map of $h\nu$ against E_B for the C 1s edge (produced by combining individual electron spectra taken at varying $h\nu$). (b) Partial electron yield NEXAFS spectrum for the C 1s edge. (c) Subtracted C resonant Auger electron spectra ($h\nu = 286.6$ eV and $h\nu = 287.4$ eV). The RAES traces were produced by subtraction of non-resonant XP contributions using the procedure outlined in ESI Section 10.3. Component labels 1 to 4 are given in (c). All electron spectra were charge referenced using procedures outlined in ESI Section 5.

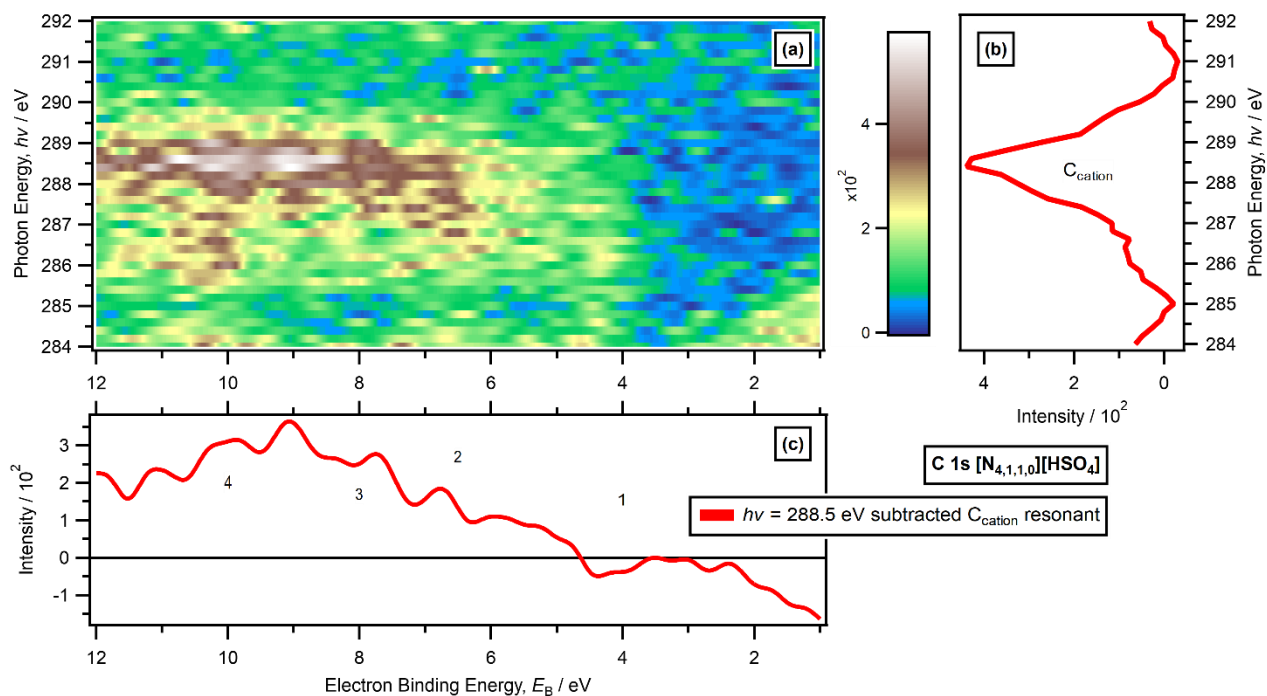


Figure S70. RAES C 1s edge data for $[N_{4,1,1,0}][HSO_4]$. (a) Heat map of $h\nu$ against E_B for the C 1s edge (produced by combining individual electron spectra taken at varying $h\nu$). (b) Partial electron yield NEXAFS spectrum for the C 1s edge. (c) Subtracted C resonant Auger electron spectrum ($h\nu = 288.5$ eV). The RAES trace was produced by subtraction of non-resonant XP contributions using the procedure outlined in ESI Section 10.3. Component labels 1 to 4 are given in (c). All electron spectra were charge referenced using procedures outlined in ESI Section 5.

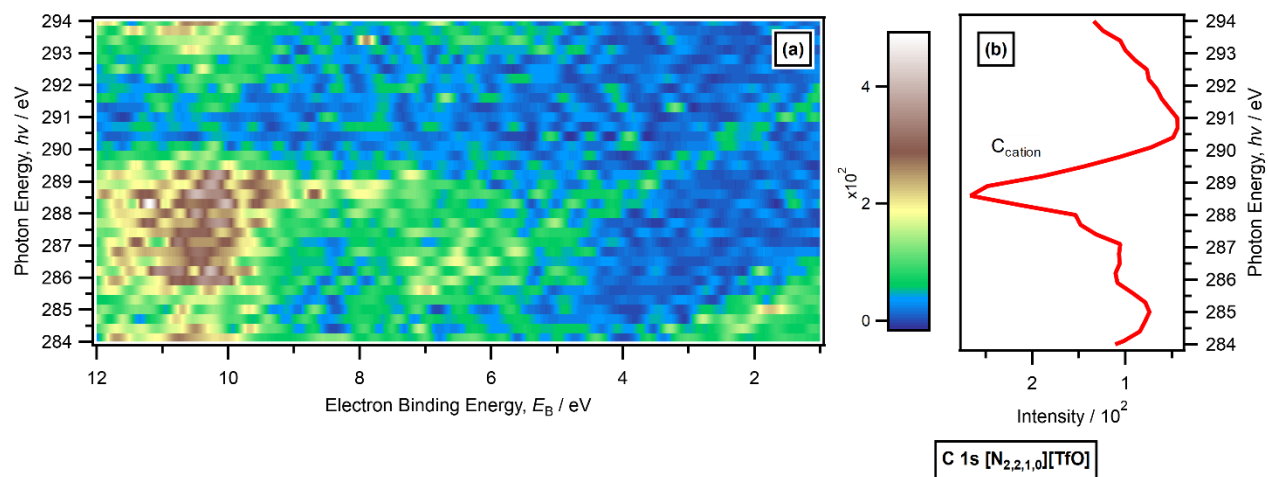


Figure S71. RAES C 1s edge data for [N_{2,2,1,0}][TfO]. (a) Heat map of $h\nu$ against E_B for the C 1s edge (produced by combining individual electron spectra taken at varying $h\nu$). (b) Partial electron yield NEXAFS spectrum for the C 1s edge. All electron spectra were charge referenced using procedures outlined in ESI Section 5. Features due to photoemission from second order light were observed (and should not be interpreted).

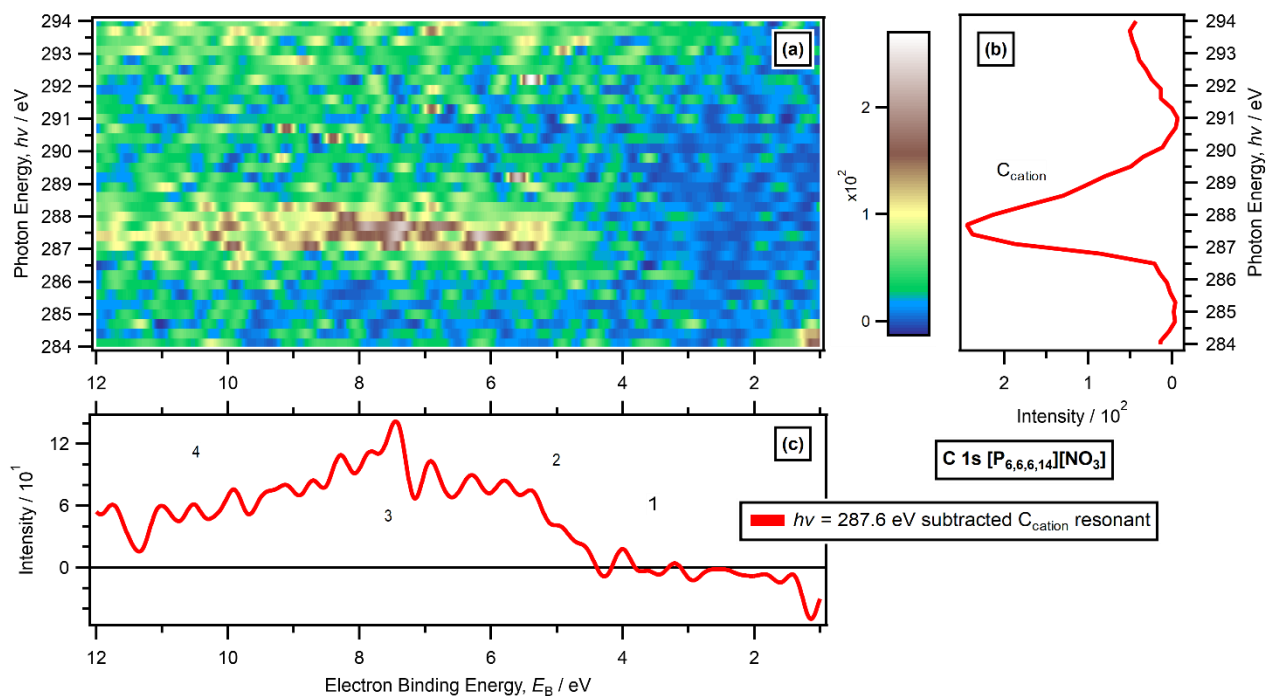


Figure S72. RAES C 1s edge data for $[P_{6,6,6,14}][NO_3]$. (a) Heat map of $h\nu$ against E_B for the C 1s edge (produced by combining individual electron spectra taken at varying $h\nu$). (b) Partial electron yield NEXAFS spectrum for the C 1s edge. (c) Subtracted C resonant Auger electron spectrum ($h\nu = 287.6$ eV). The RAES trace was produced by subtraction of non-resonant XP contributions using the procedure outlined in ESI Section 10.3. Component labels 1 to 4 are given in (c). All electron spectra were charge referenced using procedures outlined in ESI Section 5.

16.4. P 2p

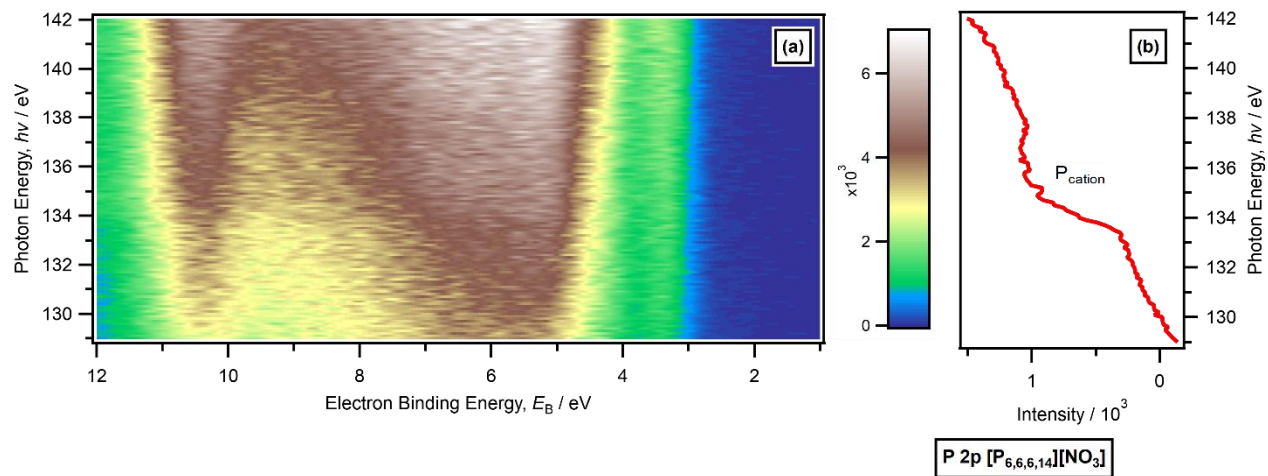


Figure S73. RAES P 2p edge data for $[P_{6,6,6,14}][NO_3]$. (a) Heat map of $h\nu$ against E_B for the P 2p edge (produced by combining individual electron spectra taken at varying $h\nu$). (b) Partial electron yield NEXAFS spectrum for the P 2p edge. All electron spectra were charge referenced using procedures outlined in ESI Section 5.

17. Results. RAES data: further descriptions

RAES: N 1s

The features at $E_B > 12$ eV were likely due to either spectator Auger transitions or a combination of both spectator Auger and participator Auger transitions (*i.e.* not solely due to participator Auger transitions); therefore, no attempts have been made to draw conclusions on valence MOs at $E_B > 12$ eV onwards for the N 1s RAES spectra of $[C_nC_1Im][A]$ ILs.

No clear peaks due to participator Auger transitions were observed for the N 1s edge for the two ammonium-based ILs (ESI Figure S62 and ESI Figure S63). In addition, no clear peaks due to participator Auger transitions were observed for the P 2p edge for $[P_{6,6,6,14}][NO_3]$ (ESI Figure S73). Therefore, MOs with significant contribution from the cationic AOs could not be identified using RAES for these three ILs. The lack of peaks due to participator Auger transitions for these cationic edges for these three ILs was most likely due to a combination of the relatively small amount of phosphorus/nitrogen atoms in the ILs and the first X-ray absorption for these three edges giving rise to electron promotion into relatively delocalised σ^* orbitals (which were unlikely to favour participator Auger transitions).⁵⁷

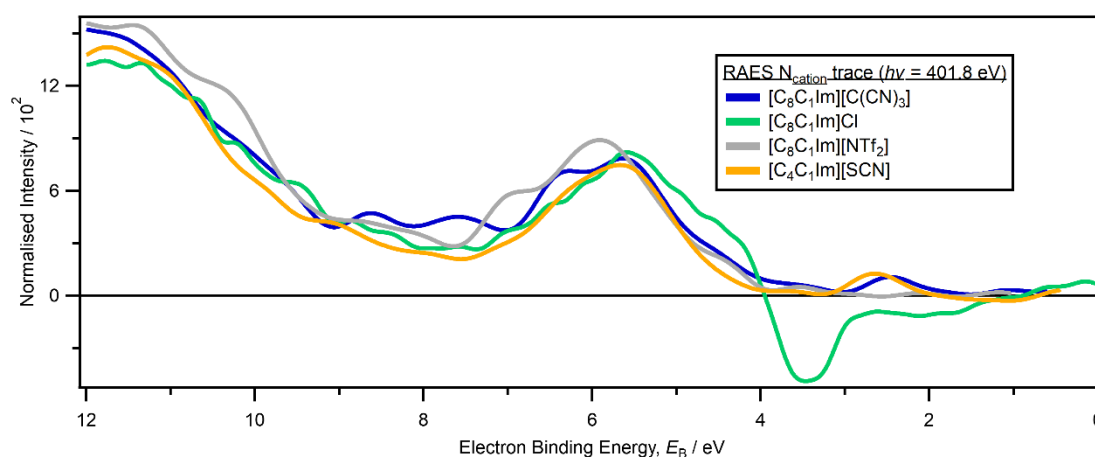


Figure S74. RAES traces for $[C_nC_1Im][A]$ recorded at $h\nu = 401.8$ eV ($N_{\text{cation}} 1s \rightarrow \pi^*$ resonance). The RAES traces were produced by subtraction of non-resonant XP contributions using the procedure outlined in ESI Section 10.3 and area normalised by eye so that the feature at $4 \text{ eV} < E_B < 7 \text{ eV}$ was approximately the same intensity. All traces were charge referenced using procedures outlined in ESI Section 5.

RAES: O 1s

For $[C_8C_1Im][NTf_2]$, the area of components 1 and 2 ($E_B \sim 6$ eV and ~ 10 eV respectively) were enhanced at the anionic O 1s edge energy ($h\nu = 535.0$ eV), relative to below the edge, due to participator Auger transitions (ESI Figure S65). Therefore, the RAES data suggests that for $[C_8C_1Im][NTf_2]$ components 1 and 2 have significant contributions from anionic oxygen. The features at $E_B > \sim 12$ eV are likely due to either spectator Auger or a combination of both spectator Auger and participator Auger transitions (*i.e.* not solely due to participator Auger transitions); therefore, no attempts have been made to draw conclusions on occupied MOs at $E_B > 12$ eV onwards for the O 1s RAES spectra of $[C_8C_1Im][NTf_2]$.

For $[N_{4,1,1,0}][HSO_4]$, the area of components 1, 2 and 3 ($E_B \sim 4$ eV, ~ 6.5 eV and ~ 8 eV respectively) were enhanced at the anionic O 1s edge energy ($h\nu = 536.7$ eV), relative to below the edge, due to participator Auger transitions (ESI Figure S66). Therefore, the RAES data suggests that for $[N_{4,1,1,0}][HSO_4]$ components 1, 2 and 3 have significant contributions from anionic oxygen. The features at $E_B > \sim 12$ eV are likely due to either spectator Auger or a combination of both spectator Auger and participator Auger transitions (*i.e.* not solely due to participator Auger transitions); therefore, no

attempts have been made to draw conclusions on occupied MOs at $E_B > 12$ eV onwards for the O 1s RAES spectra of $[N_{4,1,1,0}][HSO_4]$.

For $[P_{6,6,6,14}][NO_3]$, the areas of component 1 ($E_B \sim 3.5$ eV) and component 2 ($E_B \sim 5.0$ eV) were enhanced at the anionic O 1s edge energy ($h\nu = 532.0$ eV), relative to below the edge, due to participator Auger transitions (ESI Figure S67). Therefore, the RAES data suggests that for $[P_{6,6,6,14}][NO_3]$ component 1 and component 2 had significant contributions from anionic oxygen. The features at $E_B > \sim 12$ eV are likely due to either spectator Auger or a combination of both spectator Auger and participator Auger transitions (*i.e.* not solely due to participator Auger transitions); therefore, no attempts have been made to draw conclusions on occupied MOs at $E_B > 12$ eV onwards for the O 1s RAES spectra of $[P_{6,6,6,14}][NO_3]$. Similar conclusions were made for O 1s RAES data for Na $[NO_3]$ (ESI Section 18).⁵⁵

RAES: C 1s

For $[C_4C_1Im][SCN]$, the areas of components 2, 3 and 4 were enhanced due to peaks from participator Auger transitions at the C 1s edge energies ($h\nu = 286.6$ eV and 287.2 eV) relative to below the edge (ESI Figure S68). Therefore, MOs which gave rise to components 2, 3 and 4 had significant contributions from C 2p AOs. These contributions could be from C_{cation} or C_{anion} (see ESI Section 15 for more details). Furthermore, no peak due to a participator Auger transition was observed for component 1, strongly suggesting that there was no significant C 2p AO contribution to component 1.

For $[C_8C_1Im][C(CN)_3]$, the areas of components 2, 3 and 4 were enhanced due to peaks from participator Auger transitions at the C 1s edge energies ($h\nu = 286.6$ eV and $h\nu = 287.8$ eV) relative to below the edge (ESI Figure S69). Therefore, MOs which gave rise to components 3 and 4 had significant contributions from C 2p AOs. These contributions could be from C_{cation} or C_{anion} (see ESI Section 15 for more details). Furthermore, no peaks due to participator Auger transitions were observed for component 1 and 2, strongly suggesting that there was no significant C 2p AO contribution to components 1 and 2.

For $[N_{2,2,1,0}][TfO]$, no peak due to participator Auger transitions was observed at the C 1s edge energies (ESI Figure S71).

18. Results. RAES data: $[\text{NO}_3]^-$ comparison

RAES data has been published for the two solids $\text{Na}[\text{NO}_3]$ and $\text{Li}[\text{NO}_3]$.^{55, 58} A comparison of the first resonant $h\nu$ for both O 1s and N 1s for $\text{Na}[\text{NO}_3]$ and $[\text{P}_{6,6,6,14}][\text{NO}_3]$ showed remarkable similarities, both in terms of relative peak E_B and relative peak intensities (ESI Figure S75). For the E_B match, one shift of -1.9 eV was required for both the O 1s and N 1s data of $\text{Na}[\text{NO}_3]$ to match the E_B values of $[\text{P}_{6,6,6,14}][\text{NO}_3]$. Both sets of data were referenced to E_F , but little should be read into the magnitude and direction of these shifts, given that there a number of potential contributors to this difference.

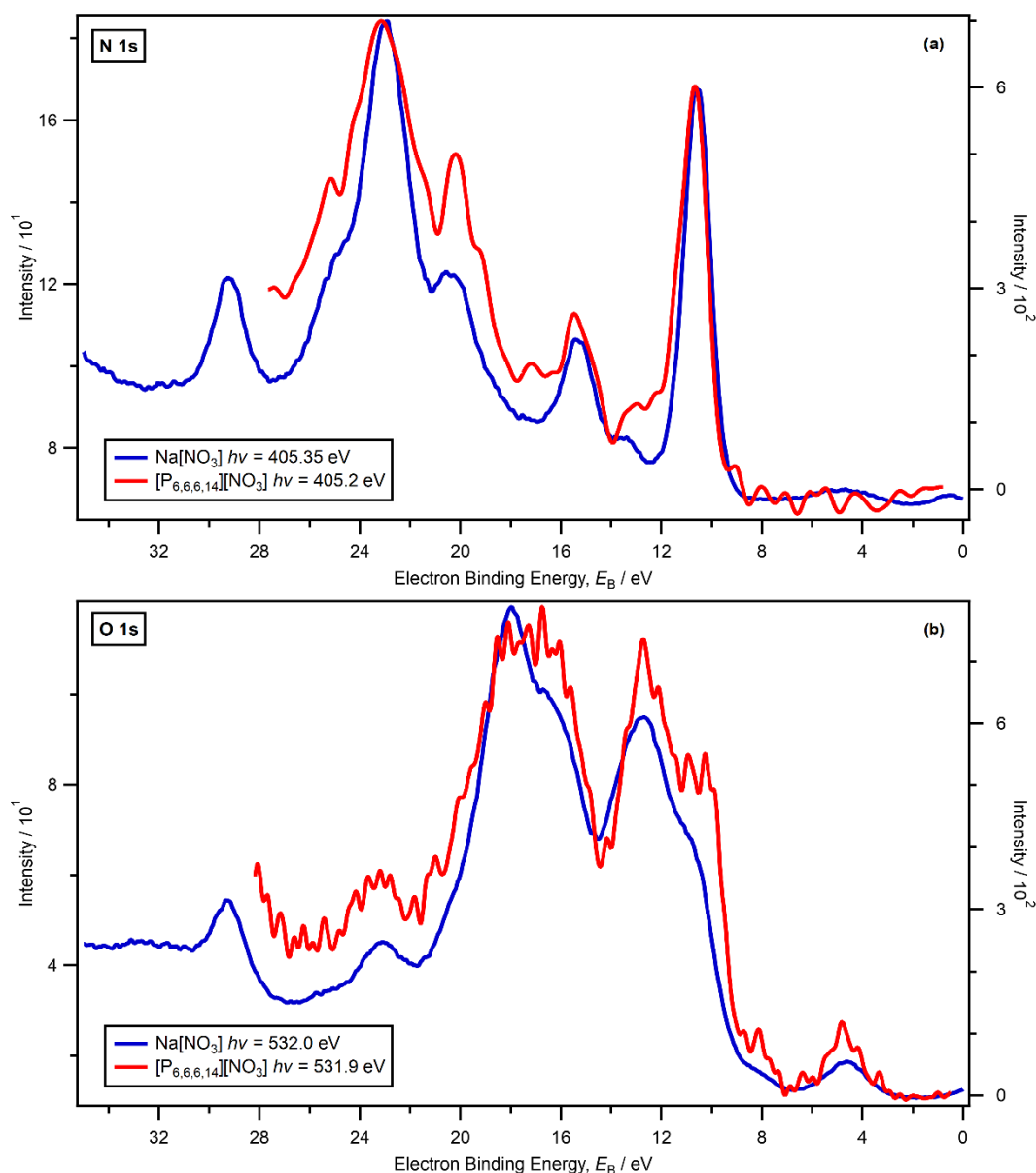


Figure S75. Electron spectra for the on-resonance absorption. (a) N 1s edge: $\text{Na}[\text{NO}_3]$ on-resonance value of $h\nu = 405.35$ eV and $[\text{P}_{6,6,6,14}][\text{NO}_3]$ on-resonance value of $h\nu = 405.2$ eV. (b) O 1s edge: $\text{Na}[\text{NO}_3]$ on-resonance value of $h\nu = 532.0$ eV and $[\text{P}_{6,6,6,14}][\text{NO}_3]$ on-resonance value of $h\nu = 531.9$ eV. The IL RAES traces were produced by subtraction of non-resonant XP contributions using the procedure outlined in ESI Section 10.3. The data for $[\text{P}_{6,6,6,14}][\text{NO}_3]$ has significantly lower signal-to-noise due to how the data was recorded (small $h\nu$ steps, relatively small dwell time at each E_B). The data for $\text{Na}[\text{NO}_3]$ is shifted -2.4 eV to give the best visual match to the data for $[\text{P}_{6,6,6,14}][\text{NO}_3]$. The two arrows on (a) label peaks due to non-resonant valence XPS transitions. Data for $\text{Na}[\text{NO}_3]$ taken from reference⁵⁵.

19. Results. Component identification: summary

Table S8. Component electron binding energies, E_B , for $[C_8C_1Im][C(CN)_3]$ and experimentally-determined atomic orbital contributions to valence electronic structure (see Figure 5 for component labels)

Component	Electron binding energy, E_B / eV	Atomic orbital contributions to valence molecular orbitals determined using variable $h\nu$ XPS and the fingerprint method	Atomic orbital contributions to valence electronic structure determined using RAES
1	2.8		N_{anion}
2	5.0	N_{cation} 2p and/or C_{cation} 2p	N_{anion} , N_{cation} , C
3	5.9		N_{anion} , N_{cation} , C
4	7.5		N_{anion} , C

Table S9. Component electron binding energies, E_B , for $[C_8C_1Im][NTf_2]$ and experimentally-determined atomic orbital contributions to valence electronic structure (see Figure 7 for component labels)

Component	Electron binding energy, E_B / eV	Atomic orbital contributions to valence molecular orbitals determined using variable $h\nu$ XPS and the fingerprint method	Atomic orbital contributions to valence electronic structure determined using RAES
1	~6	N_{cation} 2p and/or C_{cation} 2p	N_{cation} , O_{anion} , C_{cation}
2	~10	F 2p	O_{anion} , C_{cation}

Table S10. Component electron binding energies, E_B , for $[N_{4,1,1,0}][HSO_4]$ and experimentally-determined atomic orbital contributions to valence electronic structure (see ESI Figure S59d for component labels)

Component	Electron binding energy, E_B / eV	Atomic orbital contributions to valence molecular orbitals determined using variable $h\nu$ XPS and the fingerprint method	Atomic orbital contributions to valence electronic structure determined using RAES
1	~4	p	O_{anion}
2	~6.5	p	O_{anion} , C_{cation}
3	~8	p	C_{cation}
4	~10	p	O_{anion} , C_{cation}

Table S11. Component electron binding energies, E_B , for $[N_{2,2,1,0}][TfO]$ and experimentally-determined atomic orbital contributions to valence electronic structure (see Figure 6 for component labels)

Component	Electron binding energy, E_B / eV	Atomic orbital contributions to valence molecular orbitals determined using variable $h\nu$ XPS and the fingerprint method	Atomic orbital contributions to valence electronic structure determined using RAES
1	~6	p	O_{anion}
2	~10	F 2p	O_{anion}

Table S12. Component electron binding energies, E_B , for $[P_{6,6,6,14}][NO_3]$ and experimentally-determined atomic orbital contributions to valence electronic structure (see ESI Figure S59f for component labels)

Component	Electron binding energy, E_B / eV	Atomic orbital contributions to valence molecular orbitals determined using variable $h\nu$ XPS and the fingerprint method	Atomic orbital contributions to valence electronic structure determined using RAES
1	~3.5	p	O_{anion}
2	~5	p	O_{anion} , C_{cation}
3	~7.5	p	C_{cation}
4	~10.5	N_{anion} or O_{anion} 2p	N_{anion} , C_{cation}

20. Results. Fingerprint method: visual comparisons

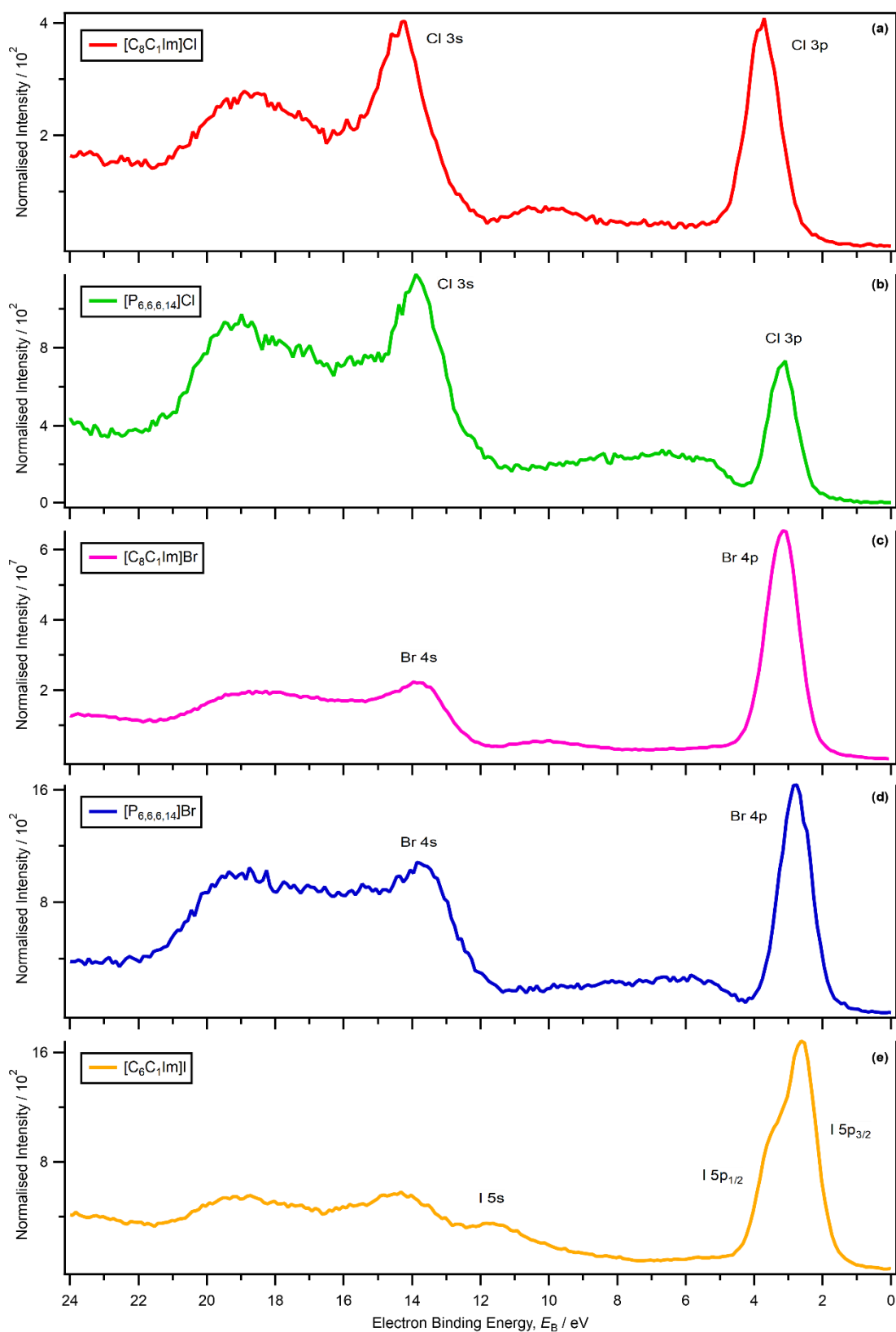


Figure S76. Valence XP spectra, all recorded at $h\nu = 1486.6$ eV for: (a) $[C_8C_7Im]Cl$, (b) $[P_{6,6,6,14}]Cl$, (c) $[C_8C_7Im]Br$, (d) $[P_{6,6,6,14}]Br$ and (e) $[C_6C_1Im]I$. All electron spectra were charge referenced using procedures outlined in ESI Section 5.

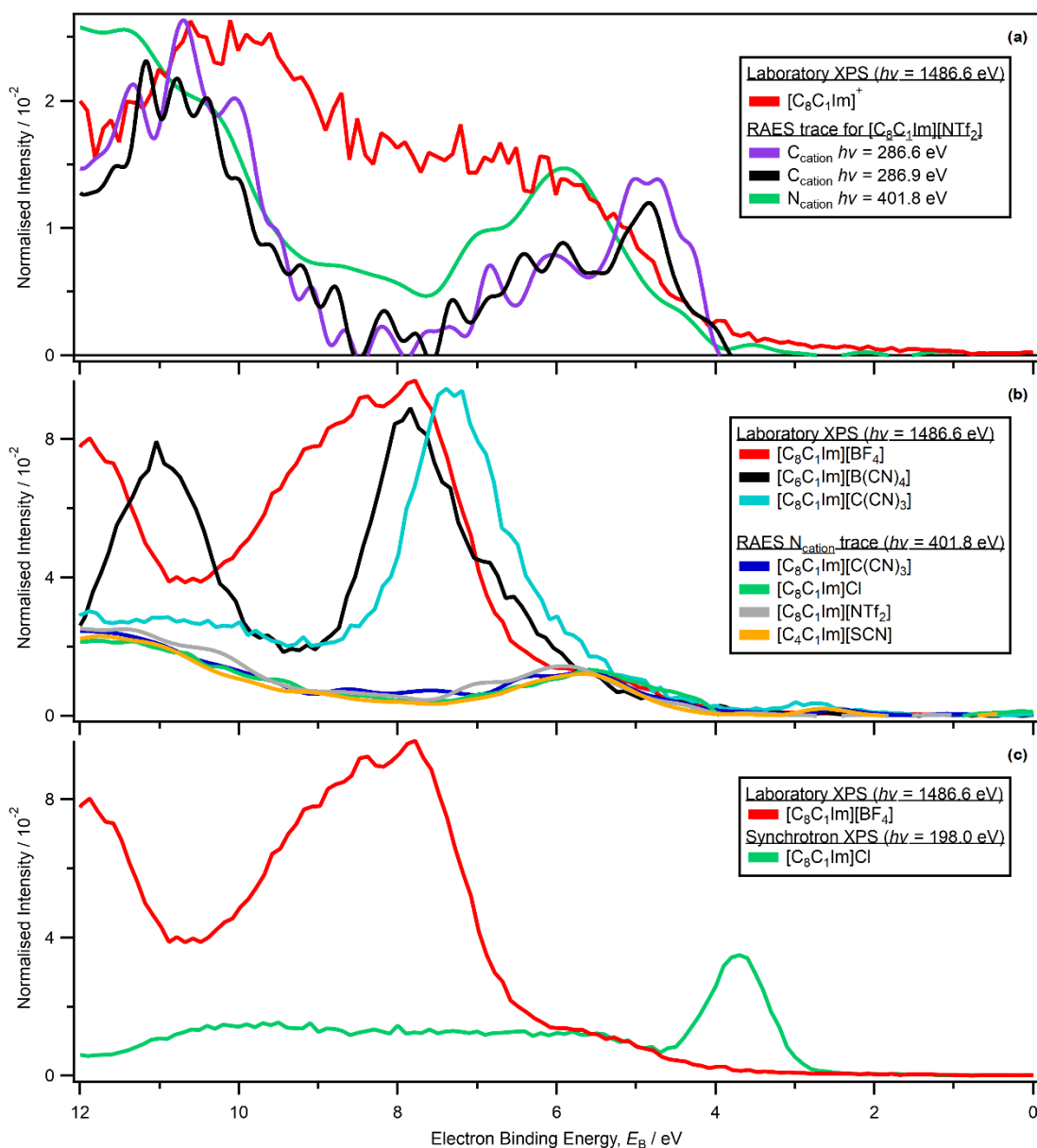


Figure S77. (a) Cation trace for $[\text{C}_8\text{C}_1\text{Im}]^+$ for data recorded at $h\nu = 1486.6$ eV, and RAES traces for $[\text{C}_8\text{C}_1\text{Im}][\text{NTf}_2]$ recorded at $h\nu = 401.8$ eV ($\text{N}_{\text{cation}} 1s \rightarrow \pi^*$ resonance), and $h\nu = 286.6$ eV and $h\nu = 286.9$ eV ($\text{C}_{\text{cation}} 1s \rightarrow \pi^*$ resonance). The area for the $[\text{C}_8\text{C}_1\text{Im}]^+$ trace was normalised using procedures outlined in ESI Section 8.2. The cation trace was obtained using procedures outlined in ESI Section 9. The RAES traces were produced by subtraction of non-resonant XP contributions using the procedure outlined in ESI Section 10.3 and area normalised by eye so that the feature at $E_B \sim 5$ eV was the same intensity as for the cation trace for $[\text{C}_8\text{C}_1\text{Im}]^+$. (b) Area normalised valence XP spectra for $[\text{C}_8\text{C}_1\text{Im}][\text{BF}_4]$, $[\text{C}_6\text{C}_1\text{Im}][\text{B}(\text{CN})_4]$ and $[\text{C}_8\text{C}_1\text{Im}][\text{C}(\text{CN})_3]$ recorded at $h\nu = 1486.6$ eV, and RAES traces for $[\text{C}_n\text{C}_1\text{Im}][\text{A}]$ recorded at $h\nu = 401.8$ eV ($\text{N}_{\text{cation}} 1s \rightarrow \pi^*$ resonance). For the valence XP spectra, the areas were normalised using procedures outlined in ESI Section 8.2. The RAES traces were produced by subtraction of non-resonant XP contributions using the procedure outlined in ESI Section 10.3 and area normalised by eye so that the feature at $E_B \sim 5$ eV was the same intensity as for the area normalised valence XP spectra for $[\text{C}_8\text{C}_1\text{Im}][\text{BF}_4]$, $[\text{C}_6\text{C}_1\text{Im}][\text{B}(\text{CN})_4]$ and $[\text{C}_8\text{C}_1\text{Im}][\text{C}(\text{CN})_3]$. (c) Valence XP spectra for $[\text{C}_8\text{C}_1\text{Im}]\text{Cl}$ and $[\text{C}_8\text{C}_1\text{Im}][\text{BF}_4]$ recorded at $h\nu = 198.0$ eV and $h\nu = 1486.6$ eV respectively. The areas were normalised by eye to make the feature at 4.5 eV $< E_B < 6$ eV the same intensity for both spectra. All electron spectra were charge referenced using procedures outlined in ESI Section 5.

Comparing area normalised (using a region of the valence XP spectra where no peaks appeared, 22 eV $< E_B < 34$ eV) valence XP spectra at $h\nu = 1486.6$ eV for $[\text{C}_8\text{C}_1\text{Im}]\text{Cl}$ and $[\text{C}_8\text{C}_1\text{Im}]\text{Br}$ (ESI Figure S78a), the features at 5 eV $< E_B < 11.5$ eV were essentially identical (as was the area normalisation region at 22 eV $< E_B < 34$ eV). The peaks due to the anions have already been identified using a simple visual comparison. Therefore, this comparison suggests that the features at 5 eV $< E_B < 11.5$ eV were from the $[\text{C}_8\text{C}_1\text{Im}]^+$ cation. Again, more quantitative data analysis by means of area normalisation using core

level peak areas can give far more insight into the valence electronic structure of these types of IL families (see Section 3.4).

A relatively qualitative data analysis approach is to normalise valence XP spectra recorded at $h\nu = 1486.6$ eV for structurally similar ILs using the intensity of valence peaks. For example, when changing the alkyl chain length for $[C_nC_1Im][NTf_2]$ (where $n = 4, 6$ and 8) the valence XP spectra normalised to the area of component 1 looked almost identical (ESI Figure S79a). For the IL families $[C_nC_1Im][SCN]$ and $[C_nC_1Im][TfO]$ (where $n = 4$ and 8), a similar conclusion can be drawn (ESI Figure S79b and ESI Figure S79c). These comparisons suggest that there were subtle differences for the s region when the alkyl chain was varied (ESI Figure S79). However, more quantitative data analysis by means of area normalisation using core level peak areas (followed by subtraction) can give far more insight into the valence electronic structure of ILs (Section 3.4).

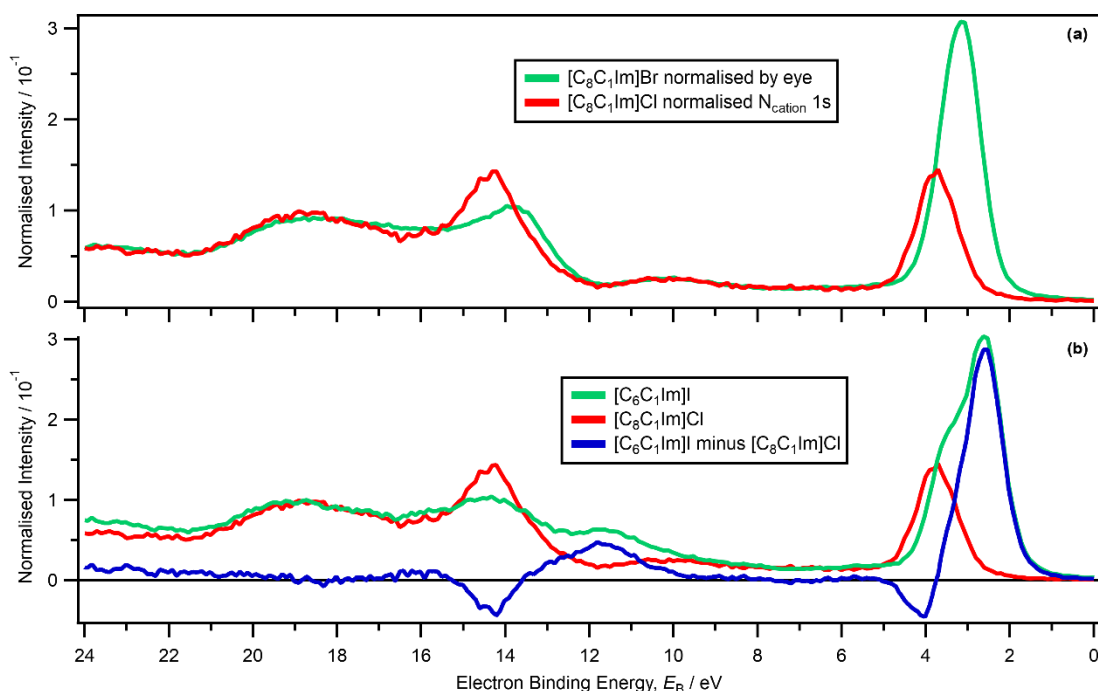


Figure S78. Area normalised (using intensity data at $22 \text{ eV} < E_B < 34 \text{ eV}$) valence XP spectra for $[C_8C_1Im]Cl$ and $[C_6C_1Im]Br$ recorded at $h\nu = 1486.6$ eV. (b) Area normalised valence XP spectra for $[C_6C_1Im]I$ and $[C_8C_1Im]Cl$ recorded at $h\nu = 1486.6$ eV and the subtracted trace $[C_6C_1Im]I$ minus $[C_8C_1Im]Cl$. The areas were normalised using procedures outlined in ESI Section 8.2; subtraction was performed using procedures outlined in ESI Section 10.1. All electron spectra were charge referenced using procedures outlined in ESI Section 5.

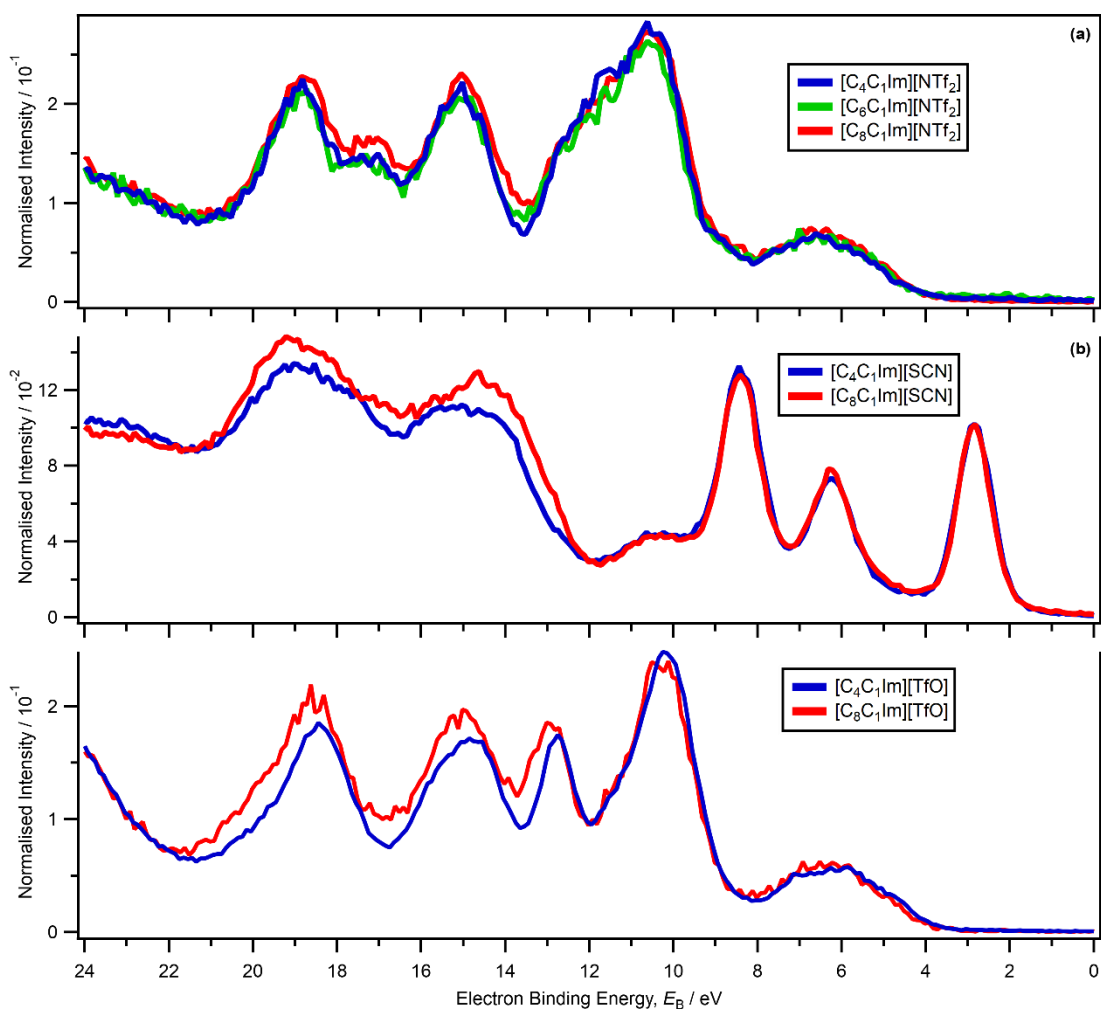


Figure S79. Valence XP spectra, all recorded at $h\nu = 1486.6$ eV, normalised visually to the area of component 1, for: (a) $[C_nC_1Im][NTf_2]$ where $n = 4, 6$ and 8 , (b) $[C_nC_1Im][SCN]$ where $n = 4$ and 8 , (c) $[C_nC_1Im][TfO]$ where $n = 4$ and 8 . The areas were normalised using procedures outlined in ESI Section 8.1. All electron spectra were charge referenced using procedures outlined in ESI Section 5.

21. Results. Subtraction method: identifying cationic and anionic alkyl contributions

In the s AO region at $12 \text{ eV} < E_B < 24 \text{ eV}$ greater deviations were observed than for the p AO region for data recorded at $h\nu = 1486.6 \text{ eV}$. The subtracted traces for $[\text{N}_{8,8,8,1}][\text{NTf}_2]$ minus $[\text{N}_{4,1,1,1}][\text{NTf}_2]$, $[\text{C}_8\text{C}_1\text{Im}][\text{HSO}_4]$ minus $[\text{C}_4\text{C}_1\text{Im}][\text{HSO}_4]$, $[\text{N}_{8,1,1,0}][\text{HSO}_4]$ minus $[\text{N}_{4,1,1,0}][\text{HSO}_4]$, and $[\text{C}_4\text{C}_1\text{Im}][\text{OcSO}_4]$ minus $[\text{C}_4\text{C}_1\text{Im}][\text{MeSO}_4]$ showed broad positive deviations from the zero line in the s AO region at $12 \text{ eV} < E_B < 24 \text{ eV}$ (ESI Figure S80a, ESI Figure S80b, ESI Figure S81b and ESI Figure S82a respectively). In the s AO region at $12 \text{ eV} < E_B < 24 \text{ eV}$ $[\text{N}_{4,1,1,1}][\text{NTf}_2]$ minus $[\text{N}_{3,2,1,1}][\text{NTf}_2]$, $[\text{S}_{2,2,2}][\text{NTf}_2]$ minus $[\text{S}_{2,2,1}][\text{NTf}_2]$, and $[\text{C}_4\text{C}_0\text{Im}][\text{NTf}_2]$ minus $[\text{C}_2\text{C}_0\text{Im}][\text{NTf}_2]$ showed minimal deviations from the zero line (ESI Figure S80d).

These observed differences for p and s AO regions can be explained by comparing photoionisation cross-sections for C 2s against C 2p; the C 2s AO photoionisation cross-section is ~ 30 times larger than the C 2p AO photoionisation cross-section at $h\nu = 1486.6 \text{ eV}$.³⁸ The minimal effects on the p AO region caused by significant changes in the amount of the alkyl carbon in ILs is most likely due to photoionisation cross-sections, and not due to the p AO contributions being essentially the same.

The s AO contributions are not expected to control the reactivity of the ILs, as the p AO contributions would be expected to; in addition, multielectron effects could occur in the s AO region, leading to challenges relating MOs to AOs. Therefore, no attempt will be made to use the data from the region at $E_B > 12 \text{ eV}$ to identify s AO contributions.

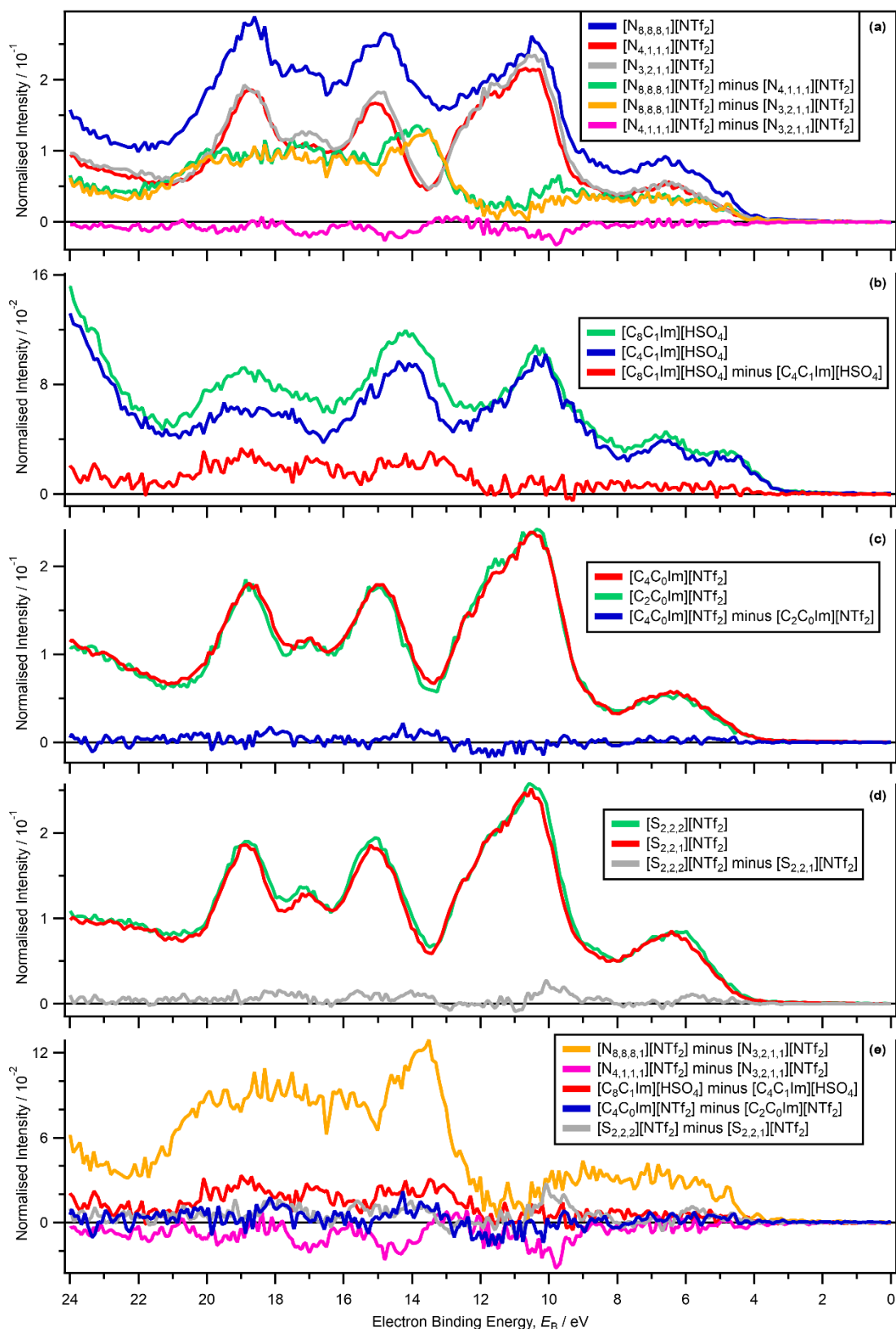


Figure S80. Area normalised valence XP spectra recorded at $h\nu = 1486.6$ eV and subtracted traces, focusing on ILs with the same cation core and anion, whilst varying the alkyl chains. (a) $[N_{8,8,8,1}][NTf_2]$, $[N_{4,1,1,1}][NTf_2]$, $[N_{3,2,1,1}][NTf_2]$, $[N_{8,8,8,1}][NTf_2]$ minus $[N_{4,1,1,1}][NTf_2]$, $[N_{8,8,8,1}][NTf_2]$ minus $[N_{3,2,1,1}][NTf_2]$, and $[N_{4,1,1,1}][NTf_2]$ minus $[N_{3,2,1,1}][NTf_2]$. (b) $[C_8C_1Im][HSO_4]$, $[C_4C_1Im][HSO_4]$, and $[C_8C_1Im][HSO_4]$ minus $[C_4C_1Im][HSO_4]$. (c) $[C_4C_0Im][NTf_2]$, $[C_2C_0Im][NTf_2]$, and $[C_4C_0Im][NTf_2]$ minus $[C_2C_0Im][NTf_2]$. (d) $[S_{2,2,2}][NTf_2]$, $[S_{2,2,1}][NTf_2]$, and $[S_{2,2,2}][NTf_2]$ minus $[S_{2,2,1}][NTf_2]$. (e) $[N_{8,8,8,1}][NTf_2]$ minus $[N_{3,2,1,1}][NTf_2]$, $[N_{4,1,1,1}][NTf_2]$ minus $[N_{3,2,1,1}][NTf_2]$, $[C_8C_1Im][HSO_4]$ minus $[C_4C_1Im][HSO_4]$, $[C_4C_0Im][NTf_2]$ minus $[C_2C_0Im][NTf_2]$, and $[S_{2,2,2}][NTf_2]$ minus $[S_{2,2,1}][NTf_2]$. The areas were normalised using procedures outlined in ESI Section 8.2; subtraction was

performed using procedures outlined in ESI Section 10.1. All electron spectra were charge referenced using procedures outlined in ESI Section 5.

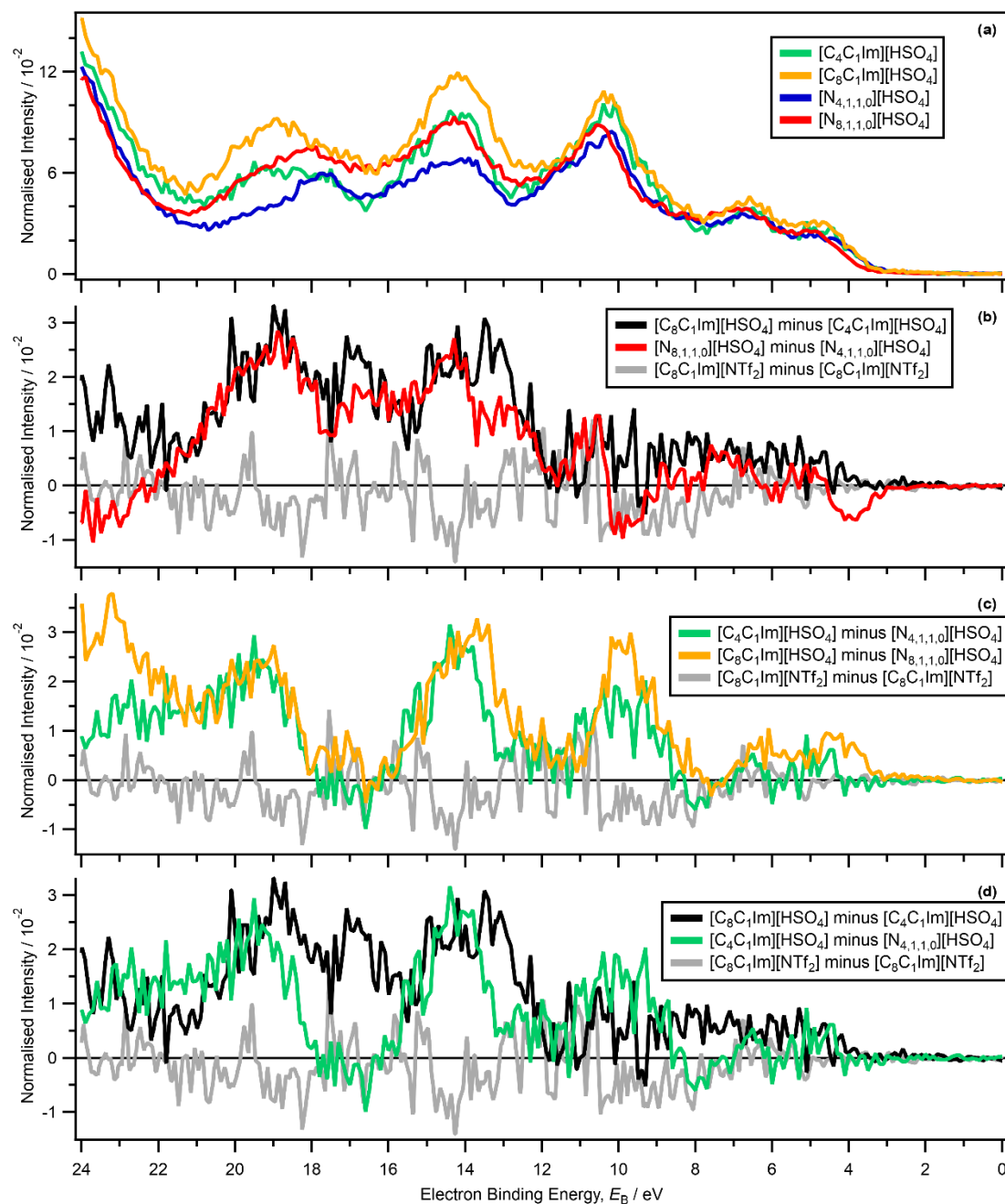


Figure S81. (a) Area normalised valence XP spectra recorded at $h\nu = 1486.6$ eV for $[C_4C_1Im][HSO_4]$, $[C_8C_1Im][HSO_4]$, $[N_{4,1,1,0}][HSO_4]$ and $[N_{8,1,1,0}][HSO_4]$. Subtracted traces for: (b) $[C_8C_1Im][HSO_4]$ minus $[C_4C_1Im][HSO_4]$, $[N_{8,1,1,0}][HSO_4]$ minus $[N_{4,1,1,0}][HSO_4]$ and $[C_8C_1Im][NTf_2]$ minus $[C_8C_1Im][NTf_2]$ (recorded on different days, ESI Section 7.2), (c) $[C_4C_1Im][HSO_4]$ minus $[N_{4,1,1,0}][HSO_4]$, $[C_8C_1Im][HSO_4]$ minus $[N_{8,1,1,0}][HSO_4]$ and $[C_8C_1Im][NTf_2]$ minus $[C_8C_1Im][NTf_2]$ (recorded on different days, ESI Section 7.2), (d) $[C_8C_1Im][HSO_4]$ minus $[C_4C_1Im][HSO_4]$, $[C_4C_1Im][HSO_4]$ minus $[N_{4,1,1,0}][HSO_4]$ and $[C_8C_1Im][NTf_2]$ minus $[C_8C_1Im][NTf_2]$ (recorded on different days, ESI Section 7.2). The areas were normalised using procedures outlined in ESI Section 8.2; subtraction was performed using procedures outlined in ESI Section 10.1. All electron spectra were charge referenced using procedures outlined in ESI Section 5.

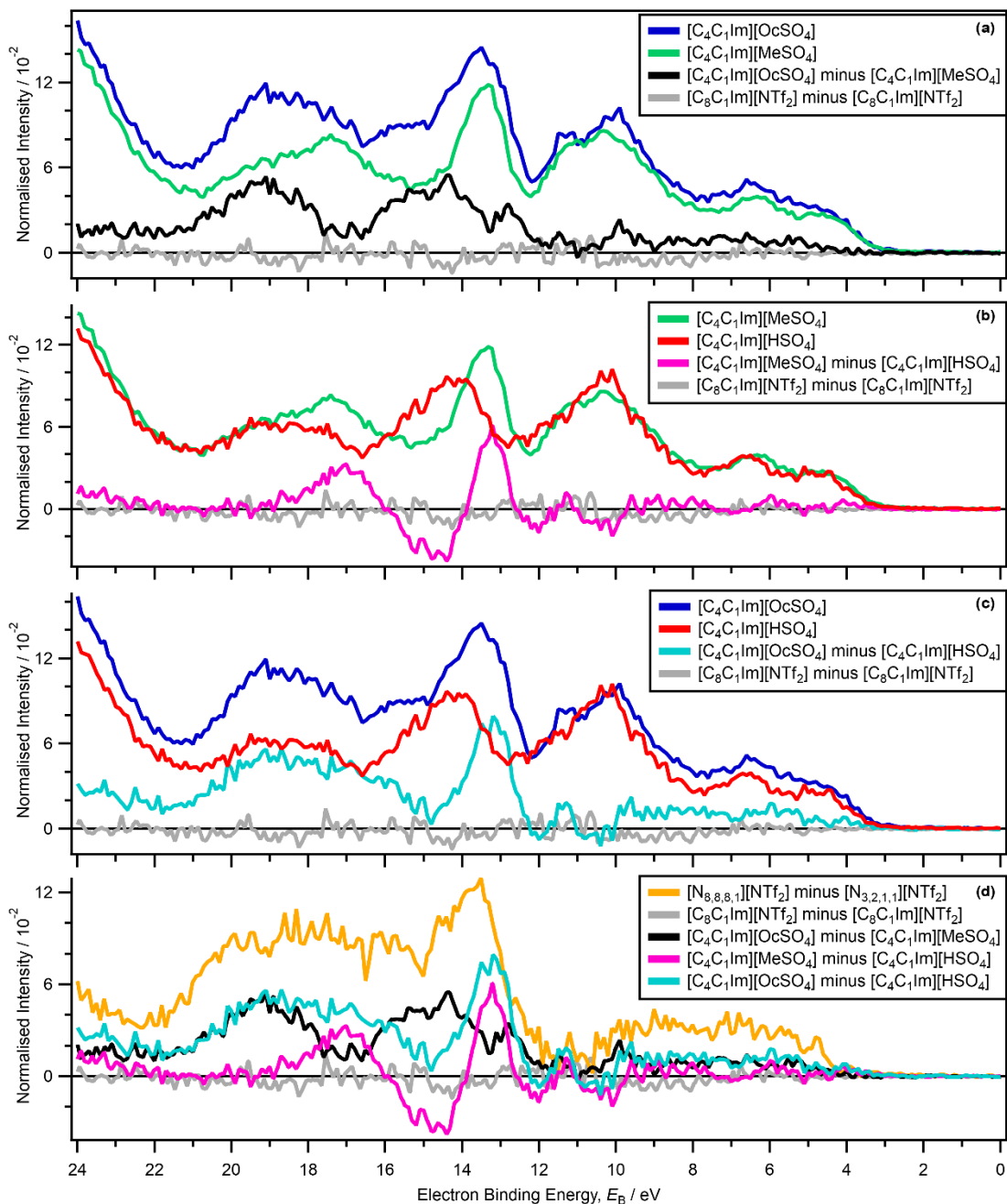


Figure S82. Area normalised valence XP spectra recorded at $h\nu = 1486.6$ eV and subtracted traces, focusing on $[C_4C_1Im][XSO_4]$ ILs. (a) $[C_4C_1Im][OcSO_4]$, $[C_4C_1Im][MeSO_4]$, $[C_4C_1Im][OcSO_4]$ minus $[C_4C_1Im][MeSO_4]$, and $[C_8C_1Im][NTf_2]$ minus $[C_8C_1Im][NTf_2]$ (recorded on different days, ESI Section 7.2). (b) $[C_4C_1Im][MeSO_4]$, $[C_4C_1Im][HSO_4]$, $[C_4C_1Im][MeSO_4]$ minus $[C_4C_1Im][HSO_4]$, and $[C_8C_1Im][NTf_2]$ minus $[C_8C_1Im][NTf_2]$ (recorded on different days, ESI Section 7.2). (c) $[C_4C_1Im][OcSO_4]$, $[C_4C_1Im][HSO_4]$, $[C_4C_1Im][OcSO_4]$ minus $[C_4C_1Im][HSO_4]$, and $[C_8C_1Im][NTf_2]$ minus $[C_8C_1Im][NTf_2]$ (recorded on different days, ESI Section 7.2). (d) $[N_{8,8,8,1}][NTf_2]$ minus $[N_{3,2,1,1}][NTf_2]$, $[C_8C_1Im][NTf_2]$ minus $[C_8C_1Im][NTf_2]$ (recorded on different days, ESI Section 7.2), $[C_4C_1Im][OcSO_4]$ minus $[C_4C_1Im][MeSO_4]$, $[C_4C_1Im][MeSO_4]$ minus $[C_4C_1Im][HSO_4]$, and $[C_4C_1Im][OcSO_4]$ minus $[C_4C_1Im][HSO_4]$. Me = CH₃ and Oc = C₈H₁₇. The areas were normalised using procedures outlined in ESI Section 8.2; subtraction was performed using procedures outlined in ESI Section 10.1. All electron spectra were charge referenced using procedures outlined in ESI Section 5.

22. Results. Subtraction method: identifying cationic non-alkyl contributions

The anion trace for I⁻ ($[\text{C}_6\text{C}_1\text{Im}]\text{I}$ minus $[\text{C}_8\text{C}_1\text{Im}]^+$) showed a very close match to the zero line at $5 \text{ eV} < E_B < 10 \text{ eV}$ (Figure 86b). Therefore, the feature at $5 \text{ eV} < E_B < 10 \text{ eV}$ can be identified as arising from the $[\text{C}_n\text{C}_1\text{Im}]^+$ cation. This identification matched very well to the identification from area normalised valence XP spectra for $[\text{C}_8\text{C}_1\text{Im}]\text{Cl}$ and $[\text{C}_8\text{C}_1\text{Im}]\text{Br}$ (ESI Figure S78a), where the features at $5 \text{ eV} < E_B < 11.5 \text{ eV}$ were essentially identical. The anion trace for I⁻ ($[\text{C}_6\text{C}_1\text{Im}]\text{I}$ minus $[\text{C}_8\text{C}_1\text{Im}]^+$) did not show a very close match to the zero line at $10 \text{ eV} < E_B < 11.5 \text{ eV}$ (Figure 86b) due to an anionic I 5s contribution (ESI Section 22). Therefore, this comparison suggests that the features at $5 \text{ eV} < E_B < 11.5 \text{ eV}$ were from the $[\text{C}_n\text{C}_1\text{Im}]^+$ cation. The area normalised traces for $[\text{C}_8\text{C}_1\text{Im}]\text{Cl}$ and $[\text{C}_8\text{C}_1\text{Im}]\text{Br}$ showed a feature at $9 \text{ eV} < E_B < 11.5 \text{ eV}$ (ESI Figure S78a). Furthermore, the area normalised traces for $[\text{C}_4\text{C}_1\text{Im}][\text{SCN}]$, $[\text{C}_4\text{C}_1\text{Im}][\text{N}(\text{CN})_2]$, $[\text{C}_8\text{C}_1\text{Im}][\text{C}(\text{CN})_3]$ and $[\text{C}_8\text{C}_1\text{Im}]\text{Cl}$ showed a feature of approximately the same intensity at $9 \text{ eV} < E_B < 11.5 \text{ eV}$ (ESI Figure S85). The anion traces for $[\text{SCN}]^-$, $[\text{N}(\text{CN})_2]^-$ and $[\text{C}(\text{CN})_3]^-$ all matched well to the zero line at $9 \text{ eV} < E_B < 11.5 \text{ eV}$ (ESI Figure S87a, ESI Figure S87b and ESI Figure S87c respectively), showing that the peak at $9 \text{ eV} < E_B < 11.5 \text{ eV}$ was from the $[\text{C}_n\text{C}_1\text{Im}]^+$ cation and not from the anions. In addition, the valence XP spectra for $[\text{C}_4\text{C}_1\text{Im}][\text{SCN}]$ and $[\text{C}_8\text{C}_1\text{Im}]\text{Cl}$ recorded at $h\nu = 161.0 \text{ eV}$ and $h\nu = 198.0 \text{ eV}$ respectively showed a peak at $9 \text{ eV} < E_B < 11.5 \text{ eV}$ (Figure 2a and Figure 2b respectively), labelled as component 5. This feature at $9 \text{ eV} < E_B < 11.5 \text{ eV}$ may be related to an intensity enhancement observed in the N 1s RAES for all four $[\text{C}_n\text{C}_1\text{Im}][\text{A}]$ ILs studied here with N 1s RAES (Figure 3, Figure 4, Figure 5 and ESI Figure S61).

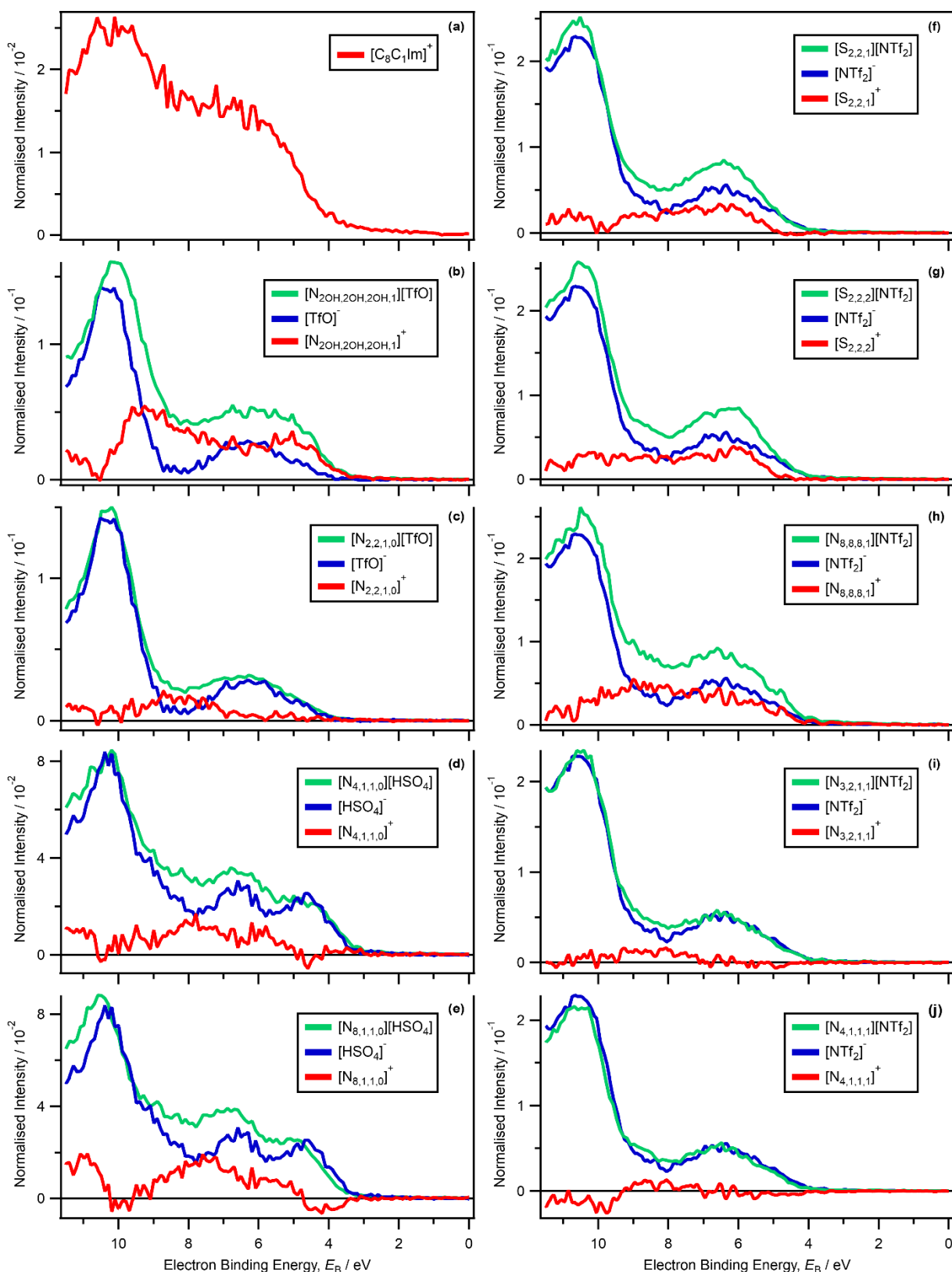


Figure S83. (a) Cation trace for $[C_8C_1Im]^+$. Area normalised valence XP spectrum recorded at $h\nu = 1486.6$ eV, anion trace and cation trace for: (b) $[N_{2OH,2OH,2OH,1}][TfO]$, (c) $[N_{2,2,1,0}][TfO]$, (d) $[N_{4,1,1,0}][HSO_4]$, (e) $[N_{8,1,1,0}][HSO_4]$, (f) $[S_{2,2,1}][NTf_2]$, (g) $[S_{2,2,2}][NTf_2]$, (h) $[N_{8,8,8,1}][NTf_2]$, (i) $[N_{3,2,1,1}][NTf_2]$, (j) $[N_{4,1,1,1}][NTf_2]$. The areas were normalised using procedures outlined in ESI Section 8.2; subtraction was performed using procedures outlined in ESI Section 10.1. The cation and anion traces were obtained using procedures outlined in ESI Section 8.4. All electron spectra were charge referenced using procedures outlined in ESI Section 5.

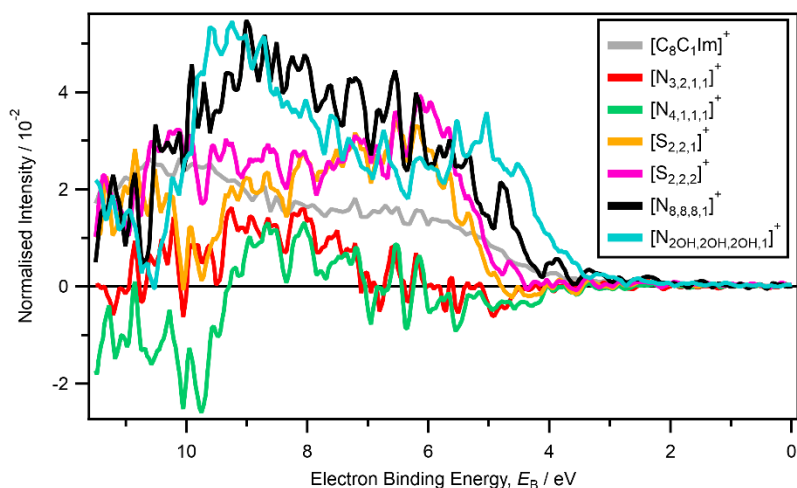


Figure S84. Subtracted ion traces for $[\text{C}_8\text{C}_1\text{Im}]^+$, $[\text{N}_{3,2,1,1}]^+$, $[\text{N}_{4,1,1,1}]^+$, $[\text{S}_{2,2,1}]^+$, $[\text{S}_{2,2,2}]^+$, $[\text{N}_{8,8,8,1}]^+$ and $[\text{N}_{2\text{OH},2\text{OH},2\text{OH},1}]^+$. Subtraction was performed using procedures outlined in ESI Section 10.1. All electron spectra were charge referenced using procedures outlined in ESI Section 5.

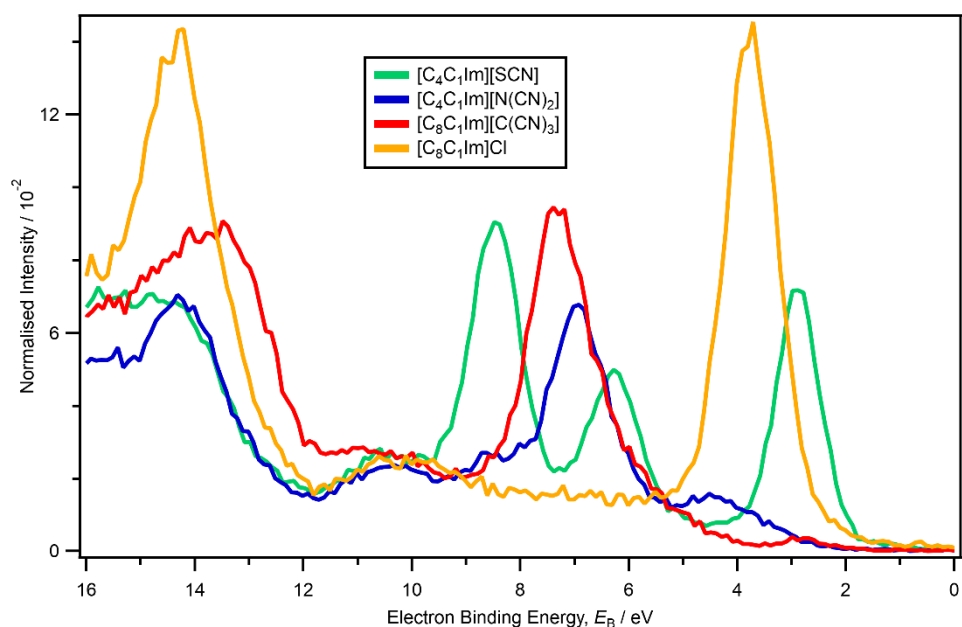


Figure S85. Area normalised valence XP spectra recorded at $h\nu = 1486.6$ eV for $[\text{C}_4\text{C}_1\text{Im}][\text{SCN}]$, $[\text{C}_4\text{C}_1\text{Im}][\text{N}(\text{CN})_2]$, $[\text{C}_8\text{C}_1\text{Im}][\text{C}(\text{CN})_3]$ and $[\text{C}_8\text{C}_1\text{Im}]\text{Cl}$. The areas were normalised using procedures outlined in ESI Section 8.2. All electron spectra were charge referenced using procedures outlined in ESI Section 5.

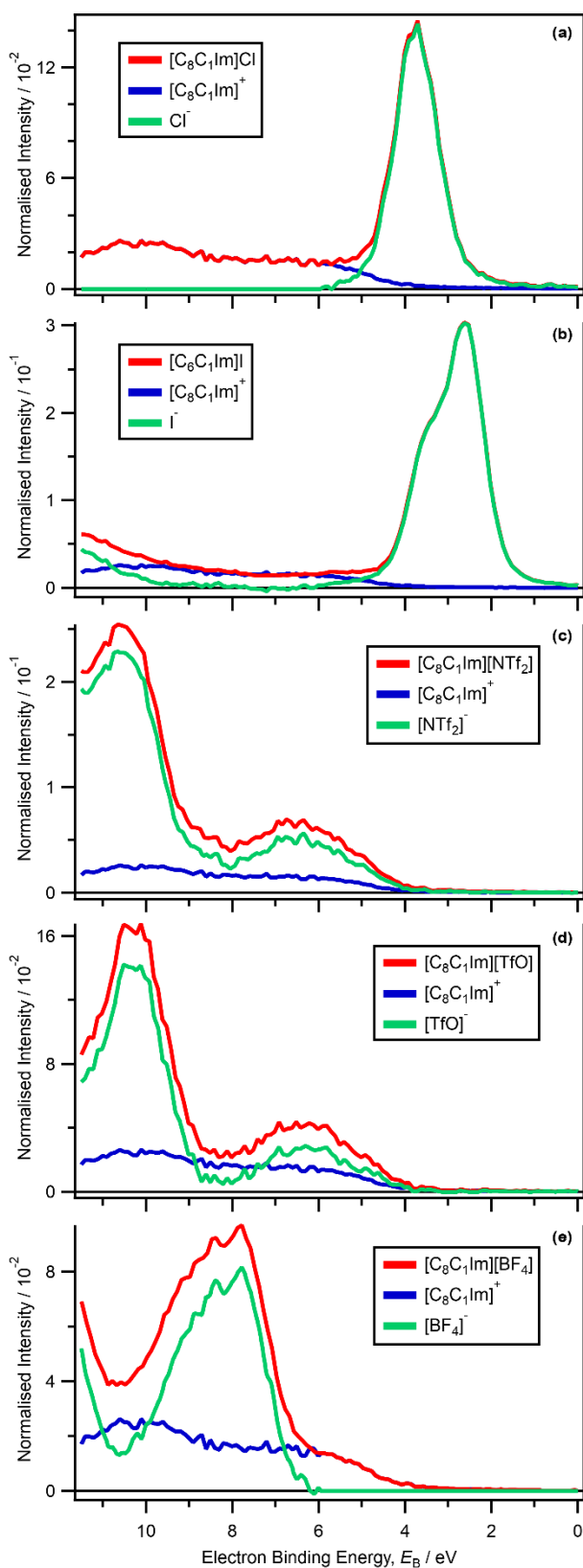


Figure S86. Area normalised valence XP spectrum recorded at $h\nu = 1486.6$ eV, spliced $[\text{C}_8\text{C}_1\text{Im}]^+$ trace and subtracted anion trace for: (a) $[\text{C}_8\text{C}_1\text{Im}]\text{Cl}$, (b) $[\text{C}_8\text{C}_1\text{Im}]\text{I}$, (c) $[\text{C}_8\text{C}_1\text{Im}][\text{NTf}_2]$, (d) $[\text{C}_8\text{C}_1\text{Im}][\text{TfO}]$, (e) $[\text{C}_8\text{C}_1\text{Im}][\text{BF}_4]$. The areas were normalised using procedures outlined in ESI Section 8.2; subtraction was performed using procedures outlined in ESI Section 10.1. The spliced $[\text{C}_8\text{C}_1\text{Im}]^+$ trace and the subtracted anion traces were obtained using procedures outlined in ESI Section 9. All electron spectra were charge referenced using procedures outlined in ESI Section 5.

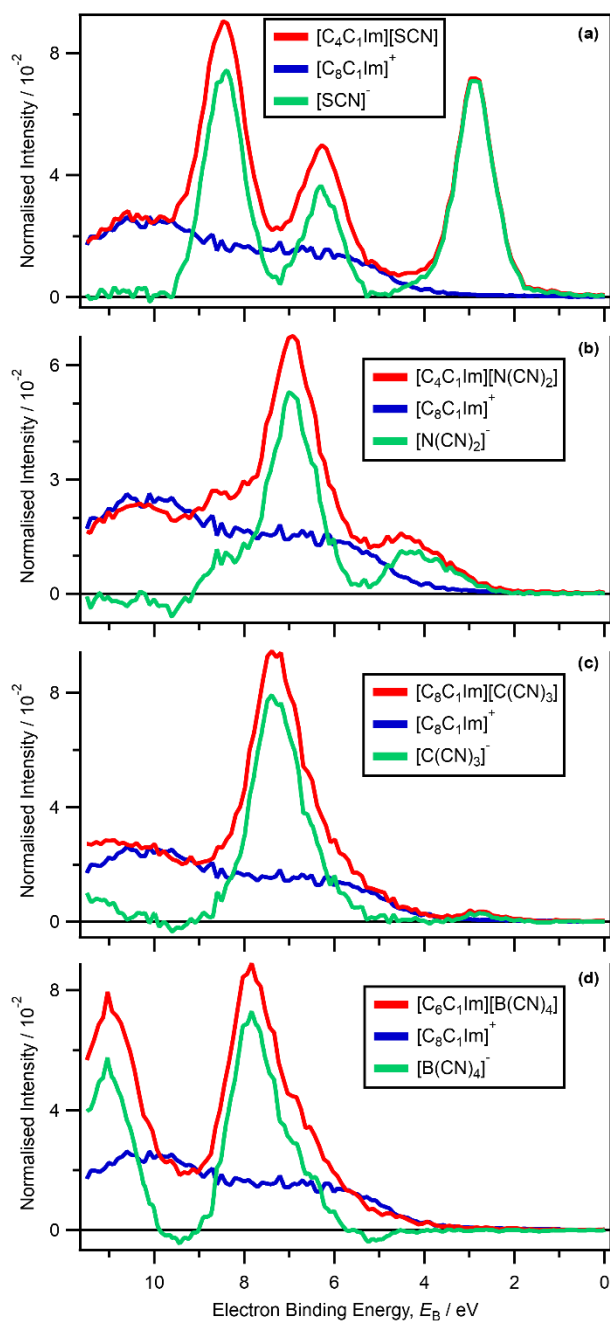


Figure S87. Area normalised valence XP spectrum recorded at $h\nu = 1486.6$ eV, spliced $[\text{C}_8\text{C}_1\text{Im}]^+$ trace and subtracted anion trace for: (a) $[\text{C}_4\text{C}_1\text{Im}][\text{SCN}]$, (b) $[\text{C}_4\text{C}_1\text{Im}][\text{N}(\text{CN})_2]$, (c) $[\text{C}_8\text{C}_1\text{Im}][\text{C}(\text{CN})_3]$, (d) $[\text{C}_8\text{C}_1\text{Im}][\text{B}(\text{CN})_4]$. The areas were normalised using procedures outlined in ESI Section 8.2; subtraction was performed using procedures outlined in ESI Section 10.1. The spliced $[\text{C}_8\text{C}_1\text{Im}]^+$ trace and the subtracted anion traces were obtained using procedures outlined in ESI Section 9. All electron spectra were charge referenced using procedures outlined in ESI Section 5.

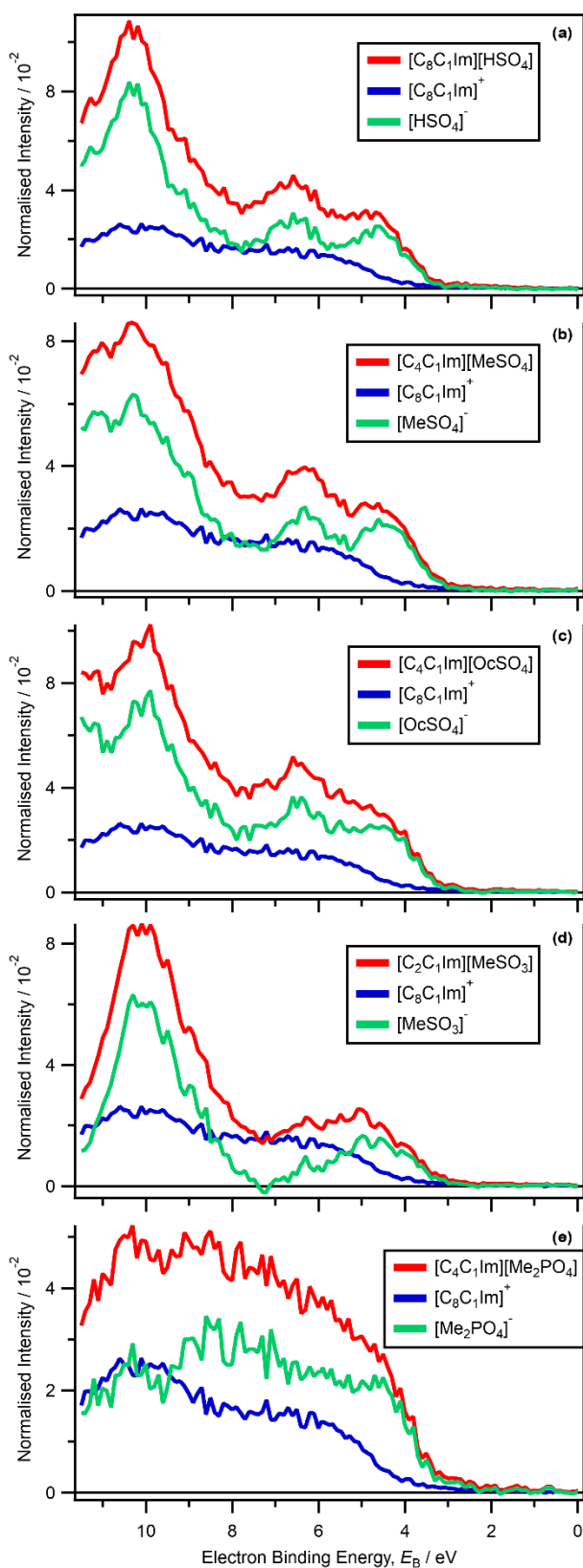


Figure S88. Area normalised valence XP spectrum recorded at $h\nu = 1486.6$ eV, spliced $[\text{C}_8\text{C}_1\text{Im}]^+$ trace and subtracted anion trace for: (a) $[\text{C}_4\text{C}_1\text{Im}][\text{HSO}_4]$, (b) $[\text{C}_4\text{C}_1\text{Im}][\text{MeSO}_4]$, (c) $[\text{C}_4\text{C}_1\text{Im}][\text{OcSO}_4]$, (d) $[\text{C}_2\text{C}_1\text{Im}][\text{MeSO}_3]$, (e) $[\text{C}_4\text{C}_1\text{Im}][\text{Me}_2\text{PO}_4]$. The areas were normalised using procedures outlined in ESI Section 8.2; subtraction was performed using procedures outlined in ESI Section 10.1. The spliced $[\text{C}_8\text{C}_1\text{Im}]^+$ trace and the subtracted anion traces were obtained using procedures outlined in ESI Section 9. All electron spectra were charge referenced using procedures outlined in ESI Section 5.

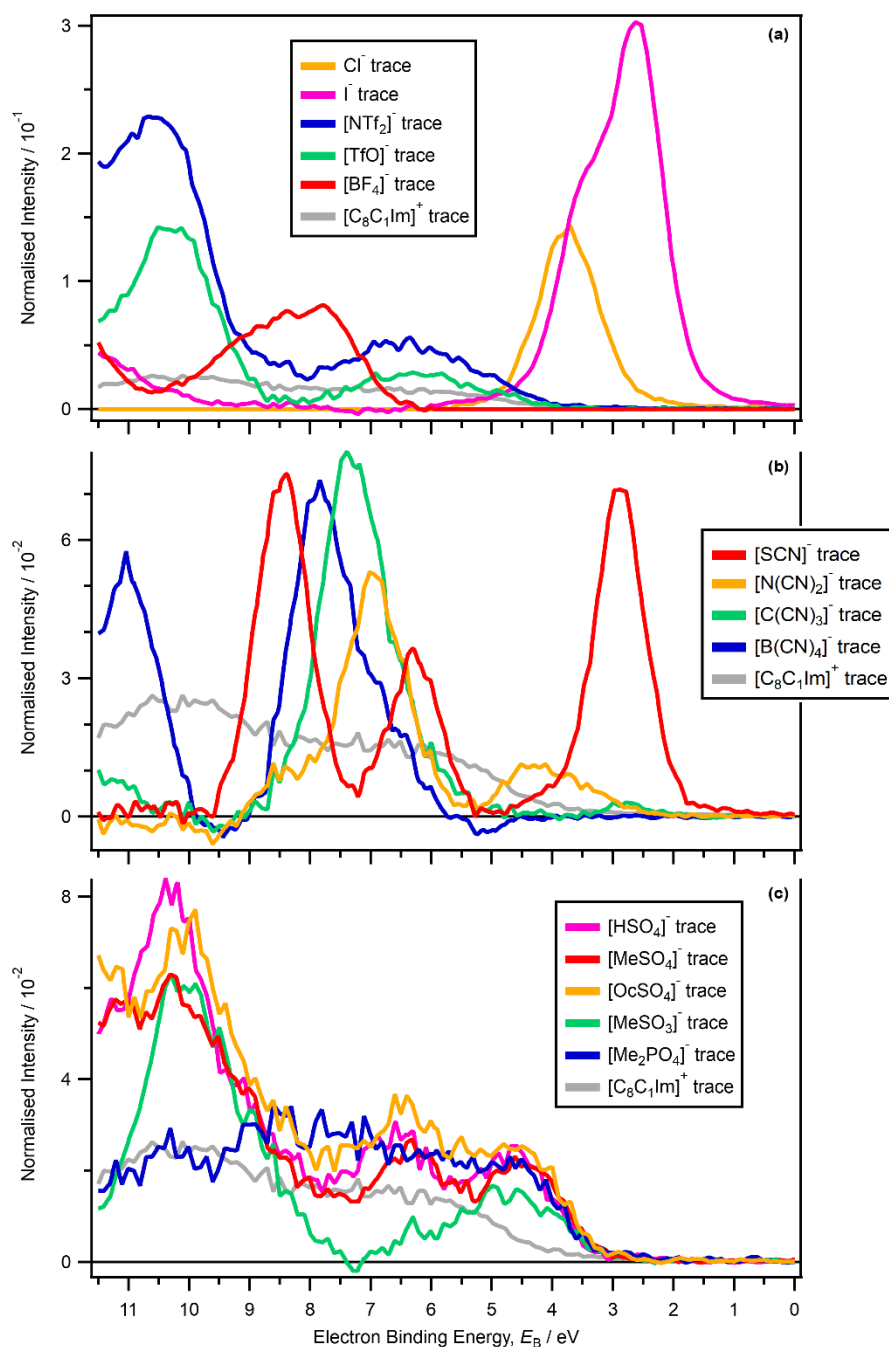


Figure S89. Subtracted ion traces for: (a) Cl^- , I^- , $[\text{NTf}_2]^-$, $[\text{TfO}]^-$, $[\text{BF}_4]^-$ and $[\text{C}_8\text{C}_1\text{Im}]^+$, (b) $[\text{SCN}]^-$, $[\text{N}(\text{CN})_2]^-$, $[\text{C}(\text{CN})_3]^-$, $[\text{B}(\text{CN})_4]^-$ and $[\text{C}_8\text{C}_1\text{Im}]^+$, (c) $[\text{HSO}_4]^-$, $[\text{MeSO}_4]^-$, $[\text{OcSO}_4]^-$, $[\text{MeSO}_3]^-$, $[\text{Me}_2\text{PO}_4]^-$ and $[\text{C}_8\text{C}_1\text{Im}]^+$. Subtraction was performed using procedures outlined in ESI Section 10.1. All electron spectra were charge referenced using procedures outlined in ESI Section 5.

It is important to consider the effect of a protic versus an aprotic cation. However, this is difficult to investigate, for two reasons: (i) changing from an aprotic to a protic IL generally makes the IL more likely to be solid at room temperature, (ii) for valence XP spectra recorded at $h\nu = 1486.6$ eV the C 2p photoionisation cross-section is relatively small,³⁸ meaning that anion peaks usually dominated these valence XP spectra. The subtracted trace for $[\text{C}_4\text{C}_1\text{Im}][\text{HSO}_4]$ (with an aprotic cation) minus $[\text{C}_4\text{C}_0\text{Im}][\text{HSO}_4]$ (with a protic cation) showed some differences above the zero line (ESI Figure S90a). However, the majority of these differences can be explained by the different methods of charge referencing these two ILs;¹⁹ the differences were caused by anion peaks being effectively offset by ~ 0.2 eV, leading to what appear to be peaks in the subtracted trace. The only feature that cannot be explained by this charge referencing issue was the feature at $16.5 \text{ eV} < E_B < 21 \text{ eV}$ (ESI Figure S90a).

This feature was in the s AO region, which means that it is of limited use for identifying the MOs most likely to be important for IL reactivity. However, this difference suggests that there is a small but potentially significant difference between the electronic structures of $[\text{C}_4\text{C}_1\text{Im}][\text{HSO}_4]$ and $[\text{C}_4\text{C}_0\text{Im}][\text{HSO}_4]$. As for identifying differences caused by alkyl carbon atoms (ESI Section 21), valence XP spectra need to be recorded at $h\nu$ significantly lower than $h\nu = 1486.6$ eV to give the chance to identify any differences due to p AO contributions. The subtracted trace for $[\text{C}_8\text{C}_1\text{Im}][\text{NTf}_2]$ (with an aprotic cation) minus $[\text{C}_4\text{C}_0\text{Im}][\text{NTf}_2]$ (with a protic cation) also showed some differences above the zero line (ESI Figure S90b). However, most of these differences were in the s AO region, strongly suggesting that the differences were due to the different alkyl chain lengths of the ILs, and not due to the protic/aprotic nature of the IL cations.

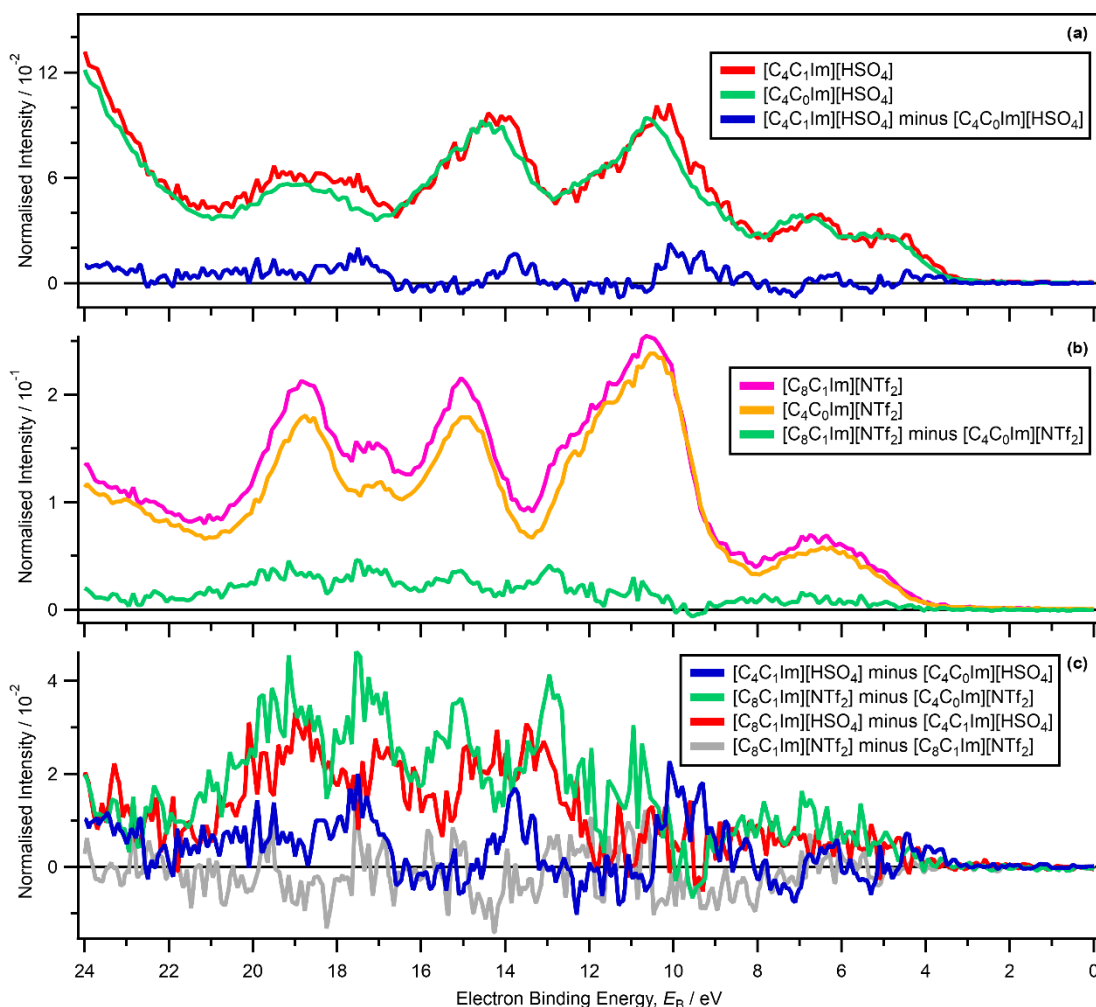


Figure S90. Area normalised valence XP spectra recorded at $h\nu = 1486.6$ eV and subtracted traces, focusing on ILs with protic cations. (a) $[\text{C}_4\text{C}_1\text{Im}][\text{HSO}_4]$, $[\text{C}_4\text{C}_0\text{Im}][\text{HSO}_4]$, and $[\text{C}_4\text{C}_1\text{Im}][\text{HSO}_4]$ minus $[\text{C}_4\text{C}_0\text{Im}][\text{HSO}_4]$. (b) $[\text{C}_8\text{C}_1\text{Im}][\text{NTf}_2]$, $[\text{C}_4\text{C}_0\text{Im}][\text{NTf}_2]$, and $[\text{C}_8\text{C}_1\text{Im}][\text{NTf}_2]$ minus $[\text{C}_4\text{C}_0\text{Im}][\text{NTf}_2]$. (c) $[\text{C}_4\text{C}_1\text{Im}][\text{HSO}_4]$ minus $[\text{C}_4\text{C}_0\text{Im}][\text{HSO}_4]$, $[\text{C}_8\text{C}_1\text{Im}][\text{NTf}_2]$ minus $[\text{C}_4\text{C}_0\text{Im}][\text{NTf}_2]$, $[\text{C}_8\text{C}_1\text{Im}][\text{HSO}_4]$ minus $[\text{C}_4\text{C}_1\text{Im}][\text{HSO}_4]$, and $[\text{C}_8\text{C}_1\text{Im}][\text{NTf}_2]$ minus $[\text{C}_8\text{C}_1\text{Im}][\text{NTf}_2]$ (recorded on different days, ESI Section 7.2). The areas were normalised using procedures outlined in ESI Section 8.2; subtraction was performed using procedures outlined in ESI Section 10.1. All electron spectra were charge referenced using procedures outlined in ESI Section 5.

The combination of data from RAES, variable $h\nu$ XPS and the fingerprint method has proved unsuccessful in identifying cation-based MOs for $[\text{N}_{2,2,1,0}][\text{TfO}]$. Possible reasons are: lack of π^* conduction MOs on the $[\text{N}_{2,2,1,0}]^+$ cation gave spectator Auger instead of participator Auger transitions, no alkyl chain longer than ethyl on the $[\text{N}_{2,2,1,0}]^+$ cation (compared to a butyl chain on $[\text{N}_{4,1,1,0}]^+$), relatively low photoionisation cross-sections for the cationic valence MOs compared to the anionic valence MOs and an inability to identify all anionic-based MOs (due to the relatively large $[\text{TfO}]^-$ anion

paired with the ammonium cations here). Therefore, cation MOs have not been experimentally identified for $[N_{2,2,1,0}][TfO]$. These observations serve to highlight the limitations of the fingerprint method for MO identification, even when other experimental data is available to further aid MO identification.

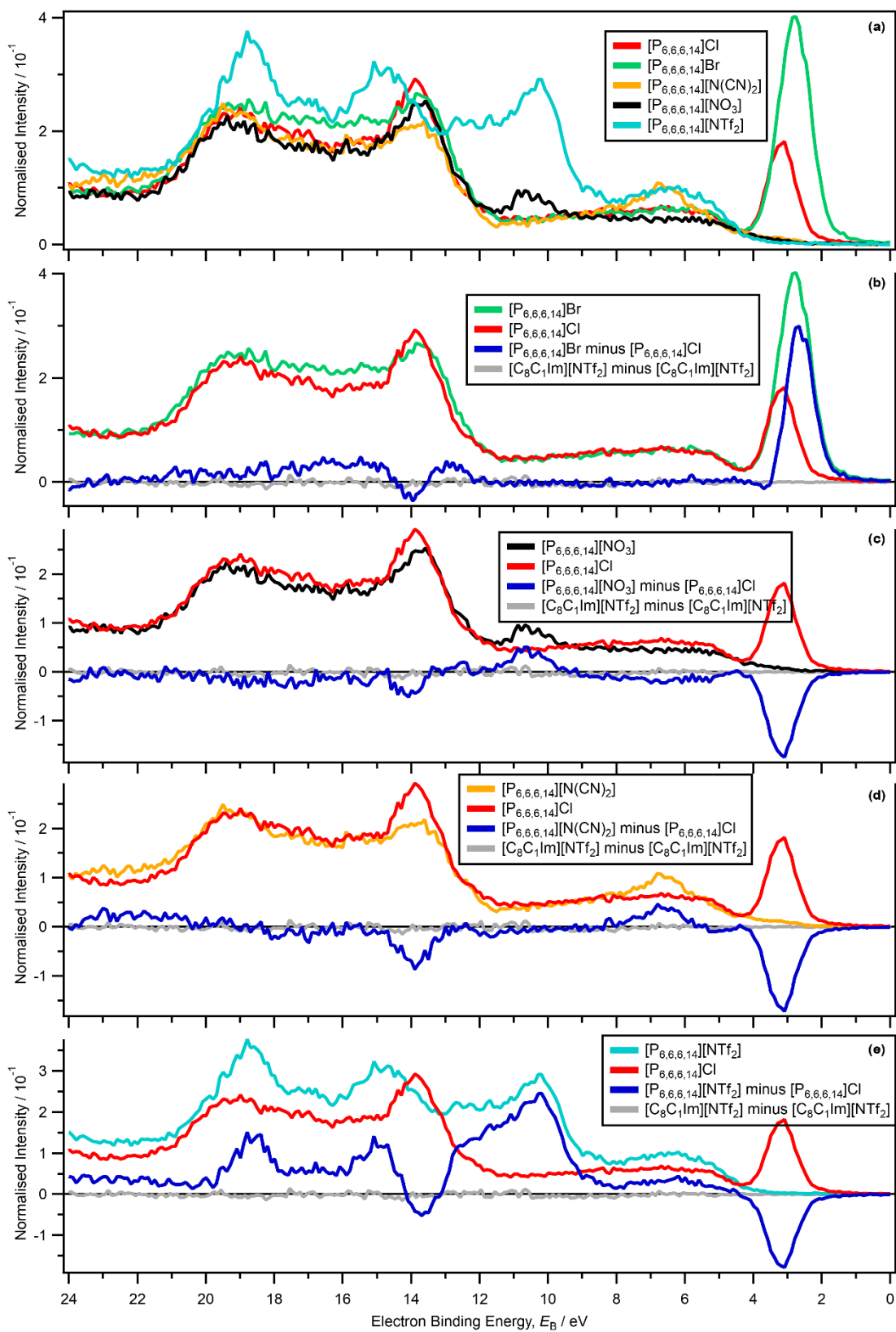


Figure S91. Area normalised valence XP spectra recorded at $h\nu = 1486.6$ eV and subtracted traces, focusing on $[P_{6,6,6,14}][A]$ ILs with different [A]: (a) $[P_{6,6,6,14}][Cl]$, $[P_{6,6,6,14}][Br]$, $[P_{6,6,6,14}][N(CN)_2]$, $[P_{6,6,6,14}][NO_3]$ and $[P_{6,6,6,14}][NTf_2]$. (b) $[P_{6,6,6,14}][Br]$, $[P_{6,6,6,14}][Cl]$, $[P_{6,6,6,14}][Br]$ minus $[P_{6,6,6,14}][Cl]$, and $[C_8C_{1Im}][NTf_2]$ minus $[C_8C_{1Im}][NTf_2]$ (recorded on different days, ESI Section 7.2). (c) $[P_{6,6,6,14}][NO_3]$, $[P_{6,6,6,14}][Cl]$, $[P_{6,6,6,14}][NO_3]$ minus $[P_{6,6,6,14}][Cl]$, and $[C_8C_{1Im}][NTf_2]$ minus $[C_8C_{1Im}][NTf_2]$ (recorded on different days, ESI Section 7.2). (d) $[P_{6,6,6,14}][N(CN)_2]$, $[P_{6,6,6,14}][Cl]$, $[P_{6,6,6,14}][N(CN)_2]$ minus $[P_{6,6,6,14}][Cl]$, and $[C_8C_{1Im}][NTf_2]$ minus $[C_8C_{1Im}][NTf_2]$ (recorded on different days, ESI Section 7.2). (e) $[P_{6,6,6,14}][NTf_2]$, $[P_{6,6,6,14}][Cl]$, $[P_{6,6,6,14}][NTf_2]$ minus $[P_{6,6,6,14}][Cl]$, and $[C_8C_{1Im}][NTf_2]$ minus $[C_8C_{1Im}][NTf_2]$ (recorded on different days, ESI Section 7.2). The areas were normalised using procedures outlined in ESI Section 8.2; subtraction was performed using procedures outlined in ESI Section 10.1. All electron spectra were charge referenced using procedures outlined in ESI Section 5.

In Section 3.4.2 of the article, it was demonstrated using the subtraction method that cationic contributions to the p AO region could be identified for $[N_{2OH,2OH,2OH,1}][TfO]$ and $[S_{2,2,n}][NTf_2]$. The s AO regions for the relevant subtracted traces showed similar magnitude peaks to the p AO regions (ESI Figure S92a and ESI Figure S93a). Therefore, the differences observed in the p AO regions were very unlikely to be due to alkyl carbon contributions, as these would have led to more significant differences in the s AO regions.

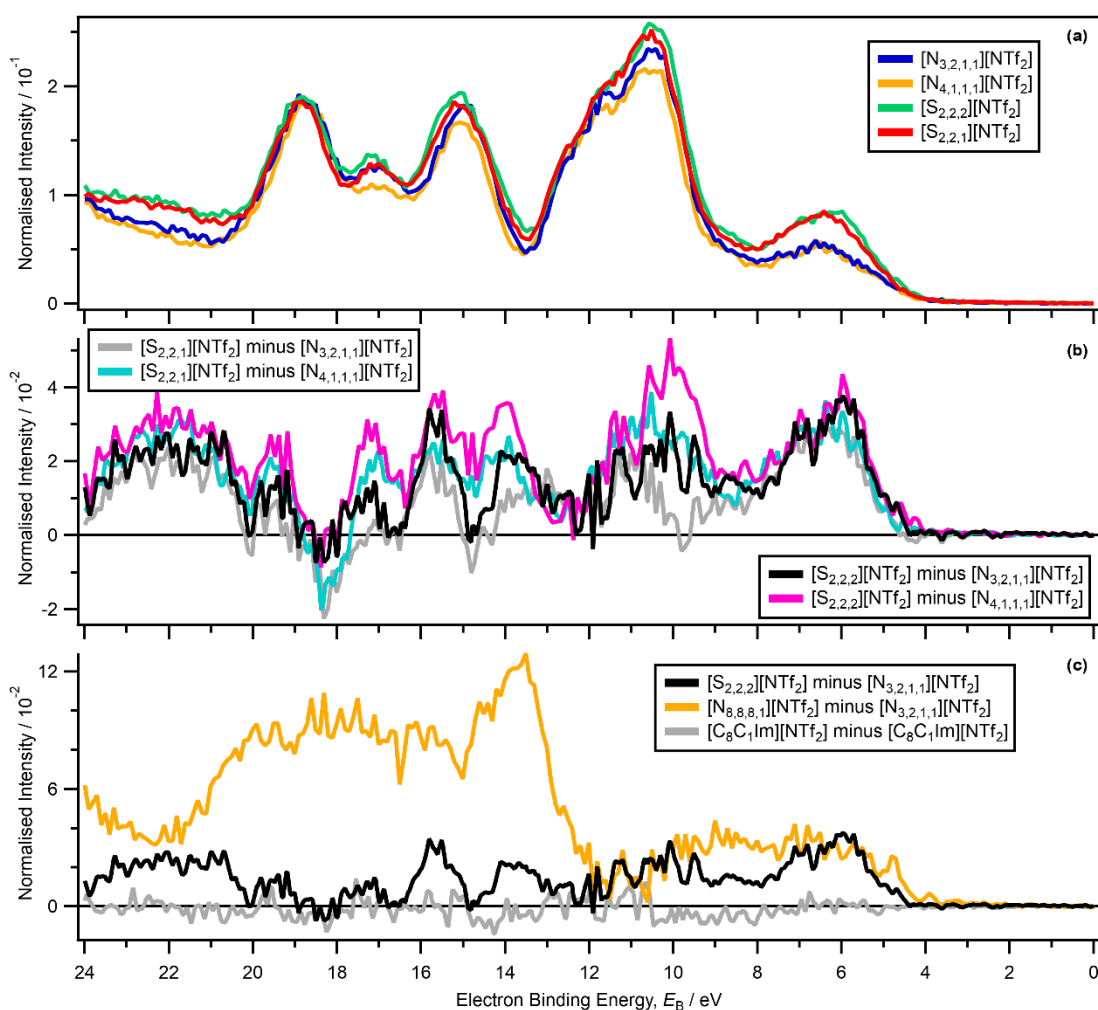


Figure S92. Area normalised valence XP spectra recorded at $h\nu = 1486.6$ eV and subtracted traces, focusing on [cation][NTf₂] ILs, where the cation core was different, and all ILs had relatively short alkyl chains. (a) $[N_{3,2,1,1}][NTf_2]$, $[N_{4,1,1,1}][NTf_2]$, $[S_{2,2,2}][NTf_2]$ and $[S_{2,2,1}][NTf_2]$. (b) $[S_{2,2,1}][NTf_2]$ minus $[N_{3,2,1,1}][NTf_2]$, $[S_{2,2,1}][NTf_2]$ minus $[N_{4,1,1,1}][NTf_2]$, $[S_{2,2,2}][NTf_2]$ minus $[N_{3,2,1,1}][NTf_2]$, and $[S_{2,2,2}][NTf_2]$ minus $[N_{4,1,1,1}][NTf_2]$. (c) $[S_{2,2,2}][NTf_2]$ minus $[N_{3,2,1,1}][NTf_2]$, $[N_{8,8,8,1}][NTf_2]$ minus $[N_{3,2,1,1}][NTf_2]$, and $[C_8C_{1Im}][NTf_2]$ minus $[C_8C_{1Im}][NTf_2]$ (recorded on different days, ESI Section 7.2). The areas were normalised using procedures outlined in ESI Section 8.2; subtraction was performed using procedures outlined in ESI Section 10.1. All electron spectra were charge referenced using procedures outlined in ESI Section 5.

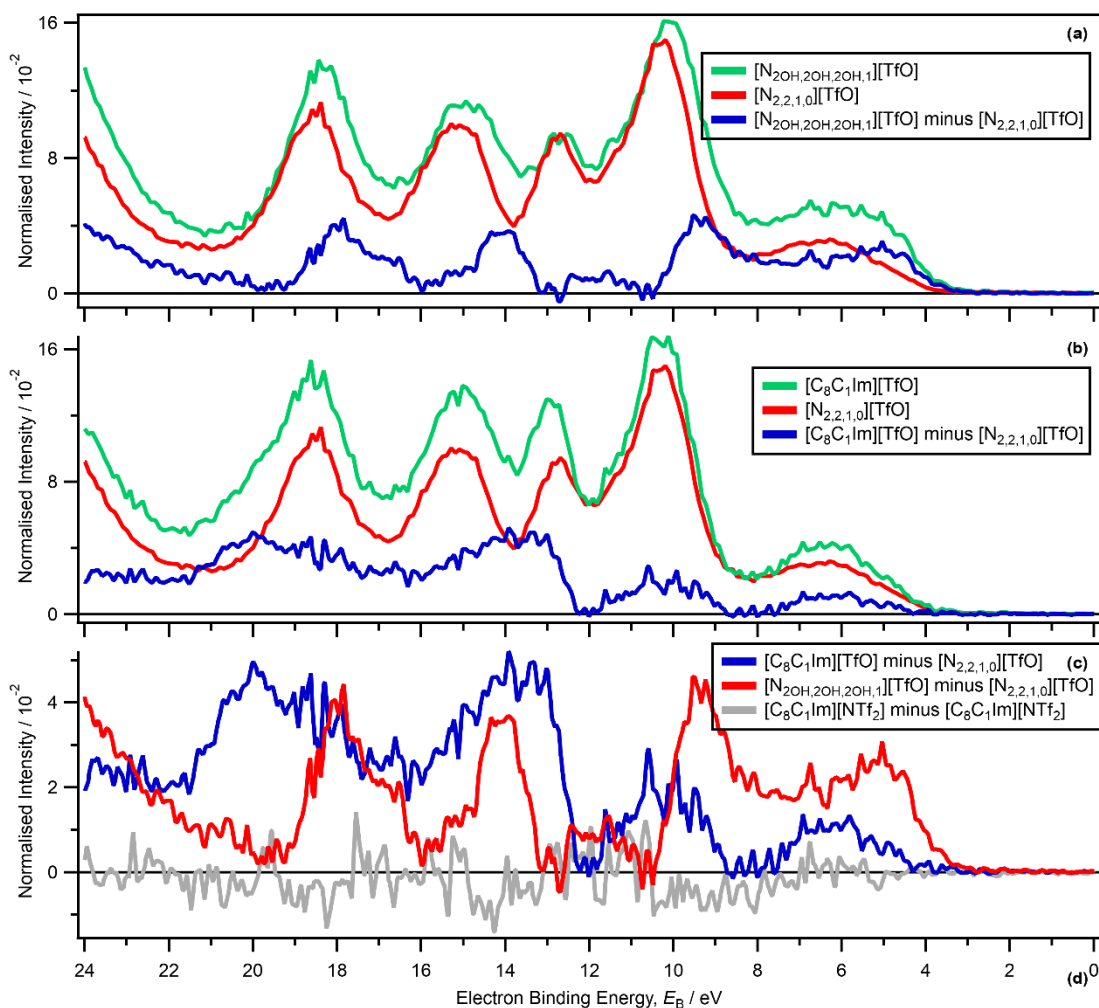


Figure S93. Area normalised valence XP spectra recorded at $h\nu = 1486.6$ eV and subtracted traces, focusing on [cation][TfO] ILs. (a) $[N_{2OH,2OH,2OH,1}][TfO]$, $[N_{2,2,1,0}][TfO]$, $[N_{2OH,2OH,2OH,1}][TfO]$ minus $[N_{2,2,1,0}][TfO]$. (b) $[C_8C_1Im][TfO]$, $[N_{2,2,1,0}][TfO]$, $[C_8C_1Im][TfO]$ minus $[N_{2,2,1,0}][TfO]$. (c) $[C_8C_1Im][TfO]$ minus $[N_{2,2,1,0}][TfO]$, $[N_{2OH,2OH,2OH,1}][TfO]$ minus $[N_{2,2,1,0}][TfO]$, and $[C_8C_1Im][NTf_2]$ minus $[C_8C_1Im][NTf_2]$ (recorded on different days, ESI Section 7.2). The areas were normalised using procedures outlined in ESI Section 8.2; subtraction was performed using procedures outlined in ESI Section 10.1. All electron spectra were charge referenced using procedures outlined in ESI Section 5.

12 comparisons were attempted for ILs with the same anion and different cation cores (and for many examples with very different alkyl chain lengths too) that did not allow MO identification. These comparisons are included here for completeness. For most of these comparisons the subtracted trace gave significantly more intense features in the s AO region than in the p AO region: $[C_8C_1Im][TfO]$ minus $[N_{2,2,1,0}][TfO]$ (ESI Figure S93b), $[P_{6,6,6,14}][NTf_2]$ minus $[C_8C_1Im][NTf_2]$ (ESI Figure S94b), $[P_{6,6,6,14}][NTf_2]$ minus $[N_{8,8,8,1}][NTf_2]$ (ESI Figure S94b), $[P_{6,6,6,14}][Cl]$ minus $[C_8C_1Im][Cl]$ (ESI Figure S97d), $[P_{6,6,6,14}][N(CN)_2]$ minus $[C_8C_1Im][N(CN)_2]$ (ESI Figure S97d), $[N_{8,8,8,1}][NTf_2]$ minus $[C_8C_1Im][NTf_2]$ (ESI Figure S94b), $[C_8C_1Im][NTf_2]$ minus $[N_{3,2,1,1}][NTf_2]$ (ESI Figure S95c) and $[C_8C_1Im][NTf_2]$ minus $[N_{4,1,1,1}][NTf_2]$ (ESI Figure S95c).

For ammonium-based cations with the $[HSO_4]^-$ anion, the ILs in this study were those with protic cations (ESI Table S1). Given the challenges presented by charge referencing, as already explained in ESI Section 5 and reference¹⁹, the relatively small differences observed in the subtracted traces were not analysed here (ESI Figure S81). For comparisons of the cations with similar alkyl chain lengths ($[C_4C_0Im][NTf_2]$ minus $[N_{3,2,1,1}][NTf_2]$ and $[C_4C_0Im][NTf_2]$ minus $[N_{4,1,1,1}][NTf_2]$), the subtracted traces showed relatively small intensities, not far above the zero line (ESI Figure S95). Therefore, these traces were not used for MO identification.

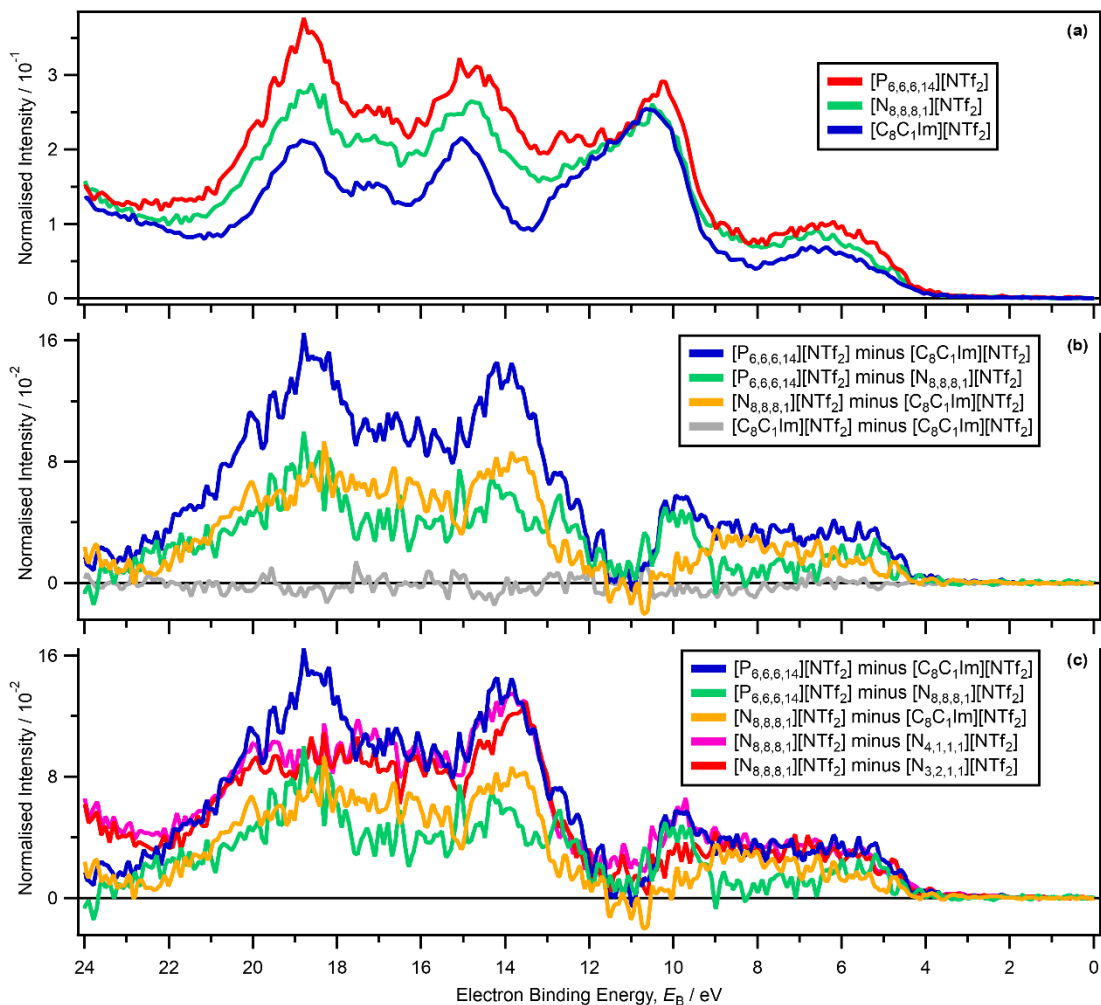


Figure S94. Area normalised valence XP spectra recorded at $h\nu = 1486.6$ eV and subtracted traces, focusing on [cation][NTf₂] ILs, where the cation core was different, and all ILs had relatively long alkyl chains. (a) $[P_{6,6,6,14}][NTf_2]$, $[N_{8,8,8,1}][NTf_2]$ and $[C_8C_1Im][NTf_2]$. (b) $[P_{6,6,6,14}][NTf_2]$ minus $[C_8C_1Im][NTf_2]$, $[P_{6,6,6,14}][NTf_2]$ minus $[N_{8,8,8,1}][NTf_2]$, $[N_{8,8,8,1}][NTf_2]$ minus $[C_8C_1Im][NTf_2]$, and $[C_8C_1Im][NTf_2]$ minus $[C_8C_1Im][NTf_2]$ (recorded on different days, ESI Section 7.2). (c) $[P_{6,6,6,14}][NTf_2]$ minus $[C_8C_1Im][NTf_2]$, $[P_{6,6,6,14}][NTf_2]$ minus $[N_{8,8,8,1}][NTf_2]$, $[N_{8,8,8,1}][NTf_2]$ minus $[C_8C_1Im][NTf_2]$, $[N_{8,8,8,1}][NTf_2]$ minus $[N_{4,1,1,1}][NTf_2]$, and $[N_{8,8,8,1}][NTf_2]$ minus $[N_{3,2,1,1}][NTf_2]$. The areas were normalised using procedures outlined in ESI Section 8.2; subtraction was performed using procedures outlined in ESI Section 10.1. All electron spectra were charge referenced using procedures outlined in ESI Section 5.

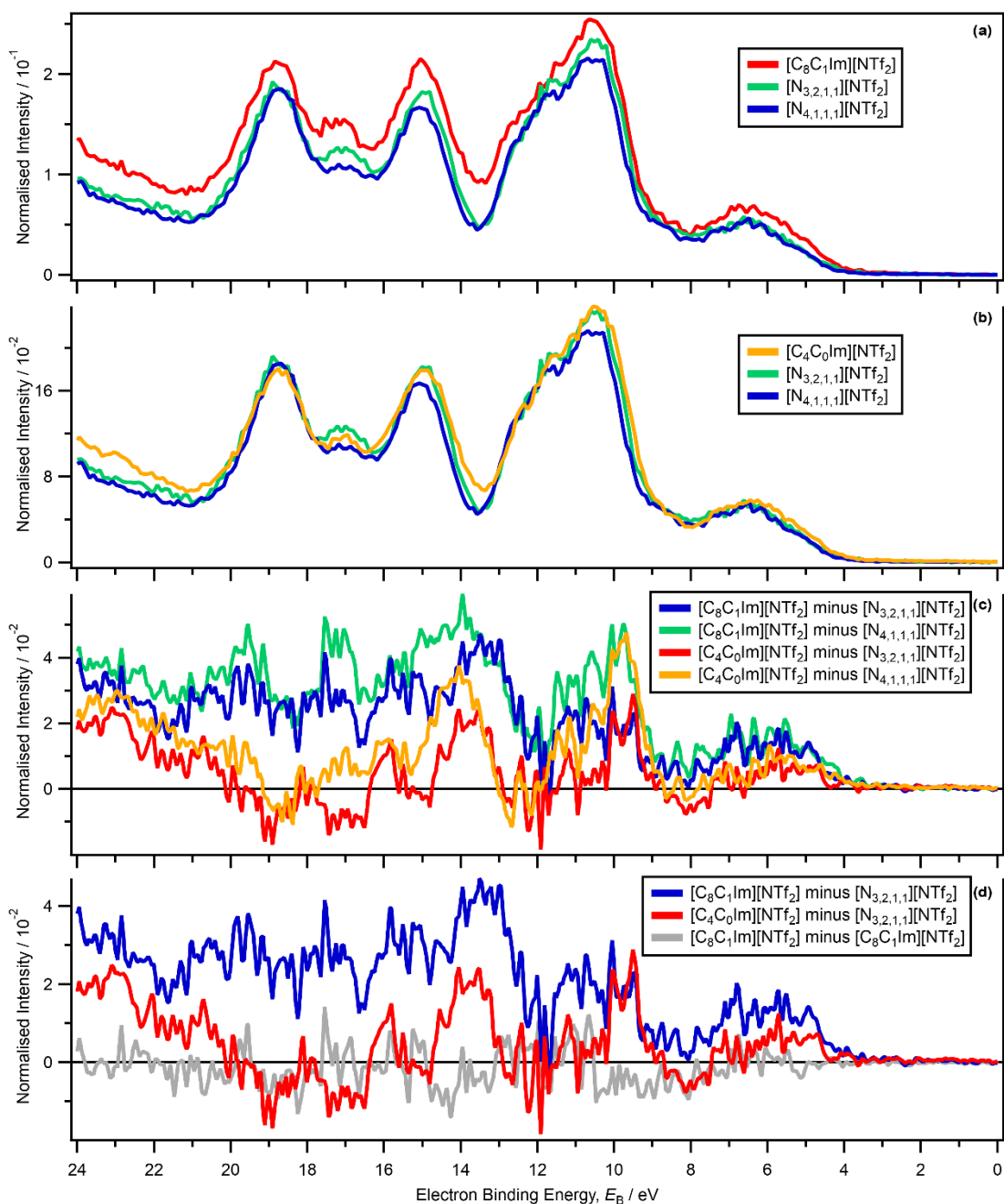


Figure S95. Area normalised valence XP spectra recorded at $h\nu = 1486.6$ eV and subtracted traces, focusing on [cation][NTf₂] ILs, where the cation core was different. (a) [C₈C₁Im][NTf₂], [N_{3,2,1,1}][NTf₂] and [N_{4,1,1,1}][NTf₂]. (b) [C₄C₀Im][NTf₂], [N_{3,2,1,1}][NTf₂] and [N_{4,1,1,1}][NTf₂]. (c) [C₈C₁Im][NTf₂] minus [N_{3,2,1,1}][NTf₂], [C₈C₁Im][NTf₂] minus [N_{4,1,1,1}][NTf₂], [C₄C₀Im][NTf₂] minus [N_{3,2,1,1}][NTf₂], and [C₄C₀Im][NTf₂] minus [N_{4,1,1,1}][NTf₂]. (d) [C₈C₁Im][NTf₂] minus [N_{3,2,1,1}][NTf₂], [C₄C₀Im][NTf₂] minus [N_{3,2,1,1}][NTf₂], and [C₈C₁Im][NTf₂] minus [C₈C₁Im][NTf₂] (recorded on different days, ESI Section 7.2). The areas were normalised using procedures outlined in ESI Section 8.2; subtraction was performed using procedures outlined in ESI Section 10.1. All electron spectra were charge referenced using procedures outlined in ESI Section 5.

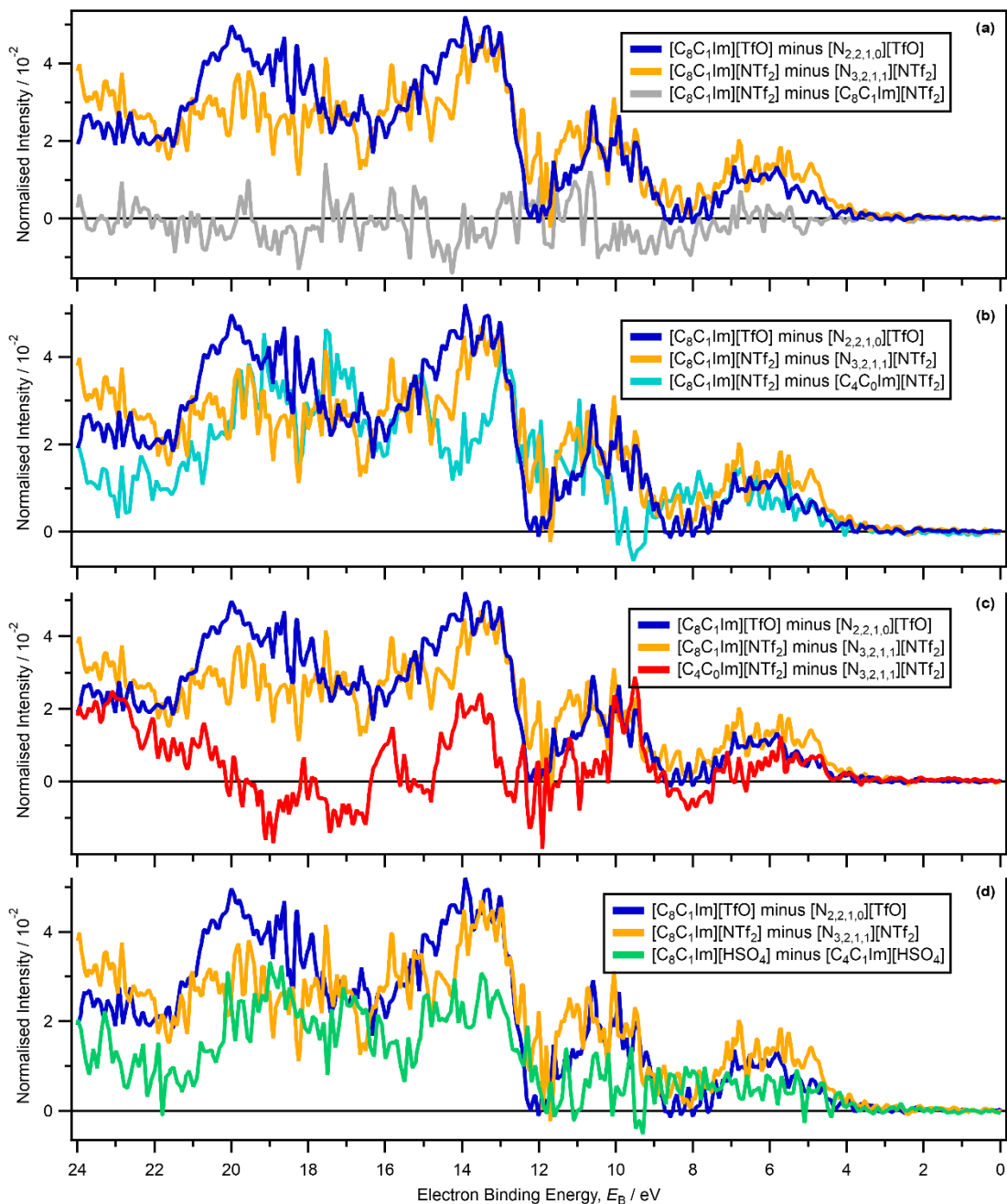


Figure S96. Subtracted traces for valence XP spectra recorded at $h\nu = 1486.6$ eV, focusing on [cation][NTf₂] ILs, where the cation core was different. (a) [C₈C₁Im][TfO] minus [N_{2,2,1,0}][TfO], [C₈C₁Im][NTf₂] minus [N_{3,2,1,1}][NTf₂], and [C₈C₁Im][NTf₂] minus [C₈C₁Im][NTf₂] (recorded on different days, ESI Section 7.2). (b) [C₈C₁Im][TfO] minus [N_{2,2,1,0}][TfO], [C₈C₁Im][NTf₂] minus [N_{3,2,1,1}][NTf₂], and [C₈C₁Im][NTf₂] minus [C₄C₀Im][NTf₂]. (c) [C₈C₁Im][TfO] minus [N_{2,2,1,0}][TfO], [C₈C₁Im][NTf₂] minus [N_{3,2,1,1}][NTf₂], and [C₄C₀Im][NTf₂] minus [N_{3,2,1,1}][NTf₂]. (d) [C₈C₁Im][TfO] minus [N_{2,2,1,0}][TfO], [C₈C₁Im][NTf₂] minus [N_{3,2,1,1}][NTf₂], and [C₈C₁Im][HSO₄] minus [C₄C₁Im][HSO₄]. The areas were normalised using procedures outlined in ESI Section 8.2; subtraction was performed using procedures outlined in ESI Section 10.1. All electron spectra were charge referenced using procedures outlined in ESI Section 5.

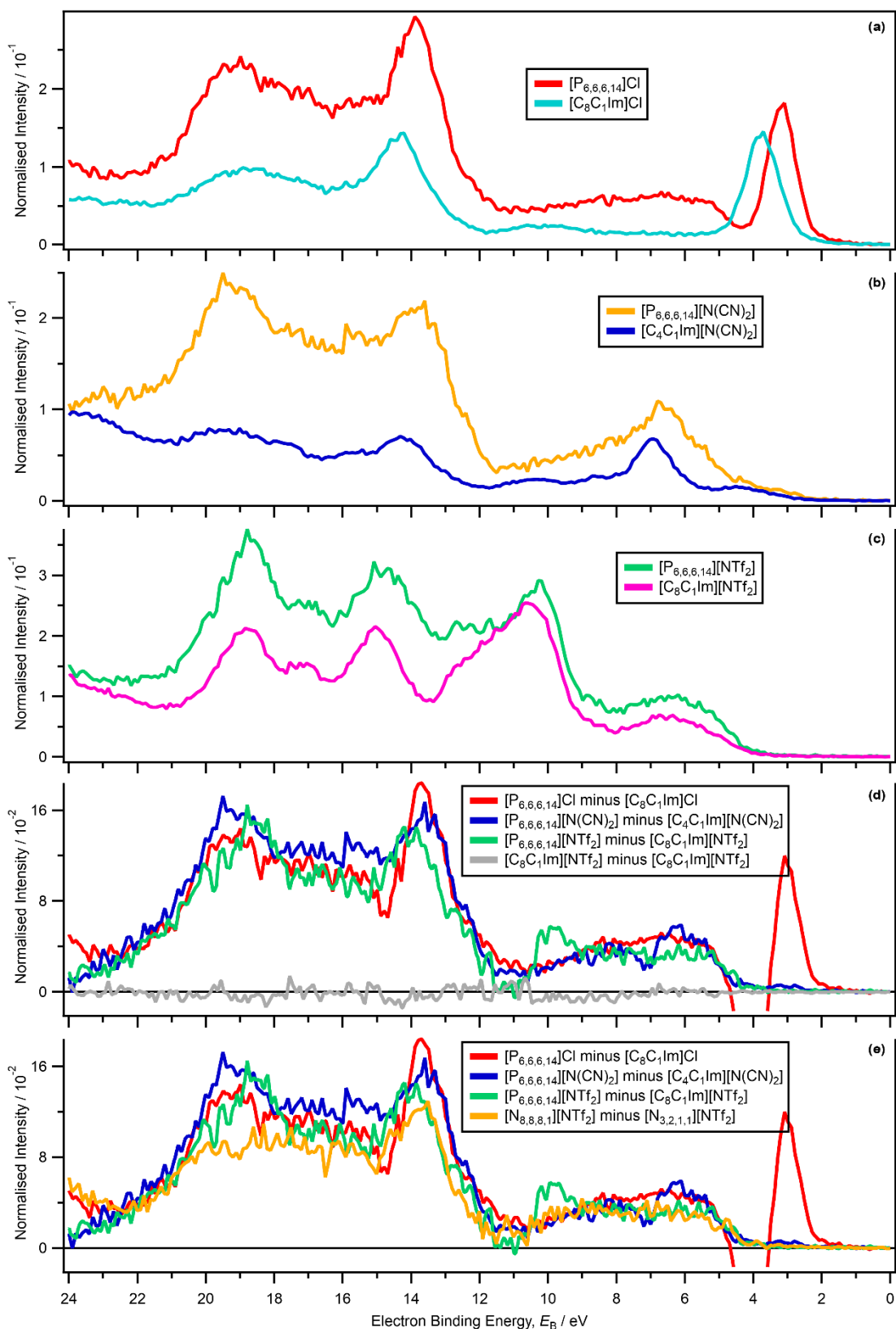


Figure S97. Area normalised valence XP spectra recorded at $h\nu = 1486.6$ eV and subtracted traces, focusing on $[P_{6,6,6,14}][A]$ and $[C_8C_1Im][A]$ ILs, where $[A]^-$ was the same for each comparison. (a) $[P_{6,6,6,14}]Cl$ and $[C_8C_1Im]Cl$. (b) $[P_{6,6,6,14}][N(CN)_2]$ and $[C_8C_1Im][N(CN)_2]$. (c) $[P_{6,6,6,14}][NTf_2]$ and $[C_8C_1Im][NTf_2]$. (d) $[P_{6,6,6,14}]Cl$ minus $[C_8C_1Im]Cl$, $[P_{6,6,6,14}][N(CN)_2]$ minus $[C_8C_1Im][N(CN)_2]$, $[P_{6,6,6,14}][NTf_2]$ minus $[C_8C_1Im][NTf_2]$, and $[C_8C_1Im][NTf_2]$ minus $[C_8C_1Im][NTf_2]$ (recorded on different days, ESI Section 7.2). (e) $[P_{6,6,6,14}]Cl$ minus $[C_8C_1Im]Cl$, $[P_{6,6,6,14}][N(CN)_2]$ minus $[C_8C_1Im][N(CN)_2]$, $[P_{6,6,6,14}][NTf_2]$ minus $[C_8C_1Im][NTf_2]$, and $[N_{8,8,8,1}][NTf_2]$ and $[N_{3,2,1,1}][NTf_2]$. The areas were normalised using procedures outlined in ESI Section

8.2; subtraction was performed using procedures outlined in ESI Section 10.1. All electron spectra were charge referenced using procedures outlined in ESI Section 5.

23. Results. Subtraction method: identifying anionic non-alkyl contributions

23.1. Identifying anionic non-alkyl contributions: component 1

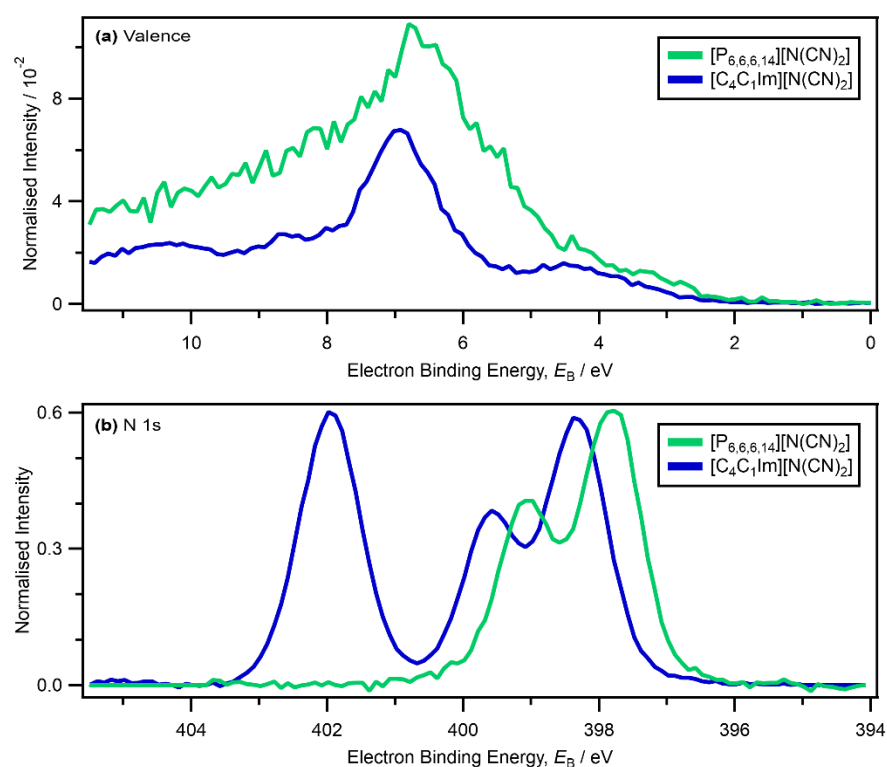


Figure S98. Area normalised XP spectra recorded at $h\nu = 1486.6$ eV for [P_{6,6,6,14}][N(CN)₂] and [C₈C₁Im][N(CN)₂]: (a) valence, (b) N 1s. The areas were normalised using procedures outlined in ESI Section 8.2 (after background subtraction for the N 1s XP spectra shown in ESI Figure S22c and ESI Figure S23c). All electron spectra were charge referenced using procedures outlined in ESI Section 5.

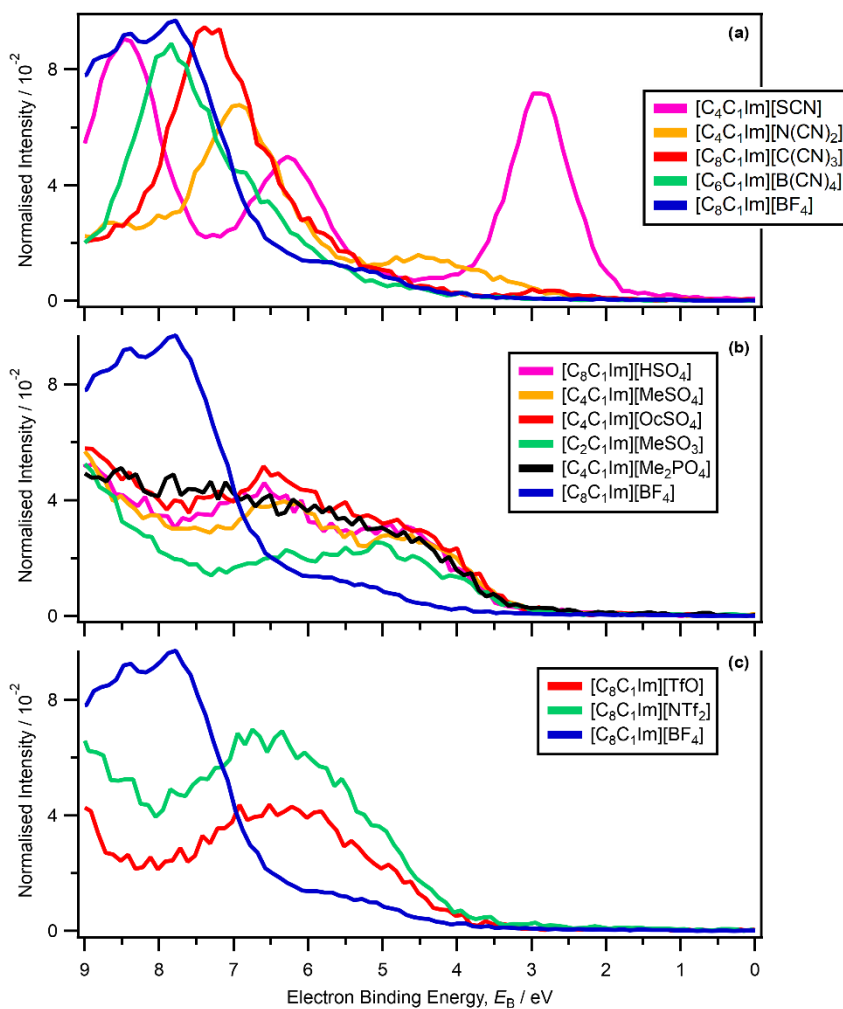


Figure S99. Area normalised valence XP spectra recorded at $h\nu = 1486.6$ eV. (a) $[\text{C}_4\text{C}_1\text{Im}][\text{SCN}]$, $[\text{C}_4\text{C}_1\text{Im}][\text{N}(\text{CN})_2]$, $[\text{C}_8\text{C}_1\text{Im}][\text{C}(\text{CN})_3]$, $[\text{C}_6\text{C}_1\text{Im}][\text{B}(\text{CN})_4]$ and $[\text{C}_8\text{C}_1\text{Im}][\text{BF}_4]$. (b) $[\text{C}_8\text{C}_1\text{Im}][\text{HSO}_4]$, $[\text{C}_4\text{C}_1\text{Im}][\text{MeSO}_4]$, $[\text{C}_4\text{C}_1\text{Im}][\text{OcSO}_4]$, $[\text{C}_2\text{C}_1\text{Im}][\text{MeSO}_3]$, $[\text{C}_4\text{C}_1\text{Im}][\text{Me}_2\text{PO}_4]$ and $[\text{C}_8\text{C}_1\text{Im}][\text{BF}_4]$. (c) $[\text{C}_8\text{C}_1\text{Im}][\text{TfO}]$, $[\text{C}_8\text{C}_1\text{Im}][\text{NTf}_2]$ and $[\text{C}_8\text{C}_1\text{Im}][\text{BF}_4]$. The areas were normalised using procedures outlined in ESI Section 8.2. All electron spectra were charge referenced using procedures outlined in ESI Section 5.

23.2. Identifying anionic non-alkyl contributions: the region $5 \text{ eV} < E_B < 12 \text{ eV}$

The $[\text{N}(\text{CN})_2]^-$ trace ($[\text{C}_4\text{C}_1\text{Im}][\text{N}(\text{CN})_2]$ minus $[\text{C}_8\text{C}_1\text{Im}]^+$) gave a relatively sharp and intense feature at $5.5 \text{ eV} < E_B < 8 \text{ eV}$; the rest of the $5 \text{ eV} < E_B < 12 \text{ eV}$ region was close to the zero line (ESI Figure S87b). The subtracted trace for $[\text{P}_{6,6,6,14}][\text{N}(\text{CN})_2]$ minus $[\text{P}_{6,6,6,14}]\text{Cl}$ also gave a relatively sharp and intense feature at $5.5 \text{ eV} < E_B < 8 \text{ eV}$; the rest of the $4.5 \text{ eV} < E_B < 11.5 \text{ eV}$ region was close to the zero line (ESI Figure S91d). Consequently, it can be concluded that for $[\text{cation}][\text{N}(\text{CN})_2]$ the second lowest E_B contribution from the $[\text{N}(\text{CN})_2]^-$ anion was at $5.5 \text{ eV} < E_B < 8 \text{ eV}$. Using just the XP spectra for $[\text{C}_4\text{C}_1\text{Im}][\text{N}(\text{CN})_2]$ and $[\text{P}_{6,6,6,14}][\text{N}(\text{CN})_2]$, the feature at $5.5 \text{ eV} < E_B < 8 \text{ eV}$ would have been hard to identify as being from the same feature from the anion, as the cationic contributions of $[\text{C}_4\text{C}_1\text{Im}]^+$ and $[\text{P}_{6,6,6,14}]^+$ were relatively different (ESI Figure S98a). Therefore, this identification of a second $[\text{N}(\text{CN})_2]^-$ anion contribution to the valence XP spectra for $[\text{P}_{6,6,6,14}][\text{N}(\text{CN})_2]$ and $[\text{C}_4\text{C}_1\text{Im}][\text{N}(\text{CN})_2]$ highlights the power of the subtraction method.

The $[\text{C}(\text{CN})_3]^-$ trace ($[\text{C}_8\text{C}_1\text{Im}][\text{C}(\text{CN})_3]$ minus $[\text{C}_8\text{C}_1\text{Im}]^+$) gave a relatively sharp and intense feature at $6 \text{ eV} < E_B < 8.5 \text{ eV}$; the rest of the $5 \text{ eV} < E_B < 12 \text{ eV}$ region was close to the zero line (ESI Figure S87c). This feature is the second lowest E_B feature from the $[\text{C}(\text{CN})_3]^-$ anion, after the peak at $E_B = 2.8 \text{ eV}$ (Section 3.2).

All $[\text{C}_n\text{C}_1\text{Im}][\text{A}]^-$ ILs studied here, where $[\text{A}]^-$ contained at least one cyano group, showed at least one peak/feature due to the cyano-containing anion in the region $5 \text{ eV} < E_B < 11.5 \text{ eV}$ (ESI Figure S89b). The $[\text{SCN}]^-$ trace ($[\text{C}_4\text{C}_1\text{Im}][\text{SCN}]$ minus $[\text{C}_8\text{C}_1\text{Im}]^+$) gave two features in the region $5 \text{ eV} < E_B < 11.5 \text{ eV}$ originating from the $[\text{SCN}]^-$ anion (ESI Figure S87a). The feature at $5 \text{ eV} < E_B < 7 \text{ eV}$ corresponded to component 3, whilst the feature at $7 \text{ eV} < E_B < 9 \text{ eV}$ corresponded to component 4. Variable $h\nu$ XPS showed that the feature at $5 \text{ eV} < E_B < 7 \text{ eV}$ (*i.e.* component 3) was mainly composed of N 2p and/or C 2p AOs (Section 3.1). Therefore, the feature at $5 \text{ eV} < E_B < 7 \text{ eV}$ was from N 2p and/or C 2p AOs from the $[\text{SCN}]^-$ anion. The $[\text{C}(\text{CN})_3]^-$ trace ($[\text{C}_8\text{C}_1\text{Im}][\text{C}(\text{CN})_3]$ minus $[\text{C}_8\text{C}_1\text{Im}]^+$) gave a feature at $6 \text{ eV} < E_B < 8.5 \text{ eV}$ originating from the $[\text{C}(\text{CN})_3]^-$ anion (Figure 10a); RAES showed that there was a significant contribution from N_{anion} to this feature (Section 3.2.2). One method to identify atomic contributions to valence regions is to use the separation between the core and valence levels.⁵⁹ $E_B(\text{N}_{\text{cyano}} 1s)$ values showed the trend $[\text{B}(\text{CN})_4]^- > [\text{C}(\text{CN})_3]^- > [\text{N}(\text{CN})_2]^- > [\text{SCN}]^-$.⁴¹ The feature in the region $6 \text{ eV} < E_B < 9 \text{ eV}$ showed the same trend: $[\text{B}(\text{CN})_4]^- > [\text{C}(\text{CN})_3]^- > [\text{N}(\text{CN})_2]^- > [\text{SCN}]^-$ (ESI Figure S89b). Overall, we conclude that the feature at $6 \text{ eV} < E_B < 9 \text{ eV}$ for the $[\text{C}_n\text{C}_1\text{Im}][\text{A}]^-$ ILs (where $[\text{A}]^-$ contained at least one cyano group) originated from the cyano group of the anion, *i.e.* for all four cyano-containing anions, the feature at $6 \text{ eV} < E_B < 9 \text{ eV}$ had significant contributions from N 2p and C 2p AO contribution.

The $[\text{TfO}]^-$ trace ($[\text{C}_8\text{C}_1\text{Im}][\text{TfO}]$ minus $[\text{C}_8\text{C}_1\text{Im}]^+$) gave two features in the region $0 \text{ eV} < E_B < 11.5 \text{ eV}$ (ESI Figure S86d). The feature at $4 \text{ eV} < E_B < 8 \text{ eV}$ was relatively low intensity, a more intense feature at $9 \text{ eV} < E_B < 11.5 \text{ eV}$ (the maximum intensity of the feature was at $E_B \sim 10.2 \text{ eV}$, ESI Figure S86d). These features for $[\text{C}_8\text{C}_1\text{Im}][\text{TfO}]$ can be identified as originating from the $[\text{TfO}]^-$ anion. The $[\text{NTf}_2]^-$ trace ($[\text{C}_8\text{C}_1\text{Im}][\text{NTf}_2]$ minus $[\text{C}_8\text{C}_1\text{Im}]^+$) gave two features in the region $0 \text{ eV} < E_B < 11.5 \text{ eV}$ (ESI Figure S86c). The feature at $4 \text{ eV} < E_B < 8 \text{ eV}$ was relatively low intensity and a more intense feature at $9 \text{ eV} < E_B < 11.5 \text{ eV}$ (the maximum intensity of the feature was at $E_B \sim 10.8 \text{ eV}$, ESI Figure S86c). At $h\nu = 1486.6 \text{ eV}$, the S 3p, F 2p and O 2p AO photoionisation cross-sections are relatively similar (ESI Section 6 and reference³⁸). Therefore, further atomic identification of these features for $[\text{C}_8\text{C}_1\text{Im}][\text{TfO}]$ and $[\text{C}_8\text{C}_1\text{Im}][\text{NTf}_2]$ using solely photoionisation cross-section values is very difficult. One possible way to identify atomic contributions to valence regions is to use the separation between the core and valence levels; values for $E_B(\text{O } 1s)$ minus $E_B(\text{O } 2s)$ have been used to identify oxygen contributions to polymers.⁵⁹ For $[\text{C}_8\text{C}_1\text{Im}][\text{BF}_4]$, $E_B(\text{F}_{\text{anion}} 1s) = 686.0 \text{ eV}$ and $E_B(\text{F}_{\text{anion}} \text{ valence}) = 7.8 \text{ eV}$ (where the F_{anion} valence contribution was judged as the E_B value that gave the maximum intensity for the F_{anion} valence contribution). The difference between these two values was $678.2 \pm 0.4 \text{ eV}$. For $[\text{C}_8\text{C}_1\text{Im}][\text{NTf}_2]$ and

[C₈C₁Im][TfO] $E_B(F_{\text{anion}} 1s) = 688.8 \text{ eV}$ and 688.4 eV respectively. Therefore, predicted $E_B(\text{valence})$ values for [C₈C₁Im][NTf₂] and [C₈C₁Im][TfO] would be 10.6 eV and 10.2 eV respectively. The measured $E_B(\text{valence})$ values for [C₈C₁Im][NTf₂] and [C₈C₁Im][TfO] were 10.8 eV and 10.2 eV respectively, almost identical to the predicted values, a superb match to the predicted values. Consequently, we can positively identify the features at $9 \text{ eV} < E_B < 12 \text{ eV}$ for [C₈C₁Im][TfO] and at $9 \text{ eV} < E_B < 13.5 \text{ eV}$ for [C₈C₁Im][NTf₂] as arising principally from F_{anion} valence contributions, *i.e.* F 2p.

[C₄C₁Im][Me₂PO₄], [C₂C₁Im][MeSO₃], [C₄C₁Im][HSO₄], [C₄C₁Im][MeSO₄] and [C₄C₁Im][OcSO₄] all gave visually similar anion traces at $3 \text{ eV} < E_B < 5 \text{ eV}$ (Section 3.4.3, ESI Figure S88 and ESI Figure S89c). The [HSO₄]⁻ trace ([C₈C₁Im][HSO₄] minus [C₈C₁Im]⁺) gave two features in the $5 \text{ eV} < E_B < 12 \text{ eV}$ region (ESI Figure S88a). The feature at $5.5 \text{ eV} < E_B < 7.5 \text{ eV}$ was relatively low intensity and a more intense feature at $9.5 \text{ eV} < E_B < 11.5 \text{ eV}$ (ESI Figure S88a). These features for [C₈C₁Im][HSO₄] can be identified as originating from the [HSO₄]⁻ anion. As identified in Section 3.4.3, the contributions in the 2p region of the anion traces for [C₄C₁Im][HSO₄], [C₄C₁Im][MeSO₄] and [C₄C₁Im][OcSO₄] were very similar; hence, the identifications made here for [C₈C₁Im][HSO₄] hold for [C₄C₁Im][MeSO₄] and [C₄C₁Im][OcSO₄]. The [MeSO₃]⁻ trace ([C₂C₁Im][MeSO₃] minus [C₈C₁Im]⁺) gave one feature in the $5 \text{ eV} < E_B < 12 \text{ eV}$ region, at $9 \text{ eV} < E_B < 11.5 \text{ eV}$, with the subtracted trace matching close to the zero line elsewhere (ESI Figure S88d). This feature can be identified as originating from the [MeSO₃]⁻ anion. The anion traces for [C₂C₁Im][MeSO₃] compared to [C₈C₁Im][HSO₄] highlights a difference that could not be discerned from just the area normalised XP spectra; the [C_nC₁Im][XSO₄] IIs gave an anionic feature at $5.5 \text{ eV} < E_B < 7.5 \text{ eV}$ which [C₂C₁Im][MeSO₃] did not, again highlighting the power of the subtraction method. The [Me₂PO₄]⁻ trace ([C₄C₁Im][Me₂PO₄] minus [C₈C₁Im]⁺) gave one very broad feature that covered the whole of the $5 \text{ eV} < E_B < 12 \text{ eV}$ region, with no clear peaks (ESI Figure S88e). This broad feature can be identified as originating from the [Me₂PO₄]⁻ anion. At $h\nu = 1486.6 \text{ eV}$, the S 3p, P 3p and O 2p AO photoionisation cross-sections are relatively similar (ESI Section 6 and reference³⁸). Therefore, further atomic identification of these features for [C₄C₁Im][Me₂PO₄], [C₂C₁Im][MeSO₃], [C₈C₁Im][HSO₄], [C₄C₁Im][MeSO₄], [C₄C₁Im][OcSO₄] and [C₄C₁Im][Me₂PO₄] using this data is difficult, and will not be attempted here.

The subtracted traces in the s AO region for [C₄C₁Im][MeSO₄] minus [C₄C₁Im][HSO₄] and [C₄C₁Im][OcSO₄] minus [C₄C₁Im][HSO₄] gave significant deviation from the zero line, in particular at $12 \text{ eV} < E_B < 16 \text{ eV}$ (ESI Figure S82b and ESI Figure 82c). These observations suggest that just adding one CH₂-R group on [XSO₄]⁻ to replace the H on [HSO₄]⁻ with a CH₂-R group had a relatively dramatic effect on the valence electronic structure. However, this effect was not observed in the p AO region due to the relatively small C 2p photoionisation cross-section.³⁸

The subtracted trace for [P_{6,6,6,14}][NO₃] minus [P_{6,6,6,14}]Cl gave a peak at $E_B \sim 10.5 \text{ eV}$ was readily observed; the rest of the $4.5 \text{ eV} < E_B < 11.5 \text{ eV}$ region was close to the zero line (ESI Figure S91c). Therefore, this peak at $E_B \sim 10.5 \text{ eV}$ was clearly due to the [NO₃]⁻ anion. This fingerprint identification for [P_{6,6,6,14}][NO₃] confirms the identification of a $N_{\text{anion}} 2p$ MO at $E_B = 10 \text{ eV}$ from N 1s RAES data (ESI Figure S67 and ESI Table S12).

As explained in Section 3.3, the I 5s contribution for [C₆C₁Im]I was hard to discern using the fingerprint method (with no area normalisation or subtraction used). The I⁻ trace ([C₆C₁Im]I minus [C₈C₁Im]⁺) gave a feature in the $10 \text{ eV} < E_B < 11.5 \text{ eV}$. This feature can be identified as originating from the I⁻ anion; hence, this feature must originate from the I 5s AO. There was probably no contribution from the I⁻ anion in the $13 \text{ eV} < E_B < 16 \text{ eV}$ region; however, it is hard to be certain, due to the contribution in that region from the Cl 3s AOs from Cl⁻.

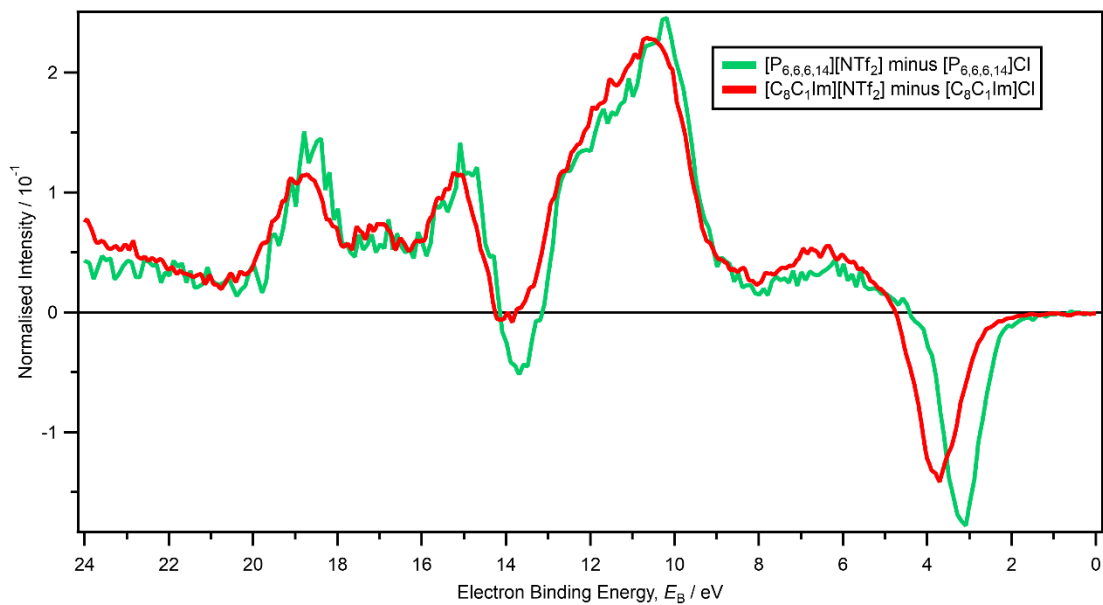


Figure S100. Subtracted traces recorded at $h\nu = 1486.6$ eV for $[P_{6,6,6,14}][NTf_2]$ minus $[P_{6,6,6,14}]Cl$ and $[C_8C_1Im][NTf_2]$ minus $[C_8C_1Im]Cl$. The areas were normalised using procedures outlined in ESI Section 8.2; subtraction was performed using procedures outlined in ESI Section 10.1. All electron spectra were charge referenced using procedures outlined in ESI Section 5.

24. Results. Identification of MOs that were not the ion HOFO

Using a combination of variable $h\nu$ XPS, RAES and the subtraction method, non-HOFO MO contributions have been identified for $[C_nC_1Im]^+$, including a feature at $9\text{ eV} < E_B < 11.5\text{ eV}$.

Using a combination of variable $h\nu$ XPS, RAES and the subtraction method, non-HOFO MO contributions have been identified for $[P_{6,6,6,14}]^+$. In the $5\text{ eV} < E_B < 11.5\text{ eV}$ region, no clear peaks or features were identified, suggesting that the relatively large number of $[P_{6,6,6,14}]^+$ cationic MOs gave a range of E_B values.

For both $[N_{4,1,1,0}]^+$ and $[N_{8,8,8,1}]^+$ alkyl carbon contributions have been identified in the regions at $6\text{ eV} < E_B < 12\text{ eV}$ and $4\text{ eV} < E_B < 12\text{ eV}$ respectively. As for $[P_{6,6,6,14}]^+$, these alkyl contributions gave no clear peaks, again suggesting that the cationic MOs gave a range of E_B values.

For halide anion-containing ILs the non-HOFO MO contributions identified were those with significant s AO contributions.

For $[SCN]^-$, $[N(CN)_2]^-$ and $[C(CN)_3]^-$, non-HOFO MOs have been identified in the region $5\text{ eV} < E_B < 8\text{ eV}$ as arising principally from N 2p and/or C 2p AOs, *i.e.* cyano-based MOs; for $[B(CN)_4]^-$ this feature was the anion HOFO. In addition, for $[SCN]^-$ a feature at $7\text{ eV} < E_B < 9\text{ eV}$ had a significant contribution from $S_{\text{anion}} 3p$ AOs.

Using a combination of variable $h\nu$ XPS, RAES and the subtraction method, non-HOFO MO contributions have been identified for $[NO_3]^-$. A peak at $E_B \sim 10.5\text{ eV}$ had a significant contribution from $N_{\text{anion}} 2p$, and potentially a contribution from $O_{\text{anion}} 2p$.

Using the subtraction method, non-HOFO MO contributions at $9\text{ eV} < E_B < 12\text{ eV}$ for $[C_8C_1Im][TfO]$ and at $9\text{ eV} < E_B < 13.5\text{ eV}$ for $[C_8C_1Im][NTf_2]$ have been identified as arising principally from F 2p AOs.

Peaks due to non-HOFO MOs have been identified for the anions $[BF_4]^-$, $[B(CN)_4]^-$, $[Me_2PO_4]^-$, $[MeSO_3]^-$, $[HSO_4]^-$, $[MeSO_4]^-$ and $[OCSO_4]^-$. However, AO contributions to these MOs have not been identified here.

25. Results. ΔE_B (valence level – valence level)

For $[C_nC_1Im][A]$ the cation HOFO and a feature at $9 \text{ eV} < E_B < 11.5 \text{ eV}$ have both been identified for a range of $[A]^-$. The E_B separation between the feature due to the cation HOFO and the feature at $9 \text{ eV} < E_B < 11.5 \text{ eV}$ was challenging to judge, but there was certainly no very large variation in this E_B separation for $[C_nC_1Im]^+$ when counteranion $[A]^-$ was varied.

As already discussed in Section 3.4.3, the E_B values for $[N(CN)_2]^-$ -based MOs for $[C_4C_1Im][N(CN)_2]$ and $[P_{6,6,6,14}][N(CN)_2]$ were different by $\sim 0.3 \text{ eV}$ (ESI Figure S98a). However, the E_B separations between the two features due to $[N(CN)_2]^-$ -based MOs were approximately the same. Furthermore, $[cation][NTf_2]$ with a variety of cations, including $[C_4C_1Im]^+$ and $[P_{6,6,6,14}]^+$, also showed minimal impact of the counteranion on the E_B separations between the two features due to $[NTf_2]^-$ -based MOs. For example, $[P_{6,6,6,14}][NTf_2]$ minus $[P_{6,6,6,14}Cl]$ and $[C_8C_1Im][NTf_2]$ minus $[C_8C_1ImCl]$ showed very similar subtracted traces, apart from where the Cl^- -based MOs contributed (at $E_B \sim 3.5 \text{ eV}$ and $E_B \sim 14 \text{ eV}$, ESI Figure S100). The E_B values for $[NTf_2]^-$ -based MOs for $[C_8C_1Im][NTf_2]$ and $[P_{6,6,6,14}][NTf_2]$ were different by $\sim 0.15 \text{ eV}$. However, the E_B separations between the two features due to $[NTf_2]^-$ -based MOs were approximately the same. Therefore, when the cation core was varied and the anion was kept constant, the counteranion appeared to have minimal effect on the anionic-based MOs.

26. Results. $E_B(\text{ion HOFO})$ and $E_B(\text{ion onset})$

26.1. $E_B(\text{ion HOFO})$

$E_B(\text{anion HOFO})$ was readily obtained for ILs that gave a peak from the anion HOFO that was well-resolved and relatively symmetrical, *e.g.* those with Cl^- , Br^- , I^- , $[\text{SCN}]^-$ and $[\text{C}(\text{CN})_3]^-$. For the other anion HOFOs and all of the cation HOFOs, determining $E_B(\text{ion HOFO})$ was more difficult, as there was no peak from the ion HOFO that was well-resolved or relatively symmetrical (*e.g.* for $[\text{C}_n\text{C}_1\text{Im}]^+$). Therefore, a combination of data from different methods was used to establish $E_B(\text{ion HOFO})$ for these ILs.

The N 1s RAES data for the four $[\text{C}_n\text{C}_1\text{Im}][\text{A}]$ ILs studied here showed a relatively broad feature due to cation contributions at $4 \text{ eV} < E_B < 7 \text{ eV}$. This feature was significantly broader than key N_{anion} 1s RAES features. For example, for $[\text{C}_4\text{C}_1\text{Im}][\text{SCN}]$ the lowest E_B RAES N_{anion} feature was significantly narrower than the lowest E_B RAES N_{cation} feature (Figure 4). This observation strongly suggests that the lowest E_B RAES N_{cation} feature for $[\text{C}_n\text{C}_1\text{Im}]^+$ had contributions from at least two MOs. The C 1s RAES data for $[\text{C}_8\text{C}_1\text{Im}][\text{NTf}_2]$, showed a C_{cation} feature at $4 \text{ eV} < E_B < 5.5 \text{ eV}$. $[\text{C}_4\text{C}_1\text{Im}][\text{SCN}]$ and $[\text{C}_8\text{C}_1\text{Im}][\text{C}(\text{CN})_3]$ very likely had anionic contributions to the C 1s RAES at the $h\nu$ values of interest. However, for both $[\text{C}_4\text{C}_1\text{Im}][\text{SCN}]$ and $[\text{C}_8\text{C}_1\text{Im}][\text{C}(\text{CN})_3]$ a feature was observed at $4 \text{ eV} < E_B < 5.5 \text{ eV}$ (ESI Figure S68 and ESI Figure S69); at the same E_B values, no N_{anion} features were observed (Figure 4 and Figure 5). For $[\text{C}_4\text{C}_1\text{Im}][\text{SCN}]$ and $[\text{C}_8\text{C}_1\text{Im}]\text{Cl}$ variable $h\nu$ valence XPS data (Figure 2) showed the component due to $E_B(\text{cation HOFO})$ was at $4.5 \text{ eV} < E_B < 5.0 \text{ eV}$. However, as component 2 for both of these ILs had a low relatively low intensity peak and had significantly more intense peaks due to anionic contributions at similar E_B , only an approximate E_B could be determined for this component from variable $h\nu$ valence XPS data. Data from the fingerprint method and the subtraction method strongly suggested that other $[\text{C}_n\text{C}_m\text{Im}][\text{A}]$ ILs (with a wide range of anions) gave similar $E_B(\text{cation HOFO})$ values. The anions studied here with a $[\text{C}_n\text{C}_1\text{Im}]^+$ cation were relatively different in both size and IL properties with the same countercation,⁶⁰ yet gave the same $E_B(\text{cation HOFO})$ value (within experimental error). Given this evidence, when IL E_B values are charge referenced to $E_B(\text{C}_{\text{alkyl}} 1s) = 285.0 \text{ eV}$ (see ESI Section 5 for more details) we expect $E_B(\text{cation HOFO}) = 4.8 \pm 0.4 \text{ eV}$ for all $[\text{C}_n\text{C}_m\text{Im}][\text{A}]$ ILs, independent of n and $[\text{A}]^-$ (at least for $n \leq 8$, $m = 0$ or 1).

Using a combination of C 1s RAES data for $[\text{P}_{6,6,6,14}][\text{NO}_3]$ and the subtraction method for four $[\text{P}_{6,6,6,14}][\text{A}]$ ILs, $E_B(\text{cation HOFO}) = 5.0 \pm 0.4 \text{ eV}$. As was the case for the $[\text{C}_n\text{C}_1\text{Im}][\text{A}]$ ILs studied here, the four anions studied in combination with the $[\text{P}_{6,6,6,14}]^+$ cation were relatively structurally diverse. Therefore, we conclude that when IL E_B values are referenced to $E_B(\text{C}_{\text{alkyl}} 1s) = 285.0 \text{ eV}$ we expect $[\text{P}_{6,6,6,14}]^+ E_B(\text{cation HOFO}) \sim 5 \text{ eV}$ for all $[\text{P}_{6,6,6,14}][\text{A}]$ ILs, independent of the anion identity.

For $[\text{N}_{4,1,1,0}][\text{HSO}_4]$ $E_B(\text{cation HOFO}) = 6.5 \pm 1.0 \text{ eV}$ was determined using C 1s RAES data. For $[\text{N}_{2,2,1,0}][\text{TfO}]$ no $E_B(\text{cation HOFO})$ was determined using C 1s RAES. A visual inspection of subtraction data showed that the onset energies were similar for $[\text{NTf}_2]^-$ and $[\text{N}_{8,8,8,1}]^+$. Therefore, for $[\text{N}_{8,8,8,1}][\text{NTf}_2]$ $E_B(\text{cation HOFO}) = 5.0 \pm 0.4 \text{ eV}$ (see below). The length of the alkyl chain had a significant impact on $E_B(\text{cation HOFO})$. For ammonium-based cations with a relatively similar number and length of alkyl chains to the $[\text{N}_{4,1,1,0}]^+$ cation, we expect $E_B(\text{cation HOFO})$ for these cations (*e.g.* $[\text{N}_{2,2,1,0}]^+$, $[\text{N}_{4,1,1,1}]^+$, $[\text{N}_{3,2,1,1}]^+$) to be relatively similar to $E_B(\text{cation HOFO})$ for the $[\text{N}_{4,1,1,0}]^+$ cation.

For $[\text{S}_{2,2,n}][\text{NTf}_2]$ ($n = 1$ and 2) and $[\text{N}_{2\text{OH},2\text{OH},2\text{OH},1}][\text{TfO}]$ $E_B(\text{cation HOFO})$ values were determined using the subtraction method. For $[\text{S}_{2,2,n}][\text{NTf}_2]$ $E_B(\text{cation HOFO})$ were found to be the same for $n = 1$ and 2 (Table 3); it is unclear at this stage what the effect on $E_B(\text{cation HOFO})$ will be for significantly larger n values for $[\text{S}_{2,2,n}][\text{NTf}_2]$.

E_B (anion HOFO) for $[\text{NO}_3]^-$ was determined using a combination of RAES data and the subtraction method. E_B (anion HOFO) for both $[\text{N}(\text{CN})_2]^-$ was determined using the subtraction method. E_B (anion HOFO) for $[\text{HSO}_4]^-$ was determined using a combination of RAES data and the subtraction method. Given the similarity of the valence XP spectra in the E_B region near the anion HOFO between $[\text{HSO}_4]^-$ ILs and a range of other anions studied here ($[\text{Me}_2\text{PO}_4]^-$, $[\text{MeSO}_3]^-$, $[\text{MeSO}_4]^-$ and $[\text{OcSO}_4]^-$), we have determined E_B (anion HOFO) for all of these ILs as the same value (Table 3).

The $[\text{NTf}_2]^-$ E_B (anion HOFO) and the $[\text{C}_8\text{C}_1\text{Im}]^+$ E_B (cation HOFO) were similar (as demonstrated using a combination of N 1s and O 1s RAES data), so no clear $[\text{NTf}_2]^-$ anion HOFO peak was observed. However, the $[\text{NTf}_2]^-$ trace ($[\text{C}_8\text{C}_1\text{Im}][\text{NTf}_2]^-$ minus $[\text{C}_8\text{C}_1\text{Im}]^+$) showed a similar onset to the $[\text{C}_8\text{C}_1\text{Im}]^+$ trace. Therefore, the $[\text{NTf}_2]^-$ E_B (anion HOFO) could be estimated as E_B (cation HOFO) = 5.0 ± 0.4 eV; this value was given to all $[\text{NTf}_2]^-$ -containing ILs studied here (Table 3). Similarly, the $[\text{TfO}]^-$ E_B (anion HOFO) and the $[\text{C}_8\text{C}_1\text{Im}]^+$ E_B (cation HOFO) were similar, leading to E_B (anion HOFO) = 5.0 ± 0.4 eV for $[\text{TfO}]^-$; again, this value was given to all $[\text{TfO}]^-$ -containing ILs studied here (Table 3).

For both $[\text{BF}_4]^-$ and $[\text{B}(\text{CN})_4]^-$ no clear anion HOFO peak was observed. Using the anion traces, for $[\text{BF}_4]^-$ E_B (anion HOFO) = 7.8 ± 0.6 eV and for $[\text{B}(\text{CN})_4]^-$ E_B (anion HOFO) = 6.6 ± 0.6 eV were determined. The larger errors (than other E_B (ion HOFO) values determined here) reflect the challenge of determining E_B (anion HOFO) for ILs where the lowest E_B anionic contributions were strongly overlapping with the cationic contributions (and the lack of any confirmation from another technique such as RAES).

26.2. E_B (ion onset)

The onset binding energy, E_B (ion onset), was readily determined for component 1 using the method outlined in ESI Section 12. Furthermore, for three ILs ($[\text{C}_8\text{C}_1\text{Im}][\text{BF}_4]^-$, $[\text{C}_6\text{C}_1\text{Im}][\text{B}(\text{CN})_4]^-$ and $[\text{C}_8\text{C}_1\text{Im}][\text{C}(\text{CN})_3]^-$) E_B (ion onset) was determined for a second component, as for these three ILs the nature of the XP spectra meant that this was possible (ESI Table S13). Overall, E_B (anion onset) was determined for all 37 ILs; E_B (cation onset) was determined for 3 ILs.

For the three ILs studied here for which E_B (cation onset) could be determined ($[\text{C}_8\text{C}_1\text{Im}][\text{BF}_4]^-$, $[\text{C}_6\text{C}_1\text{Im}][\text{B}(\text{CN})_4]^-$ and $[\text{C}_8\text{C}_1\text{Im}][\text{C}(\text{CN})_3]^-$), an average value of E_B (cation onset) = 3.7 eV was obtained. Given the relatively low intensity cation HOFO feature used to determine E_B (cation onset), a relatively conservative error value of ± 0.3 eV was given for this E_B (cation onset) value. We expect E_B (cation onset) = 3.7 ± 0.3 eV to be valid for all $[\text{C}_n\text{C}_m\text{Im}][\text{A}]$ ILs; hence, we have used this value for all $[\text{C}_n\text{C}_m\text{Im}][\text{A}]$ ILs studied here. E_B (cation onset) could not be determined for certain cations (ammonium, sulfonium, phosphonium) as contributions from the anion at lower E_B masked the onset of the cationic contributions.

For most of the ILs, it was clear that the E_B (ion onset) value determined for component 1 could be assigned to either the cation or the anion. For $[\text{cation}][\text{NTf}_2]^-$ and $[\text{cation}][\text{TfO}]^-$ ILs in particular, the E_B (ion onset) value could be due to either the cation or the anion. As we already have a good measure of E_B (cation onset) for $[\text{C}_n\text{C}_m\text{Im}][\text{A}]$, in Table 3 we presented the E_B (ion onset) values determined here for $[\text{cation}][\text{NTf}_2]^-$ and $[\text{cation}][\text{TfO}]^-$ ILs as originating from the anion (although clearly, they could have originated from the cation also).

27. Results. HOMO identification

Examples of the fitted traces to obtain $E_B(\text{ion onset})$ are provided (ESI Figure S101).

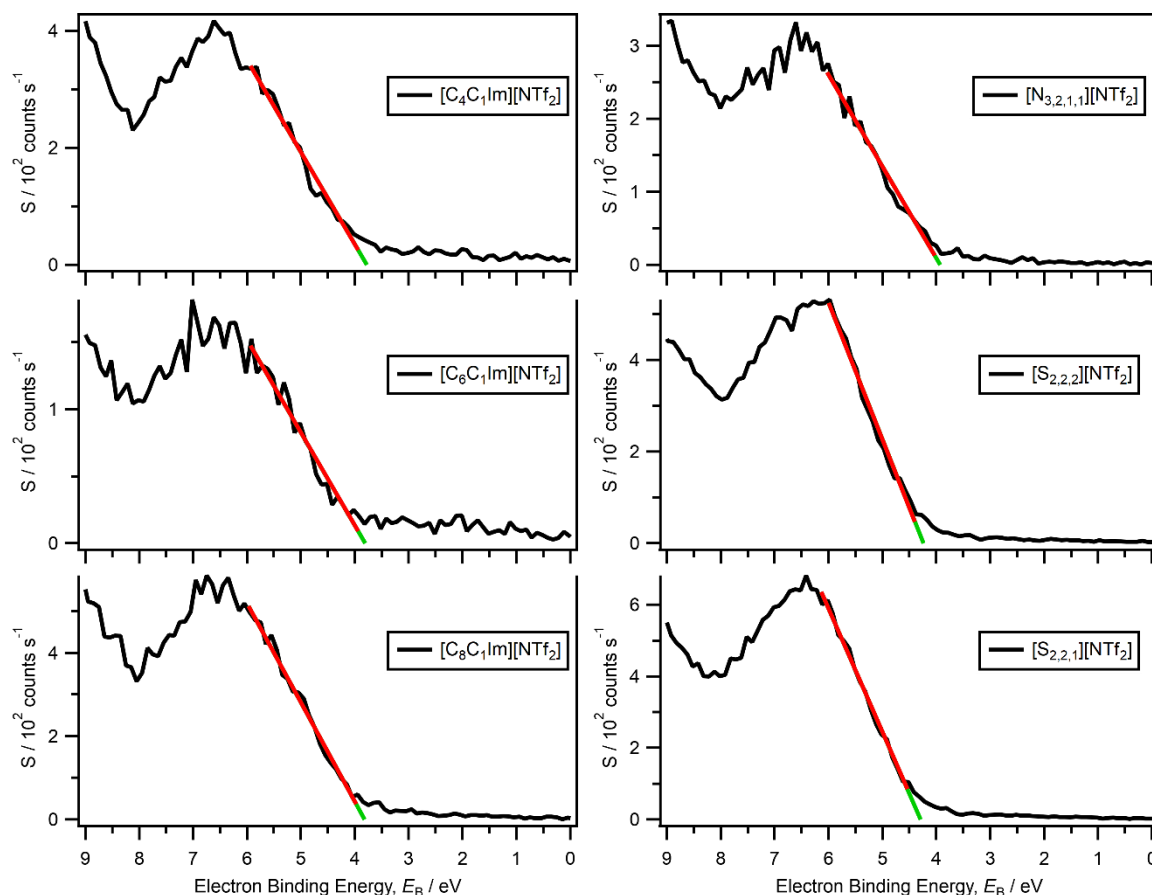


Figure S101. Valence XP spectra and fitted onset energy traces for: (a) $[\text{C}_4\text{C}_1\text{Im}][\text{NTf}_2]$, (b) $[\text{C}_6\text{C}_1\text{Im}][\text{NTf}_2]$, (c) $[\text{C}_8\text{C}_1\text{Im}][\text{NTf}_2]$, (d) $[\text{N}_{3,2,1,1}][\text{NTf}_2]$, (e) $[\text{S}_{2,2,2}][\text{NTf}_2]$, (f) $[\text{S}_{2,2,1}][\text{NTf}_2]$, all recorded at $h\nu = 1486.6$ eV. All spectra are charge referenced using the values given in ESI Table S3. The red traces are the fitted range. The green traces are the extrapolation to the x-intercept. $E_B(\text{ion onset})$ is the x-intercept. All electron spectra were charge referenced using procedures outlined in ESI Section 5.

The correlation between $\Delta E_B(\text{ion HOFO})$ and $\Delta E_B(\text{ion onset})$ was excellent. A gradient of 1.01 and an R^2 of 0.98 was obtained for a linear correlation (ESI Figure S102).

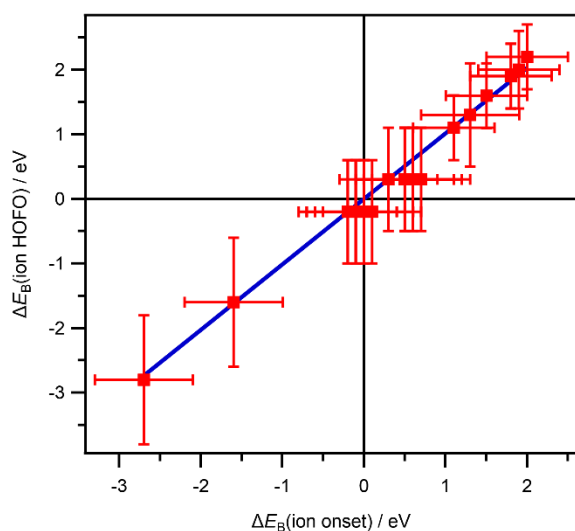


Figure S102. $\Delta E_B(\text{ion HOFO})$ versus $\Delta E_B(\text{ion onset})$.

Table S13. Experimental E_B (HOMO onset) and E_B (2nd component onset).

IL no.	IL	E_B (HOMO onset) / eV	E_B (2 nd component onset) / eV
1	[C ₈ C ₁ Im]Cl	2.6 ± 0.2	
2	[C ₈ C ₁ Im]Br	2.2 ± 0.2	
3	[C ₆ C ₁ Im]I	1.7 ± 0.2	
4	[P _{6,6,6,14}]Cl	2.2 ± 0.2	
5	[P _{6,6,6,14}]Br	1.8 ± 0.2	
6	[C ₄ C ₁ Im][SCN]	1.9 ± 0.2	
7	[C ₈ C ₁ Im][SCN]	1.9 ± 0.2	
8	[C ₄ C ₁ Im][N(CN) ₂]	2.4 ± 0.3	
9	[P _{6,6,6,14}][N(CN) ₂]	2.0 ± 0.3	
10	[C ₈ C ₁ Im][C(CN) ₃]	1.8 ± 0.3	3.8 ± 0.3
11	[C ₆ C ₁ Im][B(CN) ₄]	3.7 ± 0.3	5.3 ± 0.3
12	[C ₈ C ₁ Im][BF ₄]	3.7 ± 0.3	6.4 ± 0.3
13	[P _{6,6,6,14}][NO ₃]	2.3 ± 0.3	
14	[C ₄ C ₁ Im][HSO ₄]	3.2 ± 0.3	
15	[C ₈ C ₁ Im][HSO ₄]	3.2 ± 0.3	
16	[C ₄ C ₀ Im][HSO ₄]	3.4 ± 0.3	
17	[N _{4,1,1,0}][HSO ₄]	3.1 ± 0.3	
18	[N _{8,1,1,0}][HSO ₄]	3.5 ± 0.3	
19	[C ₄ C ₁ Im][MeSO ₄]	3.1 ± 0.3	
20	[C ₄ C ₁ Im][OcSO ₄]	3.1 ± 0.3	
21	[C ₂ C ₁ Im][MeSO ₃]	3.0 ± 0.3	
22	[C ₄ C ₁ Im][Me ₂ PO ₄]	3.2 ± 0.3	
23	[C ₄ C ₁ Im][TfO]	3.6 ± 0.3	
24	[C ₈ C ₁ Im][TfO]	3.7 ± 0.3	
25	[N _{2,2,1,0}][TfO]	3.7 ± 0.3	
26	[N _{2OH,2OH,2OH,1}][TfO]	3.6 ± 0.3	
27	[C ₄ C ₁ Im][NTf ₂]	3.8 ± 0.3	
28	[C ₆ C ₁ Im][NTf ₂]	3.8 ± 0.3	
29	[C ₈ C ₁ Im][NTf ₂]	3.8 ± 0.3	
30	[C ₂ C ₀ Im][NTf ₂]	3.9 ± 0.3	
31	[C ₄ C ₀ Im][NTf ₂]	3.9 ± 0.3	
32	[N _{4,1,1,1}][NTf ₂]	4.0 ± 0.3	
33	[N _{3,2,1,1}][NTf ₂]	3.9 ± 0.3	
34	[N _{8,8,8,1}][NTf ₂]	3.8 ± 0.3	
35	[S _{2,2,1}][NTf ₂]	4.3 ± 0.3	
36	[S _{2,2,2}][NTf ₂]	4.2 ± 0.3	
37	[P _{6,6,6,14}][NTf ₂]	3.7 ± 0.3	

Table S14. E_B (cation HOFO), E_B (anion HOFO), HOFO identities, E_B difference between the respective ion HOFO E_B values, ΔE_B (ion HOFO) = E_B (cation HOFO) – E_B (anion HOFO) and HOMO identity. Entries are listed by ΔE_B (ion HOFO) ^a

Ionic Liquid	E_B (cation HOFO) / eV	E_B (cation onset) / eV	Cation HOFO contribution	E_B (anion HOFO) / eV	E_B (anion onset) / eV	Anion HOFO contribution	ΔE_B (ion onset) / eV	ΔE_B (ion HOFO) / eV	HOMO identify
[C ₆ C ₁ Im]I	4.8 ± 0.4	3.7 ± 0.3	N 2p + C 2p	2.6 ± 0.1	1.7 ± 0.2	I 5p	2.0 ± 0.5	2.2 ± 0.5	Anion
[P _{6,6,6,14}]Br	5.0 ± 0.4	Unknown	C 2p	2.9 ± 0.1	1.8 ± 0.2	Br 4p	Unknown	2.1 ± 0.5	Anion
[N _{4,1,1,0}][HSO ₄]	6.5 ± 1.0	Unknown	C 2p	4.5 ± 0.4	3.1 ± 0.3	O 2p	Unknown	2.0 ± 1.4	Anion
[N _{8,1,1,0}][HSO ₄]	6.5 ± 1.0	Unknown	C 2p	4.5 ± 0.4	3.5 ± 0.3	O 2p	Unknown	2.0 ± 1.4	Anion
[C ₈ C ₁ Im][C(CN) ₃]	4.8 ± 0.4	3.7 ± 0.3	N 2p + C 2p	2.8 ± 0.2	1.8 ± 0.2	N 2p	1.9 ± 0.5	2.0 ± 0.6	Anion
[C ₄ C ₁ Im][SCN]	4.8 ± 0.4	3.7 ± 0.3	N 2p + C 2p	2.9 ± 0.1	1.9 ± 0.2	N 2p + S 3p	1.8 ± 0.5	1.9 ± 0.5	Anion
[C ₈ C ₁ Im][SCN]	4.8 ± 0.4	3.7 ± 0.3	N 2p + C 2p	2.9 ± 0.1	1.9 ± 0.2	N 2p + S 3p	1.8 ± 0.5	1.9 ± 0.5	Anion
[P _{6,6,6,14}]Cl	5.0 ± 0.4	Unknown	C 2p	3.1 ± 0.1	2.2 ± 0.2	Cl 3p	Unknown	1.9 ± 0.5	Anion
[P _{6,6,6,14}][N(CN) ₂]	5.0 ± 0.4	Unknown	C 2p	3.2 ± 0.4	2.0 ± 0.3	N 2p and/or C 2p	Unknown	1.8 ± 0.5	Anion
[C ₈ C ₁ Im]Br	4.8 ± 0.4	3.7 ± 0.3	N 2p + C 2p	3.2 ± 0.1	2.2 ± 0.2	Br 4p	1.5 ± 0.5	1.6 ± 0.5	Anion
[P _{6,6,6,14}][NO ₃]	5.0 ± 0.4	Unknown	C 2p	3.5 ± 0.4	2.3 ± 0.3	O 2p	Unknown	1.5 ± 0.5	Anion
[C ₄ C ₁ Im][N(CN) ₂]	4.8 ± 0.4	3.7 ± 0.3	N 2p + C 2p	3.5 ± 0.4	2.4 ± 0.3	N 2p and/or C 2p	1.3 ± 0.6	1.3 ± 0.8	Anion
[C ₈ C ₁ Im]Cl	4.8 ± 0.4	3.7 ± 0.3	N 2p + C 2p	3.7 ± 0.1	2.6 ± 0.2	Cl 3p	1.1 ± 0.5	1.1 ± 0.5	Anion
[S _{2,2,2}][NTf ₂]	6.0 ± 0.4	Unknown	S 3p	5.0 ± 0.4	4.2 ± 0.3	All elements	Unknown	1.0 ± 0.8	Anion
[S _{2,2,1}][NTf ₂]	6.0 ± 0.4	Unknown	S 3p	5.0 ± 0.4	4.3 ± 0.3	All elements	Unknown	1.0 ± 0.8	Anion
[C ₄ C ₁ Im][HSO ₄]	4.8 ± 0.4	3.7 ± 0.3	N 2p + C 2p	4.5 ± 0.4	3.2 ± 0.3	O 2p	0.5 ± 0.6	0.3 ± 0.8	Anion
[C ₈ C ₁ Im][HSO ₄]	4.8 ± 0.4	3.7 ± 0.3	N 2p + C 2p	4.5 ± 0.4	3.2 ± 0.3	O 2p	0.5 ± 0.6	0.3 ± 0.8	Anion
[C ₄ C ₀ Im][HSO ₄]	4.8 ± 0.4	3.7 ± 0.3	N 2p + C 2p	4.5 ± 0.4	3.4 ± 0.3	O 2p	0.3 ± 0.6	0.3 ± 0.8	Anion
[C ₄ C ₁ Im][MeSO ₄]	4.8 ± 0.4	3.7 ± 0.3	N 2p + C 2p	4.5 ± 0.4	3.1 ± 0.3	O 2p	0.6 ± 0.6	0.3 ± 0.8	Anion
[C ₄ C ₁ Im][OcSO ₄]	4.8 ± 0.4	3.7 ± 0.3	N 2p + C 2p	4.5 ± 0.4	3.1 ± 0.3	O 2p	0.6 ± 0.6	0.3 ± 0.8	Anion
[C ₂ C ₁ Im][MeSO ₃]	4.8 ± 0.4	3.7 ± 0.3	N 2p + C 2p	4.5 ± 0.4	3.0 ± 0.3	O 2p	0.7 ± 0.6	0.3 ± 0.8	Anion
[C ₄ C ₁ Im][Me ₂ PO ₄]	4.8 ± 0.4	3.7 ± 0.3	N 2p + C 2p	4.5 ± 0.4	3.2 ± 0.3	O 2p	0.5 ± 0.6	0.3 ± 0.8	Anion
[N _{2,2,1,0}][TfO]	Unknown	Unknown	Not identified	5.0 ± 0.4	3.7 ± 0.3	O 2p	Unknown	Not determined	Anion
[N _{4,1,1,1}][NTf ₂]	Unknown	Unknown	Not identified	5.0 ± 0.4	4.0 ± 0.3	O 2p	Unknown	Not determined	Anion
[N _{3,2,1,1}][NTf ₂]	Unknown	Unknown	Not identified	5.0 ± 0.4	3.9 ± 0.3	O 2p	Unknown	Not determined	Anion
[C ₄ C ₁ Im][TfO]	4.8 ± 0.4	3.7 ± 0.3	N 2p + C 2p	5.0 ± 0.4	3.6 ± 0.3	O 2p	0.1 ± 0.6	-0.2 ± 0.8	Cation/Anion
[C ₈ C ₁ Im][TfO]	4.8 ± 0.4	3.7 ± 0.3	N 2p + C 2p	5.0 ± 0.4	3.7 ± 0.3	O 2p	0.0 ± 0.6	-0.2 ± 0.8	Cation/Anion
[C ₄ C ₁ Im][NTf ₂]	4.8 ± 0.4	3.7 ± 0.3	N 2p + C 2p	5.0 ± 0.4	3.8 ± 0.3	O 2p	-0.1 ± 0.6	-0.2 ± 0.8	Cation/Anion
[C ₆ C ₁ Im][NTf ₂]	4.8 ± 0.4	3.7 ± 0.3	N 2p + C 2p	5.0 ± 0.4	3.8 ± 0.3	O 2p	-0.1 ± 0.6	-0.2 ± 0.8	Cation/Anion
[C ₈ C ₁ Im][NTf ₂]	4.8 ± 0.4	3.7 ± 0.3	N 2p + C 2p	5.0 ± 0.4	3.8 ± 0.3	O 2p	-0.1 ± 0.6	-0.2 ± 0.8	Cation/Anion
[C ₂ C ₀ Im][NTf ₂]	4.8 ± 0.4	3.7 ± 0.3	N 2p + C 2p	5.0 ± 0.4	3.9 ± 0.3	O 2p	-0.2 ± 0.6	-0.2 ± 0.8	Cation/Anion
[C ₄ C ₀ Im][NTf ₂]	4.8 ± 0.4	3.7 ± 0.3	N 2p + C 2p	5.0 ± 0.4	3.9 ± 0.3	O 2p	-0.2 ± 0.6	-0.2 ± 0.8	Cation/Anion
[P _{6,6,6,14}][NTf ₂]	5.0 ± 0.4	Unknown	C 2p	5.0 ± 0.4	3.6 ± 0.3	O 2p	Unknown	0.0 ± 0.8	Cation/Anion
[N _{8,8,8,1}][NTf ₂]	5.0 ± 0.4	Unknown	C 2p	5.0 ± 0.4	3.8 ± 0.3	O 2p	Unknown	0.0 ± 0.8	Cation/Anion
[N _{2OH,2OH,2OH,1}][TfO]	4.8 ± 0.4	3.6 ± 0.3	O 2p	5.0 ± 0.4	3.6 ± 0.3	O 2p	0.0 ± 0.6	-0.2 ± 0.8	Cation/Anion
[C ₆ C ₁ Im][B(CN) ₄]	4.8 ± 0.4	3.7 ± 0.3	N 2p + C 2p	6.6 ± 0.6	5.3 ± 0.3	N 2p and/or C 2p	-1.6 ± 0.6	-1.6 ± 1.0	Cation
[C ₈ C ₁ Im][BF ₄]	4.8 ± 0.4	3.7 ± 0.3	N 2p + C 2p	7.8 ± 0.6	6.4 ± 0.3	F 2p	-2.7 ± 0.6	-2.8 ± 1.0	Cation

^a The HOMO identity assignments for [N_{2,2,1,0}][TfO], [N_{4,1,1,1}][NTf₂] and [N_{3,2,1,1}][NTf₂] were based upon a combination of E_B (anion HOFO) for these ILs and E_B (cation HOFO) for [N_{4,1,1,0}][HSO₄]

28. References

1. R. M. Fogarty, R. P. Matthews, M. T. Clough, C. R. Ashworth, A. Brandt-Talbot, P. J. Corbett, R. G. Palgrave, R. A. Bourne, T. W. Chamberlain, T. Vander Hoogerstraete, P. B. J. Thompson, P. A. Hunt, N. A. Besley and K. R. J. Lovelock, *Phys. Chem. Chem. Phys.*, 2017, **19**, 31156-31167.
2. I. J. Villar-Garcia, S. Fearn, G. F. De Gregorio, N. L. Ismail, F. J. V. Gschwend, A. J. S. McIntosh and K. R. J. Lovelock, *Chem. Sci.*, 2014, **5**, 4404-4418.
3. T. Vander Hoogerstraete and K. Binnemans, *Green Chem.*, 2014, **16**, 1594-1606.
4. T. Q. To, Ph.D. Thesis, Imperial College London, 2013.
5. M. T. Clough, C. R. Crick, J. Grasvik, P. A. Hunt, H. Niedermeyer, T. Welton and O. P. Whitaker, *Chem. Sci.*, 2015, **6**, 1101-1114.
6. M. T. Clough, K. Geyer, P. A. Hunt, S. Son, U. Vagt and T. Welton, *Green Chem.*, 2015, **17**, 231-243.
7. P. Verdia, A. Brandt, J. P. Hallett, M. J. Ray and T. Welton, *Green Chem.*, 2014, **16**, 1617-1627.
8. G. F. De Gregorio, C. C. Weber, J. Grasvik, T. Welton, A. Brandt and J. P. Hallett, *Green Chem.*, 2016, **18**, 5456-5465.
9. K. Kanai, T. Nishi, T. Iwahashi, Y. Ouchi, K. Seki, Y. Harada and S. Shin, *J. Electron Spectrosc. Relat. Phenom.*, 2009, **174**, 110-115.
10. D. Briggs and J. T. Grant, eds., *Surface Analysis by Auger and X-ray Photoelectron Spectroscopy*, IM Publications, Manchester, 2003.
11. S. Thurmer, R. Seidel, M. Faubel, W. Eberhardt, J. C. Hemminger, S. E. Bradforth and B. Winter, *Phys. Rev. Lett.*, 2013, **111**, 5.
12. C. Kolbeck, M. Killian, F. Maier, N. Paape, P. Wasserscheid and H. P. Steinrück, *Langmuir*, 2008, **24**, 9500-9507.
13. K. R. J. Lovelock, I. J. Villar-Garcia, F. Maier, H. P. Steinrück and P. Licence, *Chem. Rev.*, 2010, **110**, 5158-5190.
14. I. J. Villar-Garcia, E. F. Smith, A. W. Taylor, F. L. Qiu, K. R. J. Lovelock, R. G. Jones and P. Licence, *Phys. Chem. Chem. Phys.*, 2011, **13**, 2797-2808.
15. E. F. Smith, F. J. M. Rutten, I. J. Villar-Garcia, D. Briggs and P. Licence, *Langmuir*, 2006, **22**, 9386-9392.
16. K. R. J. Lovelock, E. F. Smith, A. Deyko, I. J. Villar-Garcia, P. Licence and R. G. Jones, *Chem. Commun.*, 2007, 4866-4868.
17. A. Broderick, Y. Khalifa, M. B. Shiflett and J. T. Newberg, *J. Phys. Chem. C*, 2017, **121**, 7337-7343.
18. Y. Khalifa, A. Broderick and J. T. Newberg, *J. Electron Spectrosc. Relat. Phenom.*, 2018, **222**, 162-166.
19. R. M. Fogarty, R. G. Palgrave and K. R. J. Lovelock, 2019, In preparation.
20. R. K. Blundell and P. Licence, *Phys. Chem. Chem. Phys.*, 2014, **16**, 15278-15288.
21. R. K. Blundell, A. E. Delorme, E. F. Smith and P. Licence, *Phys. Chem. Chem. Phys.*, 2016, **18**, 6122-6131.
22. S. Men, K. R. J. Lovelock and P. Licence, *Phys. Chem. Chem. Phys.*, 2011, **13**, 15244-15255.
23. R. K. Blundell and P. Licence, *Chem. Commun.*, 2014, **50**, 12080-12083.
24. Q. H. Zhang, S. M. Liu, Z. P. Li, J. Li, Z. J. Chen, R. F. Wang, L. J. Lu and Y. Q. Deng, *Chem.-Eur. J.*, 2009, **15**, 765-778.
25. K. R. J. Lovelock, C. Kolbeck, T. Cremer, N. Paape, P. S. Schulz, P. Wasserscheid, F. Maier and H. P. Steinrück, *J. Phys. Chem. B*, 2009, **113**, 2854-2864.
26. D. Yoshimura, T. Yokoyama, T. Nishi, H. Ishii, R. Ozawa, H. Hamaguchi and K. Seki, *J. Electron Spectrosc. Relat. Phenom.*, 2005, **144**, 319-322.
27. T. Nishi, T. Iwahashi, H. Yamane, Y. Ouchi, K. Kanai and K. Seki, *Chem. Phys. Lett.*, 2008, **455**, 213-217.

28. K. Kanai, T. Nishi, T. Iwahashi, Y. Ouchi, K. Seki, Y. Harada and S. Shin, *J. Chem. Phys.*, 2008, **129**, 224507.
29. S. Krischok, R. Ötting, W. J. D. Beenken, M. Himmerlich, P. Lorenz, O. Höfft, S. Bahr, V. Kempter and J. A. Schaefer, *Z. Phys. Chemie-Int. J. Res. Phys. Chem. Chem. Phys.*, 2006, **220**, 1407-1416.
30. M. Reinmöller, A. Ulbrich, T. Ikari, J. Preiss, O. Höfft, F. Endres, S. Krischok and W. J. D. Beenken, *Phys. Chem. Chem. Phys.*, 2011, **13**, 19526-19533.
31. A. Ulbrich, M. Reinmöller, W. J. D. Beenken and S. Krischok, *ChemPhysChem*, 2012, **13**, 1718-1724.
32. A. Ulbrich, M. Reinmöller, W. J. D. Beenken and S. Krischok, *J. Mol. Liq.*, 2014, **192**, 77-86.
33. S. Krischok, M. Eremtchenko, M. Himmerlich, P. Lorenz, J. Uhlig, A. Neumann, R. Ötting, W. J. D. Beenken, O. Höfft, S. Bahr, V. Kempter and J. A. Schaefer, *J. Phys. Chem. B*, 2007, **111**, 4801-4806.
34. T. Iwahashi, T. Nishi, H. Yamane, T. Miyamae, K. Kanai, K. Seki, D. Kim and Y. Ouchi, *J. Phys. Chem. C*, 2009, **113**, 19237-19243.
35. J. C. Green and P. Decleva, *Coord. Chem. Rev.*, 2005, **249**, 209-228.
36. U. Gelius and K. Siegbahn, *Faraday Discuss.*, 1972, **54**, 257-268.
37. U. Gelius, *J. Electron Spectrosc. Relat. Phenom.*, 1974, **5**, 985-1057.
38. J. J. Yeh and I. Lindau, *At. Data Nucl. Data Tables*, 1985, **32**, 1-155.
39. S. Men, D. S. Mitchell, K. R. J. Lovelock and P. Licence, *ChemPhysChem*, 2015, **16**, 2211-2218.
40. C. Kolbeck, T. Cremer, K. R. J. Lovelock, N. Paape, P. S. Schulz, P. Wasserscheid, F. Maier and H. P. Steinrück, *J. Phys. Chem. B*, 2009, **113**, 8682-8688.
41. R. M. Fogarty, R. P. Matthews, C. R. Ashworth, A. Brandt-Talbot, R. G. Palgrave, R. A. Bourne, T. V. Hoogerstraete, P. A. Hunt and K. R. J. Lovelock, *J. Chem. Phys.*, 2018, **148**, 193817.
42. F. Rodrigues, G. M. do Nascimento and P. S. Santos, *J. Electron Spectrosc. Relat. Phenom.*, 2007, **155**, 148-154.
43. F. Rodrigues, D. Galante, G. M. do Nascimento and P. S. Santos, *J. Phys. Chem. B*, 2012, **116**, 1491-1498.
44. J. K. Chang, M. T. Lee, W. T. Tsai, M. J. Deng, H. F. Cheng and I. W. Sun, *Langmuir*, 2009, **25**, 11955-11960.
45. C. Ehlert, M. Holzweber, A. Lippitz, W. E. S. Unger and P. Saalfrank, *Phys. Chem. Chem. Phys.*, 2016, **18**, 8654-8661.
46. Y. Horikawa, T. Tokushima, O. Takahashi, H. Hoke and T. Takamuku, *J. Phys. Chem. B*, 2016, **120**, 7480-7487.
47. R. Dudde, M. L. M. Rocco, E. E. Koch, S. Bernstorff and W. Eberhardt, *J. Chem. Phys.*, 1989, **91**, 20-28.
48. A. B. Preobrajenski, A. S. Vinogradov and N. Mårtensson, *J. Electron Spectrosc. Relat. Phenom.*, 2005, **148**, 59-64.
49. P. A. Brühwiler, O. Karis and N. Mårtensson, *Rev. Mod. Phys.*, 2002, **74**, 703-740.
50. M. Mauerer, P. Zebisch, M. Weinelt and H. P. Steinrück, *J. Chem. Phys.*, 1993, **99**, 3343-3352.
51. R. Friedlein, S. L. Sorensen, A. Baev, F. Gel'mukhanov, J. Birgerson, A. Crispin, M. P. de Jong, W. Osikowicz, C. Murphy, H. Agren and W. R. Salaneck, *Phys. Rev. B*, 2004, **69**, 125204.
52. H. Peisert, I. Biswas, L. Zhang, B. E. Schuster, M. B. Casu, A. Haug, D. Batchelor, M. Knupfer and T. Chasse, *J. Chem. Phys.*, 2009, **130**, 194705.
53. J. J. Gallet, F. Bournel, S. Kubsky, G. Dufour, F. Rochet and F. Sirotti, *J. Electron Spectrosc. Relat. Phenom.*, 2002, **122**, 285-295.
54. W. Osikowicz, R. Friedlein, M. P. de Jong, S. L. Sorensen, L. Groenendaal and W. R. Salaneck, *New J. Phys.*, 2005, **7**, 104.
55. A. B. Preobrajenski, A. S. Vinogradov, S. L. Molodtsov, S. K. Krasnikov, T. Chasse, R. Szargan and C. Laubschat, *Phys. Rev. B*, 2002, **65**, 205116.

56. U. Hergenbahn, A. Rüdell, K. Maier, A. M. Bradshaw, R. F. Fink and A. T. Wen, *Chem. Phys.*, 2003, **289**, 57-67.
57. R. M. Fogarty, R. A. Bourne, R. G. Palgrave and K. R. J. Lovelock, 2019, In preparation.
58. A. B. Preobrajenski, A. S. Vinogradov, S. L. Molodtsov, S. A. Krasnikov, R. Szargan and C. Laubschat, *Chem. Phys. Lett.*, 2003, **368**, 125-131.
59. D. Briggs and G. Beamson, *Anal. Chem.*, 1993, **65**, 1517-1523.
60. T. Cremer, C. Kolbeck, K. R. J. Lovelock, N. Paape, R. Wölfel, P. S. Schulz, P. Wasserscheid, H. Weber, J. Thar, B. Kirchner, F. Maier and H. P. Steinrück, *Chem.-Eur. J.*, 2010, **16**, 9018-9033.